SUBTASK 2.18 – ADVANCING CO_2 CAPTURE TECHNOLOGY: PARTNERSHIP FOR CO_2 CAPTURE (PCO_2C) PHASE III

Final Report

(for the period of July 1, 2013, through March 31, 2016)

Prepared for:

AAD Document Control

National Energy Technology Laboratory
U.S. Department of Energy
626 Cochrans Mill Road
PO Box 10940, MS 921-107
Pittsburgh, PA 15236-0940

Cooperative Agreement No.: DE-FC26-08NT43291
DOE Technical Monitor: I. Andrew Aurelio

Prepared by:

John P. Kay
Alexander Azenkeng
Nathan J. Fiala
Melanie D. Jensen
Jason D. Laumb
Kerryanne M. Leroux
Donald P. McCollor
Joshua J. Stanislowski
Scott C. Tolbert
Tyler J. Curran

Energy & Environmental Research Center
University of North Dakota
15 North 23rd Street, Stop 9018
Grand Forks, ND 58202-9018

2016-EERC-03-13 March 2016

EERC DISCLAIMER

LEGAL NOTICE This research report was prepared by the Energy & Environmental Research Center (EERC), an agency of the University of North Dakota, as an account of work sponsored by the U.S. Department of Energy, the North Dakota Industrial Commission (NDIC), PPL Montana, Nebraska Public Power District, Tri-Mer Corporation, Montana–Dakota Utilities Co., Basin Electric Power Cooperative, Korea Carbon Capture and Sequestration Research and Demonstration Center/Korean Institute of Energy Research, Cansolv Technologies, and CO_2 Solutions, Inc. Because of the research nature of the work performed, neither the EERC nor any of its employees makes any warranty, express or implied, or assumes any legal liability or responsibility for the accuracy, completeness, or usefulness of any information, apparatus, product, or process disclosed or represents that its use would not infringe privately owned rights. Reference herein to any specific commercial product, process, or service by trade name, trademark, manufacturer, or otherwise does not necessarily constitute or imply its endorsement or recommendation by the EERC.

DISCLAIMER

This report was prepared as an account of work sponsored by an agency of the United States Government. Neither the United States Government, nor any agency thereof, nor any of their employees, makes any warranty, express or implied, or assumes any legal liability or responsibility for the accuracy, completeness, or usefulness of any information, apparatus, product, or process disclosed, or represents that its use would not infringe privately owned rights. Reference herein to any specific commercial product, process, or service by trade name, trademark, manufacturer, or otherwise does not necessarily constitute or imply its endorsement, recommendation, or favoring by the United States Government or any agency thereof. The views and opinions of authors expressed herein do not necessarily state or reflect those of the United States Government or any agency thereof.

NDIC DISCLAIMER

This report was prepared by the EERC pursuant to an agreement partially funded by the Industrial Commission of North Dakota, and neither the EERC nor any of its subcontractors nor the North Dakota Industrial Commission nor any person acting on behalf of either:

(A) Makes any warranty or representation, express or implied, with respect to the accuracy, completeness, or usefulness of the information contained in this report or that the use of any information, apparatus, method, or process disclosed in this report may not infringe privately owned rights; or

(B) Assumes any liabilities with respect to the use of, or for damages resulting from the use of, any information, apparatus, method, or process disclosed in this report.

Reference herein to any specific commercial product, process, or service by trade name, trademark, manufacturer, or otherwise does not necessarily constitute or imply its endorsement, recommendation, or favoring by the North Dakota Industrial Commission. The views and opinions of authors expressed herein do not necessarily state or reflect those of the North Dakota Industrial Commission.

SUBTASK 2.18 – ADVANCING CO_2 CAPTURE TECHNOLOGY: PARTNERSHIP FOR CO_2 CAPTURE (PCO_2C) PHASE III

ABSTRACT

Industries and utilities continue to investigate ways to decrease their carbon footprint. Carbon capture and storage (CCS) can enable existing power generation facilities to meet the current national CO_2 reduction goals. The Partnership for CO_2 Capture Phase III focused on several important research areas in an effort to find ways to decrease the cost of capture across both precombustion and postcombustion platforms.

Two flue gas pretreatment technologies for postcombustion capture, an SO_2 reduction scrubbing technology from Cansolv Technologies Inc. and the Tri-Mer filtration technology that combines particulate, NO_x, and SO_2 control, were evaluated on the Energy & Environmental Research Center's (EERC's) pilot-scale test system. Pretreating the flue gas should enable more efficient, and therefore less expensive, CO_2 capture. Both technologies were found to be effective in pretreating flue gas prior to CO_2 capture.

Two new postcombustion capture solvents were tested, one from the Korea Carbon Capture and Sequestration R&D Center (KCRC) and one from CO_2 Solutions Incorporated. Both of these solvents showed the ability to capture CO_2 while requiring less regeneration energy, which would reduce the cost of capture.

Hydrogen separation membranes from Commonwealth Scientific and Industrial Research Organisation were evaluated through precombustion testing. They are composed of vanadium alloy, which is less expensive than the palladium alloys that are typically used. Their performance was comparable to that of other membranes that have been tested at the EERC.

Aspen Plus® software was used to model the KCRC and CO_2 Solutions solvents and found that they would result in significantly improved overall plant performance. The modeling effort also showed that the parasitic steam load at partial capture of 45% is less than half that of 90% overall capture, indicating savings that could be accrued if 90% capture is not required.

Modeling of three regional power plants using the Carnegie Mellon Integrated Environmental Control Model showed that, among other things, the use of a bypass during partial capture may minimize the size of the capture tower(s) and result in a slight reduction in the revenue required to operate the capture facility. The results reinforced that a one-size-fits-all approach cannot be taken to adding capture to a power plant.

Laboratory testing indicated that Fourier transform infrared spectroscopy could be used to continuously sample stack emissions at CO_2 capture facilities to detect and quantify any residual amine or its degradation products, particularly nitrosamines.

The information gathered during Phase III is important for utility stakeholders as they determine how to reduce their CO_2 emissions in a carbon-constrained world.

This subtask was funded through the EERC–U.S. Department of Energy (DOE) Joint Program on Research and Development for Fossil Energy-Related Resources Cooperative Agreement No. DE-FC26-08NT43291. Nonfederal funding was provided by the North Dakota Industrial Commission, PPL Montana, Nebraska Public Power District, Tri-Mer Corporation, Montana–Dakota Utilities Co., Basin Electric Power Cooperative, KCRC/Korean Institute of Energy Research, Cansolv Technologies, and CO_2 Solutions, Inc.

TABLE OF CONTENTS

Continued…

TABLE OF CONTENTS (continued)

Continued…

TABLE OF CONTENTS (continued)

LIST OF FIGURES

Continued…

LIST OF FIGURES (continued)

Continued…

LIST OF FIGURES (continued)

Continued…

LIST OF FIGURES (continued)

Continued…

LIST OF FIGURES (continued)

Continued…

LIST OF FIGURES (continued)

LIST OF TABLES

Continued…

LIST OF TABLES (continued)

LIST OF ACRONYMS AND ABBREVIATIONS

A/D	analog/digital
AACE	Association for the Advancement of Cost Engineering (International)
acmm	actual cubic meter per minute
AGFC	advanced gasification fuel cell
APEA	Aspen Process Economic Analyzer
ARL	Analytical Research Laboratory
ASME	American Society of Mechanical Engineers
ATR	attenuated total reflectance
bby	billion barrels per year
bcc	body-centered cubic
BOP	balance of plant
Btu	British thermal unit
°C	degree Celsius
CCF	capital charge factor
CCS	carbon capture and storage
CF	plant capacity factor
CGE	cold gas efficiency
cm	centimeter
CO_2	carbon dioxide
COE	cost of electricity
CPP	Clean Power Plan
CPU	central processing unit
CSES	CO_2 Solutions enzyme solvent
CSIRO	Commonwealth Scientific and Industrial Research Organisation
CTF	combustion test facility
CTI	Cansolv Technologies Inc.
DEA	diethanolamine
DGM	dry gas meter
DI	deionized
DOE	U.S. Department of Energy
dP	differential pressure
DSI	direct sorbent injection
EERC	Energy & Environmental Research Center
EOR	enhanced oil recovery
EPA	U.S. Environmental Protection Agency
ESP	electrostatic precipitator
°F	degree Fahrenheit
FBG	fluidized-bed gasifier
fcc	face-centered cubic
FEED	front-end engineering design
FGD	flue gas desulfurization
ft	foot
ft^2	square foot
FT-IR	Fourier-transform infrared

FV	filter vessel
g/scm	gram/standard cubic meter
gal	gallon
GC	gas chromatograph
GC–FID	gas chromatography–flame ionization detection
GHG	greenhouse gas
GJ/t	gigajoule per ton
gpm	gallon per minute
H2	hertz
H_2S	hydrogen sulfide
HGFV	hot-gas filter vessel
HHV	higher heating value
HMTS	hydrogen membrane test system
HP	high pressure
hp	horsepower
HPLC	high-performance liquid chromatography
hr	hour
HRSG	heat recovery steam generator
HSS	heat-stable salts
IC	ion chromatography
ICEV	internal combustion engine vehicle
i.d.	inside diameter
ID	induced draft
IEAGHG	International Energy Agency Greenhouse Gas R&D Programme
IECM	Integrated Environmental Control Model
IGCC	integrated gasification combined cycle
in.	inch
IP	intermediate pressure
KCRC	Korea Carbon Capture and Sequestration R&D Center
kg	kilogram
kPa	kilopascal
kPag	kilopascal gauge
Kscf	thousand standard cubic foot
kW	kilowatt
L	liter
lb/MWh	pound per megawatt-hour
LC–MS	liquid chromatography–mass spectrometry
L/G	liquid/gas ratio
LGA	laser gas analyzer
LOI	loss on ignition
LP	low pressure
m	meter
m^2	square meter
m^3	cubic meter
m^3/min	cubic meter per minute
Macm	million actual cubic meter

MEA	monoethanolamine
MFC	mass flow controller
MHI	Mitsubishi Heavy Industries, Ltd.
mL	milliliters
µm	micrometer
MMBtu	million British thermal unit
MOP	maximum allowable pressure
MPa	megapascal
MW	megawatt
MW_e	megawatt-electric
MWh	megawatt-hour
MW_{th}	megawatt-thermal
NBS	National Bureau of Standards
NETL	National Energy Technology Laboratory
NGCC	natural gas combined cycle
NH_3	ammonia
NIOSH	National Institute for Occupational Safety and Health
nm	nanometer
NO_x	nitrogen oxides
NRC	National Research Council
O&M	operating and maintenance
o.d.	outside diameter
OC_{FIX}	fixed annual operating costs
OC_{VAR}	variable annual operating costs
OFA	overfire air
P&ID	piping and instrumentation diagram
pc	pulverized coal
PCD	particulate control device
PCO_2C	Partnership for CO_2 Capture
PFD	process flow diagram
PHEV	plug-in hybrid electric vehicle
PID	proportional integral derivative
ppb	parts per billion
ppm	parts per million
PRB	Powder River Basin
PSA	pressure swing adsorption
psia	pound per square inch, absolute
psig	pound per square inch, gauge
PTC	particulate test combustor
R&D	research and development
s	second
scf	standard cubic feet
scfm	standard cubic foot per minute
scmh	standard cubic meter per hour
scmm	standard cubic meter per minute
SCR	selective catalytic reduction

SEPA	Scottish Environmental Protection Agency
SO_2	sulfur dioxide
SO_x	sulfur oxides
SS	stainless steel
TASC	total as-spent cost
TC	thermal conductivity
TCM	Norwegian Technology Centre Mongstad
TIC	total inorganic carbon
TOC	total organic carbon
TPC	total plant cost
TRDU	transport reactor development unit
TRIG™	transport integrated gasification
Tri-Mer	Tri-Mer flue gas filtration technology
TSS	total suspended solids
UND	University of North Dakota
VFD	variable frequency drive
V-L	vapor–liquid
VLE	vapor–liquid equilibrium
vol%	volume percent
WFGD	wet flue gas desulfurization
WGS	water–gas shift
XRF	x-ray fluorescence

SUBTASK 2.18 – ADVANCING CO_2 CAPTURE TECHNOLOGY: PARTNERSHIP FOR CO_2 CAPTURE (PCO_2C) PHASE III

EXECUTIVE SUMMARY

Industries and utilities continue to investigate ways to decrease their carbon footprint as concerns mount about the potential role of carbon dioxide in global climate change. Carbon capture and storage (CCS) can enable existing power generation facilities to meet the current national CO_2 reduction goals. Unfortunately, capture is currently expensive and additional research is needed to find ways to decrease the cost. Under the Partnership for CO_2 Capture (PCO_2C) at the Energy & Environmental Research Center (EERC), ways to reduce the cost of capturing CO_2 have been sought. PCO_2C Phase III focused on several important areas as follows.

Two flue gas pretreatment technologies that can enhance the performance and reduce the cost of postcombustion CO_2 capture systems were evaluated. First, PCO_2C worked with Cansolv Technologies Inc. to test the operability of a benchmark solvent and an improved formulation for removal of SO_2 from the flue gas. Removal of SO_2 from the flue gas extends the life of a CO_2 capture solvent by reducing the formation of heat-stable salts. Both solvents were equally easy to run in the pilot-scale PCO_2C system, although the advanced formulation has a propensity to foam and should always be employed with an antifoaming agent. The testing indicated that the choice of solvent should be made based on both SO_2 removal effectiveness and the energy input required for regeneration rather than on solvent operability.

The second pretreatment technology tested was the Tri-Mer flue gas filtration technology, which combines particulate, NO_x, and SO_2 control. Testing with the Tri-Mer filter system resulted in high levels of capture for particulate, NO_x, and SO_2. NO_x capture and SO_2 capture were highly dependent on temperature, ammonia injection rate, and the amount of sorbent used. Two sorbents produced by Sorbacal, SP and SPS, were used in testing. The SPS material achieved higher levels of SO_2 removal than did the same amount of SP material. The Tri-Mer system was found to be effective for the removal of impurities prior to postcombustion CO_2 capture, although the testing showed that it may be necessary to additionally trim SO_2 levels.

Two new postcombustion capture solvents were tested on the PCO_2C small pilot-scale system. The first solvent tested was from the Korea Carbon Capture and Sequestration R&D Center (KCRC). Capture rates of 70% to 94% were observed for KCRC's Solvent-B, with steady-state data collected at several different test points. Solvent-B appeared to perform at least as well as 30 wt% monoethanolamine (MEA). It achieved 90% capture with an approximately 40% lower liquid/gas ratio (L/G) and 30% lower regeneration energy input than MEA at the same capture level.

The second postcombustion capture solvent evaluated was developed by CO_2 Solutions Incorporated. CO_2 Solutions' proprietary technology employs the enzyme carbonic anhydrase as a catalyst within a salt solution. The solvent requires that the stripping column be run at a slight vacuum. Most of the tests were performed with natural gas-derived flue gas, with a few test periods during which solvent performance using coal-derived flue gas was measured. The test campaign showed no degradation in performance of the enzyme catalyst, showed no generation of toxic waste by-products, and demonstrated the ability to use low-grade heat for regeneration, significantly reducing the cost to capture CO_2.

Nine membranes for the separation of hydrogen and CO_2 from coal-derived syngas were provided by Commonwealth Scientific and Industrial Research Organisation (CSIRO) for

evaluation as a precombustion CO_2 capture technology. The testing was performed on syngas produced in the EERC's fluidized-bed gasifier using warm-gas cleanup techniques and CSIRO's hydrogen separation membranes. The membranes' performance increased as the temperature increased and was comparable to the performance of other membranes tested at the EERC.

A detailed process-modeling effort was undertaken to develop the basis for determining the cost of CO_2 capture using advanced postcombustion capture technologies and techniques, including the solvents from KCRC and CO_2 Solutions. Partial capture with MEA was also modeled. The models were developed using Aspen Plus® software and mimicked the boiler and steam cycle for Cases 11 and 12 from the U.S. Department of Energy (DOE) report entitled "Cost and Performance Baseline for Fossil Energy Plants, Volume 1: Bituminous Coal and Natural Gas to Electricity" (Black, J. Revision 2a; DOE/2010/1397; Sept 2013.). Plant performance for the KCRC solvent is significantly improved over Case 12, which uses MEA solvent. If adequate waste heat can be gathered from the power plant for solvent regeneration and if the CO_2 Solutions solvent performs comparably to MEA, significant increases in overall plant efficiency and reductions in coal feed rate versus Case 12 can be realized. Kinetic and mass transfer limitations were seen to be significantly reduced for 75% partial capture. At 45% overall capture, the parasitic steam load is less than one-half that of 90% overall capture, improving the overall Case 12 plant efficiency from 28.4% to 33.6%.

Three power plants from the region were modeled using the Carnegie Mellon Integrated Environmental Control Model (IECM) to show the effects that the addition of capture would have on specific net power production, water usage, and revenue requirements for various levels of capture. Important findings included that sulfur removal devices must be installed if not already present; space for the capture plant and storage of solvent and reclaimer waste must be available; use of a bypass during partial capture may minimize the size of the capture tower(s), resulting in a reduction of revenue required to operate the capture facility; and power plants in arid areas may find that addition of a cooling tower could minimize water usage. The results reinforced that a one-size-fits-all approach cannot be taken to adding capture to a power plant.

A laboratory test was performed to determine the feasibility of detecting and quantifying any residual amine as well as its degradation products (particularly nitrosamines) that can be potentially emitted to the atmosphere with the stack flue gases. It was found that solutions of alkanolamine solvents containing pure solvent components as well as their degradation products and flue gas species can be monitored using the Fourier transform infrared spectroscopy (FT-IR) technique and that FT-IR would be amenable to continuous sampling of stack emissions at CO_2 capture facilities.

PCO_2C Program Phase III placed a strong emphasis on the integration of technologies into total systems so that substantial economic and environmental benefit could be realized. The type of information gathered during Phase III is important for utility stakeholders as they determine how to reduce their CO_2 emissions in a carbon-constrained world.

This subtask was funded through the EERC–DOE Joint Program on Research and Development for Fossil Energy-Related Resources Cooperative Agreement No. DE-FC26-08NT43291. Nonfederal funding was provided by the North Dakota Industrial Commission (NDIC), PPL Montana, Nebraska Public Power District, Tri-Mer Corporation, Montana–Dakota Utilities Co., Basin Electric Power Cooperative, KCRC/Korean Institute of Energy Research, Cansolv Technologies, and CO_2 Solutions, Inc.

SUBTASK 2.18 – ADVANCING CO_2 CAPTURE TECHNOLOGY: PARTNERSHIP FOR CO_2 CAPTURE (PCO_2C) PHASE III

1.0 INTRODUCTION

Industries and utilities continue to investigate ways to decrease their carbon footprint as concerns mount about the potential role of carbon dioxide in global climate change. These methods include improving process efficiencies so that less carbon-based fuel is used, switching to fuels with lower fossil carbon content (e.g., biomass or biomass blends, augmentation by wind or solar power), and capture of the CO_2 produced for either beneficial use or for permanent storage. Capture and storage of the CO_2 can enable existing power generation facilities to meet the current national CO_2 reduction goals. This approach is being demonstrated at large scale in several tests around the world and at commercial scale at the SaskPower Boundary Dam power station in Saskatchewan. Unfortunately, the capture portion of the approach is currently expensive, and additional research is needed to find ways to decrease the cost.

Reducing the cost of CO_2 capture will require that new technologies be developed across the various platforms (precombustion, postcombustion, oxyfuel combustion), the efficiency and effectiveness of existing technologies be improved, and pretreatment technologies that can improve the performance of a capture technology continue to be developed and optimized. Under the Partnership for CO_2 Capture (PCO_2C), the Energy & Environmental Research Center (EERC) has worked in each of these areas in order to reduce the cost of capturing CO_2. Pilot-scale testing of pretreatment technologies has produced new options for removing sulfur or nitrogen oxides (SO_x or NO_x, respectively) from flue gas prior to capture of the CO_2. Capture technologies covering all three platforms have been evaluated during pilot-scale tests and, when possible, changes in operation that could improve the technologies' effectiveness were identified. This method of evaluation permits identification of the strengths and weaknesses of a particular technology and allows for strategies to be developed to enhance performance and decrease costs for future applications.

2.0 CO_2 CAPTURE BACKGROUND

As countries around the world work to balance the concern about increases in CO_2 emission with the ever-increasing demand for power, regulation in some form appears to be inevitable. The following text briefly reviews two of the most recent regulatory initiatives regarding greenhouse gases (GHGs) and summarizes some of the commercial CO_2 capture demonstrations being undertaken and the technologies that are being employed at those demonstrations.

2.1 GHG Regulatory Initiatives

2.1.1 EPA's Clean Power Plan

The U.S. Environmental Protection Agency (EPA) developed the Clean Power Plan (CPP) as a means to reduce power plant CO_2 emissions by 32% below 2005 levels by 2030 (E&E

Publishing, LLC, 2015). The CPP sets a target emission rate for each state. This rate is the amount of CO_2 that can be emitted per megawatt hour (MWh) of power produced. State emission rate reductions range from 7% for Connecticut to 47% for Montana. These percentages represent the amount a state must reduce the emissions from its power plants below 2012 levels (E&E Publishing, LLC, 2015). The states are expected to submit either a final carbon-cutting plan or an initial plan with a 2-year extension by September 6, 2016. Starting in 2022, states are expected to begin working to attain their interim emission goals. They must meet the final goals in 2030 and beyond (E&E Publishing, LLC, 2015).

States first must decide whether they want to follow a rate- or a mass-based plan. A rate-based plan would mean that the state's entire power plant fleet would have to adhere to an average amount of CO_2 per unit of power produced (E&E Publishing, LLC, 2015). A mass-based plan would cap the total amount of CO_2 the state's power plants could emit each year.

States can assign standards to generators of CO_2, called an "emissions standards plan," or include a combination of emission limits and other programs, such as renewable energy and energy efficiency standards. This is called a "state measures plan" (E&E Publishing, LLC, 2015). Both of these plans may involve trading programs in which generators are able to purchase compliance credits from entities inside or outside of their states in order to offset carbon emissions, including zero-carbon renewable power producers (E&E Publishing, LLC, 2015).

EPA used three building blocks to determine what could "reasonably" be done to cut CO_2: 1) operate coal plants more efficiently, 2) run existing gas plants more often to enable existing coal plants to be run less often, and 3) ramp up renewable power. States are not required to employ the building blocks (E&E Publishing, LLC, 2015). The standard emission rate for coal-fired power stations in the United States will be 1305 lb/MWh for coal/steam plants, while the rate for natural gas-fired power plants will be 771 lb/MWh (E&E Publishing, LLC, 2015). A state with a mix of coal and gas units will have a rate that reflects its mix and falls somewhere between the two rates (E&E Publishing, LLC, 2015).

More than two dozen states and numerous industry groups filed five separate stay applications with the U.S. Supreme Court to prevent the CPP from being implemented. The Court granted a stay on February 9, 2016, pending disposition of the various applicant petitions for review in the U.S. Court of Appeals for the District of Columbia Circuit (Adler, 2016).

2.1.2 Paris Climate Agreement

Nearly 200 countries met in Paris in December 2015 to craft an agreement to reduce CO_2 emissions worldwide. The most important points in the agreement include (as summarized in Kavanagh, 2015):

- A commitment by countries to keep global temperatures at no more than 2°C above preindustrial levels. A more ambitious target of 1.5°C is mentioned as this is touted as necessary to prevent low-lying island nations from disappearing as sea levels rise in a warmer climate. Current pledges indicate that global temperatures could rise by as much

as 2.7°C if existing targets are maintained; therefore, experts are concerned that additional reductions will be needed.

- Submission for review of a nation's self-determined emission reduction plan beginning in 2020 and every 5 years thereafter. Each plan must provide successive improvement over the previous one. There is no official requirement that pledges must be reviewed or upgraded prior to 2030, although parties may do so voluntarily.

- The requirement that wealthy, developed countries provide financial assistance to poorer countries so as to assist them in transitioning to renewable energy and technologies that emit less CO_2.

2.2 Current Commercial-Scale CO_2 Capture Technology Demonstrations

Over 30 years of carbon capture and storage (CCS) experience has been collected from the Sleipner, Snøhvit, In Salah, and Weyburn–Midale projects. These four projects feature CO_2 captured from various source types and injected into different types of geologic sinks (Jensen and others, 2014). The Sleipner project takes CO_2 from a gas-processing facility and stores it in a deep saline reservoir at the bottom of the North Sea. Snøhvit sources its CO_2 from a liquid natural gas-processing plant; the CO_2 is injected into a deep saline reservoir under the North Sea. The In Salah project stores CO_2 from a gas-processing facility in a depleted portion of the nearby gas field. Finally, CO_2 produced during gasification of lignite is transported to the Weyburn and Midale oil fields for enhanced oil recovery (EOR). Although considerable information has been collected during these projects, capture at a coal-fired electricity-generating facility has not yet been demonstrated at commercial scale. Three projects are either in development or have begun capturing and storing their CO_2: the Kemper project in Mississippi, the WA Parish project in Texas, and the Boundary Dam project in Saskatchewan, Canada.

2.2.1 Kemper Project

The Kemper project will demonstrate CO_2 capture from a coal gasification process called TRIG™ (transport integrated gasification) that was developed by Southern Company and KBR in partnership with the U.S. Department of Energy (DOE). The Kemper plant will use two commercial-scale TRIG units to produce syngas by gasifying lignite (Global CCS Institute, 2013). Following cleaning, the syngas will be used to fuel two combined-cycle power-generating units having a net output of 582 MW of electricity.

The Selexol™ physical solvent will be used to capture at least 65% of the CO_2 produced at the plant (Nelson, 2011). This degree of capture will reduce the CO_2 emissions to nominally what is emitted by a natural gas-fired combined-cycle unit. The CO_2 will be compressed to a supercritical fluid for pipeline transport to an oil field for EOR. The roughly 3 million tons/yr of CO_2 from the Kemper plant will displace the current Denbury Resources Inc. Jackson Dome (a natural CO_2 reservoir) CO_2 source (Global CCS Institute, 2013).

2.2.2 WA Parish Project

Plans are being made to install commercial-scale postcombustion CO_2 capture on a 240-MW slipstream from NRG Energy's WA Parish generating station in Thompsons, Texas. The project is being developed by Petra Nova, a joint venture between NRG Energy and JX Nippon Oil & Gas Exploration and is designed to capture 90% of the CO_2 produced by the WA Parish plant. This CO_2, expected to total 1.6 million tons each year, will be used for EOR. The capture will be accomplished using an amine process developed by Mitsubishi Heavy Industries, Ltd. (MHI) and Kansai Electric Power Company (NRG Energy, 2014). When completed, the project will be the largest postcombustion capture facility installed on an existing coal-fired power plant and the first commercial-scale facility of its type in the United States (NRG Energy, 2014).

2.2.3 Boundary Dam Project

The Boundary Dam Integrated CCS project is the world's first and largest commercial-scale CCS project associated with an existing coal-fired power plant. Amine-based capture (using the Cansolv solvent) was installed on Boundary Dam Unit 3 to capture 90% of the CO_2 produced. The unit produces 115 MW of electricity. The capture system is capable of capturing up to 1 million tonnes of CO_2 each year, which is transported via pipeline to nearby oil fields for EOR and to the Aquistore site for injection into a deep saline formation.

The plant commenced operation in 2014 and achieved an 80% capture rate during early operation. As might be expected for a first-of-a-kind plant, SaskPower has experienced various issues with a number of subsystems (ZeroCO_2.NO, 2015). These are being dealt with, and the plant is again on track to produce its targeted commercial quantities of CO_2 for sale (ZeroCO2.NO, 2015).

3.0 PCO_2C BACKGROUND

The PCO_2C Program was started in 2008 to provide a platform to objectively test and compare CO_2 capture technologies at a small pilot scale. The technologies were targeted from all three of the capture platforms: precombustion, postcombustion, and oxygen-fired combustion. In addition, pretreatment of the flue gas to enable the capture technology to be more cost-effective and efficient was also studied.

During PCO_2C Phase I, one of the EERC's existing pilot-scale combustion units was retrofitted with a flexible absorption and stripping system to enable evaluation of the efficiency of several advanced and novel solvents. Baseline capture tests were performed using monoethanolamine (MEA). One of the EERC's combustion systems was retrofitted to have an oxygen-fired combustion capability. The system was tested for several weeks to identify issues that might prove challenging if oxygen firing was retrofitted to an existing coal-fired facility. Finally, economic and process models were developed for both the oxygen-fired and postcombustion systems using Aspen Plus® and Aspen Process Economic Analyzer (APEA) software packages. The results of the modeling efforts indicated that it was more expensive (on a

per-ton-CO_2 basis) to apply oxygen firing to an existing plant than to add solvent capture to the plant.

Phase II of the PCO_2C Program, which began in September 2010, moved promising technologies further toward demonstration and commercialization, with the ultimate goal being the development of lower-cost and more effective capture technologies and their integration into a system in order to provide substantial economic and environmental benefits. Using the results gained in Phase I, solvent technologies were investigated that might capture CO_2 at reduced cost and increased efficiency. An effort also was made to step away from more conventional solvents toward solid sorbents and other novel concepts, including a novel solvent contactor. Strategic studies investigated technology life cycles, balance-of-plant (BOP) issues, commercialization time scales, and by-product handling.

PCO_2C Phase III continued to build upon the successes of previous work performed at the EERC in order to provide a platform for further development of promising technologies toward demonstration and commercialization. The Phase III work effort focused on the evaluation of flue gas pretreatment technologies that can enhance the performance and reduce the cost of CO_2 capture systems. Postcombustion capture testing continued with two new solvents as well as tests during which partial capture was investigated. Precombustion capture testing using membranes was studied. The new solvent and membrane technologies were modeled using Aspen, and a technoeconomic assessment was made for each of the three approaches. Three power plants from the region were modeled using the Carnegie Mellon Integrated Environmental Control Model (IECM) to show the effects that the addition of capture would have on their net power production, water usage, and revenue requirements for various levels of capture. Finally, a portable Fourier transform infrared (FT-IR) spectrometer was used to monitor and evaluate the concentrations of flue gas constituents, including amine aerosol emissions.

The PCO_2C Program provided a small pilot-scale platform to demonstrate novel and improved CO_2 capture technologies. There was a strong emphasis on the integration of these technologies into the total systems such that substantial economic and environmental benefit could be derived. This type of information is important for utilities as they determine how to reduce their CO_2 emissions in a carbon-constrained world.

4.0 FLUE GAS PRETREATMENT FOR POSTCOMBUSTION CAPTURE

4.1 Introduction

The flue gas pretreatment task falls within the PCO_2C Phase III goal of assisting promising postcombustion CO_2 capture technologies as they move toward demonstration and commercialization. The removal of flue gas components such as SO_x, NO_x, or particulate that might reduce the efficiency or effectiveness of a postcombustion capture technology is crucial to improving the success of that particular technology. Two flue gas pretreatment technologies were studied during PCO_2C Phase III: an SO_2 removal process and a technology aimed at removing SO_x, NO_x, and particulate.

4.2 Cansolv SO_2 Capture Process

4.2.1 Introduction

PCO_2C worked with Cansolv Technologies Inc. (CTI) to test the operability of SO_2 solvents for flue gas pretreatment prior to CO_2 capture. Advanced solvents can be very sensitive to contaminant levels in the flue gas, with the levels of nitrogen oxides, sulfur dioxide, and particulate being of highest interest. CTI has developed several solvents for SO_2 pretreatment that may reduce NO_x levels as well. Two of these solvents are a benchmark solvent and a newly developed improved formulation.

The goal of this project was, therefore, to determine if the improved formulation has improved operability over the benchmark solvent for pilot-scale application. The objectives were to 1) modify the EERC's existing pilot-scale CO_2 capture system to remove SO_2 so as to simulate commercial-scale operation; 2) test the CTI solvents, noting important operability characteristics such as SO_2 removal efficiency and energy input for regeneration; and 3) compare the qualitative and quantitative observations during testing to assist in identifying the optimal solvent for full-scale operations.

4.2.2 Experimental Equipment and Methods

The existing dual-column, postcombustion CO_2 capture system at the EERC (Figure 4-1) was repurposed for use as an SO_2 capture system to simulate commercial-scale operations of solvent utilization. A test matrix was developed by CTI to best compare the solvents under several operating conditions of interest to CTI. Comparison of the heat input, HSS formation, and SO_2 removal capability results was then conducted by CTI. The EERC determined if differences in ease of use existed between the two solvent formulations. The latter analysis is the focus of this report.

4.2.2.1 Pilot-Scale Test System

The solvent-based capture system was originally designed for CO_2 capture. A process flow diagram (PFD) for the capture system is shown in Figure 4-2. As originally designed, it consisted of three columns: two absorber columns and one stripper (or regeneration) column. Each of these columns was constructed from sections of varying lengths bolted together to achieve the required total height for a given solvent. The packing in the columns, either stainless steel (SS) random packing or structured packing, enhanced the liquid–gas contact area and promoted better CO_2 absorption and regeneration. The columns were designed to handle 3.4–3.7 scmm (120–130 scfm) of flue gas generated by the EERC combustion systems, either the combustion test facility (CTF) or the particulate test combustor (PTC). The system was also equipped with a water wash column to minimize solvent entrainment in the exit gas stream. Brief descriptions of major equipment follow, with detailed information provided in Appendix A.

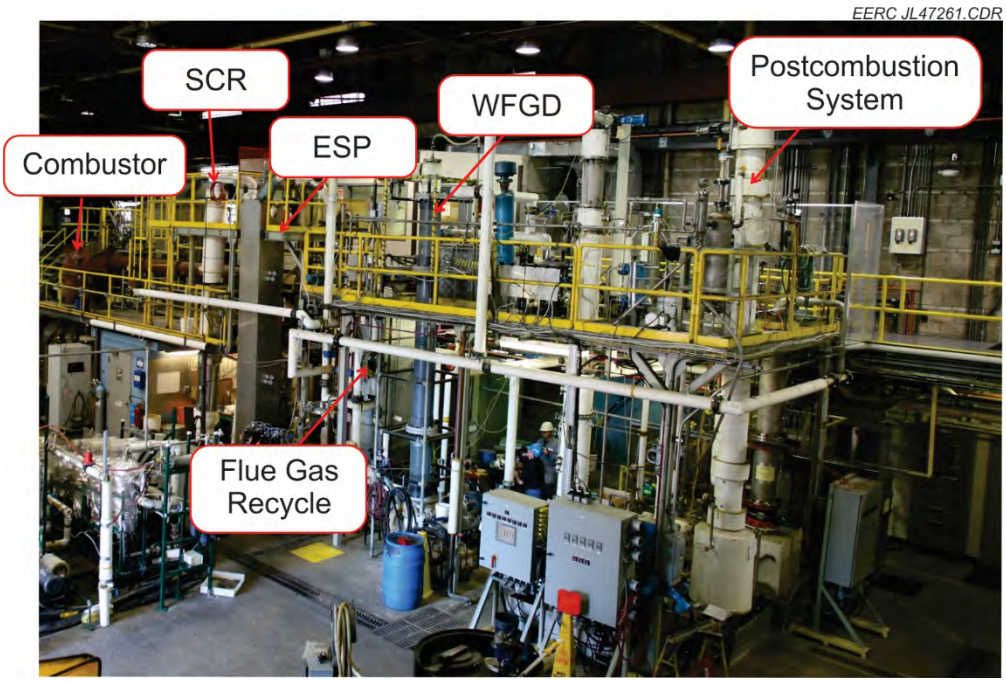

Figure 4-1. EERC pilot-scale system (SCR = selective catalytic reduction unit, ESP = electrostatic precipitator, WFGD = wet flue gas desulfurization).

4.2.2.1.1 Absorption Columns

The system featured two 25.4-cm (10-in.)-inside-diameter (i.d.) SS absorber columns. Each column is constructed of several flanged sections to allow flexibility in column height; for CTI testing, columns were configured for their maximum height of 6.40 m (21 ft) each. The absorbers treated the flue gas in series, with the gas flowing from the bottom to the top of each column, effectively doubling the total absorber packing height when compared to a single-column configuration. Total combined packing height for the two absorber columns was 7.62 m (25 ft). Each column has a series of thermocouples along its length. Both absorber columns also use a SS mesh demister in the top section to reduce solvent carryover with the flue gas.

The south, or "top," absorber column contained 3.66 m (12 ft) of Sulzer Mellapak-CC structured packing. This structured packing was installed in sections, each of which was supported by an expanded mesh base and topped with a liquid distribution plate to diminish wall effects. Although Figure 4-2 shows two heat exchanger sections in this absorber column, they were not used during the CTI testing.

The north, or "bottom," absorber column contained 0.91 m (3 ft) of the Sulzer structured packing, with the remaining column height filled with Koch–Glitsch IMTP 25 316L SS random packing, resulting in a total of 3.96 m (13 ft) of packing in the column. The "bottom" column used the same packing support and liquid distribution plate system as the other absorber column.

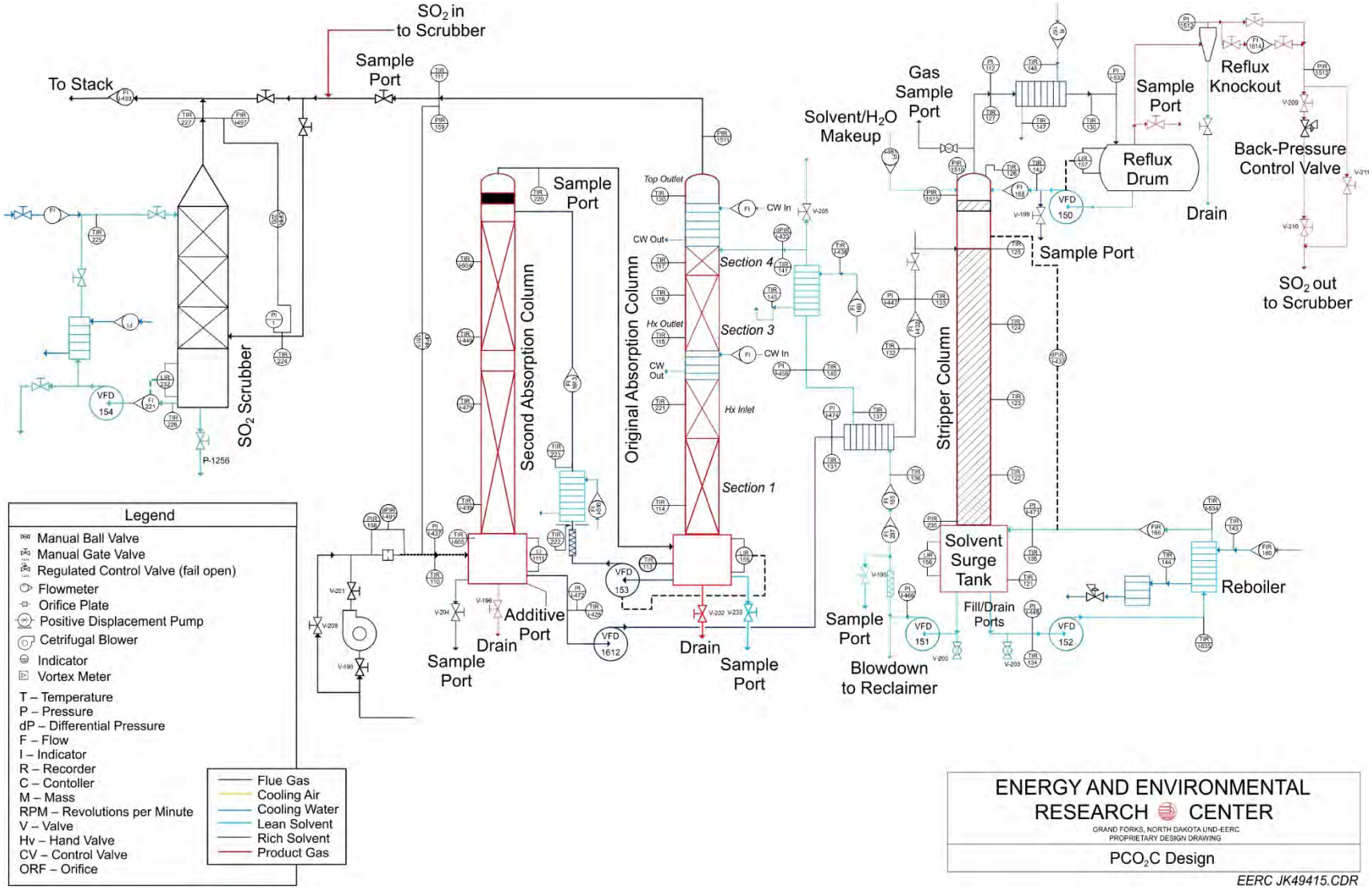

Figure 4-2. Solvent-based capture system PFD.

4.2.2.1.2 Stripper Column

The test system includes a single 6.40-m (21-ft), 10-in.-i.d. stripping column. The column has a series of thermocouples along its length. A piece of SS expanded mesh supported approximately 3.96 m (13 ft) of Koch–Glitsch IMTP 25 316L SS packing in the column. A custom-made liquid distribution plate rested on top of the packing below the rich solvent inlet. A demister was located inside the top section of the column. A back-pressure control valve was installed on the product gas line downstream of the reflux collection tank.

4.2.2.1.3 SO_2 Air Emission Control Equipment

An existing water wash column was repurposed for use as a scrubbing column to remove SO_2 from the total gas stream prior to venting to the atmosphere. For this test, an 8 wt% caustic NaOH solution was circulated through the column at a rate of approximately 113.6 L/hr (30 gal/hr), with pH levels maintained at approximately 6.0. This rate of neutralization allowed the test to meet the SO_2 emission limit for the EERC's test equipment. Typically, SO_2 emission levels were maintained below 200 ppm during the test campaign.

4.2.2.1.4 Solvent Heat Exchangers

The postcombustion capture system used two cross-flow heat exchangers. One served as the main heat exchanger between rich and lean solvent streams. The other was a smaller, secondary cooler for the lean solvent stream before it entered the absorber columns. Both heat exchangers were plate-and-frame style heat exchangers manufactured by Tranter, with all 316 SS wetted surfaces. The addition of 24 plates to the main heat exchanger between the lean and rich solvent streams expanded its heat-transfer surface area to 18.13 m^2 (195.2 ft^2). The secondary heat exchanger was used intermittently during testing to regulate temperature at the top of the absorber column.

The heat exchanger for regeneration energy input was a shell-and-tube heat exchanger manufactured by Weldon, Inc. The unit was operated with steam on the shell side and the process solvent on the tube side, with the streams flowing countercurrently. Wetted parts on the heat exchanger are 304L SS.

4.2.2.1.5 Solvent Pumps and Flowmeters

Magnetic-drive gear pumps were installed for rich and lean solvent streams. The gear pumps allowed for solvent flow rates down to 1.1 L/min (0.3 gpm). Each newly installed pump was pressure-restricted by a valve installed downstream of the pump, reducing the possibility of cavitation in the pump head. The pumps consisted of Liquiflow pump heads paired with Edelmann & Associates motors. The reboiler pump was a centrifugal pump manufactured by Magnatex and run by a ¾-hp motor.

Target solvent flow rates for the CTI test run were between 2.6 and 4.5 L/min (0.69 and 1.2 gpm). Magnetic flowmeters were installed to monitor rich solvent flow, intermediate rich solvent flow, and reboiler heater loop solvent flow. A Coriolis flowmeter measured the lean solvent stream from the stripper to the top absorber column.

Solvent filters were used upstream of the lean pump and both rich pumps. A fourth filter was in place downstream of the reboiler pump. The filters were 100-µm cotton-wound cartridge on a 304 SS perforated support. Filters, supplied by Nowata, were replaced between each test run.

4.2.2.1.6 Steam Flow and Regulation Equipment

Steam was provided by the University of North Dakota (UND) steam plant at approximately 130 psig. Steam pressure can be reduced with a sliding-gate pressure regulator, manufactured by Jordan Valve. A new vortex flowmeter, manufactured by Innova-Mass Sierra Instruments, Inc., was installed for CTI testing. A FlatPlate™ heat exchanger on the steam reboiler loop was water-cooled and used to ensure the steam was fully condensed before manual condensation collection measurements.

The steam control valve installed for the CTI test was manufactured by DFT, Inc., and operated with a pneumatically controlled valve positioner. A float-and-thermostatic steam SpiraxSarco trap was installed downstream of the reboiler heat exchangers. Downstream from the trap, on the condensate line, another pneumatically operated control valve was installed to restrict condensate flow and impart a back pressure on the steam heat exchanger. This control valve, manufactured by Badger Meter, Inc., was used exclusively to set steam flow rate during the test plan runs (detailed in the Solvent Testing section).

4.2.2.1.7 SO_2 Mass Flow Controller

SO_2 gas was metered with a mass flow controller (MFC) to maintain desired input rates. The MFC was manufactured by Brooks Instruments and factory-calibrated for SO_2 gas flow. A manifold connecting four SO_2 cylinders in parallel allowed flow to the MFC to be continuous, i.e., when one cylinder was depleted, flow was diverted to the next cylinder during replacement without discontinuing SO_2 supply to the absorber.

4.2.2.2 Solvent Testing

Testing was performed with natural gas-fired flue gas. During operation of the system, gas (both inlet flue gas composition and emission) and liquid samples were taken. Limited analyses were performed at the EERC on solvent samples, with emission gas samples and solvent samples sent to CTI for further analysis. The test plan derived by CTI is shown in Table 4-1.

4.2.2.2.1 Sampling and Analyses

4.2.2.2.1.1 Liquid Sampling

Liquid samples were taken about 3–7 times per test as designated by CTI. Samples were pulled in 60-mL vials. These samples included rich solvent, lean solvent, reflux, and water wash samples. The rich and lean solvents were analyzed by the EERC Analytical Research Laboratory (ARL) for pH, water content, amine solvent concentration, and sulfate/sulfite concentration. HSS formation was calculated from the results of these analyses.

Table 4-1. CTI Test Plan as Conducted (January 2014)

Test	Date and Time	Solvent Flow, L/min	Steam Flow, kg/hr	Notes
Benchmark Solvent				
1	Jan 16 12:02–14:08	2.6	45	Cold flow (air) emission measurement
2	Jan 19 18:00 – Jan 20 15:00	3.0	43	
3	Jan 20 15:00 – Jan 21 13:00	2.6	45	NG[1] emission measurement
4	Jan 21 13:00 – Jan 22 02:00	2.6	38	
5	Jan 22 02:00–16:00	3.0	52	
6	Jan 22 16:58–17:28	3.0	54	Baseline heat loss test
7	Jan 22 17:36–18:11	3.0	45	Baseline heat loss test
8	Jan 23 16:00 – Jan 24 04:00	3.4	50	
9	Jan 24 04:00–16:00	3.0	39	
10	Jan 24 16:00 – Jan 25 04:00	2.6	49	
11	Jan 25 04:00–12:00	3.0	43	Test 2 repeat
Improved Formulation				
1	Jan 25 19:14–19:29	3.0	52	Baseline heat loss test
2	Jan 25 19:39–19:58	3.0	44	Baseline heat loss test
3	Jan 25 21:00 – Jan 26 09:00	3.4	50	
4	Jan 26 09:00–21:00	3.0	52	
5	Jan 26 21:00 – Jan 27 09:00	3.0	43	
6	Jan 27 09:00–21:00	2.6	45	NG emission measurement
7	Jan 27 21:00 – Jan 28 09:00	3.0	43	
8	Jan 28 09:00–21:00	2.6	49	
9	Jan 28 21:00 – Jan 29 09:00	3.0	52	
10	Jan 29 09:00–21:00	3.4	Variable	Match SO_2 emissions of 194 ppm from benchmark
11	Jan 29 21:00 – Jan 30 09:00	3.0	Variable	Match SO_2 emissions of 142 ppm from benchmark
12	Jan 30 09:00–17:00	3.0	39	25% less steam than DS Test 5
13	Jan 30 17:00 – Jan 31 05:00	3.0	Variable	Match SO_2 emissions of 203 ppm from benchmark
14	Jan 31 05:00–09:00	3.0	39	
15	Jan 31 10:05–10:20	3.0	39	Baseline heat loss test, only airflow (no NG)
16	Jan 31 10:30–10:47	3.0	50	Baseline heat loss test, only airflow (no NG)
17	Jan 31 12:15–14:15	2.6	45	Air emission measurement

[1] Natural gas.

The **pH** was determined using a Fisher Scientific Accumet 950 pH/ion meter according to standard pH measurement method.

Water content was determined using an Aquamax Karl Fischer volumetric titration system. The system was calibrated daily, and at least three analyses were performed for each of the samples so as to obtain a reproducible average analytical result.

Sulfite and sulfate concentrations were determined using a Dionex ICS-3000 ion chromatography (IC) system. Analysis was performed using a method specified by CTI. The instrument was calibrated prior to the beginning of the test campaign. The calibration was verified each morning and at the end of the analytical day using a continuing calibration standard. Quality control checks (using a standard that was certified but from a different lot than the continuing calibration standard) were run between every four or five samples (or as frequently as the timing of required sampling results would allow). Blank samples were also run each day.

Amine concentrations were determined using a Mettler Toledo T50 titrator with LabX Light software. The analysis consisted of a standard acid–base titration that was run gravimetrically (rather than volumetrically) to meet CTI's request. The acid used to quantify the free amine was HCl, while NaOH was used to quantify the amine cations in solution. The total amine present was determined as the sum of the free amine and the amine cations. The calculations did not include corrections for weak acids or degradation products.

Reflux and water wash samples were shipped to CTI at CTI's request for analysis in its laboratory.

Table 4-2 provides a summary of the analyses performed on the solvent samples and location of the laboratory.

4.2.2.2.1.2 Online Analysis of SO_2 in the Flue Gas

The SO_2 concentration of the flue gas was measured using Ametek online gas analyzers located at various points in the system. These analyzers were zeroed and calibrated at least once every 24 hours.

4.2.2.2.1.3 Emission Measurement

Emission measurements were carried out during testing with both solvents under both airflow conditions and natural gas-firing conditions. Table 4-3 lists the measurement periods and conditions. During these tests, the furnace system blowers provided either air or natural gas-derived flue gas to the scrubbing system. Solvent flow was held steady, and heat input was introduced to the stripping column. Samples were extracted isokinetically (to ensure that they were representative) and sent to CTI for analysis. The measurements were modifications of NIOSH Method 2549, Volatile Organic Compounds, and NIOSH Method 3509, Aminoethanol Compounds II. Modifications to the method are described below. Figure 4-3 shows a schematic of the sampling train.

4.2.2.2.1.4 Condenser Sample

The condenser sample was collected, and the condenser and impinger bottles were rinsed with high-performance liquid chromatography (HPLC)-grade deionized (DI) water and added to the sample. Additional water was added to bring the total volume to 200 mL.

Table 4-2. Analytical Techniques Performed

Location/Analytical Technique	Laboratory
Rich Solvent	
pH	ARL
Karl Fischer Titration	ARL
Sulfites by IC	ARL
Lean Solvent	
pH	ARL
Karl Fischer Titration	ARL
Amine Concentration Using Acid–Base Titration	ARL
IC	ARL
Foaming and TSS[1]	CTI
Cation Analysis	CTI
Reflux	
pH	CTI
LC–MS[2] and GC–FID[3]	CTI
IC	CTI
Water Wash	
pH	CTI
LC–MS and GC–FID	CTI
IC	CTI
Treated Gas	
Adapted NIOSH[4] 3509 and 2549[5]	CTI
Feed Gas Quenched	
Gas Tube Sampling for NO and NO_2	CTI

[1] Total suspended solids.
[2] Liquid chromatography–mass spectrometry.
[3] Gas chromatography–flame ionization detection.
[4] National Institute for Occupational Safety and Health.
[5] See Emission Measurement section.

Table 4-3. Emission Measurement Times and Conditions*

Solvent Test	Date and Time	Solvent Flow, L/min	Steam Flow, kg/hr
Benchmark Test 1 – Air	Jan 16 12:08–14:08	2.6	45.0
Benchmark Test 3 – NG	Jan 21 10:46–12:46	2.6	45.0
Improved Formulation Test 6 – Air	Jan 27 12:20–14:20	2.6	45.3
Improved Formulation Test 17 – NG	Jan 31 12:15–14:15	2.6	45.3

* Tests included droplet collection, Method 2549, and Method 3509.

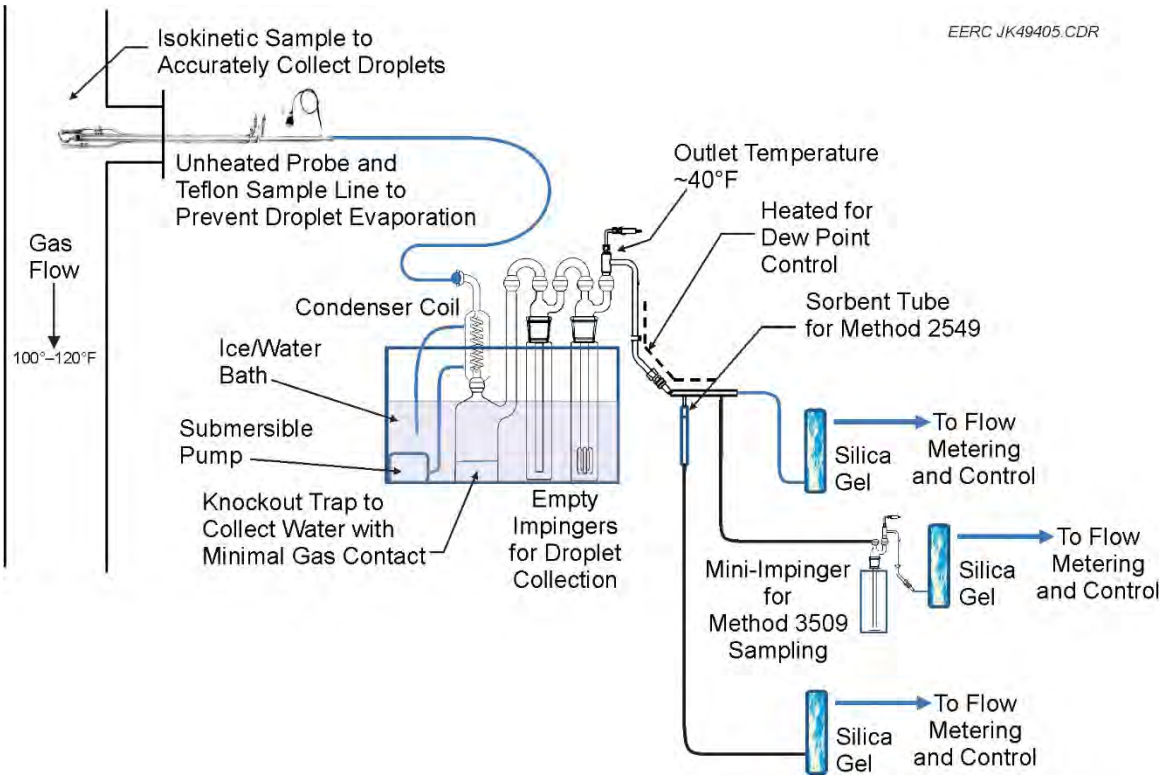

Figure 4-3. Schematic of the emission-sampling system.

4.2.2.2.1.5 NIOSH Method 2549

This method employs a multibed sorbent tube for sample collection. Figure 4-4 shows the actual sampling train and the location of the sorbent tube. A slipstream was taken of the sampled gas after droplet collection and was passed through the sorbent at a constant rate.

4.2.2.2.1.6 NIOSH Method 3509

This method was split into two separate sections. The section consisting of a condenser coil, knockout trap, and empty impingers was employed to capture any droplets and moisture in the sampled gas stream. Gas flow was then split to pull a sample to pass through a midget impinger of hexanesulfonic acid. Figure 4-5 shows the midget impinger. During actual sampling, the impinger is located inside the metal impinger box in the ice bath. Gas sampling was pulled at a steady rate through a gas-metering box. Isokinetic sampling was maintained for the upstream droplet capture portion of the sampling. Total sample size was 15 mL. If the sample did not contain that volume at the end of the test, then HPLC-grade DI water was added such that a volume of 15 mL was attained.

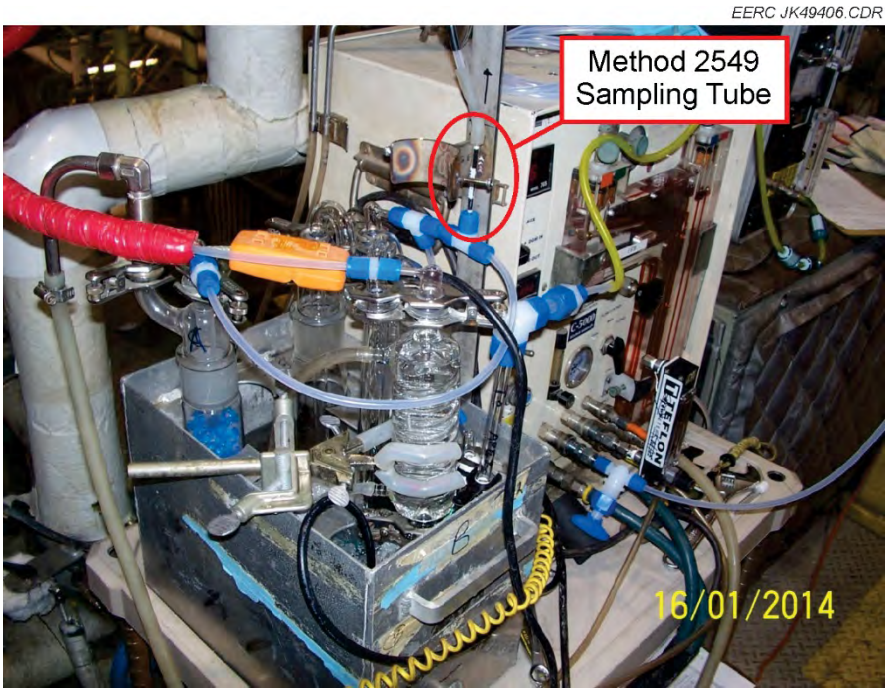

Figure 4-4. Photograph of the sampling train. The red oval shows the Method 2549 sampling tube.

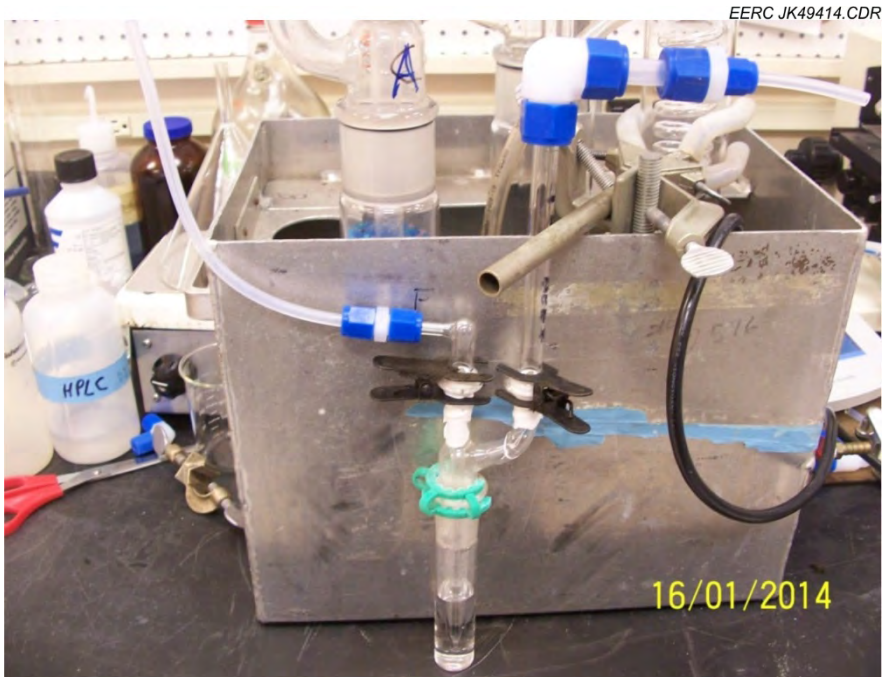

Figure 4-5. Photograph showing the midget impinger for Method 3509 sampling. During sampling, the impinger is located inside the metal box.

4.2.2.2.1.7 Sampling Data

Table 4-4 contains the data collected during the emission-sampling tests.

Table 4-4. Emission-Sampling Test Data

Sample	Test	Flue Gas Water Content, %	Actual Isokinetic Sampling, %	Total Gas Volume Sampled,* m^3
Condenser	Benchmark Test 1 – air	5	101.9	1.3380
	Benchmark Test 3 – NG	8.3	101.0	1.0984
	Improved Formulation Test 6 – air	7.9	100.6	1.1660
	Improved Formulation Test 17 – NG	4.1	99.8	1.2697
Method 2549	Benchmark Test 1 – air			0.0034
	Benchmark Test 3 – NG			0.0039
	Improved Formulation Test 6 – air			0.0039
	Improved Formulation Test 17 – NG			0.0037
Method 3509	Benchmark Test 1 – air			0.0963
	Benchmark Test 3 – NG			0.0998
	Improved Formulation Test 6 – air			0.1022
	Improved Formulation Test 17 – NG			0.1007

* Standard conditions at 68°F and 29.92 in. Hg.

4.2.3 Results and Discussion

4.2.3.1 Operational Challenges

The testing of the CTI SO_2 reduction technology at the EERC began September 30, 2013. Two solvents were evaluated utilizing the EERC repurposed dual-absorber, postcombustion pilot solvent-scrubbing system. The test plan originally called for 2 weeks of benchmark solvent evaluation, followed by a second 2-week test period evaluating the improved formulation. Several issues with the test equipment were identified during the first few days of testing.

4.2.3.2 Initial Resolutions

Minor issues with operation of the repurposed EERC system were identified during the initial utilization of the CTI SO_2 reduction technology. The flowmeter for the rich solvent flow line was not providing accurate readings for the flow rates used. The reflux pump was not usable in automatic mode, making level control problematic. In addition, steam control for regeneration energy input was not consistent. Once all issues had been mitigated, a shakedown of the system

was performed using the benchmark solvent. During this shakedown effort, there were difficulties maintaining constant pressure when using the stripper column alone. CTI, therefore, requested switching to a dual-absorber column configuration, as described in the Absorption Columns section.

A second attempt at completing the 2-week baseline tests was conducted November 12–16, 2013. During this testing, several solvent leaks and SO_2 product gas leaks were identified throughout the system. Most of these leaks were repairable during operation, but others required a full system shutdown to address, detailed in the following section.

4.2.3.3 Carbon Flange Corrosion

On the morning of November 16, a minor SO_2 gas leak was noted at the flanged connection on the outlet of the reflux drum. Tightening the flange did not eliminate the leak, so it was decided to address the issue following conclusion of the test. However, by the end of the day on November 16, a major SO_2 leak was discovered near the base of the stripper column (Figure 4-6) at the first flange on top of the stripper solvent surge tank. Testing ceased immediately.

The stripper column was built from SS pipe sections with welded-on 150-lb carbon steel slip-on flanges. Gaskets between the flanges were CGI gaskets with a 316L SS ring on the inside diameter. The absorber was built with laser-cut SS flanges rather than pressure-rated slip-on flanges. Because of this construction method, the surface area of the carbon steel flanges was exposed to the process gas and liquid during testing. These exposed surfaces corroded quickly (Figure 4-7). Each flange on the column showed signs of significant corrosion, and the bottom

Figure 4-6. Solvent leaks at the base of the stripper column.

Figure 4-7. Carbon flange corrosion.

flange where the major leak was detected was completely eroded through. The column was thus disassembled and the flanges removed.

New 316L SS weld-neck flanges were attached in their place, and the column was reassembled, retaining overall column height. The carbon steel slip-on flanges adjacent to the reflux drum were corroded as well and were nearing catastrophic failure. These were also replaced with 316L SS flanges.

4.2.3.4 Other System Improvements

While the stripper column was being rebuilt, other system improvements were performed for improved evaluation of the solvents. All SS pipe and pipe fittings on the product gas line upstream of the back-pressure control valve were replaced with SS tubing and compression fittings. This allowed any potential leaks to be addressed during the run without shutting down the system.

4.2.3.5 Solvent-Poisoning Issues

Testing resumed January 7, 2014, by filling the column surge tanks with the prescribed mix of water, solvent, and acid. Once added, the solvent was circulated through the system. Samples of the solvent were analyzed to determine whether the system inventory was within solvent specifications as prescribed by CTI. Flue gas was then brought online.

SO_2 delivery to the system was accomplished by spiking the natural gas-derived flue gas with bottled SO_2. As described previously, the SO_2 was metered from a manifold connecting four SO_2 cylinders in parallel.

By January 8, several issues were presented: a very high negative pressure was registered on both the absorber columns, SO_2 levels were unusually low at the stack, and the conditioner for the SO_2 analyzer at the stack was found to be off-line. It became apparent that gas flows to the absorber were not set up properly to test desired system conditions. Thus the unmonitored flue gas flowing through the absorber poisoned the solvent significantly by elevating the sulfite and sulfate levels in the solvent.

Draining solvent inventory and adding water, solvent, or a combination of the two, commonly referred to as a "bleed and feed" operation, was performed at 15:40 on January 10, 2014, reducing the total solvent inventory in the system. The goal of the bleed and feed was to reduce the loading level of the solvent by replacing a significant portion of the overloaded solvent with fresh solvent. Testing resumed, with analysis continuing to show high sulfite levels.

Another bleed and feed was performed on January 12, again reducing the system inventory. The system was shut down at the end of the day because of an SO_2 cylinder shortage caused by weather-related delays in delivery of replacement cylinders. The final sample before shutdown continued to show elevated levels of sulfite in the system, >12,000 ppm. The high sulfite levels led CTI to direct a restart with a fresh batch of solvent.

4.2.3.6 SO_2 Gas Cylinder Inventory

To maintain safety standards on the storage quantities and locations of SO_2 at the EERC testing facility, multiple deliveries of SO_2 cylinders were scheduled. One delivery scheduled for arrival January 10, 2014, was delayed by the supplier until January 17, which postponed the start of the benchmark test plan. A second delivery scheduled for January 21 was again delayed by the supplier until January 23. This led to a system shutdown January 22 18:15 – January 23 14:00, i.e., between benchmark Tests 7 and 8 in Table 4-1.

4.2.3.7 Modifications to Steam Metering

The downtime in testing while awaiting the first delayed shipment of SO_2 cylinders allowed the CTI team to take a more detailed look at test results thus far; the data and solvent performance were not meeting their expectations. An attempt was made to change the steam-metering method in order to increase the temperature differential between the steam in the reboiler and the solvent at the base of the column. In the previous tests conducted January 5–19, steam flow to the reboiler heat exchanger was controlled using both the steam control valve, located upstream of the heat exchanger, and the condensate control valve, which is downstream of the heat exchanger. The target flow rate was met by balancing the flow through these two valves. However, this method resulted in less heat input than was required for regenerating the solvent. Thus some tests were conducted with the condensate control valve completely open, providing the minimum amount of back pressure possible. This method led to mixed results, with good flow control at some levels and poor control at others.

On January 19, steam flow control was attempted through use of the condensate control valve exclusively, with the steam flow control valve upstream of the reboiler completely open. The new method, along with a higher steam input pressure, resulted in better-controlled higher heat input for the solvent regeneration. With the desired temperature difference between steam and solvent realized, successful tests with repeatable conditions could be performed.

4.2.3.8 Weather-Related Issues

Colder-than-average outdoor temperatures, down to −34°C (−30°F), at the EERC facility in Grand Forks, North Dakota, affected any equipment exposed to the ambient air. Slight temperature drops were apparent in the system when the pilot facility's overhead door was opened for any length of time, and both the flue gas stack and the outlet analyzer exhaust experienced icing because of the extremely cold outside temperatures.

Stack icing led to issues with flue gas flow and combustor pressure. Once identified, the stack ice was removed every few hours by an operator physically striking the stack pipe with a hammer. The periodic physical removal was sufficient to keep the system running properly.

Icing problems also affected the absorber outlet gas analyzer. Reported analyzer values were checked periodically against an adjacent gas analyzer. The values were not in agreement for much of the test, but value offsets between the two analyzers were consistent, leading to correctable data output. On January 23 during morning analyzer maintenance (between benchmark Tests 7 and 8), the issue was determined to be a result of analyzer exhaust port icing. The exhaust line was then rerouted to prevent further icing, and the reported values between the two analyzers were in agreement.

4.2.3.9 Control Program Disruptions

Starting January 5, the system operated without disruption for nearly 1 month. On January 24 at 10:10 (during benchmark Test 9), an event was noted where all temperature displays on the LabVIEW interface briefly flashed a "0" value and then returned to process conditions. At the same time, PID (proportional integral derivative) loops on pumps were reset, leading to flow excursions. This program anomaly happened again on January 27 at 06:05 (during improved formulation Test 5), resulting in nearly 2 hours of lost time while the system was recovered. The program was also restarted on January 28 at 13:48 (during improved formulation Test 8) to reset the shared variable library. This effort appeared to correct the problem, as no further system anomalies were observed.

4.2.3.10 Successful Testing Campaign

4.2.3.10.1 Operations and Schedule

Solvent inventory was drained completely January 13 in preparation to begin the full test campaign. The system was flushed with DI water, and all solvent filters were replaced before the new solvent batch was added. The new batch was circulated through the system for several hours before shutting down to await delivery of SO_2 cylinders that arrived January 17, as mentioned previously in the SO_2 Gas Cylinder Inventory section.

Cold-flow emission sampling was performed on January 16, using air rather than natural gas-derived flue gas for gas flow through the absorbers (benchmark Test 1). No SO_2 was added during this emission test. The emission test lasted approximately 2 hr. Solvent testing on natural gas-derived flue gas resumed following delivery of the SO_2 cylinders.

The test campaign was scheduled to end on January 31. Therefore, the test points were restricted to ~12-hr runs. The benchmark solvent was evaluated January 19–25. Ten test points were conducted with this solvent (benchmark Tests 2–11), with benchmark Test 11 a repeat test of benchmark Test 2.

The benchmark solvent was drained from the system on January 25 after final samples were collected. The system was charged with DI water and then drained again. All solvent filters were replaced, and the improved formulation was mixed and added to the system. The solvent was circulated for several hours to allow the components to fully mix.

The improved formulation test points were also run for ~12-hr periods. Testing was conducted mostly under the same conditions as the benchmark solvent (improved formulation Tests 1–9 and 14–17). Four additional tests were performed to identify conditions using the improved formulation that would match the SO_2 emission rates from chosen benchmark tests (improved formulation Tests 10–13).

Pump flow and regeneration energy test conditions were varied throughout the campaign to evaluate desired system conditions. Other test conditions remained constant, including flue gas inlet composition (specifically SO_2 level), temperature, and flow rate. These were typically 12,000-ppm SO_2 at the absorber inlet, with flue gas flow into the absorber at 120 scfm and 43.3°C (110°F) inlet gas temperature.

At least one set of solvent samples, including lean and rich solvents, was collected for each test set point. The select solvent sample analysis was performed daily by the ARL. Analysis results were used to determine necessary solvent changes before continuing testing, such as removing water from the reflux tank, adding acid to the solvent mix, or performing a bleed and feed.

4.2.3.10.2 Operability and Comparison of Solvents

The operability of the pilot-scale system was not noticeably different when the benchmark solvent was tested than when the improved formulation was tested. The improved formulation mixture tended to foam when circulated in the capture system because of one of its components, which could pose an operability issue. However, the addition of an antifoaming agent during the testing showed that it could be easily remedied.

4.2.4 Conclusions

Both solvents were equally easy to run in the pilot-scale system. To prevent any challenges that might be caused by foaming of the improved formulation, it should always be employed with an antifoaming agent. The testing conducted at the EERC indicated that the decision of which solvent to use should be made based on the effectiveness of the SO_2 removal from the flue gas

stream as well as the energy input required for solvent regeneration rather than on solvent operability.

4.3 Tri-Mer Flue Gas Filtration Technology

4.3.1 Introduction

The Tri-Mer flue gas filtration technology (Tri-Mer), developed by the Tri-Mer Corporation, combines particulate, NO_x, and SO_2 control. Its application as a pretreatment for postcombustion CO_2 capture was evaluated during testing at the EERC.

4.3.2 Experimental Equipment and Methods

Three pilot-scale test series were performed to evaluate the Tri-Mer combined particulate, NO_x, and SO_2 filtration technology. Test Series 1 was performed August 20–22, 2014, Test Series 2 was performed April 30 – May 2, 2015, and Test Series 3 was performed July 23–24, 2015. All tests were performed on a flue gas produced by combustion of a North Dakota lignite. In each test series, NO_x control was achieved using ammonia injection and SO_2 control was achieved by injection of dry sorbent. Two dry sorbents were evaluated during the testing. Both ash particulates and sulfated sorbent material were removed from the flue gas stream by the Tri-Mer filter vessel.

4.3.2.1 Experimental Configuration

A diagram of the pilot-scale equipment configuration used for testing is shown in Figure 4-8. Flue gas is produced by the pilot-scale CTF and the PTC. The flows are combined to provide the required flue gas volume. Gas analysis of the combined flow is performed before the point where ammonia and sorbent are injected. The gas stream then passes through the residence chamber to allow increased time for the sorbent and ammonia to react. After the residence chamber, the gas flow is split and enters the two chambers of the filter vessel. It should be noted that orifices measuring the gas flow through each filter chamber were installed upstream of the filter vessel during Test Series 1 and 2. Because of plugging by particulate and sorbent, the orifices were moved downstream of the filter vessel for Test Series 3. Downstream of the filter vessel, the gas streams from the two filter vessel chambers are recombined. The combined gas stream is analyzed before it exits to an induced draft (ID) fan and to the stack.

4.3.2.1.1 Furnaces

The pilot-scale CTF and PTC are functionally equivalent furnace systems, with a nominal feed rate of 34 kg/hr (75 lb/hr) of pulverized coal (pc) and a nominal thermal output capacity of 161 kW (550,000 Btu/hr). Flue gas for the experiments was provided by the CTF and PTC firing a North Dakota lignite. To achieve the required flue gas volume, the two furnaces were operated simultaneously, with the flue gas produced by the two units combined before being routed to the downstream systems.

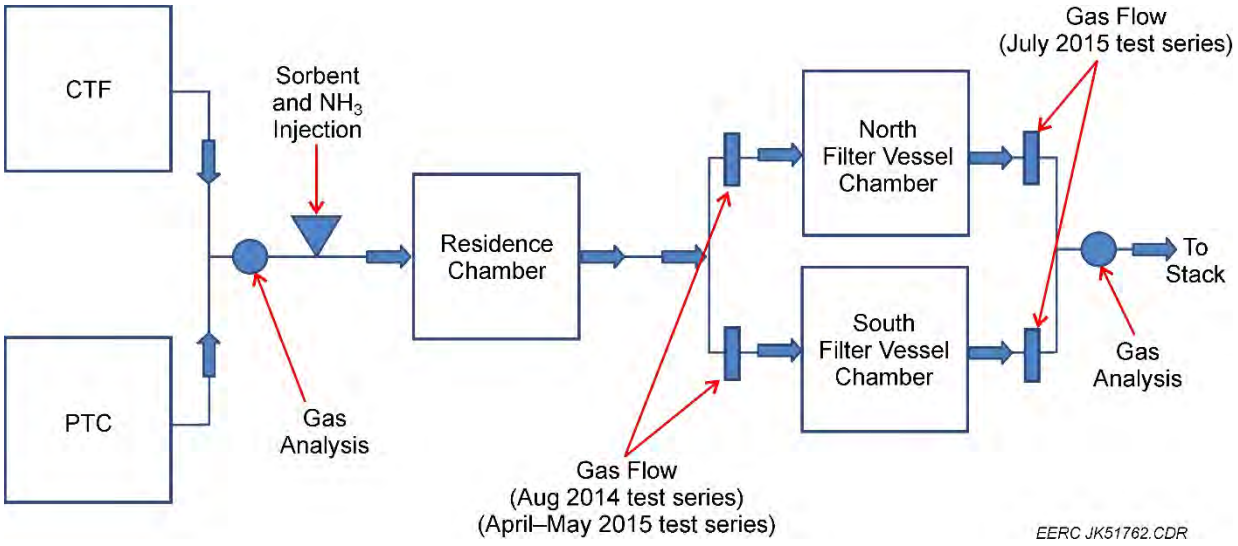

Figure 4-8. Schematic of plant configuration.

4.3.2.1.2 Residence Chamber

The residence chamber was fabricated by Tri-Mer and is designed to increase residence time to allow reaction of the SO_2 with the sorbent and NO_x with ammonia prior to the flue gas entering the filter vessel. The chamber provides an additional gas path of approximately 7.6 m (25 ft) of insulated 0.1-m (4-in.) pipe, corresponding to a residence time of approximately 0.65 s. The nominal chamber inlet temperature was between 316° and 371°C (600° and 700°F).

4.3.2.1.3 Filter Vessel

The filter vessel was fabricated by Tri-Mer and is a pilot-scale version of commercial units manufactured by the company. It consists of two filter chambers in parallel, with four ceramic candle filters in each chamber. The chambers are referenced subsequently as South or S chamber and North or N chamber. Flue gas flow enters each chamber at the bottom and exits at the top, with a decrease in temperature from bottom to top. Temperatures are reported bottom, middle, and top of each chamber. The average of the two chamber middle temperatures is taken as the representative temperature for each test.

4.3.2.2 Gas Analysis

The concentrations of O_2, CO, CO_2, SO_2, and NO_x were measured for the combined flue gas stream upstream of the ammonia and sorbent injection point. These gases were also measured downstream of the filter vessel after the gas streams from the two filter vessel chambers had been recombined. These inlet and outlet gas analyses were used to determine the NO_x and SO_2 removal efficiencies for the tests.

The downstream combined gas stream was also sampled for ammonia using a FT-IR spectroscopy gas analyzer to determine the concentration of ammonia exiting the filter vessel

(ammonia slip). These measurements were made at the downstream gas analysis location with a separate instrument and did not occur over the full time period of each individual test.

4.3.2.3 Particulate Analysis

Extractive particulate sampling was performed during Test Series 1 and 2 using EPA Method 5 sampling protocol. The sampling was performed on the combined flue gas streams at the gas analysis locations.

4.3.2.4 Ammonia and Sorbent Injection

Ammonia gas was metered into the flue gas stream at the indicated injection location. Dry sorbent was introduced using a screw feeder at the same location. Two dry sorbents, Sorbacal® SP and Sorbacal SPS, were evaluated during the testing. Both are a high-calcium hydrated lime.

4.3.3 Results and Discussion

4.3.3.1 Test Series 1

Test Series 1 was performed August 20–22, 2014. The planned testing consisted of seven tests, with ammonia and sorbent injection varied to achieve specific levels of NO_x and SO_2 removal as given in Table 4-5. Achieving the planned gas temperatures in the filter vessel was immediately found to be difficult. As a result, the gas temperatures during the testing were lower than desired.

Table 4-5. Planned Test Conditions for Test Series 1

Test	Target SO_2 Removal, %	Target NO_x Removal, %
1	50	50
2	60	60
3	70	70
4	80	80
5	90	90
6	95	95
7	98	95

SO_2 and NO_x inlet concentrations remained relatively stable during the individual tests. Generally, NO_x remained more stable than SO_2. However, the outlet concentrations exhibited large fluctuations, with NO_x being less variable than SO_2. The instability of the outlet gas concentrations was the result of the need to pulse the filter vessel filters and variation in the sorbent and ammonia injection rates. It proved to be extremely difficult to adjust the injection rates to achieve the desired removal rates, resulting in alternate overshooting and undershooting of removal rate. Perceived changes in measured flow rate because of material buildup on the orifice plates also contributed to the difficulty of determining the desired injection rates. These variations in the data also made it difficult to identify steady-state periods that could be used to quantify levels of NO_x and SO_2 for the individual test periods.

The most stable (or least unstable) period for each individual test was identified, and average values of the operating parameters and removals were determined. The results are given in Table 4-6.

Table 4-6. Operating Conditions and Results for Test Series 1

Test:		1	2	3	4	5	6	7
Date	mm/dd/yy	8/20/14	8/20/14	8/21/14	8/21/14	8/21/14	8/22/14	8/22/14
Test Start	hh:mm	12:01	14:45	9:30	12:15	14:33	9:30	12:24
Test End	hh:mm	14:44	17:05	11:30	14:15	16:51	12:00	14:33
Test Time	hh:mm	2:43	2:20	2:00	2:00	2:18	2:30	2:09
Stable Period Start	hh:mm	13:09	16:09	10:33	13:46	16:06	10:31	13:12
Stable Period End	hh:mm	14:02	17:00	10:55	14:06	16:48	11:25	14:15
Stable Period Time	hh:mm	0:53	0:51	0:21	0:20	0:41	0:53	1:03
Target SO_2 Removal	%	50	60	70	80	90	95	98
Target NO_x Removal	%	50	60	70	80	90	95	95
Sorbent		SP	SP	SP	SP	SP	SP	SP
Average Mid	°C	272	276	271	279	277	265	274
Average dP	kPa	1.59	1.59	1.71	1.89	1.87	1.79	1.84
S Top	°C	251	254	243	257	253	239	251
S Middle	°C	271	275	268	278	276	264	274
S Bottom	°C	274	276	273	281	279	268	276
S Chamber dP	kPa	1.54	1.57	1.77	1.89	1.77	1.79	1.82
N Top	°C	251	255	246	257	254	241	253
N Middle	°C	273	277	273	279	277	266	275
N Bottom	°C	276	278	276	283	281	269	278
N Chamber dP	kPa	1.67	1.62	1.67	1.89	1.97	1.79	1.89
South Flow	scmm	2.89	2.77	2.91	2.77	2.86	2.88	2.78
North Flow	scmm	2.85	2.75	2.9	2.83	2.89	2.91	2.84
Total Flow	scmm	5.74	5.52	5.81	5.61	5.74	5.79	5.62
O_2 Inlet	%	4.02	4.20	3.77	3.86	4.27	3.60	3.61
O_2 Outlet	%	4.60	4.75	4.61	4.51	5.10	4.63	4.64
DSI[1]	kg/hr	1.30	1.50	1.70	2.57	1.05	2.66	3.30
DSI	kg/Macm	3784	4549	4924	7632	3057	7666	9787
DSI	kg/kg-SO_2	2.06	2.17	2.28	3.51	1.52	3.78	4.41
SO_2 Inlet	ppm	692.6	791.4	816.3	821.0	760.9	764.8	837.7
SO_2 Outlet	ppm	359.1	380.5	240.3	159.7	388.1	148.9	97.2
SO_2 Capture	%	48.12	51.99	70.57	80.56	49.01	80.53	88.40
NO_x Inlet	ppm	370.4	417.6	433.5	453.2	435.0	389.1	466.0
NO_x Outlet	ppm	178.6	167.0	141.2	93.5	452.5	113.3	110.9
NO_x Capture	%	51.81	60.15	67.42	79.39	NA	70.84	76.24
NH_3	L/min	0.93	1.13	1.55	1.79	0.00	0.93	0.93
NH_3 Inj, Rate	kg/Macm	114.7	146.2	190.5	226.8	0.00	113.7	117.1
Molar Ratio	NH_3/NO_x	0.44	0.49	0.62	0.71	0.00	0.41	0.35
NH_3 Ratio	kg NH_3/ kg NO_x	0.25	0.28	0.35	0.40	0.00	0.23	0.20
Outlet NH_3	ppm (dry)	NA[2]	NA	NA	NA	NA	NA	NA

[1] Direct sorbent injection.
[2] Not applicable.

Test 5 appears to be anomalous in that the SO_2 capture is high for the amount of sorbent injected, and there was no ammonia injection and consequently no NO_x removal. For this reason, it has been excluded from the discussion of the test results.

No measurements of NH_3 slip were reported for the tests.

4.3.3.1.1 Average Stable Period Test Conditions

The average stable period temperatures, differential pressures, and flue gas flows were fairly constant during the tests. Figures 4-9–4-11 show these conditions. Inlet oxygen, SO_2, and NO_x concentration remained relatively constant as well, as shown in Figures 4-12 and 4-13.

The stable period average middle chamber temperature remained between 265° and 277°C (509° and 530°F) for the tests. The average differential pressure showed a slight increasing trend as the tests progressed. This may be the result of particulate plugging of pressure taps along with conditioning of the new ceramic filters. The total flue gas flow remained between 5.5 and 5.8 scmm (195 and 205 scfm) over the tests and remained nearly equally divided between the two filter vessel chambers.

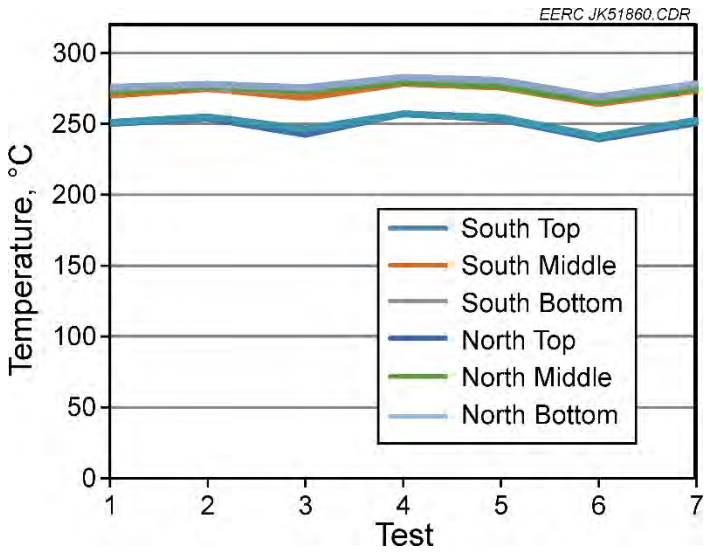

Figure 4-9. Average stable period temperatures for Test Series 1.

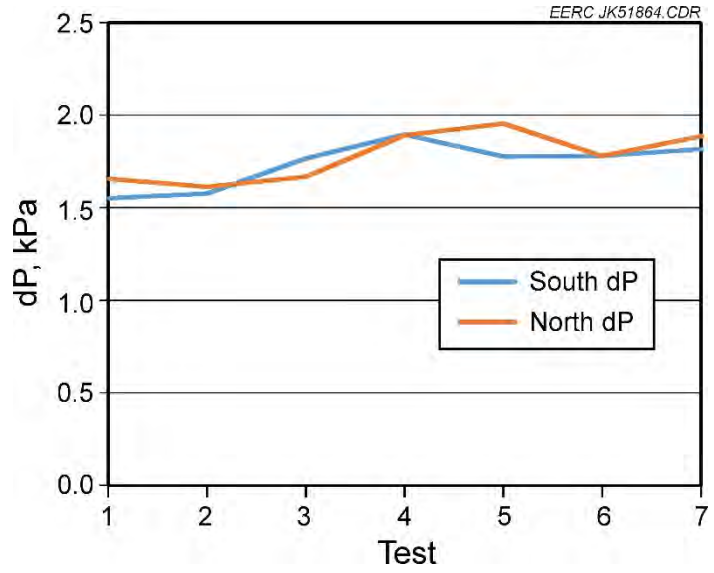

Figure 4-10. Average stable period differential pressures for Test Series 1.

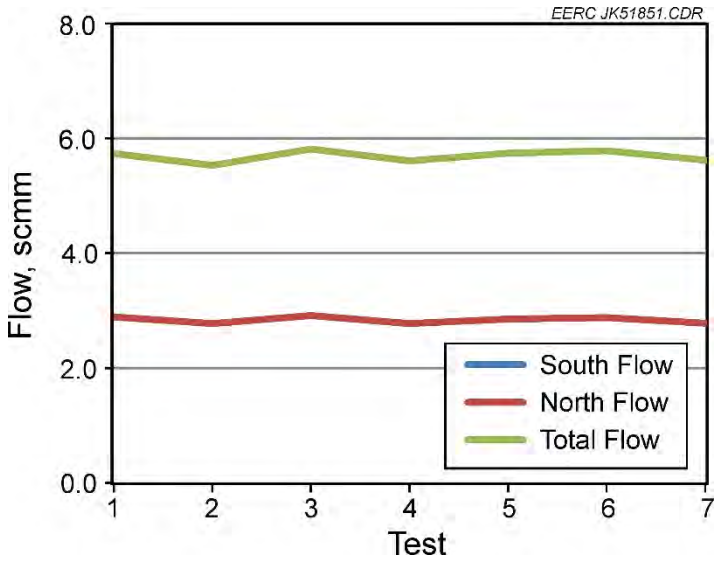

Figure 4-11. Average stable period flow rates for Test Series 1.

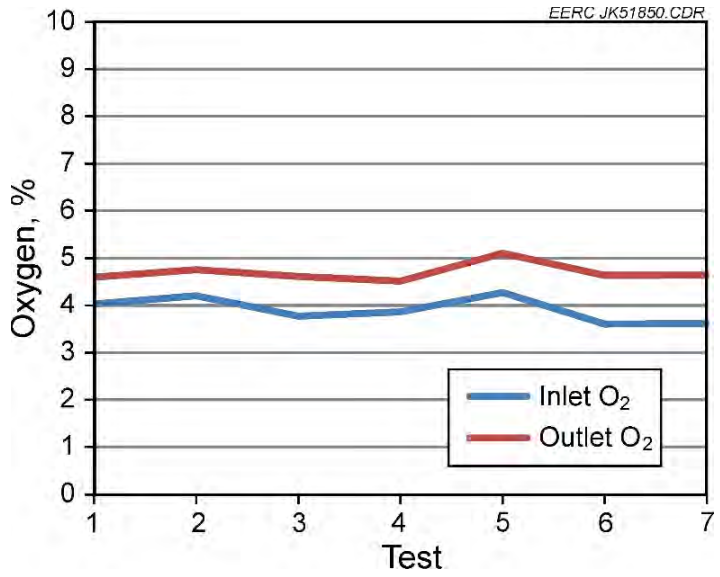

Figure 4-12. Average stable period inlet oxygen concentrations for Test Series 1.

4.3.3.1.2 SO_2 and NO_x Removal

The test plan had targeted specific SO_2 removals of between 50% and 98% and NO_x removals of between 50% and 95% for the individual tests. Figures 4-14 and 4-15 give a comparison of the target removal for each test versus the actual average stable period removals. It should be noted that Test 5 is not included because of its anomalous results. There was good agreement between the target and actual SO_2 removals during Tests 1–4, achieving up to 80% removal. Test 7 was able to reach 90% removal, but not the desired 95% removal. Tests 1–4 also showed good agreement with the target NO_x removals. However, Tests 6 and 7 appear to have been run at lower NH_3 injection rates than the previous four tests. Despite this, the removals were still 70% and 76%, respectively, but did not achieve the 90%–95% NO_x removal targets.

Figure 4-16 shows SO_2 average stable period removal plotted versus lb sorbent injected/lb SO_2 in the inlet flue gas. The removal from 50% to 90% shows an approximately linear trend with the sorbent/SO_2 ratio, although it may flatten out as SO_2 removal rises above 90%. A similar graph of NO_x removal versus the molar ratio of NH_3 injected/NO_x in the inlet gas stream can be found in Figure 4-17. Four points, corresponding to Tests 1–4, also show a linear trend between 50% and 80% NO_x removal. The other two points, corresponding to Tests 6 and 7, show anomalous behavior, with high NO_x removal at a low NH_3/NO_x molar ratio. This may be the result of a "memory effect" of ammonia adsorbed on sorbent accumulating in the inlet ducting.

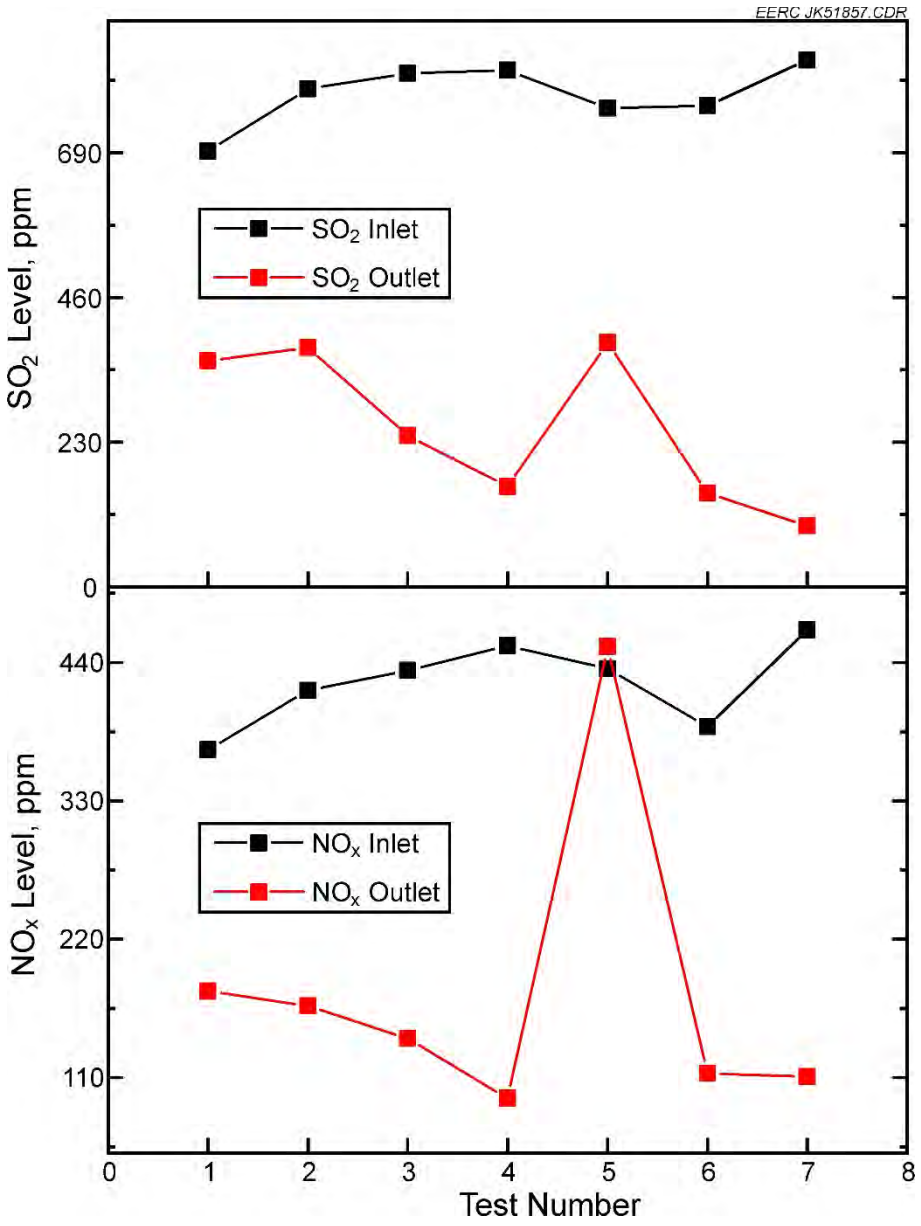

Figure 4-13. Average stable period inlet and outlet SO_2 and NO_x concentrations for Test Series 1.

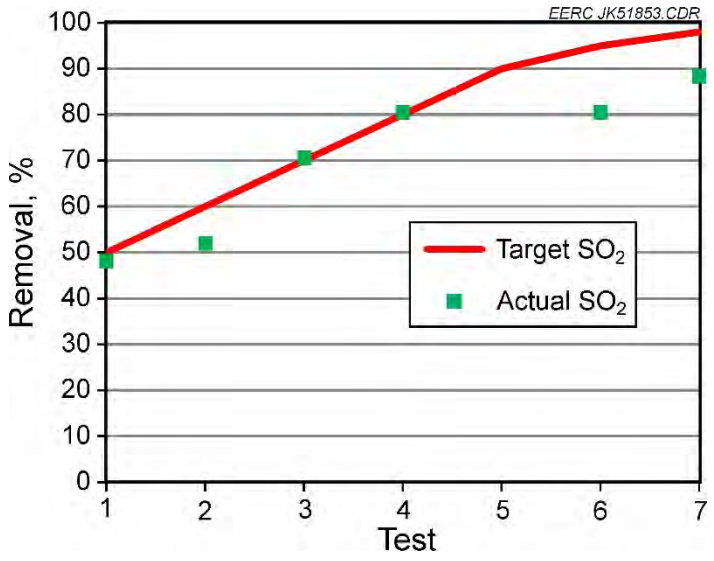

Figure 4-14. Target and actual stable period SO_2 removals for Test Series 1.

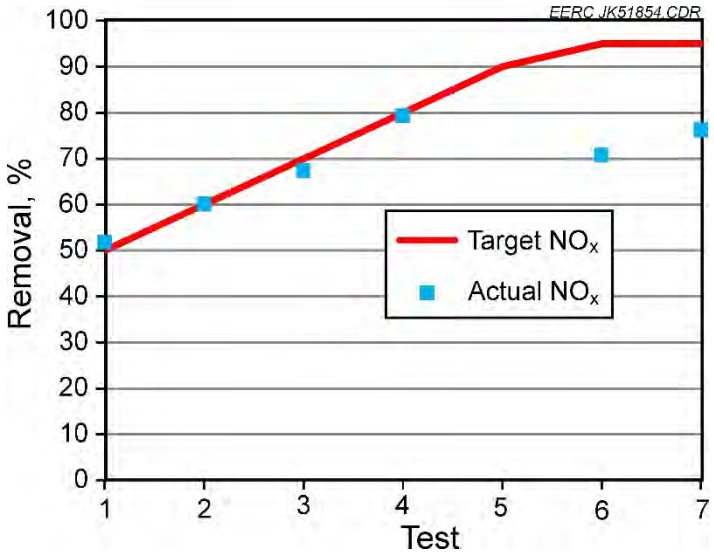

Figure 4-15. Target and actual stable period NO_x removals for Test Series 1.

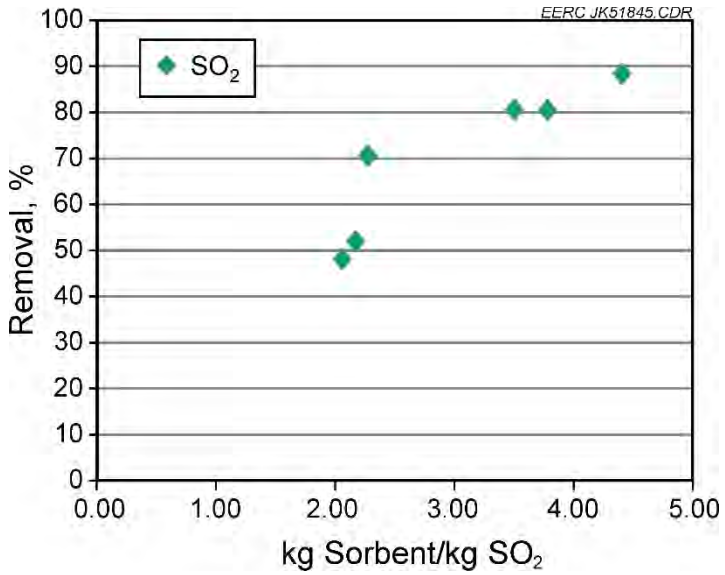

Figure 4-16. SO_2 removal versus lb sorbent injected/lb SO_2 in the inlet gas stream for Test Series 1.

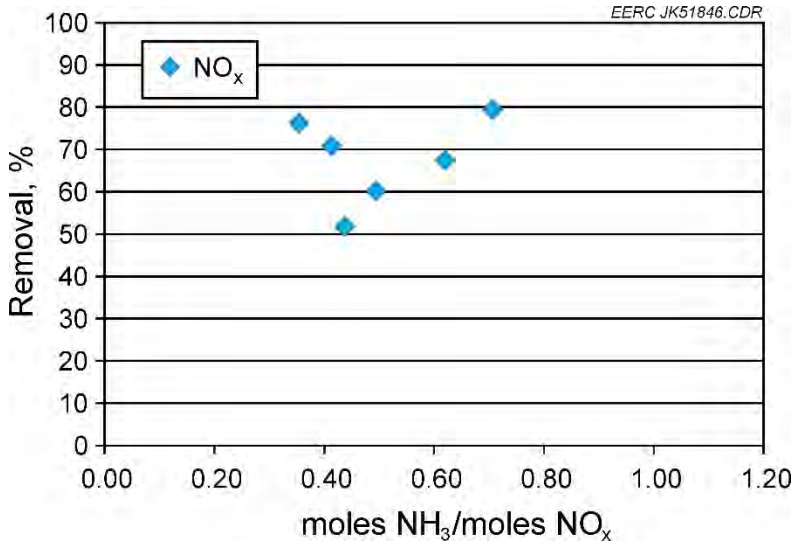

Figure 4-17. NO_x removal versus NH_3/NO_x molar ratio for Test Series 1.

4.3.3.1.3 EPA Method 5 Particulate Sampling

Method 5 sampling was performed at the inlet and outlet ports. Pitot measurements were first made to determine the isokinetic flue gas-sampling rate. Both pitot measurements and Method 5 sampling were performed with the respective probes at the center line of the duct. Sampling was performed for 120 min. At the completion of sampling, the filter assembly was disassembled and the dust collected on the filter recovered and carefully weighed. The sampling tests were performed nearly isokinetically, 106.7% at the inlet port and 105.6% at the outlet port. Other sampling parameters were also consistent. Table 4-7 provides sampling conditions, sampling times, and amounts of particulate collected.

Table 4-7. EPA Method 5 Particulate-Sampling Results for Test Series 1

Location:	**Inlet**	**Outlet**
Test Date	8/21/2014	8/21/2014
Start Time, hr:min	14:33	14:35
End Time, hr:min	16:33	16:35
Duration, min	2:00	2:00
Barometric Pressure, kPa	97.3	97.3
Stack Temperature, °C	374	221
Stack Pressure, kPa	−2.36	−2.36
dP Pitot, Pa	67.2	846
Nozzle Diameter, cm	0.64	0.38
Dry Sample Volume, scm	1.25	1.76
Total Sample Volume, scm	1.46	2.04
Flue Gas H_2O, %	14.30	13.90
Isokinetic, %	106.7	105.6
Filter, g	6.2662	0.01013
Total Dust, g	6.2662	0.01013
Dust Loading, grains/scf	2.1904	0.0025
Dust Loading, g/scm	5.0116	0.0058
Particulate Removal, %		99.88

The Method 5 sampling was performed August 21, 2014, beginning at 14:33 and ending at 16:35, during Tests 4 and 5. Sampling began at 14:33 and ended at 16:33 at the inlet and from 14:35 to 16:35 at the outlet for a sampling duration of 120 min. The sampling was nearly isokinetic, with 6.2662 g of dust collected at the inlet, corresponding to 5.0116 g/scm (2.1904 grains/dry scf). At the outlet, 0.01013 g of dust was collected, corresponding to a dust loading of 0.0058 g/scm (0.0025 grains/dry scf). Based on the Method 5 sampling, the particulate collection efficiency across the filter vessel was 99.88%. It should be noted that the actual collection efficiency would be higher if the injected sorbent particulate loading (not measured by the inlet Method 5 sampling) removed by the filter vessel was taken into account.

4.3.3.1.4 Summary of Test Series 1

The average stable period temperatures, differential pressures, and flue gas flows were fairly constant during the tests. Inlet oxygen, SO_2, and NO_x concentration remained relatively constant as well. However, outlet concentrations exhibited significant fluctuation. NO_x showed less fluctuation than SO_2. The outlet gas concentration instability was the result of trying to achieve the targeted removals by pulsing the filter vessel filters and varying the sorbent and ammonia injection rates. There was good agreement between the target and actual SO_2 removals up to 80% removal. The testing was able to reach 90% removal, but not the desired 95% removal. Target NO_x removals were achieved up to 80% removal, but testing could not achieve the 90%–95% NO_x removal targets. Extractive particulate sampling indicated the particulate collection efficiency across the filter vessel was 99.88%. The testing also provided experience used to improve operation in the test series conducted later.

4.3.3.2 Test Series 2

Test Series 2 was performed April 30 – May 2, 2015. The series consisted of 20 tests with ammonia and sorbent injection fixed and the NO_x and SO_2 removals monitored. The test plan is given in Table 4-8. The test series was conducted at three target filter vessel temperatures 177°, 232°, and 288°C (350°, 450°, and 550°F) and with two sorbents (SP and SPS). In this test series, the sorbent and ammonia injection rates were selected for a desired sorbent/inlet SO_2 ratio and NH_3/inlet NO_x ratio and then kept fixed, rather than attempting to achieve specific removal rates. This improved the stability of the tests. The SO_2 and NO_x inlet concentrations remained relatively stable during the individual tests. Generally, NO_x remained more stable than SO_2. The outlet concentrations exhibited fluctuation, with NO_x showing less fluctuation than the SO_2, although they were more stable than in Test Series 1. It should be noted that the measured gas flows were very erratic because of deposits forming on the flow orifices. For this reason, no individual chamber flows are given, and a constant value is assumed for the average flow over the entire Test Series 2. As a consequence, there is an increased uncertainty in the values of SO_2 and NO_x removal since their mass is calculated using the flue gas flow.

The stable period for each individual test was identified and average values for the operating parameters and removals determined. The results are given in Table 4-9. Measurements of outlet NH_3 (NH_3 slip) are reported for all but one of the tests. It should be noted that the outlet NH_3 measurements do not necessarily correspond to the stable periods that are averaged, since the measurements were performed over only a part of each test period.

4.3.3.2.1 Average Stable Period Test Conditions

Figure 4-18 shows the target temperature desired for the tests along with the actual average of the middle temperature of the two chambers. The tests with a target 232°C (450°F) temperature were slightly higher, from 240° to 248°C (465° to 478°F). For the 288°C (550°F) target temperature, the actual temperatures were slightly lower, from 277° to 287°C (531° to 549°F). Actual temperatures were higher, from 200° to 206°C (392° to 403°F) for the tests with a target temperature of 177°C (350°F).

Table 4-8. Planned Test Conditions for Test Series 2

Test	Target Filter Vessel Temperature, °C	Sorbent	Target Sorbent Feed, kg sorbent/kg inlet SO_2	Target Ammonia Feed, kg NH_3/kg inlet NO_x
1	232	SP	2	0.60
2	232	SP	3	0.60
3	232	SP	4	0.70
4	232	SPS	5	0.70
5	232	SPS	3	0.80
6	232	SPS	4	0.90
7	288	SP	2	0.60
8	288	SP	3	0.60
9	288	SP	4	0.70
10	288	SP	5	0.70
11	288	SPS	3	0.80
12	288	SPS	4	0.90
13	288	SPS	5	0.95
14	177	SP	2	0.60
15	177	SP	3	0.60
16	177	SP	4	0.70
17	177	SP	5	0.70
18	177	SPS	3	0.80
19	177	SPS	4	0.90
20	177	SPS	5	0.95

The actual versus target sorbent and ammonia injections for the tests are shown in Figures 4-19 and 4-20. Both the mass sorbent/mass SO_2 and the mass NH_3/mass NO_x injection rates are consistently lower than the target values. The sorbent injection rate was approximately 60% of the target value, and the NH_3 injection rate was approximately 80% of the target value.

The average stable period temperatures and differential pressures were reasonably stable during the tests; Figures 4-21 and 4-22 show these conditions. As noted previously, a single average value for gas flow was assumed for all tests in Test Series 2, and flue gas flows were stable during the tests. Inlet oxygen, SO_2, and NO_x concentration remained relatively constant as well, as shown in Figures 4-23 and 4-24. Likely as a result of the fuel composition, inlet SO_2 increased approximately 100 ppm during the middle third of the tests. Inlet NO_x decreased toward the end of the tests, decreasing by approximately 50 ppm for Tests 14–20.

The stable period average middle chamber temperature remained steady over the course of each of the three target temperatures. The average differential pressure showed some variation between individual tests, probably as a result of particulate plugging of pressure taps.

Table 4-9. Operating Conditions and Results for Test Series 2

Test:		1	2	3	4	5	6	7	8	9	10	11	12	13	14	15	16	17	18	19	20
Date	mm:dd:yy	4/30/15	4/30/15	4/30/15	4/30/15	4/30/15	4/30/15	5/1/15	5/1/15	5/1/15	5/1/15	5/1/15	5/1/15	5/1/15	5/2/15	5/2/15	5/2/15	5/2/15	5/2/15	5/2/15	5/2/15
Test Start	hh:mm	11:08	12:28	14:25	16:00	17:00	18:00	14:00	15:14	16:01	17:00	18:20	19:19	20:08	9:20	10:55	11:56	12:50	14:10	15:00	15:52
Test End	hh:mm	12:24	14:00	15:25	16:50	17:49	18:50	15:00	15:59	16:50	17:55	19:09	20:05	21:10	10:50	11:53	12:49	13:55	14:59	15:51	17:39
Test Time	hh:mm	1:16	1:32	1:00	0:50	0:49	0:50	1:00	0:44	0:49	0:55	0:49	0:45	1:01	1:29	0:58	0:53	1:05	0:49	0:51	1:47
Stable Period Start	hh:mm	11:44	13:20	15:05	16:30	17:23	18:33	14:30	15:33	16:30	17:39	18:44	19:39	20:47	10:14	11:24	12:38	13:35	14:41	15:36	17:00
Stable Period End	hh:mm	12:07	13:35	15:25	16:43	17:44	18:50	15:00	15:53	16:50	17:55	19:09	20:05	21:10	10:50	11:49	12:49	13:55	14:59	15:51	17:39
Stable Period Time	hh:mm	0:22	0:14	0:20	0:12	0:21	0:17	0:30	0:19	0:20	0:15	0:24	0:25	0:22	0:35	0:25	0:11	0:19	0:18	0:15	0:38
Sorbent		SP	SP	SP	SPS	SPS	SPS	SP	SP	SP	SP	SPS	SPS	SPS	SP	SP	SP	SP	SPS	SPS	SPS
Target FV Temperature	°C	232	232	232	232	232	232	288	288	288	288	288	288	288	177	177	177	177	177	177	177
Target Sorbent Feed	kg sorbent/kg inlet SO_2	2	3	4	5	3	4	2	3	4	5	3	4	5	2	3	4	5	3	4	5
Target Ammonia Feed	kg NH_3/kg inlet NO_x	0.60	0.60	0.70	0.70	0.80	0.90	0.60	0.60	0.70	0.70	0.80	0.90	0.95	0.60	0.60	0.70	0.70	0.80	0.90	0.95
Average Mid	°C	245	246	241	237	243	248	277	280	282	284	281	283	287	203	200	201	202	202	203	206
Average dP	kPa	1.74	1.84	1.82	1.94	1.74	1.84	1.94	1.82	1.94	2.09	1.97	1.89	2.09	1.89	2.21	1.67	2.02	1.72	1.99	1.62
S Top	°C	225	229	227	219	226	230	255	257	259	261	257	259	262	188	187	187	189	187	188	191
S Middle	°C	247	246	241	238	243	248	277	280	282	284	282	285	288	203	199	199	201	201	203	206
S Bottom	°C	245	249	245	237	248	251	281	283	284	287	280	287	292	206	203	203	205	201	202	208
S Chamber dP	kPa	1.69	1.74	1.84	1.97	1.77	1.87	1.97	1.84	1.97	2.12	1.99	1.92	2.12	1.92	2.21	1.69	2.04	1.74	2.02	1.64
N Top	°C	227	229	227	220	227	232	257	260	263	266	260	263	267	192	189	191	192	190	191	194
N Middle	°C	243	246	241	236	243	247	277	279	281	283	281	282	286	203	201	201	203	202	204	206
N Bottom	°C	247	250	244	239	247	251	281	283	284	286	283	286	290	206	204	204	207	204	206	206
N Chamber dP	kPa	1.82	1.92	1.79	1.92	1.69	1.82	1.89	1.79	1.92	2.07	1.94	1.87	2.07	1.87	2.19	1.64	1.99	1.69	1.97	1.59
South In Flow	acmm	NA	NA	NA	NA	NA	NA	NA	NA	NA	NA	NA	NA	NA	NA	NA	NA	NA	NA	NA	NA
North In Flow	acmm	NA	NA	NA	NA	NA	NA	NA	NA	NA	NA	NA	NA	NA	NA	NA	NA	NA	NA	NA	NA
Total Flow	acmm	5.83	5.83	5.83	5.83	5.83	5.83	5.83	5.83	5.83	5.83	5.83	5.83	5.83	5.83	5.83	5.83	5.83	5.83	5.83	5.83
O_2 Inlet	%	3.92	3.97	3.67	3.67	3.74	3.81	3.75	3.75	3.62	3.73	3.69	3.55	3.69	3.92	3.96	3.82	4.26	4.06	3.91	4.38
O_2 Outlet	%	4.67	4.76	4.41	4.52	4.62	4.77	4.54	4.55	4.44	4.55	4.49	4.35	4.52	4.83	4.85	4.67	5.07	4.85	4.73	5.20
DSI	kg/hr	1.45	2.75	1.26	1.63	1.82	2.45	1.21	1.82	2.28	2.74	1.64	1.64	2.45	1.21	1.82	2.28	2.74	1.64	2.05	2.45
DSI	kg/Macm	4151	7861	3606	4683	5202	7018	3464	5215	6512	7822	4683	4683	7018	3464	5215	6512	7822	4683	5851	7018
DSI	kg/kg-SO_2	1.58	3.01	1.37	1.84	2.01	2.71	1.25	1.89	2.25	2.73	1.64	1.60	2.45	1.29	1.98	2.39	2.97	1.77	2.18	2.93
SO_2 Inlet	ppm	989.1	986.3	991.5	961.3	976.0	978.1	1047.1	1042.6	1089.5	1081.4	1075.1	1104.8	1082.3	1012.7	991.2	1026.6	993.1	998.5	1012.8	904.4
SO_2 Outlet	ppm	457.4	301.0	493.4	499.8	402.1	230.3	716.3	691.8	722.1	565.4	673.7	632.2	508.7	827.9	686.5	688.0	516.7	675.4	557.2	536.6
SO_2 Capture	%	53.77	69.48	50.24	48.00	58.80	76.45	31.60	33.65	33.72	47.71	37.33	42.76	53.00	18.23	30.75	32.98	47.97	32.36	44.98	40.67
NO_x Inlet	ppm	572.3	568.1	550.2	551.1	548.9	561.3	563.8	572.1	547.0	567.3	565.1	516.6	536.3	416.2	425.9	424.4	447.0	445.6	440.3	448.8
NO_x Outlet	ppm	4.3	136.6	142.4	74.8	7.4	4.3	399.0	171.6	79.4	101.0	55.5	2.5	2.3	129.5	109.8	119.7	104.6	141.0	118.9	150.0
NO_x Capture	%	99.25	75.97	74.13	86.44	98.65	99.24	29.24	70.02	85.49	82.20	90.20	99.53	99.57	68.88	74.23	71.80	76.60	68.35	72.99	66.60
NH_3	L/min	3.61	1.35	1.35	1.85	2.31	2.50	1.40	1.40	1.60	1.60	1.80	2.30	2.00	1.40	1.40	1.40	1.40	1.60	1.60	1.10
NH_3 Inj. Rate	kg/Macm	439	163	163	224	280	304	170	170	194	194	219	280	243	170	170	170	170	194	194	133
Molar Ratio	NH_3/NO_x	1.09	0.41	0.42	0.58	0.72	0.76	0.43	0.42	0.50	0.48	0.55	0.76	0.64	0.58	0.56	0.57	0.54	0.62	0.62	0.42
NH_3 Ratio	kg NH_3/kg NO_x	0.62	0.23	0.24	0.33	0.41	0.43	0.24	0.24	0.28	0.27	0.31	0.34	0.36	0.33	0.32	0.32	0.30	0.35	0.35	0.24
Outlet NH_3	ppm (dry)	6.09	5.23	0.73	1.25	22.50	64.18	<1	<1	<1	<1	<1	33.82	75.19	0.66	14.92	30.94	32.53	35.31	75.89	NA

[1] Filter vessel.

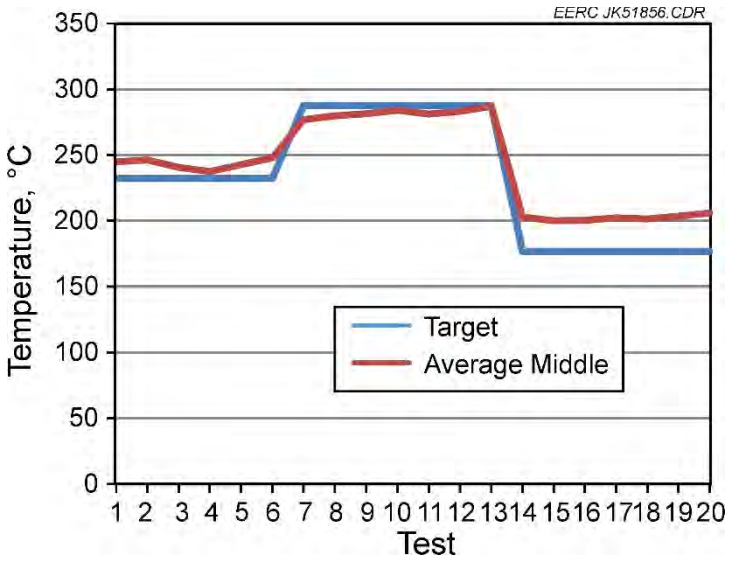

Figure 4-18. Target versus actual filter vessel temperature for Test Series 2.

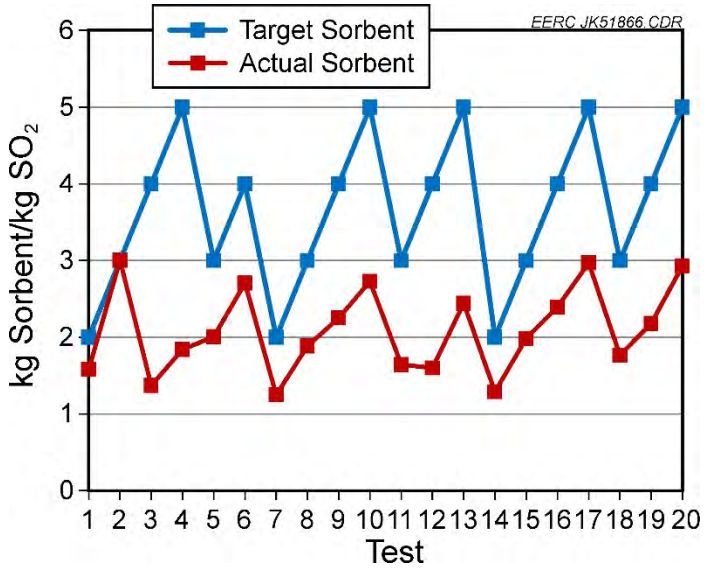

Figure 4-19. Target versus actual sorbent injection rate for Test Series 2.

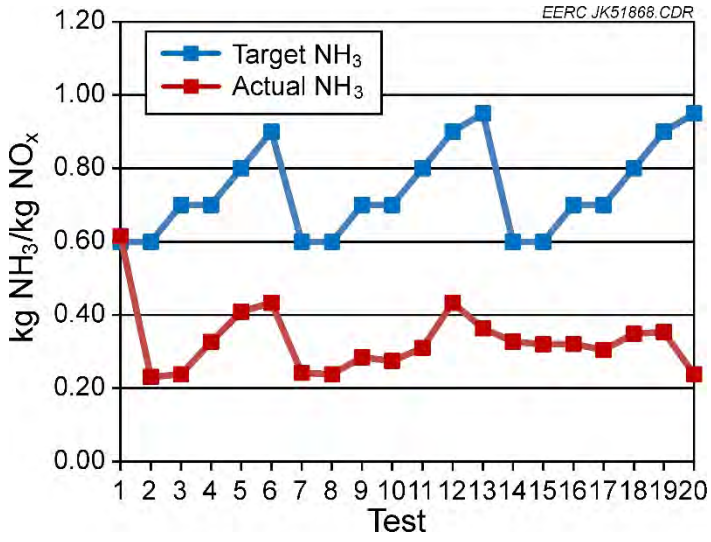

Figure 4-20. Target versus actual ammonia injection rate for Test Series 2.

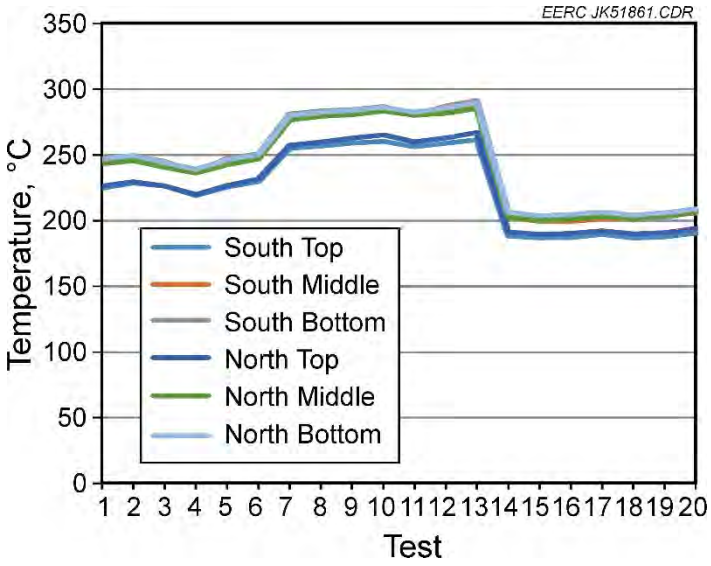

Figure 4-21. Average stable period temperatures for Test Series 2.

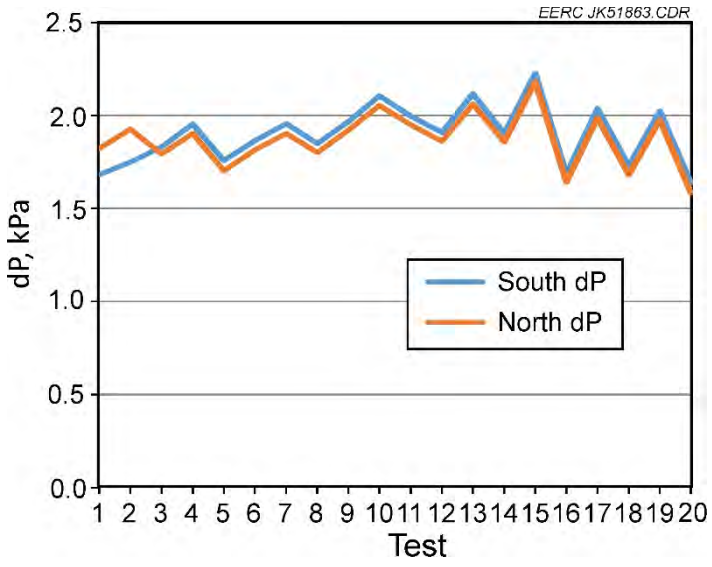

Figure 4-22. Average stable period differential pressures for Test Series 2.

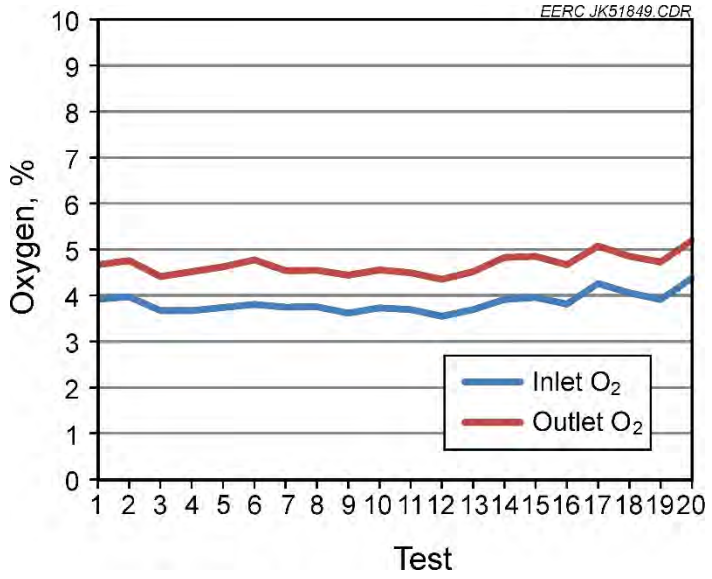

Figure 4-23. Average stable period inlet oxygen concentrations for Test Series 2.

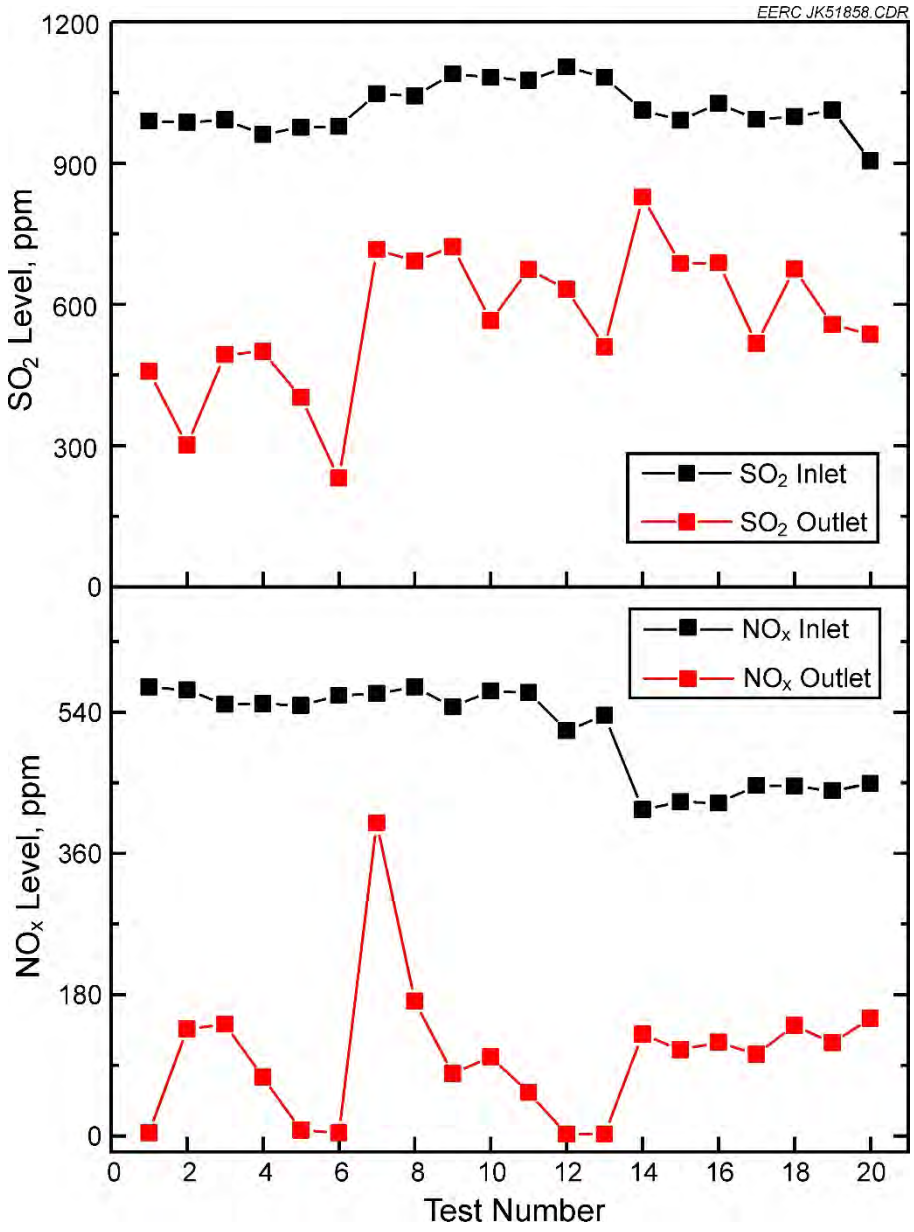

Figure 4-24. Average stable period inlet and outlet SO_2 and NO_x concentrations for Test Series 2.

4.3.3.2.2 SO_2 and NO_x Removal

The test plan had targeted specific sorbent and ammonia ratios rather than attempting to achieve specific SO_2 and NO_x removals. This improved the stability of the measurements.

The SO_2 removals were measured at three temperature conditions using two sorbent types. Figure 4-25 gives a comparison of the removals as a function of lb sorbent/lb inlet SO_2 for each condition of temperature and sorbent. Actual SO_2 removals ranged from 20% to nearly 80% for

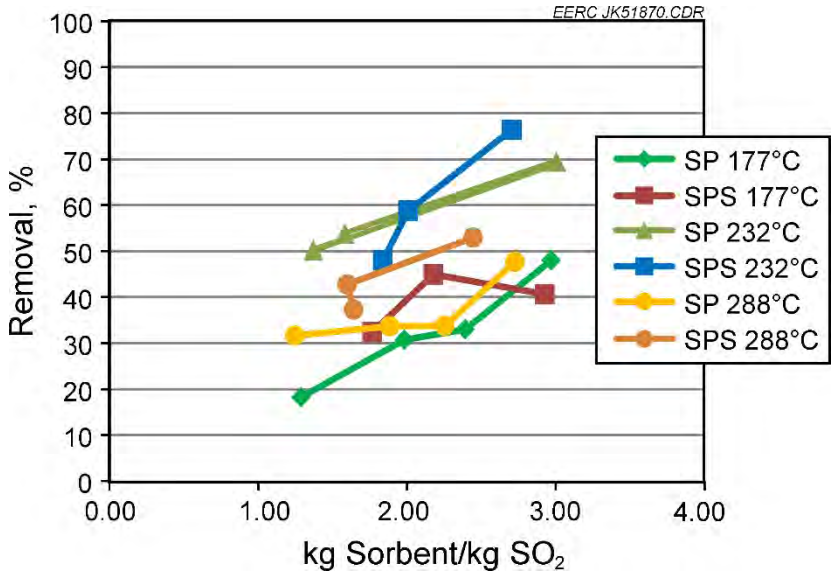

Figure 4-25. SO_2 removal versus lb sorbent injected/lb SO_2 in the inlet gas stream for Test Series 2.

the tests. There is a roughly linear trend of increasing SO_2 removal with increased sorbent injection rate, as previously seen in Test Series 1.

Two trends are seen in the data. Although there is considerable scatter, the SPS sorbent appears to show better SO_2 removal effectiveness than the SP sorbent at all three temperature conditions. Both sorbents also appear to exhibit the best SO_2 removal effectiveness at 232°C (450°F), with similar lower removal effectiveness at 177° (350°) and 288°C (550°F).

Figure 4-26 shows the NO_x removal versus the ratio of moles NH_3 injected/moles NO_x in the inlet gas steam. The data are grouped as a function of both temperature and sorbent type. Despite the scatter in the data, NO_x removals appear to be approximately the same in the presence of either sorbent. This indicates that the NO_x removal is not affected by the sorbent, as would be expected.

The NO_x removal as a function of temperature only is shown in Figure 4-27. Again, despite the data scatter, there appears to be a trend of increasing NO_x removal with increasing temperature. In several of the tests, effectively 100% NO_x removal was achieved. However, the high removal in some cases also resulted in significant ammonia slip at the exit of the filter vessel.

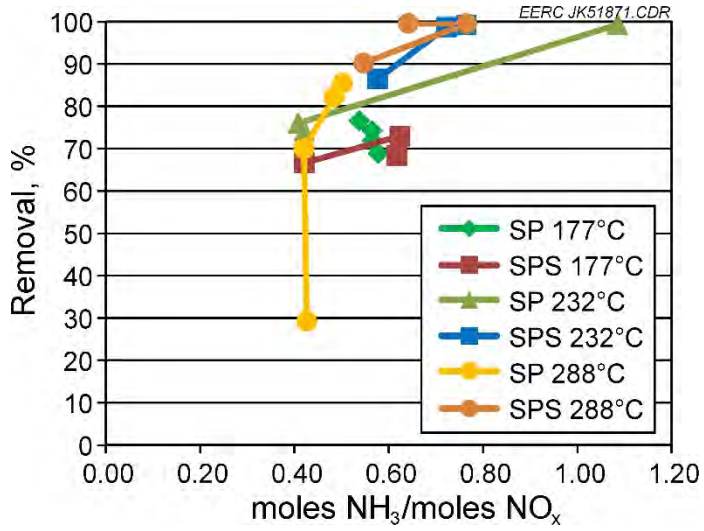

Figure 4-26. NO_x removal versus moles NH_3 injected/mole NO_x in the inlet gas stream as a function of temperature and sorbent for Test Series 2.

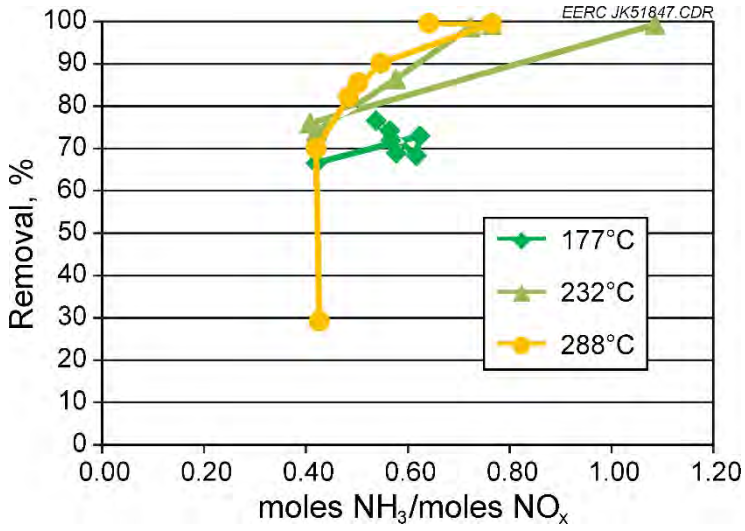

Figure 4-27. NO_x removal versus moles NH_3 injected/mole NO_x in the inlet gas stream as a function of temperature for Test Series 2.

4.3.3.2.3 EPA Method 5 Particulate Sampling

Method 5 sampling was performed at the inlet and outlet ports. Pitot measurements were first made to determine the isokinetic flue gas-sampling rate. Both pitot measurements and Method 5 sampling were performed with the respective probes at the center line of the duct. Sampling was performed for 120 min. At the completion of sampling, the filter assembly was disassembled and the dust collected on the filter recovered and carefully weighed. The sampling tests were performed nearly isokinetically, 101.1% at the inlet port and 93.6% at the outlet port. Other sampling parameters were also consistent. Table 4-10 provides sampling conditions, sampling times, and amounts of particulate collected.

The Method 5 sampling was performed May 1, 2015, beginning at 11:44 and ending at 13:47, before the start of Test 7. Sampling began at 11:44 and ended at 13:44 at the inlet and from 11:47 to 13:47 at the outlet for a 120-min sampling duration. The sampling was nearly isokinetic, with 13.29 g of dust collected at the inlet, corresponding to 5.83 grains/dry scf. At the outlet, 0.008 g of dust was collected, corresponding to a dust loading of 0.002 grains/dry scf. Based on the Method 5 sampling, the particulate collection efficiency across the filter vessel was 99.96%.

Table 4-10. EPA Method 5 Particulate-Sampling Results for Test Series 2

Location	**Inlet**	**Outlet**
Test Date:	5/1/2015	5/1/2015
Start Time, hr:min	11:44	11:47
End Time, hr:min	13:44	13:47
Duration, min	2:00	2:00
Barometric Pressure, kPa	99.1	99.1
Stack Temperature, °C	303	213
Stack Pressure, kPa	−2.16	−3.93
dP Pitot, Pa	42.3	746.5
Nozzle Diameter, in.	0.65	0.39
Dry Sample Volume, scm	1.00	1.56
Total Sample Volume, scm	1.14	1.77
Flue Gas H_2O, %	12.90	11.70
Isokinetic, %	101.1	93.6
Filter, g	13.29	0.008
Total Dust, g	13.29	0.008
Dust Loading, grains/scf	5.83	0.002
Dust Loading, g/scm	13.34	0.005
Particulate Removal, %		99.96

4.3.3.2.4 Summary of Test Series 2

Test Series 2 was performed April 30 – May 2, 2015. The series consisted of 20 tests, with ammonia and sorbent injection at specific mass ratios of sorbent/inlet SO_2 and NH_3/inlet NO_x. The test series was conducted at three target filter vessel temperatures 177°, 232°, and 288°C (350°, 450°, and 550°F) and with two sorbents (SP and SPS).

Outlet NO_x and SO_2 levels were more stable than the previous Test Series 1. The average stable period temperatures, differential pressures, and flue gas flows were stable during the tests. Inlet oxygen, SO_2, and NO_x concentration remained relatively constant as well. However, problems with flow measurements necessitated the use of a single average value of flue gas flow for the entire test series.

SO_2 removal level was measured at three temperature conditions using two sorbent types. Actual SO_2 removals ranged from 20% to nearly 80% for the tests. There is a roughly linear trend of increasing SO_2 removal with increased sorbent injection rate. The SPS sorbent appears to show better SO_2 removal effectiveness than the SP sorbent at all three temperature conditions. Both sorbents also appear to exhibit the best SO_2 removal effectiveness at 232°C (450°F), with similar lower removal effectiveness at 177° (350°) and 288°C (550°F).

The NO_x removal appears to show a trend of increasing NO_x removal with increasing temperature. In several of the tests, effectively 100% NO_x removal was achieved. However, the high removal in some cases also resulted in significant ammonia slip at the exit of the filter vessel. NO_x removals appear to be approximately the same in the presence of either sorbent. This indicates that the NO_x removal is not affected by the sorbent.

Extractive particulate sampling indicated the particulate collection efficiency across the filter vessel was 99.96%.

4.3.3.3 Test Series 3

Test Series 3 was performed July 23–24, 2015. The series consisted of 12 tests, with ammonia and sorbent injection fixed and the NO_x and SO_2 removals monitored. The test plan is given in Table 4-11. The test series was conducted at four target filter vessel temperatures: 260°, 266°, 279°, and 288°C (500°, 510°, 535°, and 550°F) and with two sorbents (SP and SPS). In this test series, the sorbent and ammonia injection rates were selected for a desired sorbent/inlet SO_2 ratio and NH_3/inlet NO_x mass ratio and then kept fixed, rather than attempting to achieve specific removal rates. This improved the stability of the tests. The SO_2 and NO_x inlet concentrations remained very stable during the individual tests. The outlet concentrations exhibited much less fluctuation than the previous two test series, with NO_x showing less fluctuation than the SO_2. The orifices were relocated to the clean flue gas stream at the exit of the filter vessel. This appeared to improve the stability of the flow measurements and the calculated SO_2 and NO_x removals. No Method 5 sampling was performed during Test Series 3.

Table 4-11. Planned Test Conditions for Test Series 3

Test	Target Filter Vessel Temperature, °C	Sorbent	Target Sorbent Feed, mass ratio sorbent/inlet SO_2	Target Ammonia Feed, mass ratio NH_3/inlet NO_x
1	279	SP	2	0.60
2	288	SP	4	0.70
3	288	SP	5	0.70
4	288	SPS	3	0.80
5	288	SPS	4	0.90
6	288	SPS	5	0.95
7	266	SPS	3	0.80
8	266	SPS	4	0.90
9	266	SPS	5	0.95
10	260	SP	3	0.60
11	260	SP	4	0.70
12	260	SP	5	0.70

The stable period for each individual test was identified and average values for the operating parameters and removals determined. The results are given in Table 4-12. Measurements of outlet NH_3 (NH_3 slip) are reported for all but one of the tests. It should be noted that the outlet NH_3 measurements do not necessarily correspond to the averaged stable periods, since the measurements were performed over only a part of each test period.

4.3.3.3.1 Average Stable Period Test Conditions

Figure 4-28 shows the target temperature desired for the tests along with the actual average of the middle temperature of the two chambers. Good agreement between the target temperature and the actual temperature for each test was achieved.

Table 4-12. Operating Conditions and Results for Test Series 3

Test:		1	2	3	4	5	6	7	8	9	10	11	12
Date	mm:dd:yy	7/23/2015	7/24/2015	7/24/2015	7/24/2015	7/24/2015	7/24/2015	7/24/2015	7/24/2015	7/24/2015	7/24/2015	7/24/2015	7/24/2015
Test Start	hh:mm	13:34	9:22	11:22	12:40	13:52	14:39	16:31	17:34	18:18	19:22	20:06	20:57
Test End	hh:mm	14:40	11:20	12:24	13:49	14:34	15:21	17:32	18:15	19:05	20:02	20:55	21:44
Test Time	hh:mm	1:06	1:58	1:02	1:09	0:42	0:42	1:01	0:41	0:47	0:40	0:48	0:47
Stable Period Start	hh:mm	14:15	10:40	12:05	13:19	14:17	15:05	17:10	18:04	18:42	19:47	20:40	21:22
Stable Period End	hh:mm	14:40	11:20	12:24	13:49	14:34	15:21	17:32	18:15	19:05	20:02	20:55	21:44
Stable Period Ttime	hh:mm	0:25	0:40	0:19	0:30	0:16	0:16	0:22	0:11	0:23	0:14	0:14	0:22
Target FV Temperature	°C	279	288	288	288	288	288	266	266	266	260	260	260
Sorbent		SP	SP	SP	SPS	SPS	SPS	SPS	SPS	SPS	SP	SP	SP
Target Sorbent Feed	kg sorbent/kg inlet SO_2	2	4	5	3	4	5	3	4	5	3	4	5
Target Ammonia Feed	kg NH_3/kg inlet NO_x	0.60	0.70	0.70	0.80	0.90	0.95	0.80	0.90	0.95	0.60	0.70	0.70
Average Mid	°C	283	289	290	287	291	292	265	268	264	259	262	263
Average dP	kPa	1.94	2.34	2.16	2.21	2.04	2.07	2.04	1.99	1.99	1.99	2.02	1.99
S Top	°C	252	263	263	261	261	265	244	244	244	238	238	241
S Middle	°C	283	291	291	287	291	293	266	269	265	258	262	264
S Bottom	°C	279	286	288	288	288	289	262	265	261	259	261	261
S Chamber dP	kPa	1.97	2.34	2.16	2.21	2.04	2.09	2.04	1.99	2.02	2.02	2.04	2.02
N Top	°C	258	267	268	266	266	268	247	248	246	241	241	243
N Middle	°C	282	289	289	288	289	291	264	267	263	259	262	262
N Bottom	°C	278	284	289	285	285	286	262	263	259	256	258	258
N Chamber dP	in H_2O	1.94	2.31	2.16	2.21	2.02	2.07	2.04	1.97	1.97	1.99	2.02	1.99
South In Flow	acmm	3.02	3.07	3.09	3.07	3.06	3.03	3.07	3.05	3.07	3.07	3.07	3.05
North In Flow	acmm	3.03	3.10	3.08	3.08	3.06	3.05	3.09	3.08	3.09	3.10	3.10	3.09
Total Flow	acmm	6.06	6.16	6.18	6.15	6.12	6.09	6.16	6.13	6.16	6.16	6.17	6.14
O_2 Inlet	%	3.76	3.76	3.74	3.72	3.75	3.81	3.99	3.85	3.82	3.96	3.81	3.82
O_2 Outlet	%	4.82	5.63	5.51	5.46	5.45	5.49	5.64	5.53	5.52	5.67	5.55	5.58
DSI	kg/hr	1.48	2.15	2.68	1.45	1.73	2.13	1.45	1.73	2.13	1.73	2.15	2.68
DSI	kg/Macm	4080	5827	7228	3923	4708	5827	3917	4698	5759	4684	5818	7278
DSI	kg/kg-SO_2	1.61	2.28	2.79	1.50	1.80	2.25	1.58	1.86	2.26	1.88	2.32	2.88
SO_2 Inlet	ppm	956.1	965.8	978.6	986.6	988.6	975.3	933.8	951.8	960.4	940.5	945.2	951.4
SO_2 Outlet	ppm	562.9	436.8	391.4	496.2	465.2	393.6	484.0	430.8	412.6	508.0	430.0	388.3
SO_2 Capture	%	41.11	54.78	60.01	49.70	52.95	59.66	48.16	54.72	57.05	45.99	54.50	59.18
NO_x Inlet	ppm	415.0	428.0	426.9	437.5	430.0	431.5	424.5	424.2	428.4	441.6	436.1	432.8
NO_x Outlet	ppm	97.0	127.2	125.4	55.4	16.2	1.6	36.3	9.8	4.5	132.9	70.0	63.2
NO_x Capture	%	76.62	70.28	70.63	87.34	96.23	99.62	91.45	97.68	98.95	69.91	83.95	85.41
NH_3	L/min	1.67	1.85	1.85	2.01	2.31	2.35	2.01	2.31	2.35	1.67	1.85	1.85
NH_3 Inj. Rate	kg/Macm	195	213	212	232	268	274	231	267	270	192	212	214
Molar Ratio	NH_3/NO_x	0.66	0.70	0.70	0.75	0.88	0.90	0.77	0.89	0.89	0.61	0.69	0.70
NH_3 Ratio	kg NH_3/kg NO_x	0.38	0.40	0.40	0.42	0.50	0.51	0.44	0.50	0.50	0.35	0.39	0.39
Outlet NH_3	ppm (dry)	0.02	0.17	0.14	0.07	0.05	0.04	0.10	0.04	8.97	0.60	0.26	0.14

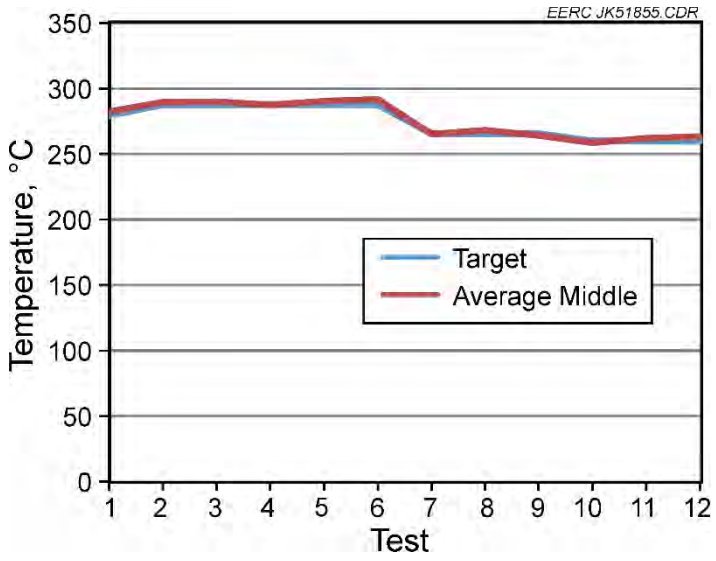

Figure 4-28. Target versus actual filter vessel temperature for Test Series 3.

The actual versus target sorbent and ammonia injections for the tests are shown in Figures 4-29 and 4-30. The mass ratio of sorbent/inlet SO_2 injection rates are consistently lower than the target values, approximately 55% of the target value. The NH_3/inlet NO_x injection rates were approximately 98% of the target value.

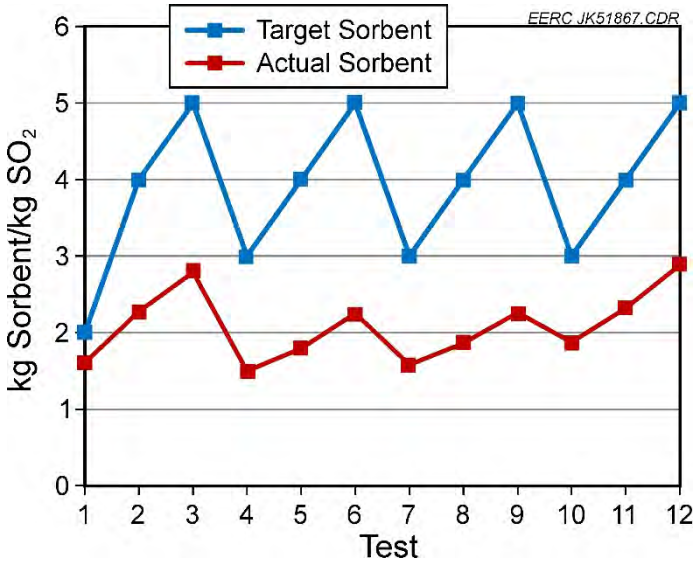

Figure 4-29. Target versus actual sorbent injection rate for Test Series 3.

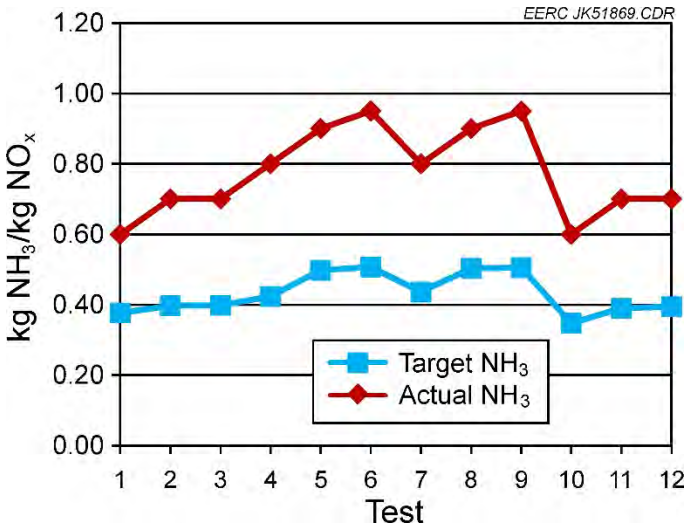

Figure 4-30. Target versus actual ammonia injection rate for Test Series 3.

The average stable period temperatures and differential pressures were relatively stable during the tests. Figures 4-31 and 4-32 show these conditions. Flue gas flows were also stable during the tests, as shown in Figure 4-33. Inlet oxygen, SO_2, and NO_x concentration remained relatively constant as well, as shown in Figures 4-34 and 4-35.

4.3.3.3.2 SO_2 and NO_x Removal

The test plan had targeted specific sorbent and ammonia ratios rather than attempting to achieve specific SO_2 and NO_x removals. As in Test Series 2, this improved measurement stability.

The SO_2 removals were measured at four temperature conditions using two sorbent types. Figure 4-36 gives a comparison of the removals as a function of lb sorbent/lb inlet SO_2 for each condition of temperature and sorbent. Actual SO_2 removals ranged from 40% to 60% for the tests. There is a roughly linear trend of increasing SO_2 removal with increased sorbent injection rate, as previously seen. The removals are clustered much more tightly than the previous two test series, which is indicative of stable operating conditions.

Two trends are seen in the data. The SPS sorbent appears to show better SO_2 removal than the SP sorbent. The two sorbents appear to show little effect of temperature on removal. This is probably because of the narrow temperature range of 266° to 288°C (510° to 550°F) used in the tests.

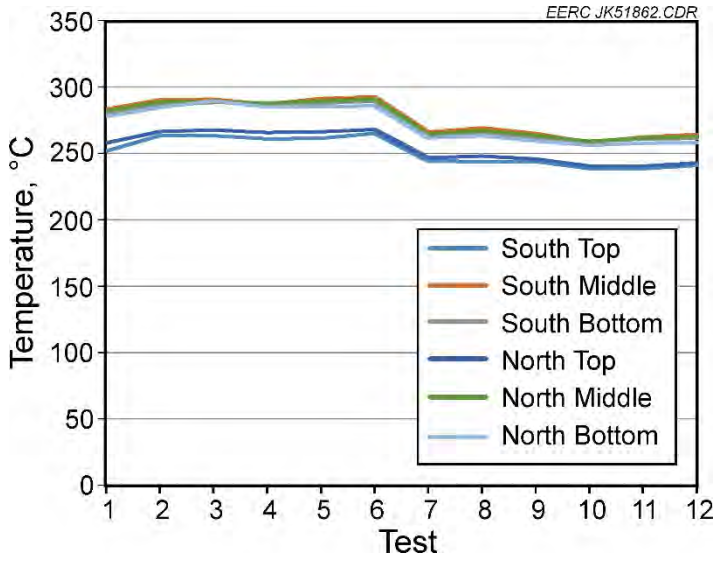

Figure 4-31. Average stable period temperatures for Test Series 3.

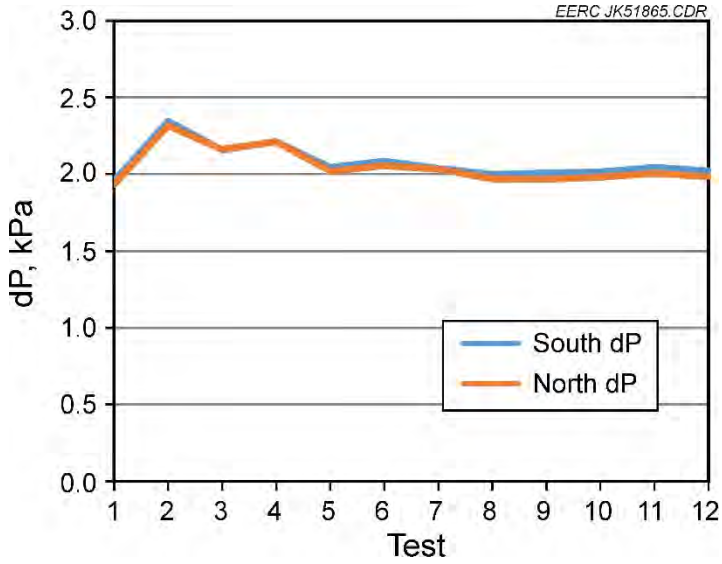

Figure 4-32. Average stable period differential pressures for Test Series 3.

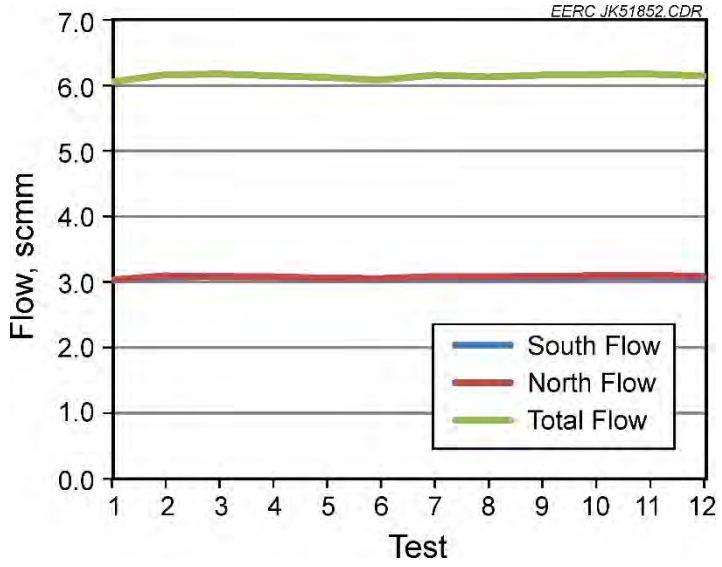

Figure 4-33. Average stable period flue gas flow for Test Series 3.

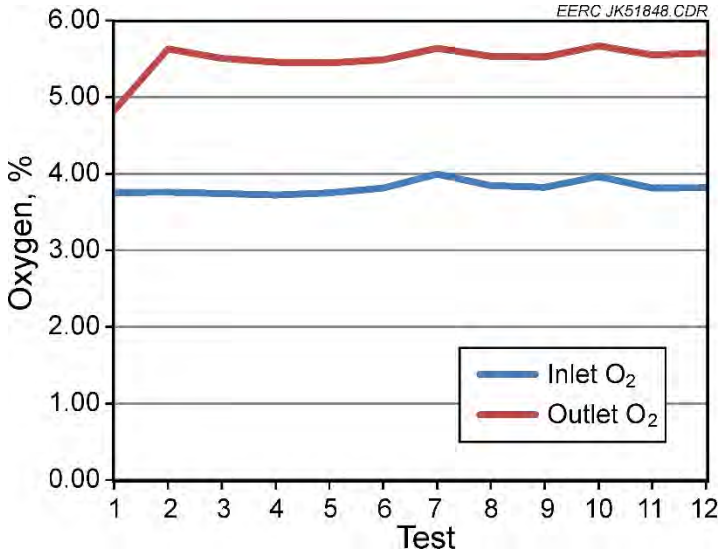

Figure 4-34. Average stable period inlet oxygen concentrations for Test Series 3.

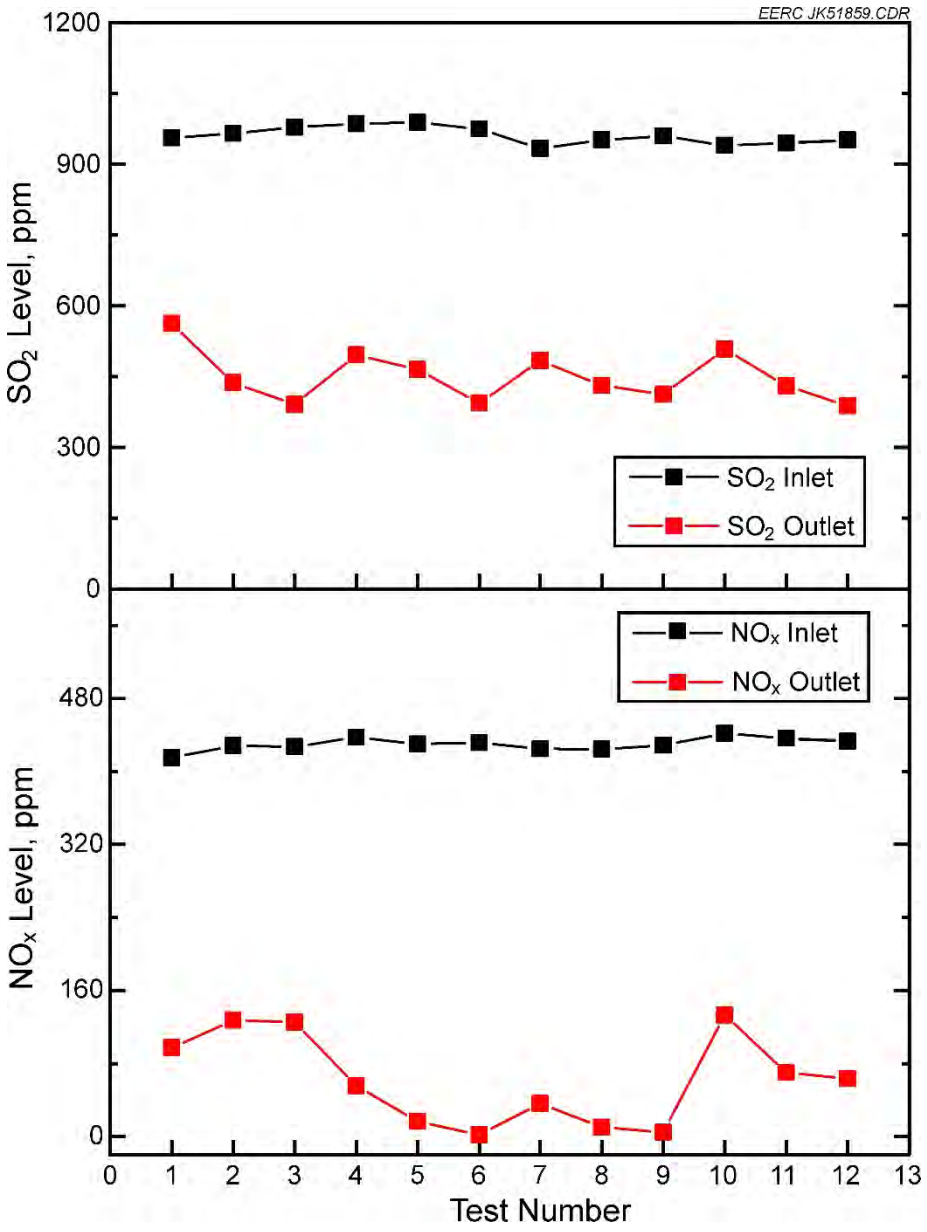

Figure 4-35. Average stable period inlet and outlet SO_2 and NO_x concentrations for Test Series 3.

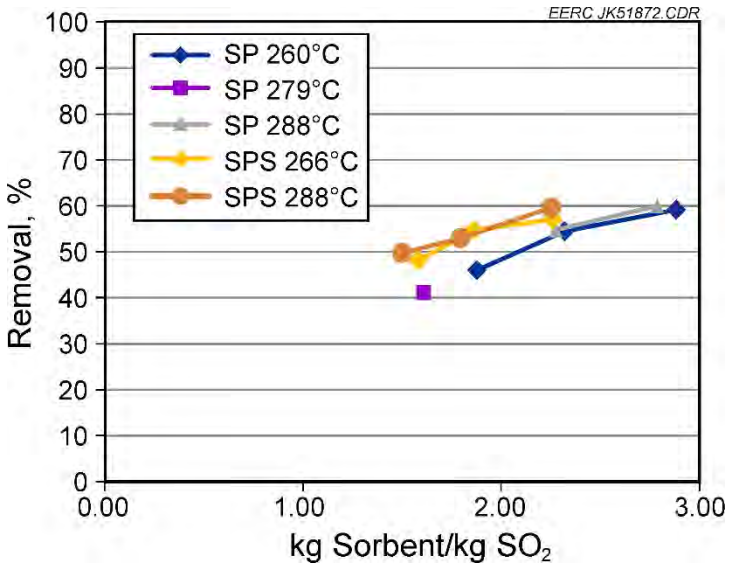

Figure 4-36. SO_2 removal versus lb sorbent injected/lb SO_2 in the inlet gas stream for Test Series 3.

Figure 4-37 shows the NO_x removal versus the ratio of moles NH_3 injected/moles NO_x in the inlet gas steam. The data are grouped as a function of both temperature and sorbent type. Again, NO_x removals appear to be approximately the same in the presence of either sorbent, indicating that the NO_x removal is not affected by the sorbent.

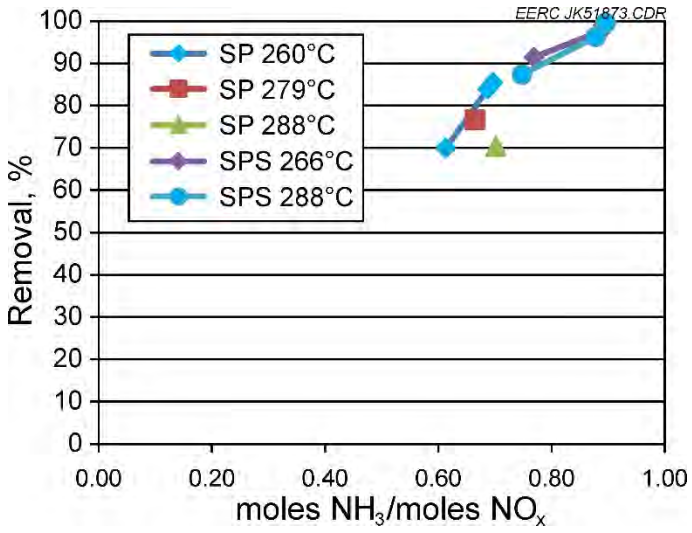

Figure 4-37. NO_x removal versus moles NH_3 injected/mole NO_x in the inlet gas stream as a function of temperature and sorbent for Test Series 3.

NO_x removal as a function of temperature only is shown in Figure 4-38. The removal appears to show little effect of temperature. This is probably because of the narrow 16°C (40°F) temperature range used in the tests. In several tests, effectively 100% NO_x removal was achieved, with very little ammonia slip at the exit of the filter vessel.

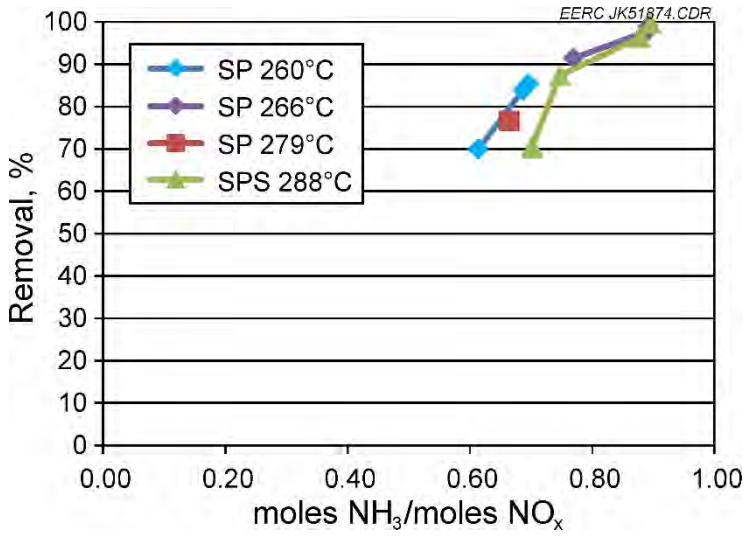

Figure 4-38. NO_x removal versus moles NH_3 injected/mole NO_x in the inlet gas stream as a function of temperature for Test Series 3.

4.3.3.3.3 Summary for Test Series 3

Test Series 3 was performed July 23–24, 2015. The series consisted of 12 tests, with ammonia and sorbent injection at specific mass ratios of sorbent/inlet SO_2 and NH_3/inlet NO_x. The test series was conducted at four target filter vessel temperatures: 260°, 266°, 279°, and 288°C (500°, 510°, 535°, and 550°F) and with two sorbents (SP and SPS).

Outlet NO_x and SO_2 levels were much more stable than the previous Test Series 1 and 2. The average stable period temperatures, differential pressures, and flue gas flows were stable during the tests. Inlet oxygen, SO_2, and NO_x concentration remained relatively constant as well. The relocation of the flow orifices to the outlet of the filter vessel appeared to significantly improve the flow measurements.

SO_2 removals were measured at four temperature conditions using two sorbent types. Actual SO_2 removals ranged from 40% to nearly 60% for the tests. There is a roughly linear trend of increasing SO_2 removal with increased sorbent injection rate. The SPS sorbent appears to show better SO_2 removal effectiveness than the SP sorbent. No significant effect of temperature on removal was noted. This is probably because of the narrow temperature range of 266° to 288°C (510° to 550°F) used in the tests.

NO_x removal did not appear to show any trend with temperature. This is probably because of the narrow 16°C (40°F) temperature range used in the tests. In several of the tests, effectively 100% NO_x removal was achieved, with very little ammonia slip at the exit of the filter vessel. NO_x removals appear to be approximately the same in the presence of either sorbent, indicating that the NO_x removal is not affected by the sorbent.

4.3.4 Conclusions

Testing with the Tri-Mer filter system resulted in high levels of capture for particulate, NO_x, and SO_2. As anticipated, NO_x and SO_2 capture were highly dependent on temperature, ammonia injection rate, and amount of sorbent. Differences were also observed between the SP and SPS SO_2 sorbent. While injecting the SPS material, higher levels of SO_2 removal were achieved at the same rate of SP injected material. The Tri-Mer system was an effective tool for the removal of impurities prior to CO_2 capture technologies. However, it may be necessary to trim SO_2 levels.

5.0 POSTCOMBUSTION CO_2 CAPTURE TESTING

5.1 Introduction

The EERC has developed a premiere program to advance the most promising carbon capture technologies, PCO_2C. Through this and other programs, world-class facilities have been designed, fabricated, and installed at the EERC. Tests in Phase III of the PCO_2C Program evaluated advanced postcombustion CO_2 capture technologies, including the Korea Carbon Capture and Sequestration R&D Center (KCRC) Solvent-B technology, the CO_2 Solutions enzyme solvent (CSES), and partial CO_2 capture with MEA.

5.2 Experimental Methods and Equipment

5.2.1 Postcombustion Test System

The solvent-based capture system, shown in Figure 5-1, consists of two absorber columns and one stripper (or regeneration) column, each constructed from 25.4 cm-(10 in.)-i.d. stainless steel column sections of varying lengths bolted together to achieve a desired total height. The absorbers treat the flue gas in series, with the gas flowing from the bottom to the top of each column, countercurrent to the solvent.

The columns contain packing designed to promote liquid–gas contact, facilitating the absorption and regeneration processes. Total combined packing height for the absorber columns is approximately 7.6 m (25 ft), including 3 m (10 ft) of Koch–Glitsch IMTP 25 316L SS random packing and 15 ft of Sulzer MellapakCC™ advanced structured packing. Liquid distribution plates are inserted at the top of each packing section to evenly distribute the solvent, mitigating wall effects. The top (south) absorber has a 0.3-m (1-ft)-high column section near the middle of the column that is used as a water-cooled heat exchanger to control column temperature. A demister is installed near the top of the absorber column to prevent the flue gas from carrying solvent overhead with the exhaust stream.

Figure 5-1. PCO_2C system and control station.

The upper (south) absorber column has an integrated intracolumn water-cooled heat exchanger section. The solvent line between the upper and lower absorber columns also has an integrated tube-and-shell heat exchanger that cools the solvent. These heat exchangers help control the exothermic reaction within the absorber column during testing.

The columns will handle up to 3.7 scmm (130 scfm) of flue gas generated by either the CTF or the PTC. KCRC's Solvent-B used flue gas from the PTC at flow rates of approximately 2.83 and 2.12 scmm (100 and 75 scfm). The piping and instrumentation diagram (P&ID) for the postcombustion test system is shown in Figure 5-2. Detailed system equipment descriptions are included in Appendix A.

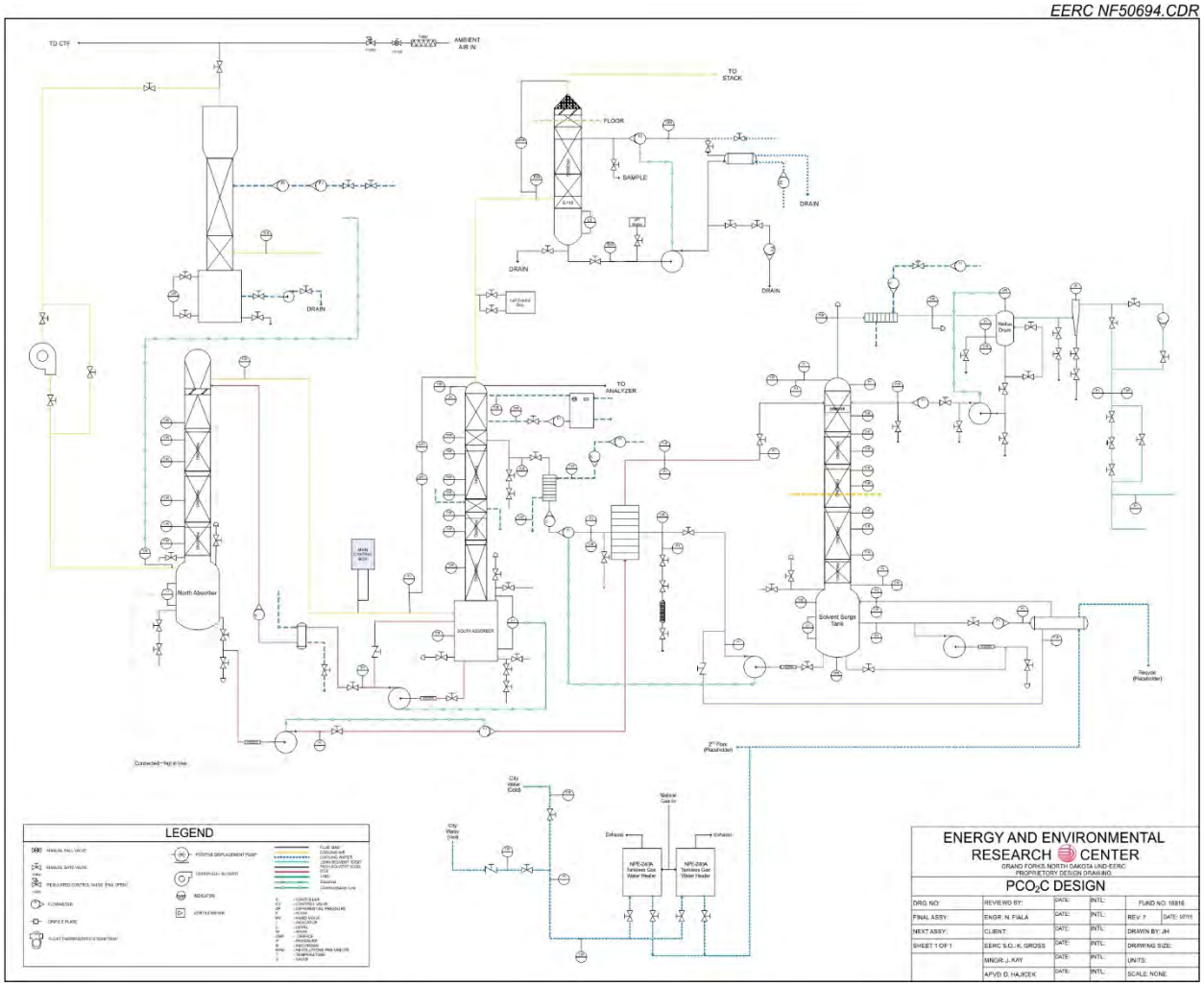

Figure 5-2. PCO_2C system P&ID.

The postcombustion capture system is controlled and monitored through a custom LabVIEW computer interface developed by the EERC. The LabVIEW control program also records all data generated by the postcombustion capture system, including temperature, pressure, and flow rate.

5.2.2 Combustion Furnace Overview

Flue gas is provided by burning coal, natural gas, or some other fuel. For each test period, the furnace was preheated by burning natural gas, but all flue gas to the absorbers was generated through coal combustion. The furnace is rated at approximately 0.2 MWth (500,000 Btu). The PTC is controlled through a separate LabVIEW interface that also controls and monitors the pollution control devices and gas analyzers. All PTC data are recorded in a file separate from the postcombustion capture data.

The facility is equipped with up to four state-of-the-art gas analyzer racks, which are used to monitor the flue gas at selected locations for levels of O_2, CO, CO_2, SO_2, and NO_x. For the

KCRC test runs, three analyzer racks were used, with one each at the combustor outlet, the CO_2 absorber inlet, and the CO_2 absorber outlet. Inlet and outlet gas analyzer data are used to determine the CO_2 capture rate of the technology.

5.2.3 Test Goals and Methods

The goal of the test effort was to evaluate the solvent's ability to capture CO_2 from coal-derived flue gas at several different process conditions. Two test campaigns for KCRC's Solvent-B were carried out, the first January 19–23, 2015, and the second March 3–5, 2015. The focus of the first test campaign was to survey several test conditions to develop a wide range of performance metrics. The second test campaign focused on finding optimum conditions for capturing 90% of the CO_2 entering the absorber column.

5.2.4 Test Parameters

The test plan was built around the PCO_2C test system limitations. Key variables for both test campaigns with Solvent-B included stripper bottom temperature, absorber inlet and outlet gas temperatures, lean solvent temperature into the absorber, solvent flow rate, and flue gas flow rate. Table 5-1 shows the system variable ranges and test plan variable ranges.

Table 5-1. System and Test Plan Variable Ranges

	Typical Range	KCRC Test Range
PTC System		
Inlet Gas Flow Rate	1.7–3.7 scmm (60–130 scfm)	2.1–3.0 scmm (75–105 scfm)
Inlet Gas Temperature	32°–49°C (90°–120°F)	39°–42°C (102°–108°F)
NO_x to Columns	0–600 ppm	0–600 ppm
SO_2 to Columns	0–600 ppm	0–200 ppm
Postcombustion Capture System		
Solvent Flow Rate Through Absorber	11–38 L/min (3–10 gpm)	6.8-17 L/min (1.8–4.5 gpm)
Condenser Cooling Water Flow Rate	3.8–23 L/min (1–6 gpm)	3.8–23 L/min (1–6 gpm)
Lean Solvent to Absorber Temperature	27°–66°C (80°–150°F)	27°–66°C (80°–150°F)
Stripper Static Pressure	20–97 kPag (3–10 psig)	20°–97 kPag (3–10 psig)
Reboiler Steam Pressure	69–345 kPag (10–50 psig)	172–345 kPag (25–50 psig)
Solvent Concentration	As requested	Target: 35 wt%
Stripper Bottom Temperature	82°–127°C (180°–260°F)	100°–113°C (212°–235°F)
H_2O Makeup Rate	0–500 mL/min	0–60 mL/min

5.3 Results and Discussion

5.3.1 KCRC Solvent-B

Although several challenges arose during testing, the main goal of demonstrating and investigating the CO_2 capture abilities of KCRC's Solvent-B was achieved through the test efforts at the EERC. The capture goal of 90% was also achieved during both test campaigns.

5.3.1.1 Operational Challenges

The January test campaign with KCRC's Solvent-B was the first test of the technology at the pilot scale. The unfamiliarity with the solvent's properties and performance levels led to some challenges in test operations. During the first test campaign, water loss from the solvent occurred throughout the test at a rate of approximately 3.8 L/hr (1 gal/hr). To correct this problem and maintain a more balanced solvent concentration, the second test used a steady makeup stream of approximately 55 mL/min of heated DI H_2O which was injected into the south absorber column base.

Another issue discovered through parametric testing at ~2.83 scmm (100 scfm) during the first campaign was that the flue gas flow rate would need to be reduced to approximately 2.12 scmm (75 scfm) in order to achieve proper liquid/gas ratio (L/G) for 90% capture.

Two separate incidents occurred during the first test campaign, leading to temporary stoppages. The first occurred at the beginning of the second test day when an ash deposit in the furnace fell down onto the swirl burner, creating a flame problem and a very high NO_x level, poor excess O_2 control, and difficulty maintaining consistent combustion.

A second unplanned temporary shutdown occurred on the third day of testing after cooling water was increased to the condensate chiller, leading the steam trap to seize. With loss of steam trap functionality, the steam system built up a significant amount of condensate. After fixing the steam trap, it took several hours to clear out the buildup of condensate before the test could continue.

5.3.1.2 Changes to System Between Tests

Following completion of the first test campaign, several changes were made to the postcombustion capture system. Thermocouples were added to the cooling water inlet and outlet of the condensate cooler, and a rotameter was added to monitor flow through the condensate cooler.

The steam vortex flowmeter was refurbished by the manufacturer following the first test before being reinstalled and rearranged for the second test campaign. A steam bypass around the vortex flowmeter was installed to prevent condensate from flowing through the vortex meter. A drain was installed on the bypass to allow staff to drain off condensate from the steam line.

5.3.1.3 Test Summary

The first test campaign with KCRC's Solvent-B was the first time the technology had been evaluated at the pilot scale, so a test plan was implemented to establish several performance characteristics of the solvent. As new information was gathered during the first day of testing, the initial test plan was discarded, and new test points were added.

The second test campaign focused on obtaining longer-term steady-state data at or near 90% CO_2 capture of coal-derived flue gas at 2.1–2.3 scmm (75–80 scfm). The initial test point called for operation at an L/G of approximately 6.1 L/scm (46 gal/Kscf), with stripper bottom temperatures near 102°C (216°F).

5.3.1.4 Solvent Performance

Data from the tests were gathered and reduced to identify periods of steady conditions in order to determine the effects of each variable parameter.

During operation of the test stand, each change in a system variable can have an effect on the performance of the solvent. To fully realize an effect from any particular variable, it is important to allow the system to come to an equilibrium state. Typically, the operating engineer allows the solvent to be cycled two to three times through the system after each variable change to ensure steady-state performance.

In the first test campaign with KCRC Solvent-B, test variables changed frequently. Often, the parameters were changed before the solvent was circulated through the system long enough to reach steady state.

Upon completion of the test, actual steady-state periods of testing were identified during data reduction by comparing the rates of change of several variables and functions, including L/G, stripper pressure, regeneration energy input, and CO_2 capture rate. Figures 5-3 and 5-4 show the real-time operation data for the two test campaigns. In Figure 5-3, CO_2 capture is highly variable, a result of rapidly changing test conditions. In Figure 5-4, CO_2 capture is much more stable, resulting from longer periods of steady-state testing.

5.3.1.4.1 Heat Duty and L/G vs. CO_2 Capture

During the first campaign, regeneration energy input for ≥90% capture ranged from 3.49 to 5.82 GJ/t CO_2 (1500 to 2500 Btu/lb CO_2), as shown in Figure 5-5. Because variable parameters were changed rapidly during the first test campaign, steady-state data were not collected for every test point. An effort was made during the second campaign to hold conditions for longer time durations to ensure the data generated were accurately representative of the solvent capabilities.

Figure 5-6 shows the results of the second test campaign for CO_2 capture when conditions were maintained for longer periods. At 90% CO_2 capture, regeneration energy input ranged from approximately 3.49 to 3.95 GJ/t CO_2 (1500 to 1700 Btu/lb CO_2). The results are consistent with the first test but show less variability. In Figures 5-5 and 5-6, error bars represent a 95% confidence interval.

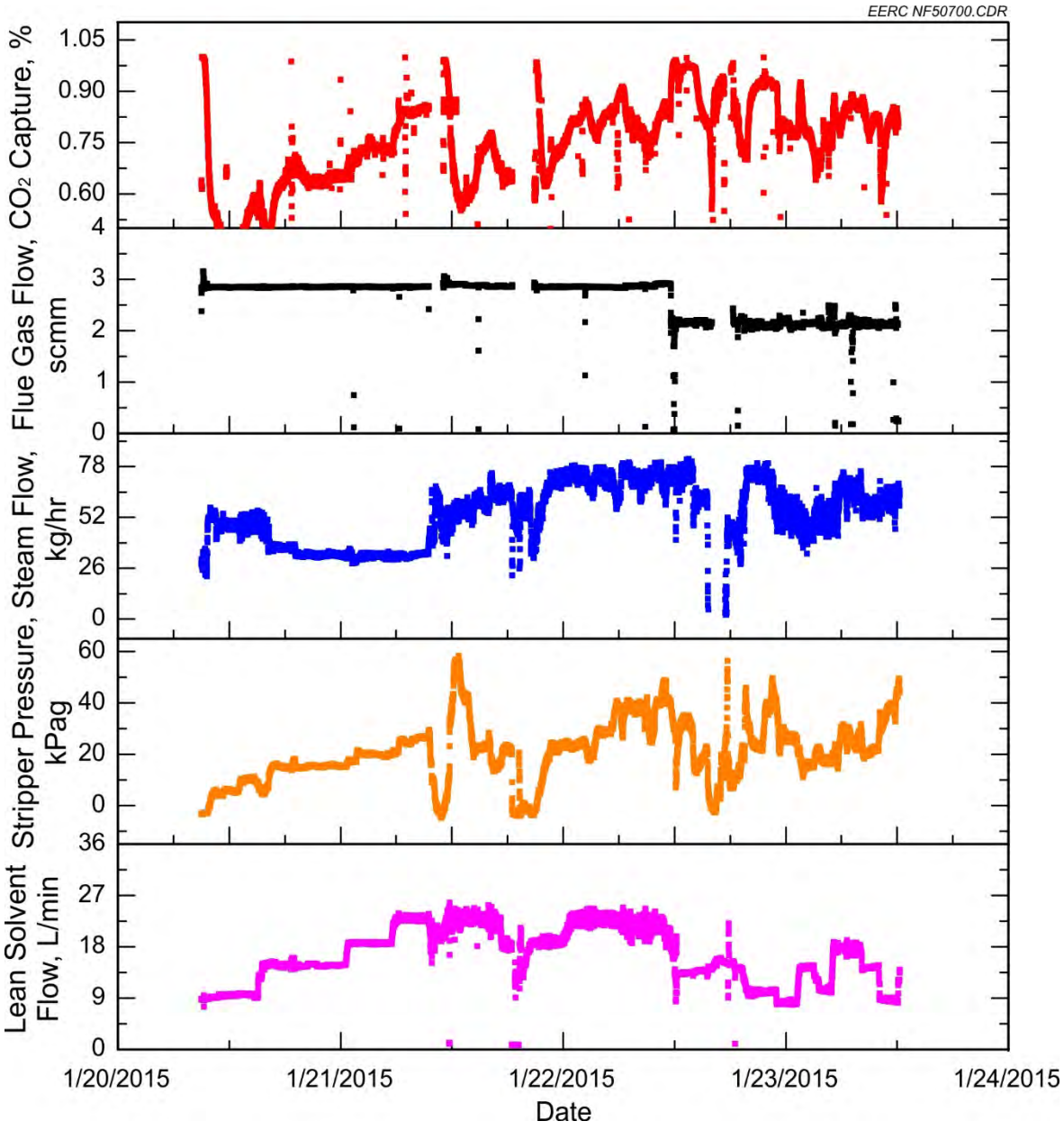

Figure 5-3. First test campaign operation data.

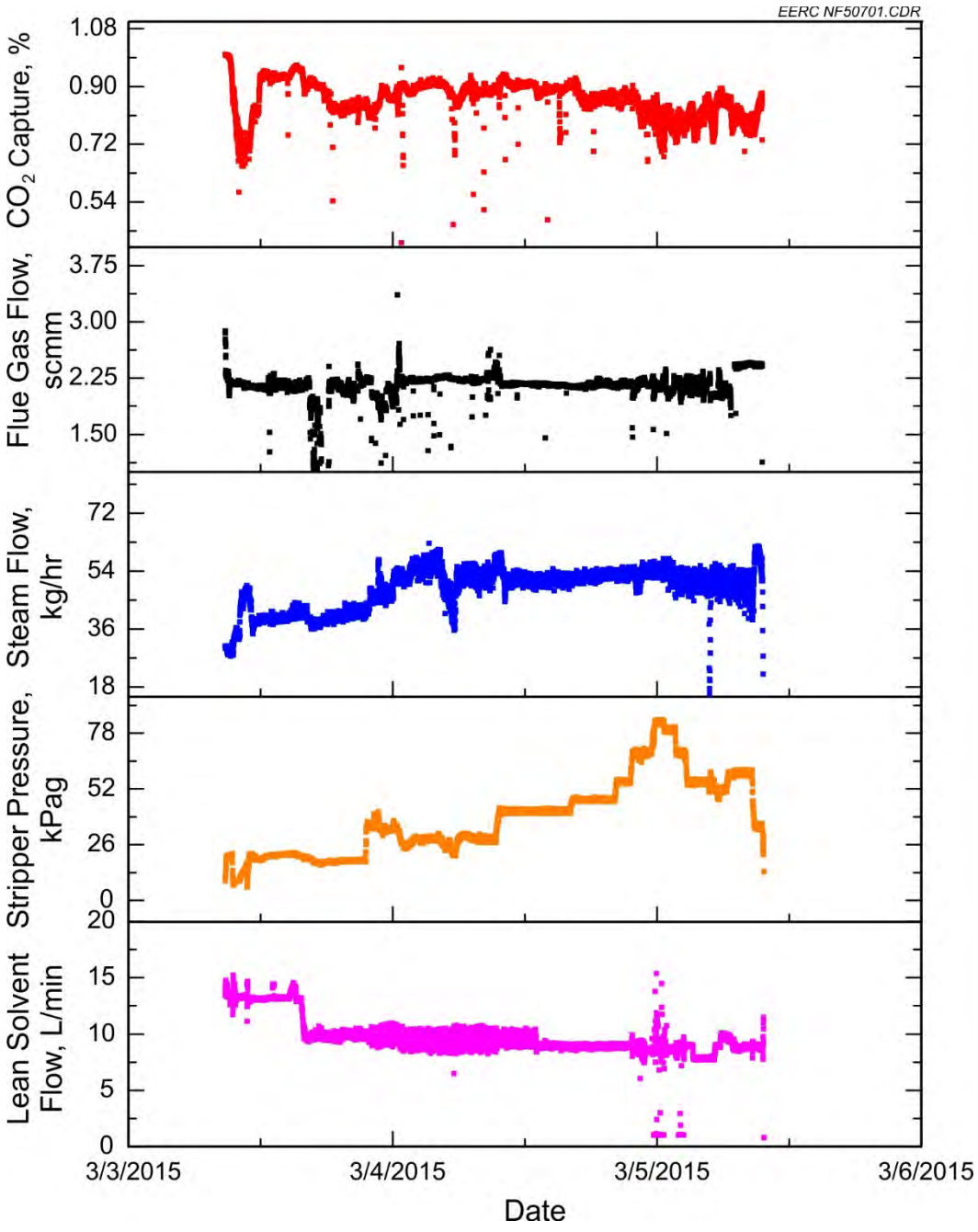

Figure 5-4. Second test campaign operation data.

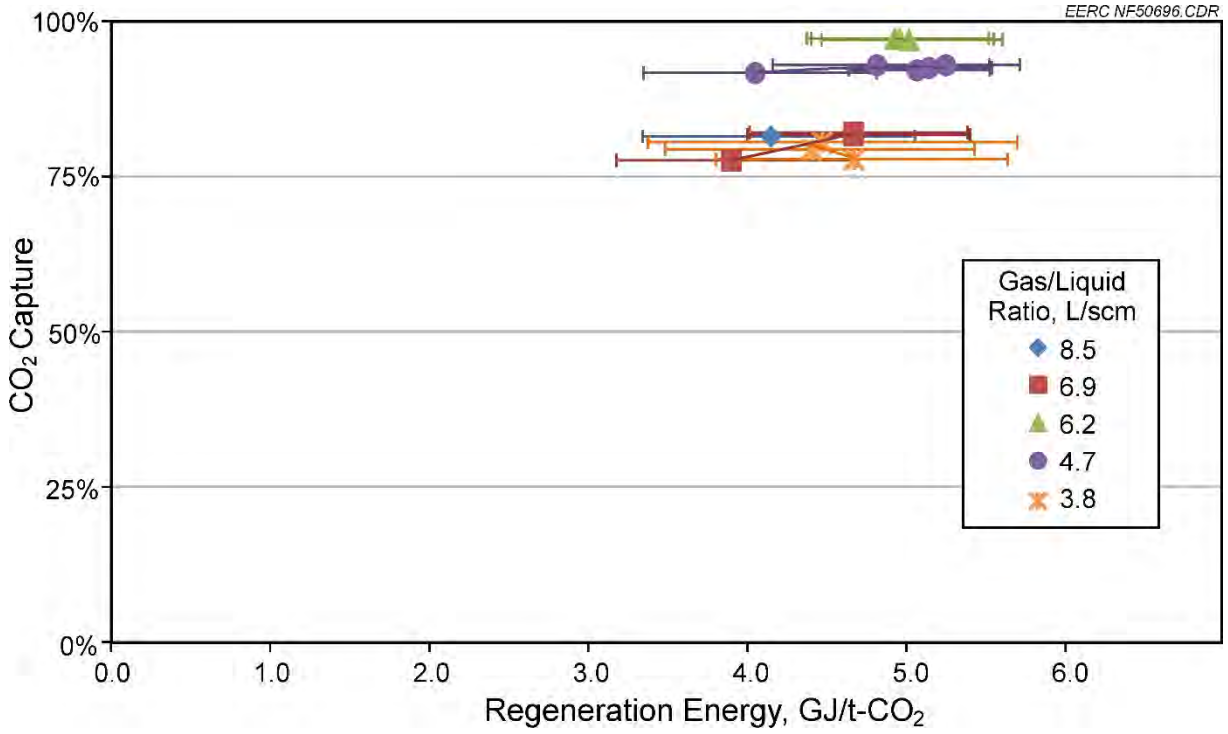

Figure 5-5. Test 1 data for CO_2 capture as a function of regeneration energy input and L/G.

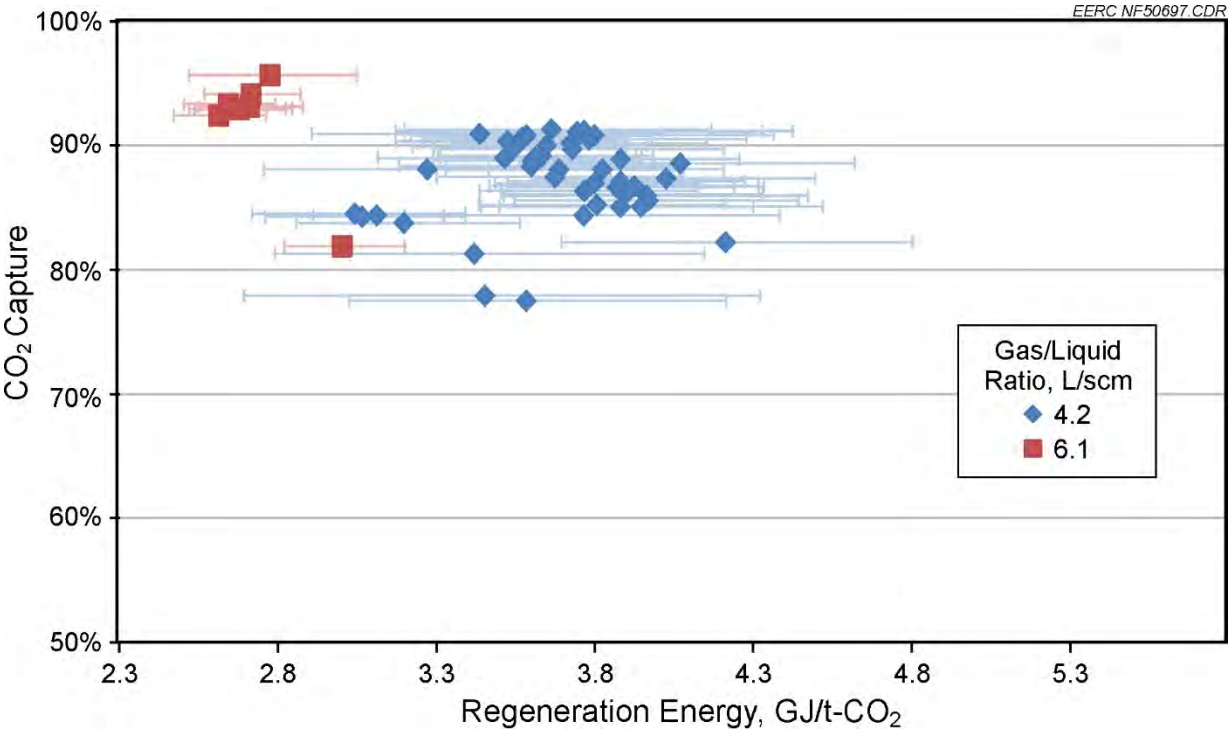

Figure 5-6. Test 2 data for CO_2 capture as a function of regeneration energy input and L/G.

The initial test point for the second campaign was run with a L/G of approximately 6.1 L/scm (46 gal/Kscf). CO_2 capture for that test point was approximately 93%, as shown in Figure 5-6.

Because the goal of the test was to explore the solvent performance at or around 90% capture, the L/G was reduced after running the experiment to approximately 4.1 L/scm (31 gal/Kscf). L/G was explored very little during the second KCRC Solvent-B test. Most data were gathered with solvent flow rate at approximately 9.5 L/min (2.5 gpm) and 2.1–2.3 scmm (75–80 scfm) flue gas flow, corresponding to a L/G of 4.1–4.3 L/scm (31–32 gal/Kscf).

5.3.1.4.2 Pressure Effects

Static pressure in the stripper column was shown to affect the regeneration rate and lean loading of the solvent. Stripper column static pressure is controlled with a pneumatically actuated valve located downstream of the reflux tank. With the valve fully open, the restriction in the product gas line caused by the control valve was enough to maintain pressure at 18.6–26.2 kPag (2.7–3.8 psig) under steady-state conditions.

As shown in Figure 5-7, system operation between 24.8 and 41.4 kPag (3.6 and 6.0 psig) in the stripper generally corresponded with CO_2 capture rates between 88% and 92% for KCRC Solvent-B. However, at pressures above 41.4 kPag (6 psig) in the stripper, CO_2 capture rates decreased to 85%–87%, even with increased regeneration energy input. It appeared that more gas was entrained in the liquid at the higher pressures, and pumping the mixed-phase lean solvent to the absorber became problematic.

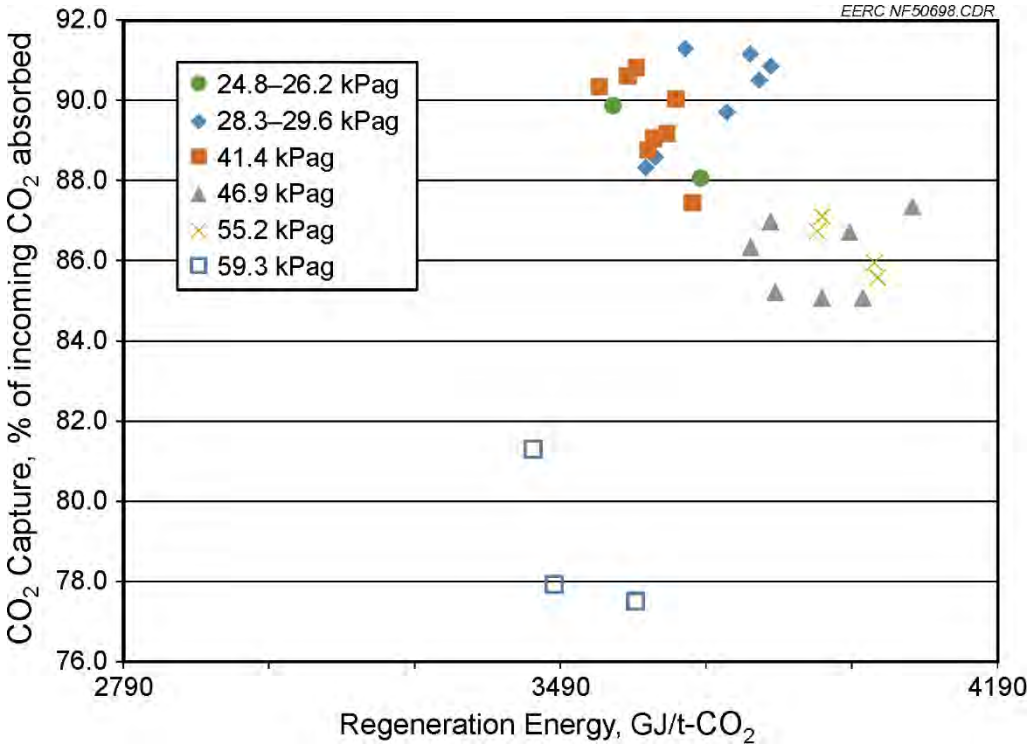

Figure 5-7. CO_2 capture as a function of regeneration energy input and stripper pressure.

5.3.1.5 Comparison to MEA

A common standard of comparison for postcombustion CO_2 capture technologies is 30 wt% MEA. The EERC has used MEA on the same test system as KCRC Solvent-B, so a direct comparison in performance can be made.

At 90% CO_2 capture, MEA required a L/G of approximately 53 and a regeneration energy input rate of approximately 5.2 GJ/t CO_2 (2243 Btu/lb CO_2). At the same capture rate, Solvent-B had a L/G of approximately 4.3 L/scm (32 gal/Kscf) and a regeneration energy input rate of about 3.6 GJ/t CO_2 (1561 Btu/lb CO_2). The data suggest that KCRC's Solvent-B performed as well as or better than MEA in the system, requiring a 40% lower L/G and 30% less regeneration energy to meet the same 90% capture benchmark. Table 5-2 illustrates the difference between MEA and Solvent-B.

Table 5-2. Solvent-B and MEA Regeneration Energy Requirement Comparison Summary

	Averaged Test Point Data		
	L/G (L/scm)	**GJ/t CO_2**	**CO_2 Capture**
KCRC Solvent-B	4.3	3.63	0.90
MEA	7.1	5.22	0.90
Solvent-B/MEA	**0.60**	**0.70**	**0.99**

5.3.1.5.1 Comparison to Literature-Reported MEA Performance

The pilot system at the EERC is significantly smaller than a utility-scale application and has inherent inefficiencies such as wall effects and heat losses that should be taken into account when extrapolating results to utility scale. Often, MEA performance results reported in the literature are used to compare data collected on the EERC test equipment. Typically, MEA regeneration energy reported in the literature is about 4.0 GJ/t CO_2 (1719 Btu/lb CO_2) (Galindo and others, 2012).

By using the literature-reported regeneration energy value for MEA, utility-scale regeneration energy requirement is estimated for KCRC Solvent-B in Table 5-3. The two solvents are assumed to exhibit the same performance ratios found at the pilot scale, as shown in Table 5-2.

Table 5-3. Solvent-B and MEA Regeneration Energy Requirement Utility Estimate

	Literature Comparison Estimate		
	L/G (L/scm)	**GJ/t CO_2**	**CO_2 Capture**
Utility Estimate MEA	7.1	4.0	0.90
Solvent-B/MEA	0.6	0.7	0.99
Utility Est. Solvent-B	**4.3**	**2.8**	**0.90**

The resulting estimate of regeneration energy for a utility-scale application is approximately 21% lower than the value generated on the pilot-scale equipment.

5.3.1.6 Sampling and Analysis

Samples of the lean and rich solvent streams were collected for each test point. During the first test campaign, each sample was analyzed for total inorganic carbon (TIC) and total organic carbon (TOC) content using the EERC's TIC/TOC analyzer. TIC and TOC analyses were used to determine CO_2 loading for lean and rich solvent streams. Select samples were also analyzed using Karl Fischer and acid/base titration methods to determine solvent concentration.

Sample analysis data for the second week of testing are included in Appendix B.

5.3.1.7 Results Summary

KCRC Solvent-B was used in the EERC's postcombustion capture system to capture CO_2 from coal-derived flue gas. Capture rates were determined by comparing real-time gas analyzer data from the absorber inlet and absorber outlet flue gas streams. Regeneration energy was provided to the stripper via a shell-and-tube heat exchanger, with steam as the heat source. Steam flow and temperatures in and out of the heat exchanger were measured to calculate total energy input.

CO_2 capture rates from 70% to 94% were observed, with steady-state data collected at several different test points. Solvent samples were collected periodically to check solvent concentration. Because the primary goal of the test was to show Solvent-B's ability to capture CO_2 at 90%, most of the test points were focused on obtaining data at or near 90% CO_2 capture rates.

One of the test goals was to determine an optimum operation condition for Solvent-B. It is difficult to definitively conclude that an optimum set of conditions for 90% CO_2 capture was achieved because of the limited scope of the test. However, at an average L/G of 4.3 L/scm (32 gal/Kscf), 90% CO_2 capture was established with a stripper pressure of 41.4 kPag (6 psig), a stripper bottom temperature of approximately 108°C (227°F), and regeneration energy input of approximately 3.6 GJ/t CO_2 (1562 Btu/lb CO_2). This combination of conditions represents the highest performance level of the solvent achieved during testing.

Pilot-scale results were used along with literature-reported values for MEA to estimate a utility-scale regeneration energy requirement for Solvent-B of 2.8 GJ/t CO_2 (1204 Btu/lb CO_2), 21% lower than the pilot-scale result.

Although L/G was not investigated thoroughly, CO_2 capture appeared to increase with higher L/G for a given regeneration energy input level.

KCRC's Solvent-B appears to perform as well as or better than 30 wt% MEA on the EERC test system. Comparing data collected for each solvent, Solvent-B achieved 90% capture with approximately 40% lower L/G and 30% lower regeneration energy input than MEA at the same capture level.

5.3.2 CO_2 Solutions Enzyme Solvent

CO_2 Solutions Incorporated, based in Québec City, Québec, Canada, has developed a platform for the capture of CO_2 from gas streams by employing a unique enzyme carbonic anhydrase which functions as a catalyst within a salt solution. This proprietary technology is involved with several test programs within Canada, and the opportunity arose for involvement in the PCO_2C Program to provide data on performance and benchmarking. Additional information about CO_2 Solutions can be found at www.co2solutions.com/en.

CO_2 Solutions joined the PCO_2C Program with the goal of conducting 3 weeks of testing on carbonate-based solvents provided by CO_2 Solutions. The testing comprised parametric-style and short-term tests applying various L/Gs to observe and measure the resulting CO_2 capture rates. The solvents required the stripping column to be run at a slight vacuum. A majority of the tests were run with natural gas-derived flue gas, with a few days set aside for determining performance with coal-derived flue gas.

The test program, being a first of its kind, was conducted by modifying the EERC's postcombustion capture system to accommodate CO_2 Solutions' process to operate under target commercial conditions. The nature of the program as the first-ever test of an enzyme-based carbon capture process at this scale was not without challenges. However, CO_2 Solutions' separate analysis showed that the enzyme in the process (known as "1T1," a proprietary carbonic anhydrase developed by CO_2 Solutions) remained stable during the test period, including during exposure to contaminants found in the coal-derived flue gas.

Overall, the CO_2 Solutions test program was successful, meeting objectives including no degradation in performance of the enzyme catalyst, no toxic waste products generated, and showing the ability to use low-grade heat for the process for significantly reduced carbon capture costs. The learnings were also valuable for a subsequent 8-tonne/day, 2500-hour demonstration run by CO_2 Solutions near Montreal, Canada, during the summer and fall of 2015.

5.3.2.1 Solvent-Specific System Modifications

The EERC's solvent-based postcombustion capture system was used for testing, but several modifications were made to accommodate the technology. Figure 5-8 shows a P&ID of the system with needed changes for testing of the solvents. The modifications included the following:

- A vacuum pump was installed to impart a negative gauge pressure on the stripper column.
- An on-demand hot-water system was installed to replace the steam heat system.
- A water recycle line was installed to bring water from the solvent heater back through the water heaters to supplement the cold-water feed. The heated water was supplied to both the existing reboiler heat exchanger and to a second heat exchanger provided by CO_2 Solutions.

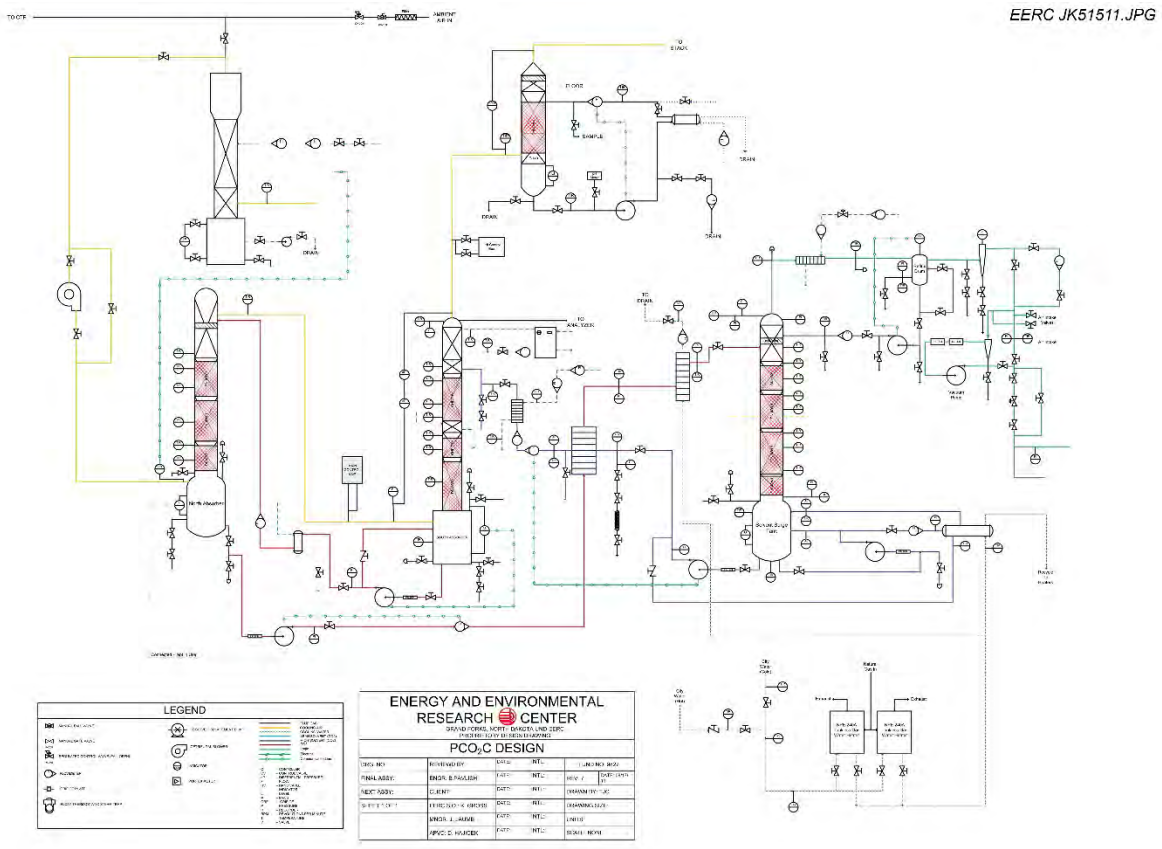

Figure 5-8. P&ID of the PCO_2C system as configured for the operation with CO_2 Solutions solvents.

- A heat exchanger, provided by CO_2 Solutions, was installed at the rich solvent inlet to the stripper column. Water flow to each exchanger was measured independently with separate flowmeters.

- Several new thermocouples were added in order to monitor the water-heating system.

- Prior to the final week of testing, a cable heater was installed on the water line at the inlet of the solvent heater in order to provide higher-temperature water than the water heaters alone could produce.

- An inline pH meter was installed downstream of the lean solvent cooler at the inlet to the south (top) absorber column. The pH meter measurements were monitored in real time and recorded in the data file.

5.3.2.2 Test Summary

CO_2 capture testing of CO_2 Solutions' solvents took place between December 1, 2014, and January 9, 2015. Several challenges were encountered in adapting the system to run the CO_2

Solutions solvent formulations and in carrying out the test plan. These challenges resulted in limited data being collected and greatly restricted the operability of the CO_2 Solutions formulations.

5.3.2.2.1 L/G Ratio and Gas Flow Limitations

CO_2 Solutions originally desired an L/G (kg solvent/kg treated flue gas) that was unattainable with the pump equipment already installed on the PCO_2C system. The pumps installed have a maximum flow rating of 30.3 L/min (8 gpm). The pumps were limited by several factors during testing, including erosion of the pump seals and blockages in the pump filter housings, leading to a maximum attainable pump rate of approximately 19–23 L/min (5–6 gpm). Pump seal erosion appeared to be attributed to inherent incompatibility of the pumps with the base solvent. Installation of new wear-resistant components in the pumps improved pump performance but did not maintain it. For larger test systems, these pumps would not be recommended. Filter blockages appeared to be from residue not removed by previous testing system cleaning from use with other solvents and were not indicative of this solvent's performance.

A gas flow rate of approximately 1.98 scmm (70 scfm) was used for testing on both coal and natural gas.

5.3.2.2.2 Maximum Temperature Limitation

The nature of some of CO_2 Solutions' solvent ingredients required system temperatures, including skin temperatures, below a certain temperature to maintain integrity. This limited the amount of regeneration energy available and is also the reason for modifying the system to use hot water as the heat-transfer media instead of steam. The existing shell-and-tube reboiler was not the correct configuration for this testing. A plate heat exchanger would have provided better performance. Temperatures of the flue gas and lean solvent streams into the absorber were controlled below the solvent integrity temperature limit for all test weeks. The temperature limitation allows for the consideration of waste heat sources for full-scale operation.

5.3.2.2.3 Water Flow Limitation

Water flow through the water-heating system was limited by pipe size and house water pressure. This flow restriction reduced the overall energy duty for solvent regeneration, much lower than the duty seen during amine-based solvent testing with steam with this system. This limited the CO_2 capture from the EERC system.

5.3.2.2.4 Vacuum Pump Operation Challenges

Throughout the first 2 weeks of testing, several challenges were noted in operating the vacuum pump to maintain partial vacuum in the stripper column. The vacuum pump installed had a much larger capacity than necessary for operating at the desired vacuum.

To compensate for the oversized vacuum pump, a valve was installed to allow the pump to pull from both the column and the external plant area. However, even with the intake valve, the

pump had to run at approximately 30 Hz, or 50% of full speed. This resulted in lower airflow through the pump's cooling fan and caused the vacuum pump to overheat. Several times during the first 2 weeks of testing, fuses for the vacuum pump were overloaded, causing temporary test interruptions.

By the end of the second week of testing, a serious leak had developed in the oil reservoir for the vacuum pump, and it was unable to maintain the same vacuum it had generated earlier in the test week.

These problems were overcome prior to the third week of testing. A second replacement pump was installed, the pump oil was flushed and replaced prior to testing, and a larger air intake valve was installed to allow the vacuum pump to run at nearly 60 Hz. The vacuum pump was completely functional for the third test week.

5.3.2.2.5 Analytical Challenges

There were two central analytical challenges during testing: consistent measurement of pH and analysis of solvent samples for carbon content. Values measured at the EERC did not fully agree with those measured by CO_2 Solutions. The issues were never fully resolved.

The inline pH meter on the test system measured the pH of the solvent prior to entering the absorption section of the system. The measurement from this meter informed operators of the condition of the solvent and stripping of the solvent as it flowed through the system. Samples of solvent were also taken and pH values measured by bench-top meters. It became clear over the first few days that the inline meter would not stay in calibration, even after several recalibration checks over many days. It was then decided to have the analytical laboratory take pH measurements of each solvent sample taken.

It was also discovered that some inconsistency remained in the measurements taken from the analytical laboratory. Several samples were measured more than once as their original values did not trend as expected. Repeat measurements yielded values that seemed more reasonable. The cause of this deviation was never discovered, and ultimately, it was decided that the samples be sent to CO_2 Solutions for final measurement. Figure 5-9 shows an example of the variation of pH measurement made at the EERC. Analytical lab measurements were of both rich and lean samples, yielding the double trends seen in the first measurement plot. pH was only used during testing to indicate significant change in solvent performance. Attempts at using the inline pH meter for relative change became suspect by the end of testing.

Carbon measurements from the TIC/TOC analyzer determined starting viability of the solvent and were used to periodically monitor the working capacity. However, CO_2 Solutions could not duplicate results measured by the EERC during the first weeks of testing. After extensive discussions between the EERC analytical lab manager and researchers from CO_2 Solutions, the discrepancy could not be resolved. It was then determined that TIC/TOC analyses be halted at the EERC and all samples would be sent to CO_2 Solutions for measurement. It was felt that CO_2 Solutions had all the prior knowledge of its solvent and measurement method experience, so it only made sense that its results would be more accurate.

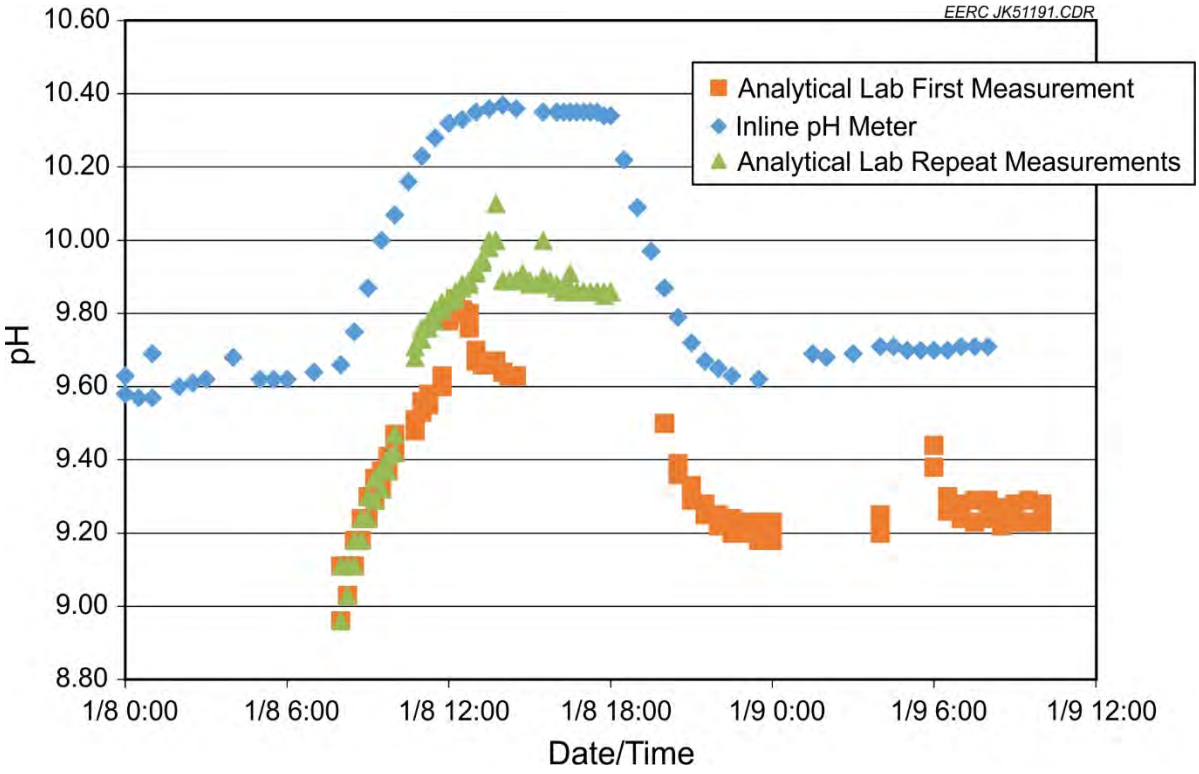

Figure 5-9. Differences in measured pH of solvent samples (data taken January 7–9).

5.3.2.2.6 Gas Analyzer Issues

Another challenge was the capture system inlet CO_2 gas analyzer. CO_2 concentration in the flue gas from firing natural gas can vary and typically runs in the range of 9.0% (dry) to 10.5% (dry). Variability is highly influenced by excess air in the system and unintended consequences due to maintenance performed on the system between projects. During the first 2 weeks of testing under natural gas-firing conditions the analyzer was reporting an inlet gas CO_2 concentration of approximately 10.4% (dry). During the final week of testing, the analyzer was measuring concentrations in the range of 8.9% (dry). All system checks, calibrations, and physical checks revealed no changes in the operation of the instrument. No physical changes or operational changes had been made to the performance of the furnace between Weeks 2 and 3, and maintenance performed was minimal because of ongoing project work. Another instrument provided a secondary check of the inlet CO_2 concentration during Week 3, and it agreed with the 8.9% value. Instrument checks against concentrations during coal firing found that it was measuring accurately. No explanations were found for the varying readings it provided during Weeks 1 and 2. O_2 concentration in the flue gas was elevated as compared to Weeks 1 and 2, which would lower the CO_2 concentration, but the difference explains the discrepancy, as flue gas composition is standardized to an O_2 concentration of 4.5% (dry). This makes direct comparison of CO_2 capture between weeks more difficult to conduct.

5.3.2.2.7 Solvent Buildup

Following testing, the system was drained and the solvent collected in barrels. After draining the solvent completely, the level gauge in the south absorber was still showing 11.4 cm (4.5 in.) of solvent. A flush of the south absorber tank was completed, and the large inspection port at the bottom of the column was removed. There was a significant buildup of solids left in the tank can. It should be noted that there was no solids buildup in the north column. Solvent residue buildup at the bottom of the south column over the course of the test could have reduced the ability of the solvent to capture CO_2. This phenomenon was a result of the south absorber tank geometry.

5.3.2.3 CSES Results Summary

The approach used for processing CO_2 capture testing data to determine capture performance and energy requirements for evaluation of capture technology involved the following primary steps: CO_2 capture estimation, steady-state determination, computation of stream averages and statistical variation, and capture energy calculation.

5.3.2.3.1 Calculated CO_2 Capture Equations

Estimated CO_2 capture was calculated using the volume fraction of gases measured at the absorber inlet and outlet, taking into account oxygen content from system air ingress. Assumptions included no air ingress between the measurements and no other constituents than CO_2 removed during capture. Equations 5.1–5.4 illustrate these assumptions; Table 5-4 provides the nomenclature. If CO_2 capture is the volume of CO_2 captured per volume of CO_2 input, then capture may be calculated using the measured volume fraction values in Equation 5.5.

If: $$(C_{inlet} + O_{inlet} + G_{inlet}) \cdot X_{inlet} = (C_{outlet} + O_{outlet} + G_{outlet}) \cdot X_{outlet} + C_{capture} \cdot X_{capture} \quad \text{[Eq. 5.1]}$$

$$C_{inlet} + O_{inlet} + G_{inlet} = C_{outlet} + O_{outlet} + G_{outlet} = C_{capture} = 1 \quad \text{[Eq. 5.2]}$$

$$C_{inlet} \cdot X_{inlet} = C_{outlet} \cdot X_{outlet} + C_{capture} \cdot X_{capture} \rightarrow = C_{inlet} \cdot X_{inlet} - C_{outlet} \cdot X_{outlet} \quad \text{[Eq. 5.3]}$$

$$O_{inlet} \cdot X_{inlet} = O_{outlet} \cdot X_{outlet} \rightarrow X_{outlet} = O_{inlet} \cdot X_{inlet}/O_{outlet} \quad \text{[Eq. 5.4]}$$

Then:

$$X_{capture}/(C_{inlet} \cdot X_{inlet}) = (C_{inlet} \cdot X_{inlet} - C_{outlet} \cdot X_{outlet})/(C_{inlet} \cdot X_{inlet}) = 1 - C_{outlet} \cdot X_{outlet}/(C_{inlet} \cdot X_{inlet}) = 1 - C_{outlet} \cdot (O_{inlet} \cdot X_{inlet}/O_{outlet})/(C_{inlet} \cdot X_{inlet}) = 1 - (C_{outlet}/C_{inlet}) \cdot (O_{inlet}/O_{outlet}) \quad \text{[Eq. 5.5]}$$

Table 5-4. Nomenclature for Equations 5.1–5.5

Symbol	Description
X_n	Gas flow rate for given absorber stream, scfm
C_n	Carbon dioxide volume fraction for given absorber stream
O_n	Oxygen volume fraction for given absorber stream
G_n	Trace gases volume fraction for given absorber stream

5.3.2.3.2 Steady-State Determination

Steady-state conditions were identified for four primary streams within the EERC CO_2 capture testing system: solvent, hot water, flue gas, and capture rate. Steady state was defined as remaining within the average variation of the set point for a minimum of 5 min. The typical noise or range in the recorded data was determined for each stream; when this variation was significant, a moving average was calculated as well. The average over the identified steady-state interval was also calculated to ensure consistency with the set point and that all data remained within the determined variation. An interruption of steady state <1 min was allowed, provided >5 min of steady state was determined to occur prior to and following the deviation, which was not included in the estimated average.

Because CO_2 capture is a result as opposed to a controlled parameter, the rate of change was calculated to identify steady-state periods. The typical noise or range in the volume fraction data and thus calculated capture were also determined, and when variation was significant, a moving average was calculated. An average capture value was then estimated over an identified period when rate of change was minimal.

Steady state was then defined as remaining within the determined variation of this average capture value for a minimum of 5 min. This is the standard process used for all solvents tested at the EERC. Steady-state intervals were then further refined as periods when all four streams (solvent, hot water, flue gas, and capture) were determined to be at steady state. Only intervals longer than 5 min are considered significant.

5.3.2.3.3 System Steady-State Averages and Statistical Variation

The averages and variation of pertinent data were calculated across the identified, significant steady-state intervals. These included solvent, hot water, and flue gas flow rates; CO_2 volume fraction into and out of the absorber and capture; and hot water and condensate temperatures into and out of the absorber, respectively. Statistical variation was estimated using a factor of 1.96 times the calculated standard deviation of the data over the steady-state intervals for each stream, representing the 95% confidence limits.

5.3.2.3.4 Capture Energy Calculations

Regeneration energy was estimated as the heat transferred per pound of CO_2 captured during an identified steady-state interval. Heat transfer was calculated using the determined steady-state averages for hot-water flow rate and hot-water and condensate temperatures. The energy content of hot water and condensate using respective temperatures and published tables (Smith and others, 1996) was estimated. Heat transfer was then calculated as the change in energy between hot water and condensate based on hot-water flow. Mass of CO_2 captured was converted from the calculated volumetric flow rate (i.e., using the determined steady-state averages for CO_2 volume fraction and flue gas flow rate). Previously calculated variation was also incorporated into the regeneration energy calculations to generate 95% confidence intervals of the results.

5.3.2.3.5 CO_2 Loading in the Solvent

The CO_2 loading (α) in the carbonate solvent is defined as follows:

$$\propto = \frac{mole\ of\ CO_2\ in\ carbonate\ solvent + mole\ of\ CO_2\ in\ bicarbonate\ solvent}{mole\ of\ carbonate\ salt^+} \quad \text{[Eq. 5.6]}$$

The definition yields a lower limit with no CO_2 content in the solvent, to 1.0, indicating fully loaded solvent in which all of the carbonate solvent has been converted into bicarbonate solvent.

5.3.2.3.6 Free Enzyme Concentration

CO_2 capture increased with the addition of CO_2 Solutions' proprietary enzyme. CO_2 capture was measured at 7% for the base solvent without the enzyme, and CO_2 capture was measured at up to 40% for the highest tested concentration of enzyme.

Because of the limited availability of hot water, a maximum of 50–60 MJ/hr (47,400–56,900 Btu/hr) was available for regenerating the solvent. Hot-water flow was split between the heat exchanger at the stripper inlet and the reboiler. Tests helped determine that the stripper inlet heat exchanger did not contribute significantly to CO_2 removal. The duty of the reboiler alone was 20–40 MJ/hr (19,000–37,900 Btu/hr). In comparison, the duty available with steam injection with the EERC test system is typically 100–160 MJ/hr (94,800–152,000 Btu/hr) for testing with amines.

This lower available duty with hot water versus the duty available for amine-steam testing has resulted in a limited stripping capacity. The targeted loading of the lean solvent approached but did not reach the desired goal because of the hot-water flow rate limitation.

5.3.2.3.7 Immobilized Enzyme Concentration

While low hot-water flow rate was certainly a limiting factor in CO_2 capture, it looks as if the percentage of CO_2 captured is lower with the immobilized enzyme when compared to the free enzyme at an equivalent enzyme concentration. This is potentially due to particle settling at the bottom of the columns during testing of the immobilized enzyme solvent. As the immobilized enzyme was initially added, the CO_2 capture percentage increased. However, capture performance began to decrease as the immobilized enzyme addition continued. It is possible that settling of some of the solvent at the base of the south column eventually counterbalanced the addition. The design of a process handling this immobilized enzyme would require column bottoms with properly adapted shapes and liquid draw-offs to avoid particle accumulation in low-velocity areas.

5.3.2.3.8 Effect of the Solvent Additive

An additive was used to validate the increase in vapor–liquid equilibria (VLE) properties of the solvent while containing a certain quantity of free enzyme. CO_2 Solutions wishes to keep the name of the additive confidential. This additive is supposed to increase the partial pressure of CO_2 in the stripper and decrease it in the absorber in order to improve the performance of the capture cycle. Testing indicated that CO_2 capture increases by a small percentage after initial addition of the additive, and as the additive concentration was increased, CO_2 capture also increased.

6.0 PRECOMBUSTION CO_2 CAPTURE TESTING

6.1 Introduction

In order to facilitate the use of hydrogen in integrated gasification combined-cycle (IGCC) applications or as a transportation fuel, hydrogen-from-coal technologies that are capable of managing carbon will be needed. Many technologies are under development for the separation of hydrogen from coal-derived syngas, and among the most promising are hydrogen separation membranes. Studies indicate a significant IGCC plant efficiency increase can be realized if warm-gas cleanup and hydrogen separation membranes are used in the place of conventional technologies. These membranes provide the potential to produce hydrogen while simultaneously separating carbon dioxide at system pressure. Membrane development activities need to take into account the impact of coal-derived impurities. Gasification syngas typically has many impurities that, if not removed, will poison most hydrogen separation materials. In order to commercialize this promising technology, scale-up to bench- and pilot-scale gasifiers is required so that the impact of impurities can be evaluated.

The work at the EERC focused on the testing of the Commonwealth Scientific and Industrial Research Organisation's (CSIRO) hydrogen separation membranes for purifying hydrogen from coal-derived syngas. CSIRO provided nine palladium–vanadium metal membranes that were tested on syngas produced in the EERC's fluidized-bed gasifier (FBG). These were the first tests of CSIRO's membranes on actual coal-derived syngas. The EERC's hydrogen membrane test system (HMTS) was used as the platform for testing the membranes. The goal of the project was to conduct tests with coal-to-hydrogen production technology using warm-gas cleanup techniques and CSIRO's hydrogen separation membranes. The FBG and warm-gas cleanup system were configured to facilitate testing in conjunction with the HMTS. The data derived will be used to support CSIRO's efforts in developing hydrogen separation membranes.

6.2 Background

Five main types of membranes are currently under development: dense polymer, microporous ceramic, porous carbon, dense metallic, and dense ceramic (Kluiters, 2004). Of these types, dense metallic and dense ceramic have the highest hydrogen selectivity. Dense metallic membranes also have very high hydrogen flux rates, making them potential candidates for large-scale commercial application if poisoning issues can be overcome. Palladium is the typical base metal for metallic membranes, and alloy combinations such as Pd–Cu, Pd–Au, and Pd–Ag have been tested. Many other formulations exist, but most are closely guarded trade secrets.

Two main applications for hydrogen separation membranes employed at large scale are envisioned. Large-scale hydrogen production facilities could provide fuel for fuel cell vehicles. Power generation facilities with CO_2 capture could employ hydrogen separation membranes to reduce the cost of separation. Both scenarios are likely to employ coal gasification to produce the hydrogen.

6.2.1 Membranes for Hydrogen Production for Transportation Applications

DOE views hydrogen as an energy carrier of the future because it can be derived from domestic resources that are clean and abundant and because hydrogen is an inherently clean fuel. According to DOE, the deployment of hydrogen technologies could lead to the creation of 675,000 green jobs in the United States (U.S. Department of Energy, 2008a). Coal gasification plants can separate hydrogen from the synthesis gas, purify the carbon for storage, and burn the hydrogen to produce power in an IGCC configuration. In this type of configuration, the only major emission from the plant is water. Hydrogen can also play a key role as a transportation fuel. If all vehicles in Los Angeles were converted to hydrogen, the urban smog problems would be virtually eliminated. Hydrogen fuel cell technologies have undergone rapid development over the past decade, and the technology exists today to produce commercial hydrogen fuel cell vehicles that have a transportation range of up to 280 miles (Ellis, 2008). The primary challenges that remain today are the economical production of hydrogen; the economical production of fuel cell vehicles; and the development of hydrogen transportation, storage, and dispensing infrastructure.

The National Hydrogen Association views hydrogen as the best pathway to both reduce oil consumption in the United States and reduce transportation-based CO_2 emissions. Figure 6-1 compares three different vehicle market penetration scenarios for light-duty vehicles (Holmes, 2008). The bar on the left represents 100% gasoline internal combustion engines, the middle bar represents market penetration for plug-in hybrid electric vehicles, and the bar on the right represents hydrogen fuel cell vehicles. Each scenario is compared to the annual oil consumption for that time period. It can be seen that if nothing changes and the United States continues to rely solely on gasoline-powered vehicles, the annual oil consumption is predicted to increase from 4 billion barrels per year (bby) to over 7 bby by the year 2100. With a significant market penetration of plug-in hybrid vehicles, oil consumption can be reduced to about 2.5 bby by 2100. However, with 98% market penetration of fuel cell vehicles, dependence on oil is virtually eliminated. While the future of transportation will certainly be a mix of several technologies, this graph illustrates that hydrogen is one of the only pathways toward eliminating the use of oil.

Figure 6-2 shows a similar set of scenarios, but compares the market penetration with annual CO_2 emissions from vehicles (Holmes, 2008). It should be noted that the study assumes hydrogen production is occurring with CCS or hydrogen is supplied from a renewable source. The graph shows that CO_2 emissions from vehicles will almost double by the year 2100 if gasoline vehicles are continued to be used exclusively. A reduction in CO_2 emissions is achieved if the course of plug-in hybrid vehicles is followed. However, with the fuel cell vehicle scenario, CO_2 emissions are reduced by over 80% in the year 2100. This illustrates that hydrogen is a potential fuel pathway in a carbon-constrained world. Increased production of natural gas and coal will be needed to meet these targets, and the data assume that the hydrogen production facility is equipped with carbon capture technology.

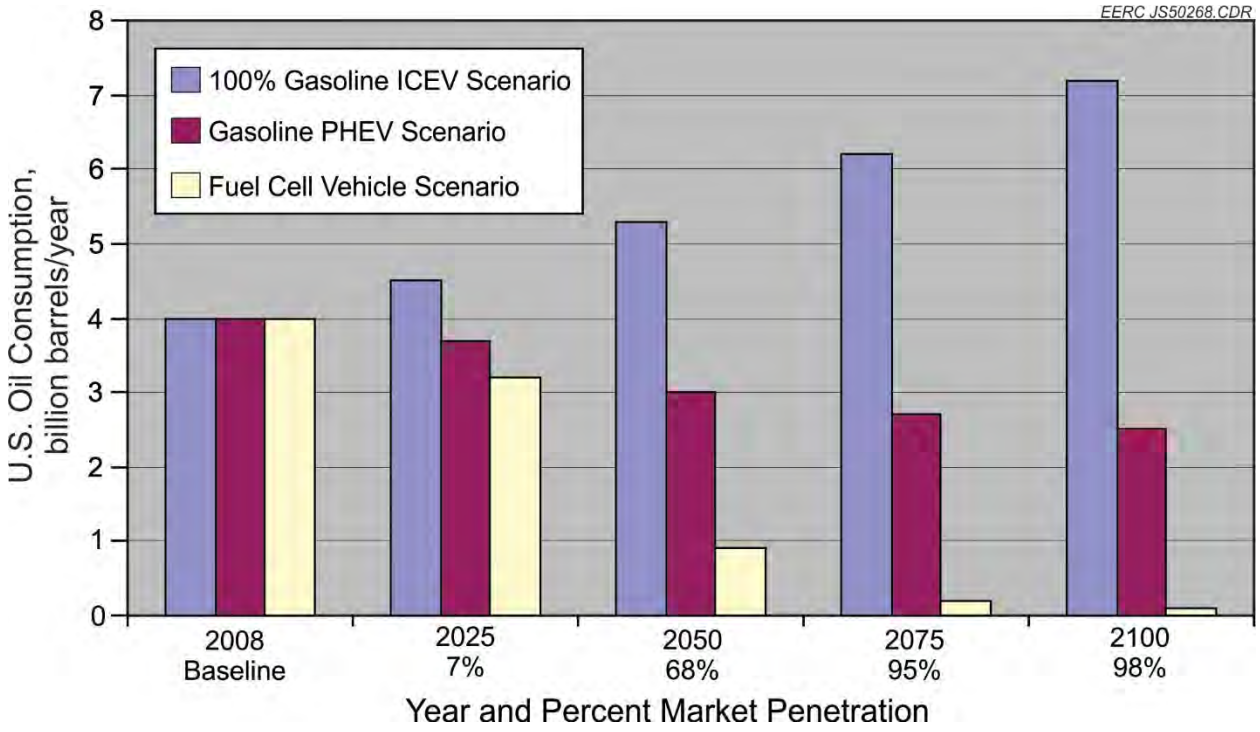

Figure 6-1. U.S. oil consumption for various vehicle scenarios (Holmes, 2008) (ICEV is internal combustion engine vehicle, and PHEV is plug-in hybrid electric vehicle).

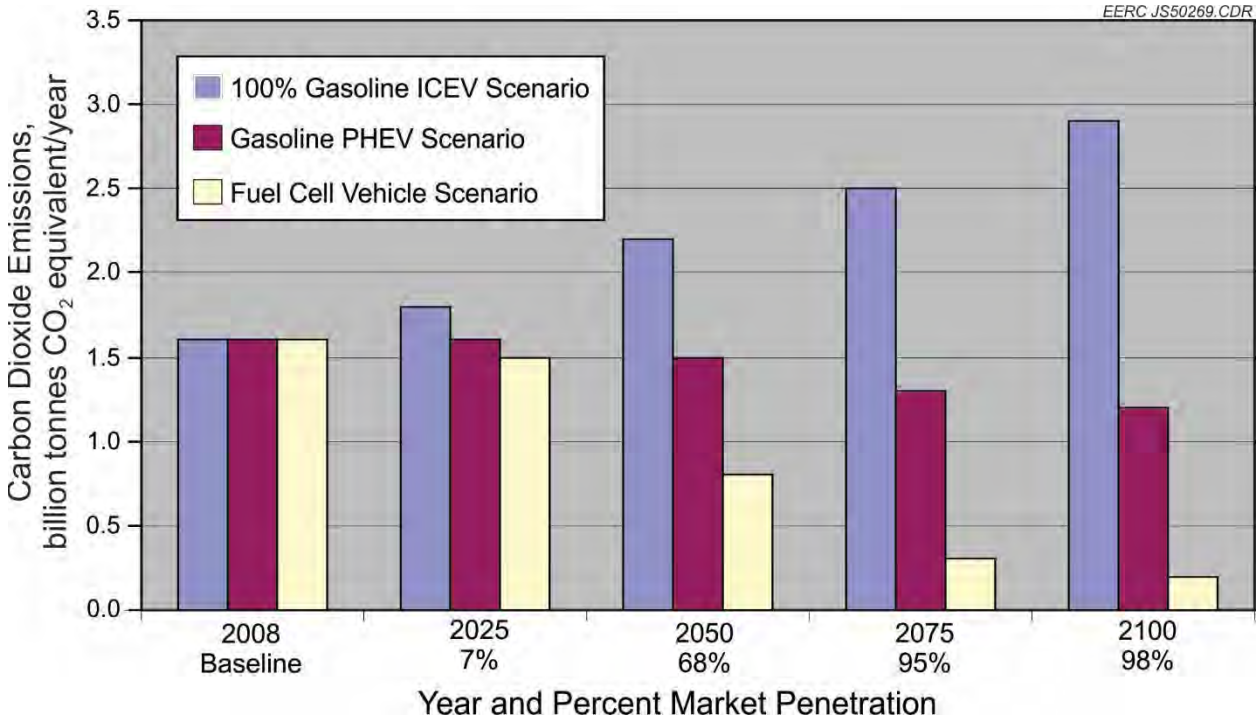

Figure 6-2. CO_2 emissions for various vehicle scenarios (Holmes, 2008).

6.2.2 Membranes Integrated with Power Systems

Coal gasification is of significant interest to the future of power generation in the United States because it can be performed more efficiently and with fewer emissions than conventional combustion. IGCC systems fire the syngas produced directly in a gas turbine and recover the heat produced, resulting in more efficient conversion of energy to electricity than a conventional steam cycle. Currently, gasification systems produce electricity at a higher cost than conventional combustion systems. One significant advantage of gasification over combustion is the ability to capture CO_2 at a much lower cost and energy penalty. The CO_2 in gasifier syngas streams is at much higher concentration and typically at elevated pressure; therefore, less energy is required to perform the separation. When the cost of CO_2 capture is considered in the overall capital and operating cost of a power system, gasification units can have advantages in the cost of electricity (COE) over conventional combustion. Figure 6-3 compares the COE for gasification versus conventional power systems with and without CO_2 capture (Black, 2010). The figure shows that for conventional power systems, the COE is significantly less if CO_2 capture is not required. In the cases where CO_2 capture is needed, the IGCC plant produces electricity at a lower cost than the pc systems. The cost of natural gas combined cycle (NGCC) is heavily dependent on the price of natural gas. With recent natural gas prices as low as $2/MMBtu, the current cost of NGCC is significantly lower than the competing technologies.

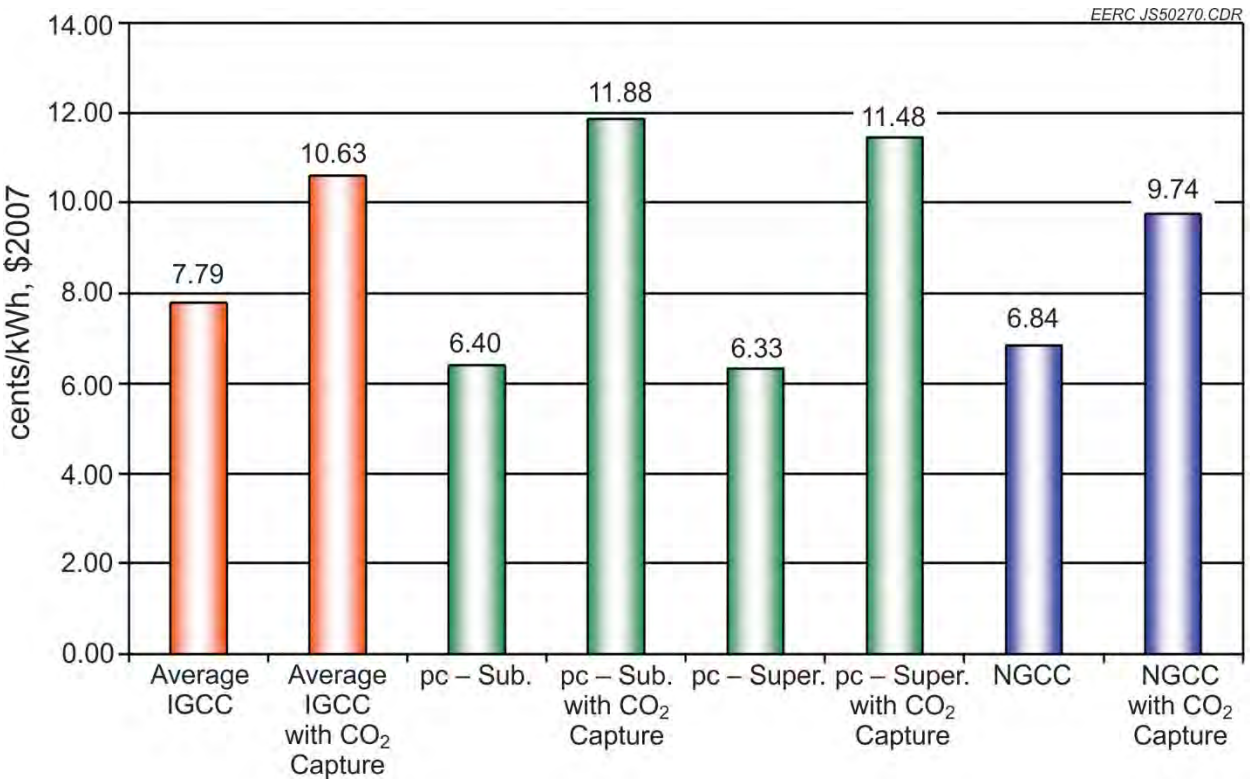

Figure 6-3. Comparison of COE for gasification vs. conventional systems with and without CO_2 capture (Black, 2010).

The cost of gasification with CO_2 capture utilizing technologies that are commercially available today is still relatively high compared to COE production with no capture. Advanced technologies are needed to further reduce the costs of capture and improve the overall efficiency of the plants. Several critical research pathways and technologies have been identified by the DOE National Energy Technology Laboratory (NETL) that will greatly improve the efficiency of gasification-based power systems. Figure 6-4 depicts the technology advancements and the incremental increase in net plant efficiency if each technology is implemented (Gerdes, 2010). The figure indicates that the technology with the highest potential for reducing the cost of gasification systems is hydrogen and CO_2 separation using hydrogen selective membranes. According to NETL, the implementation of membrane technology can result in a nearly 3% efficiency point increase for a gasification system over using a conventional Selexol process. If all of the advanced pathway technologies are realized, the efficiency of an IGCC system with hydrogen separation membrane technology and CO_2 capture and compression could reach 40%. Advanced gasification fuel cell (AGFC) technologies could push the efficiency over 50%.

EERC JS50271.CDR

Case Title	Efficiency (% HHV)	Delta* Efficiency (% points)	TPC** (S/kW)	Delta* TPC** ($/kW)	20-yr Leveraged COE (¢/kW-hr)	Delta* COE (¢/kW-hr)
Reference IGCC	30.4	0	2718	0	11.48	0
Adv. "F" Turbine	31.7	1.3	2472	-246	10.64	-0.84
Coal Feed Pump	32.5	0.8	2465	-7	10.54	-0.10
85% CF	32.5	0.0	2465	0	10.14	-0.40
WGCU/Selexol	33.3	0.8	2425	-40	10.00	-0.14
WGCU/H_2 Membrane	36.2	2.9	2047	-378	8.80	-1.20
AHT-1 Turbine	38.0	1.8	1855	-192	8.14	-0.66
ITM	38.3	0.3	1724	-131	7.74	-0.40
AHT-2 Turbine	40.0	1.7	1683	-41	7.61	-0.13
90% CF	40.0	0.0	1683	0	7.36	-0.25
IGCC Pathway		+9.6% pts (+32%)		-1035 (-38%)		-4.12 (-36%)
Advanced IGFC	56.3	+26% pts +85%	1759	-959 (-35%)	7.45	-4.03 (-35%)

* Delta shown is the incremental change as each new technology is added to previous case configuration.
** TPC is reported in January 2007 dollars and excludes owner's costs.

Figure 6-4. Advanced gasification pathways toward improving efficiency and reducing the COE for IGCC systems (Gerdes, 2010).

6.2.3 Coal Gasification Fundamentals

Coal gasification is a process in which coal is reacted with steam and oxygen at temperature and pressure to form H_2 and carbon monoxide. Pressures can range from atmospheric pressure to 8.27 MPa (1200 psi), and temperatures range from about 649° to over 1593°C (1200° to over 2900°F). Besides the typically desired products, H_2 and CO, many other by-products are formed during gasification such as CO_2, CH_4, H_2S, COS, HCl, NH_3, higher hydrocarbons, tars and oils, and particulate matter. The biggest challenge with any gasification system is dealing with the inorganic components in the coal and matching gasifier design to fuel-specific properties and desired end products. Gasifiers are typically configured as fixed beds, fluidized beds, moving beds, or entrained flow. Each gasifier type has strengths and weaknesses depending on the fuel used and the desired end products.

Entrained-flow gasifiers operate at very high temperatures and pressures, usually exceeding 1482°C (2700°F) and 4.14 MPa (600 psig). Systems are either up-fired or down-fired, and the gasifier operates like a plug-flow reactor, with the pulverized solids entrained in the gas stream. Residence times are on the order of seconds. The main advantage of entrained-flow gasifiers is that the high temperature results in the destruction of heavy organic materials, light aromatics, and hydrocarbons including methane. Carbon conversions of low-reactivity, high-rank coals and petroleum coke can exceed 99%, and most entrained-flow gasifiers are designed for high-rank fuels. The inorganic components are melted in the high-temperature environment and flow out of the gasifier as liquid slag. The elevated temperature results in lower cold gas efficiencies (CGEs) with entrained-flow gasifiers, and most gasifiers average near 80% CGE. Entrained-flow gasifiers are commercially available today and are backed by large companies such as Shell, GE, Siemens, and CB&I.

FBGs operate with a fluidized bed of unconverted carbon and inorganic particles, typically sized to approximately 1.9 mm (0.075 in). Solids residence times are typically 0.5 to 2 minutes. The temperature of the system is kept below the ash-melting point, usually below 871°C (1600°F), and the systems typically operate at elevated pressure. These systems are well-suited for high-reactivity, low-rank fuels. Fluid beds can produce high levels of tars and organic materials and can achieve CGEs of 90% and carbon conversions over 95%. Commercial systems include the High-Temperature Winkler offered by ThyssenKrupp and the U-Gas technology developed by the Gas Technology Institute and licensed to Synthesis Energy Systems.

Fixed-bed gasifiers operate with a bed of larger coal particles, ranging from 1.3 to 5.1 cm (0.5 to 2 in.) in size. Both slagging and nonslagging fixed beds have been developed. Depending on the operating conditions, fixed beds can produce high levels of tars, organics, and methane. The low temperature and relatively simple operation of nonslagging systems can lead to high CGEs and low-cost operation. The Lurgi gasifier offered by Air Liquide is currently deployed commercially at Sasol in South Africa and the Great Plains Synfuels Plant in North Dakota.

For the purposes of this test program, syngas was produced from a small pilot-scale entrained-flow gasifier and FBG. These systems were chosen because they are commercially available and tend to produce less methane than fixed-bed gasifiers. While methane is not expected

to harm membrane materials, elevated levels in syngas reduce the overall capture efficiency of an IGCC facility.

Coal gasification had taken on a renewed interest in recent years because of the rising price of oil and pending carbon legislation. Falling natural gas and oil prices over the last 2 years have made recent deployment and financing of gasification technologies more difficult. Historically, studies have shown that if CCS is required, IGCC plants will have a significant cost advantage over conventional pc boilers with retrofit carbon capture (Klara, 2006; Sondreal and others, 2006). However, the most recent studies have stated that the costs may be similar between the two technologies, especially when considering ultrasupercritical boilers (Gerdes, 2009; Hoffman, 2009; Plunkett, 2009). At this point, it is difficult to accurately estimate the cost of carbon capture from a pc power plant because no commercially available technology exists. Therefore, these studies must be reevaluated once technologies are commercially available.

6.2.4 Gas Cleanup Fundamentals

Conventionally, cold-gas cleanup methods have been employed to remove contaminants from coal gasification syngas streams. Methods such as Rectisol® or Selexol are commercially available and do a very good job removing contaminants but are also very costly from a capital and operational perspective. Significant economic benefits can be realized by utilizing warm- or hot-gas-cleaning techniques. DOE has stated thermal efficiency increases of 8% over conventional techniques can be realized by integrating warm-gas cleanup technologies into IGCC plants (Klara, 2006). Hydrogen separation membranes typically operate at warm-gas cleanup temperatures, so they are a good match for IGCC projects looking to employ warm-gas cleanup and carbon capture.

Work has been performed at the EERC in conjunction with DOE to develop methods to remove contaminants from syngas to levels suitable for a hydrogen separation membrane. The warm-gas cleanup train is capable of removing sulfur, particulate, chlorine, and trace metals including mercury at temperatures above 204°C (400°F). All of the technologies utilized are considered either commercial or near-commercial in development. One such test involved gasification of Texas lignite in the EERC's transport reactor development unit (TRDU), with a slipstream of gas being sent to the warm-gas cleanup train (Stanislowski and Laumb, 2009). Figure 6-5 shows the test setup and a sampling of the results from the test.

Sulfur in the form of hydrogen sulfide and carbonyl sulfide was removed in a transport-style gas–solid contactor at temperatures between 316° and 538°C (600° and 1000°F). The system was capable of reducing sulfur to single-digit ppm levels in the syngas. Particulate was removed in a hot-gas filter vessel (HGFV) that provided near-absolute filtration using candle filters. Mercury and trace elements were removed with a proprietary sorbent. A high-temperature water–gas shift (WGS) catalyst significantly increased the hydrogen concentration in the gas stream, while reducing CO. A sulfur-polishing bed removed hydrogen sulfide to concentrations below 0.2 ppm. A chlorine guard bed was used in front of the low-temperature WGS catalyst to prevent poisoning. CO was reduced to 0.1% in a low-temperature shift bed, and hydrogen was maximized. If the system were run under oxygen-fired conditions, the resulting syngas would have had combined H_2 and CO_2 levels greater than 90%. After passing through the cleanup train, the syngas was ready for hydrogen and CO_2 separation in a hydrogen separation membrane.

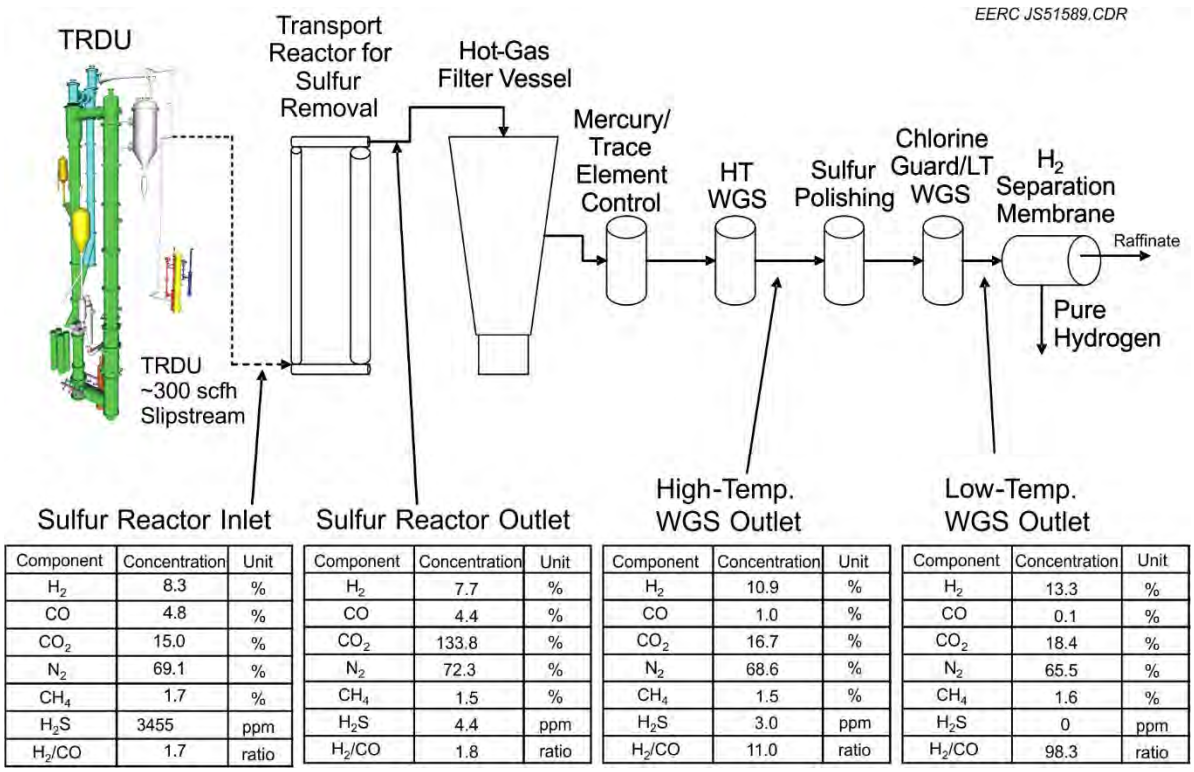

Component	Concentration	Unit
H_2	8.3	%
CO	4.8	%
CO_2	15.0	%
N_2	69.1	%
CH_4	1.7	%
H_2S	3455	ppm
H_2/CO	1.7	ratio

Component	Concentration	Unit
H_2	7.7	%
CO	4.4	%
CO_2	133.8	%
N_2	72.3	%
CH_4	1.5	%
H_2S	4.4	ppm
H_2/CO	1.8	ratio

Component	Concentration	Unit
H_2	10.9	%
CO	1.0	%
CO_2	16.7	%
N_2	68.6	%
CH_4	1.5	%
H_2S	3.0	ppm
H_2/CO	11.0	ratio

Component	Concentration	Unit
H_2	13.3	%
CO	0.1	%
CO_2	18.4	%
N_2	65.5	%
CH_4	1.6	%
H_2S	0	ppm
H_2/CO	98.3	ratio

Figure 6-5. Gasification and gas cleanup process diagram with test results (Stanislowski and Laumb, 2009).

6.2.5 Conventional Hydrogen Separation Processes

The most commonly employed method used today for hydrogen separation is a process called pressure swing adsorption (PSA). PSA technology is based on an adsorbent bed that captures the impurities in the syngas stream at higher pressure and then releases the impurities at low pressure. Multiple beds are utilized simultaneously so that a continuous stream of hydrogen may be produced. This technology can produce hydrogen with purity greater than 99.9% (Stocker and others, 1998). Temperature swing adsorption is a variation on PSA, but is not widely used because of the relatively long time it takes to heat and cool sorbents. Electrical swing adsorption has been proposed as well, but is currently in the development stage. Cryogenic processes also exist to purify hydrogen, but require extremely low temperatures and are, therefore, very expensive (Adhikari and Fernando, 2006).

6.2.6 Principles of Hydrogen Separation Membranes

Most hydrogen separation membranes operate on the principle that hydrogen selectively penetrates through the membrane because of the inherent properties of the material. The mechanism for hydrogen penetration through the membrane depends on the type of membrane in question. Most membranes rely on the partial pressure of hydrogen in the feed stream as the driving force for permeation, which is balanced with the partial pressure of hydrogen in the permeate stream. Kluiters (2004) has categorized membranes into five main types that are commercial or

appear to have commercial promise: dense polymer, microporous ceramic, porous carbon, dense metallic, and dense ceramic (Kluiters, 2004). Each membrane type has advantages and disadvantages, and research organizations and companies continue to work to develop better versions of each (U.S. Department of Energy, 2008b). Figure 6-6 illustrates the basic operating principles of hydrogen separation membranes for use in coal-derived syngas (Stanislowski and Laumb, 2009). This figure shows a dense metallic tubular membrane, but plate-and-frame-style membranes have also been developed. The "syngas in" stream refers to the feed gas into the membrane module. The permeate stream has permeated through the membrane wall, and in this case is made up of mostly hydrogen. The raffinate stream is what is left of the feed stream once the permeate is separated. A sweep gas such as nitrogen may be used on the permeate side to lower the partial pressure of hydrogen and enable more hydrogen to permeate the membrane.

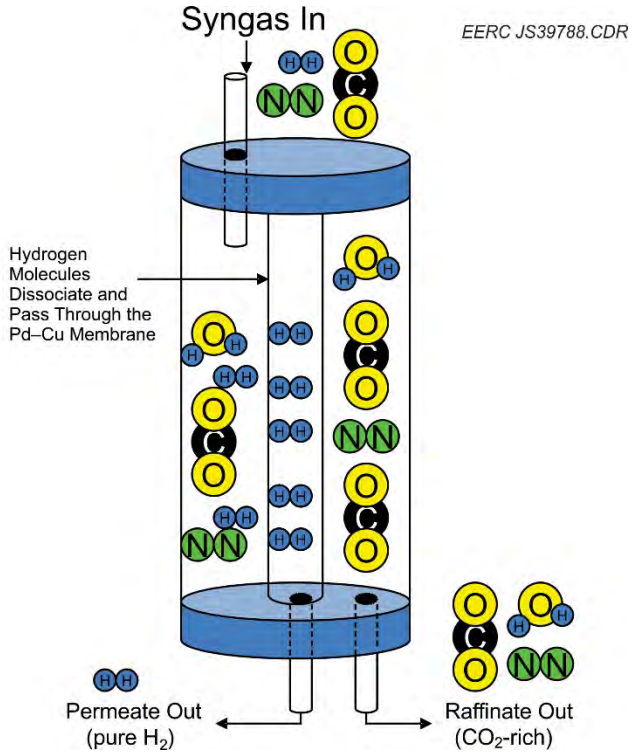

Figure 6-6. Illustration of the operating principle of hydrogen separation membranes (Stanislowski and Laumb, 2009).

The mechanisms for hydrogen transport through each membrane type are different. However, the performance of each membrane is gauged by two main principles: hydrogen selectivity and hydrogen flux. Hydrogen selectivity is defined by Equation 6.1 (Kluiters, 2004):

$$\alpha_{A/B} = \frac{y_A / y_B}{x_A / x_B} \qquad \text{[Eq. 6.1]}$$

where α is the selectivity factor of Component A over Component B in the mixture, y_A and y_B are the fractions of those components in the permeate, and x_A and x_B are the fractions of those

components in the feed. Components A and B are usually defined so that a higher selectivity factor refers to better membrane performance. A selectivity factor of 1 means there is no component separation.

Hydrogen flux is a measure of the rate of permeation of hydrogen through a membrane wall. The general equation for flux is shown by Equation 6.2 (Kluiters, 2004; Adhikari and Fernando, 2006):

$$J_x = \frac{P(p^n_{x,\,feed} - p^n_{x,\,permeate})}{t} \qquad \text{[Eq. 6.2]}$$

where J_x represents the flux of species x, P_x represents the permeability of species x, $p_{x,feed}$ and $p_{x,permeate}$ are the partial pressures of species x in the feed and permeate streams, t is the membrane thickness, and n is the partial pressure exponent. The value of n is usually between 0.5 and 2 and, like the value of P, depends on the transport mechanism assumed. When n = 1, the equation is called Fick's law. For hydrogen transport through a metal membrane, the value of n is usually 0.5, and the equation reduces to what is referred to as Sievert's law. Sievert's law is a useful way of measuring membrane performance because it takes into account the membrane thickness and the partial pressure of hydrogen on each side of the membrane.

Since most membranes operate on a partial pressure differential, there will always be some hydrogen left behind in the raffinate stream. Therefore, an additional measurement of performance is the recovery or yield, as shown by Equation 6.3 (Kluiters, 2004):

$$S = \frac{q_p}{q_f} \qquad \text{[Eq. 6.3]}$$

where S is the yield, q_p is the permeate flow, and q_f is the feed flow. There are numerous other ways to quantify the yield, including calculating the volume reduction in the raffinate or the percentage hydrogen recovery from the feed.

The five basic types of membranes mentioned earlier each have inherent advantages and disadvantages, depending on the desired operating conditions and necessary product specifications. With data presented by Kluiters (2004) and modified with Adhikari and Fernando (2006) and Ockwig and Nenoff (2007), Table 6-1 compares, in general, the relative operational performance of these five membrane types. Typical operational temperature will vary by specific membrane type, but it can be seen that the dense polymer membranes are only applicable at low temperature. Dense ceramic and dense metallic membranes have the highest hydrogen selectivity, and hydrogen flux is highest with dense metallic or microporous ceramic membranes. While dense metallic membranes seem to have the best performance relative to hydrogen, they are also very susceptible to poisoning from many compounds found in syngas, and metal alloys can be very expensive. Dense ceramic membranes also have high potential for commercial applications. They are less susceptible to poisoning than metallic membranes and, depending on the material, can be significantly less inexpensive. Development work is under way with each of these membrane types to increase the resistance to poisoning and reduce cost.

Table 6-1. Properties of Five Hydrogen-Selective Membranes (Kluiters, 2004; Adhikari and Fernando, 2006; Ockwig and Nenoff, 2007)

	Dense Polymer	Microporous Ceramic	Dense Ceramic	Porous Carbon	Dense Metallic
Temperature Range, °C	<100	200–600	600–900	500–900	300–600
H_2 Selectivity	Low	Moderate	Very high	Low	Very high
H_2 Flux	Low	High	Moderate	Moderate	High
Known Poisoning Issues	HCl, SO_x, CO_2		H_2S	Organics	H_2S, HCl, CO
Example Materials	Polymers	Silica, alumina, zirconia, titania, zeolites	$SrCeO_{3-\delta}$, $BaCeO_{3-\delta}$	Carbon	Palladium Alloys, Pd–Cu, Pd–Au
Transport Mechanism	Solution/ diffusion	Molecular sieving	Solution/ diffusion	Surface diffusion, molecular sieving	Solution/ diffusion

6.2.6.1 Hydrogen Transport Mechanisms

For porous membranes, there are four types of diffusion mechanisms that can effect hydrogen separation. They are Knudsen diffusion, surface diffusion, capillary condensation, and molecular sieving. Knudsen diffusion occurs when the Knudsen number, Kn defined by Equation 6.4, is large (Ockwig and Nenoff, 2007).

$$Kn = \frac{\lambda}{L} \qquad \text{[Eq. 6.4]}$$

where λ represents the mean free path of the gas molecules and L is the pore radius. At Knudsen numbers larger than 10, Knudsen diffusion becomes significant. Surface diffusion refers to gas molecules that are absorbed on the pore wall and migrate along the surface to the other side. Surface and Knudsen diffusion can occur simultaneously. Capillary condensation occurs if a partially condensed phase fills the pores and does not let other molecules penetrate. Molecular sieving occurs when the pores are so small that only the smaller molecules can fit through. Selectivity toward hydrogen is greatest with molecular sieving and is least with the Knudsen diffusion mechanism (Kluiters, 2004; Ockwig and Nenoff, 2007).

This work focuses on palladium-based dense metallic membranes, which rely on a solution/diffusion mechanism to transport hydrogen. The solution/diffusion mechanism is somewhat more complex than the porous diffusion mechanisms, although relatively straightforward in nature. Ockwig and Nenoff (2007) have presented a seven-step mechanism: 1) the hydrogen mixture moves to the surface of the membrane, 2) dissociation of the H_2 molecules into H^+ ions and electrons, 3) adsorption of the ions into the membrane bulk, 4) diffusion of the H^+ ions through the membrane, 5) desorption of the H^+ ions from the membrane, 6) recombination of the H^+ ions and electrons back to H_2 molecules, and 7) diffusion of the H_2 from the surface of the membrane. In the case of metal membranes, only hydrogen undergoes the solution/diffusion mechanism and, therefore, the membranes are considered 100% selective to hydrogen.

Figure 6-7 illustrates the mechanism of separation in a seven-step process that depicts hydrogen transport through dense metallic membranes as atoms. The mechanism is very similar to that proposed by Ockwig and Nenoff (2007) in the case of ion transport membranes. Key points for the mechanism of separation are the catalytic dissociation of hydrogen on the membrane surface and absorption of H atoms into the alloy structure. Both of these key steps can be hindered by the presence of sulfur on the surface of the membrane, reducing the overall flux rate. Sulfur could also be present on the reassociation side of the membrane if a significant leak in the material were ever present during operations. Diffusion of the hydrogen away from the surface is also an important point because under normal operating conditions, the gas is pure hydrogen and, therefore, the partial pressure of hydrogen can be high. In IGCC cases, a sweep gas of nitrogen would be employed to improve the overall efficiency of the separation, temper the combustion flame in the gas turbine, and provide additional mass to drive the turbine.

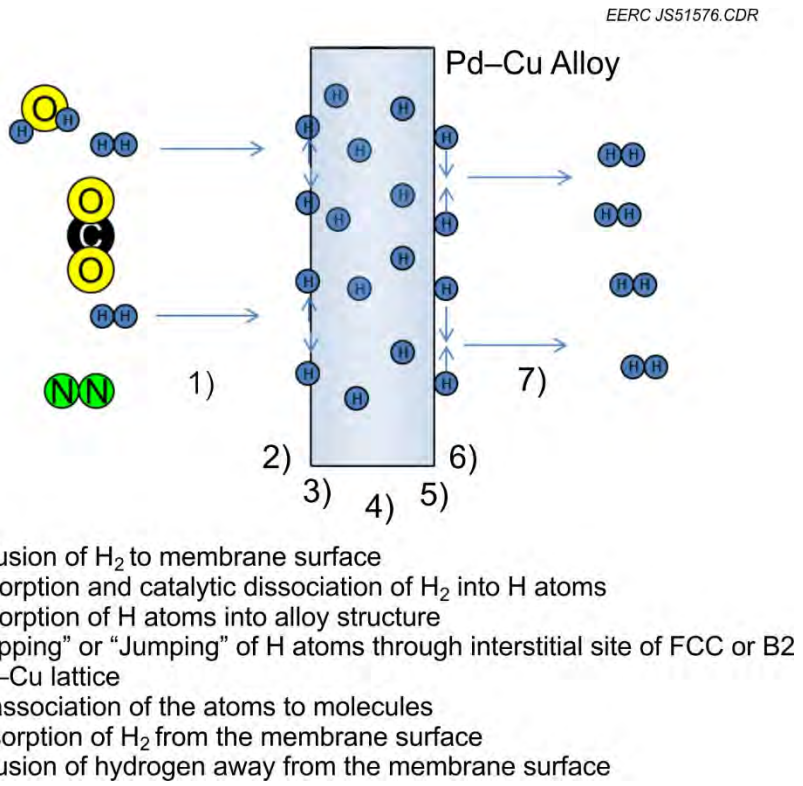

Figure 6-7. Seven-step mechanism of hydrogen separation through dense metallic membranes.

6.2.7 Impact of Sulfur on Membrane Performance

Dense metallic Pd–Cu-based metallic membranes are of great interest to researchers because they hold properties of high selectivity, high flux rates, and have shown the potential to have resistance to sulfur poisoning (Rothenberger and others, 2005). The nature of the Pd–Cu structure is of great importance when it comes to the permeation of hydrogen through the membrane. Pd–Cu either forms a body-centered cubic (bcc or b2) structure or a face-centered cubic (fcc) structure.

Figure 6-8 depicts the crystalline structure of each. The bcc structure contains copper atoms at each of the eight corners of the cubic matrix, with a palladium atom at the center of the cube. The fcc structure also contains eight copper atoms at the corners, but also a palladium atom at the center of each face of the cube.

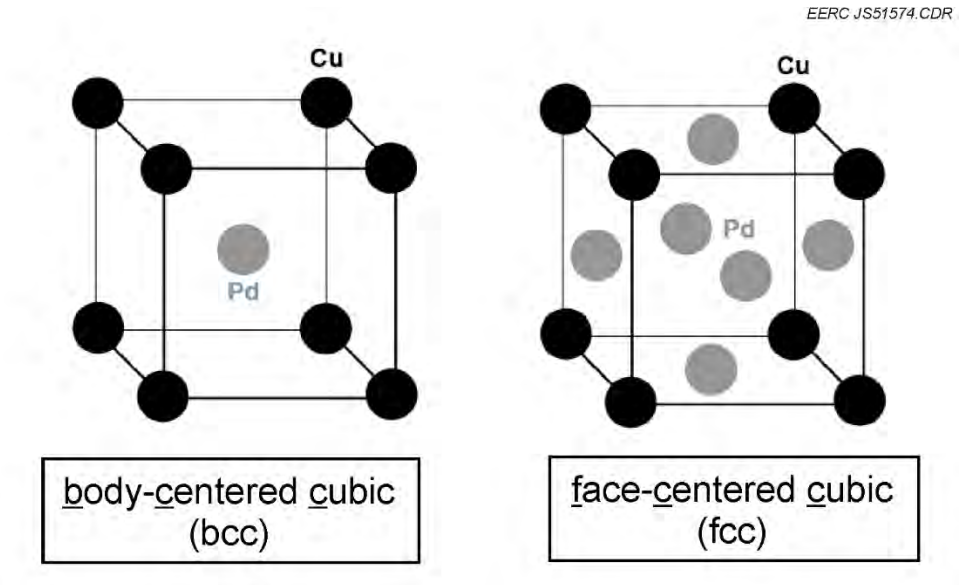

Figure 6-8. Pd–Cu crystalline structure in bcc and fcc orientations (Rothenberger and others, 2005).

As shown in Figure 6-9, the type of crystalline structure formed depends on both the composition and temperature of the material (Rothenberger and others, 2005; Subramanain and Laughlin, 1990; Volkov and others, 2008). The bcc structure is encountered in the widest temperature range at a concentration of 53 wt% Pd and 47 wt% Cu. It is for this reason that many studies have evaluated this particular composition. Studies also indicate that the bcc structure has higher hydrogen permeability but lower resistance to sulfur than the fcc structure. Rothenberger and colleagues reported that performance degradations of an order of magnitude were observed when exposing bcc structures to 1000 ppm H_2S, but performance degradations of less than 20% were observed when exposing fcc–crystalline-phase materials to the same conditions (Rothenberger and others, 2005).

The diffusion of hydrogen through a palladium membrane or a palladium copper alloy has been described in detail by a number of authors (Kamakoti and Sholl, 2003, 2005; Sholl, 2007) in an attempt to understand and predict the energies required for hydrogen atoms to diffuse through Pd–Cu lattices. Figure 6-10 depicts possible positions for H atoms to exist in bcc Pd–Cu. Sholl described the movements to and from tetrahedral sites and determined the activation energy required for each of these movements (Sholl, 2007). Understanding of the first principles of hydrogen diffusion through metal materials can lead to breakthroughs in development of new materials and crystal arrangements. Kamakoti and Sholl (2006) also studied the impact of ternary alloys on hydrogen diffusion and have undertaken a number of studies involving novel metals and amorphous materials for hydrogen separation (Hao and Sholl, 2009a, b, 2010).

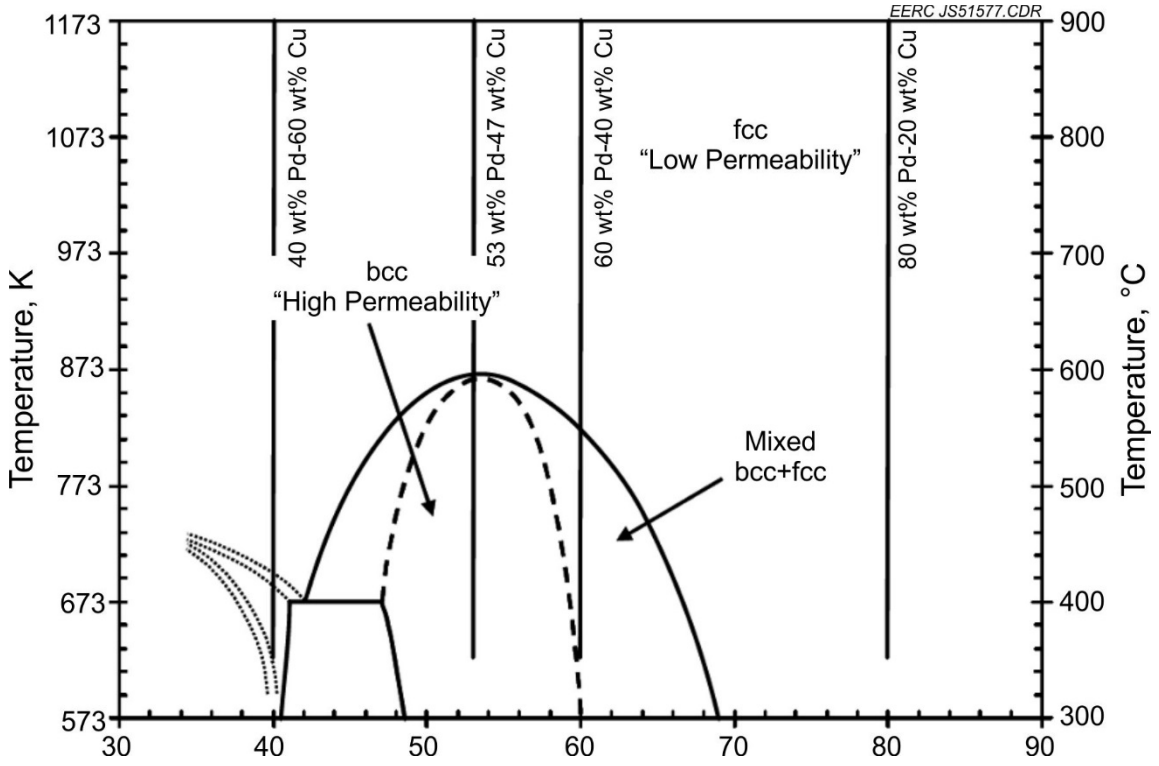

Figure 6-9. Pd–Cu phase diagram (Rothenberger and others, 2005; Subramanain and Laughlin, 1990; Volkov and others, 2008).

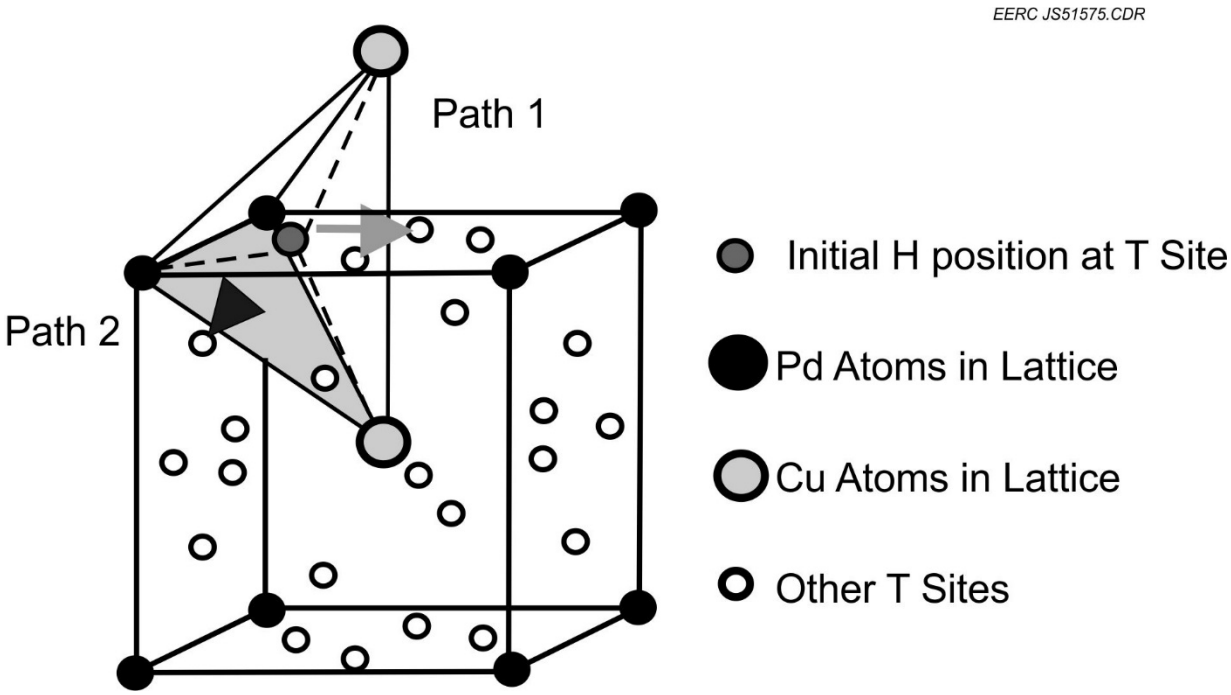

Figure 6-10. Possible pathways for H motion in bcc Pd–Cu (Kamakoti and Sholl, 2003).

Sulfur poisoning is known to impact the flux rate of hydrogen through Pd and Pd–Cu alloys. O'Brien (2011) theorized that hydrogen transport across a membrane is impacted by sulfur poisoning in two manners: 1) by producing a thin sulfide film on the surface of the membrane with low hydrogen permeability and 2) by blocking Pd from catalyzing the hydrogen dissociation reaction and, therefore, slowing the rate of dissociation. O'Brien's permeation experiments and H_2–D_2 experiments showed that both mechanisms indeed impact hydrogen flux rates through Pd–Cu membranes. The study also showed that at elevated temperature (900 K), H_2S has no impact on hydrogen permeation through $Pd_{47}Cu_{53}$ alloys.

Studies by Gabitto and Tsouris (2009) concluded that $Pd_{60}Cu_{40}$ alloys represent the best combination of high hydrogen flux and sulfur resistance. Studies have shown that sulfur poisoning of a thin membrane of fcc $Pd_{81}Cu_{19}$ was completely reversible if the sulfur was exposed to the membrane above 450°C (Ma and others, 2007). If the sulfur was exposed at 400°C, the original membrane performance could not be reestablished. Yang and colleagues (2008) evaluated the performance of a $Pd_{60}Cu_{40}$ membrane covered with a thin coating of nickel to promote resistance to H_2S. The results of this study indicated that the H_2S poisoning was reversible and that the membrane shows little performance degradation when operated above 573 K.

6.3 Experimental Methods and Equipment

6.3.1 CSIRO Hydrogen Separation Membrane Tubes

The membrane tubes supplied for this test were a novel design constructed of extruded vanadium alloy. Vanadium is highly permeable to hydrogen and much lower cost to manufacture compared to palladium alloys. The hydrogen permeability of vanadium is tens of times greater than that of palladium, making vanadium of particular interest for use in hydrogen-selective metal membranes. Self-supporting vanadium-based metal membranes, comprising a vanadium core overlaid with hydrogen dissociation and recombination catalysts, are a low-cost alternative to the current benchmark Pd-based membranes. In this configuration, Pd is applied in submicrometer layers on the inner and outer surface of dense vanadium tubes, thereby minimizing Pd consumption and its high associated cost. The vanadium tube serves the dual purposes of imparting mechanical strength against large transmembrane pressures and providing a gas-tight medium through which only atomic hydrogen can migrate. This brings the additional benefit of eliminating the requirement for costly porous supports, meaning the economic case for this technology is strong. Ultimately, however, it is the performance in realistic industrial environments, that will determine the market potential of this and other metal membrane technologies.

The hydrogen membrane separators tested during this project were formed from palladium-coated vanadium. Vanadium tubing (99.9%), with an outside diameter (o.d.) of 9.5 mm (3/8 in.), a wall thickness of 0.50 mm, and length of 330 mm, was procured from a commercial supplier. The vanadium tubes were treated to remove all traces of grease and oxides. A palladium layer of 500 nm was then electroplated onto the inner and outer surfaces. The tubes were finally annealed in a vacuum at 300°C for several hours to remove dissolved H_2 and improve adhesion of the deposited layers. The separator tubes were sealed using commercially available compression fittings and graphite ferrules. Figure 6-11 shows the as-received vanadium tube, the vanadium tube after Pd deposition, and sealed with compression fittings. A total of 12 membranes were prepared for the trials.

Figure 6-11. As-received tube (bottom), Pd-coated membrane (middle), and a membrane sealed with compression fittings (top).

CSIRO reported that in order to determine the baseline membrane performance, one membrane from the batch was subjected to pure gas permeability testing in its lab. The constant pressure method was used, whereby the outer surface of the membrane was exposed to a stream of flowing pure H_2 at a constant pressure, while the inner surface was maintained at 1.0 bar. The steady-state H_2 flux was measured for 10 min, after which the feed pressure and temperature conditions were changed.

Figure 6-12 shows the measured H_2 flux (flow per area per time) at several temperatures and pressures reported by CSIRO. Flux increases with increasing feed pressure and increasing temperature. Figure 6-13 shows the membrane performance expressed as permeability (mol m^{-1} s^{-1} $Pa^{-0.5}$), as reported by CSIRO. The nonlinearity of the data suggests hydrogen transport is at least partially limited by surface resistances, but the permeability values in excess of 2 to 3 × 10^{-7} mol m^{-1} s^{-1} $Pa^{-0.5}$ are more than 20× that of palladium under the same conditions.

6.3.2 Fluidized-Bed Gasifier

The EERC high-pressure FBG system was designed according to American Society of Mechanical Engineers (ASME) B31.3 Process Piping Code specifications. A design drawing of the main reactor is shown in Figure 6-14. The 3.0-in.-i.d. gasifier is capable of operation at a maximum operating pressure (MOP) of 6.9 MPa (1000 psig) at operational temperatures up to 843°C (1550°F). For temperatures up to 982°C (1800°F), the MOP is limited to 2.0 MPa (300 psig).

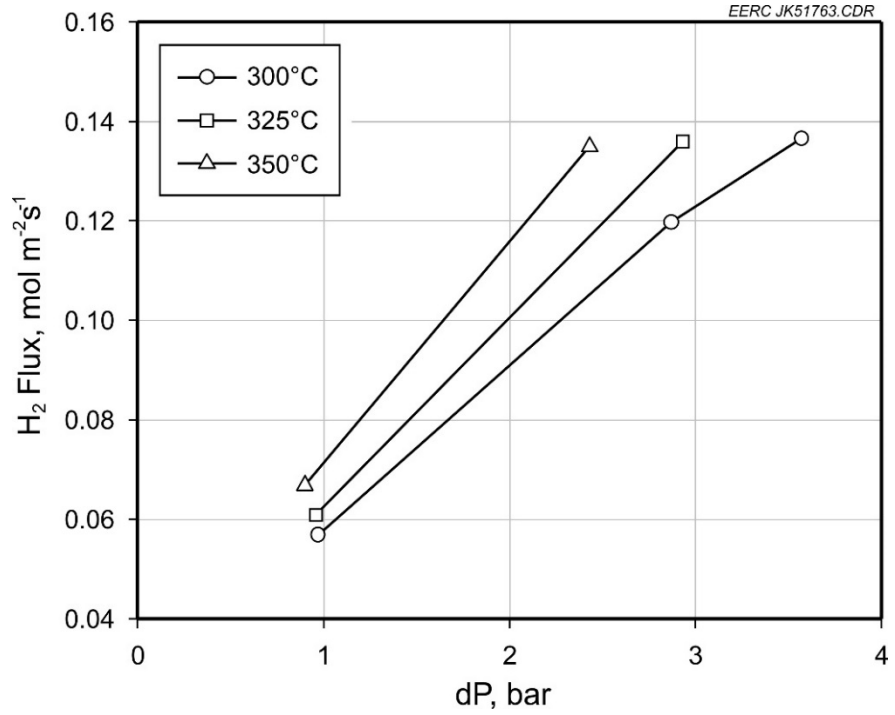

Figure 6-12. Hydrogen flux through 0.50-mm-thick Pd-coated vanadium separators with varying transmembrane pressure and temperature.

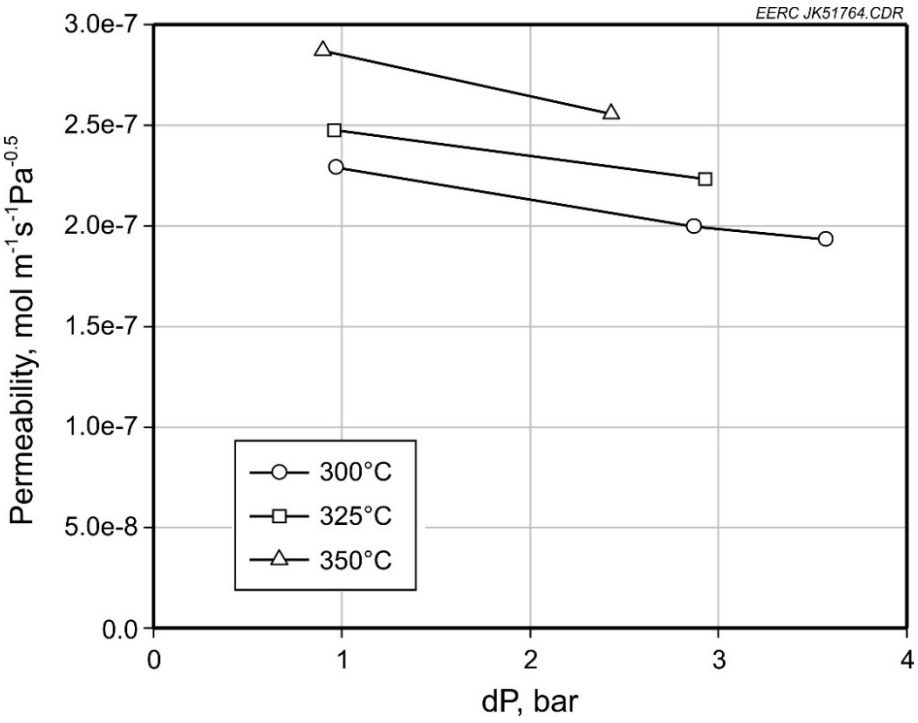

Figure 6-13. Hydrogen permeability of 0.50-mm-thick Pd-coated vanadium membranes with varying transmembrane pressure and temperature.

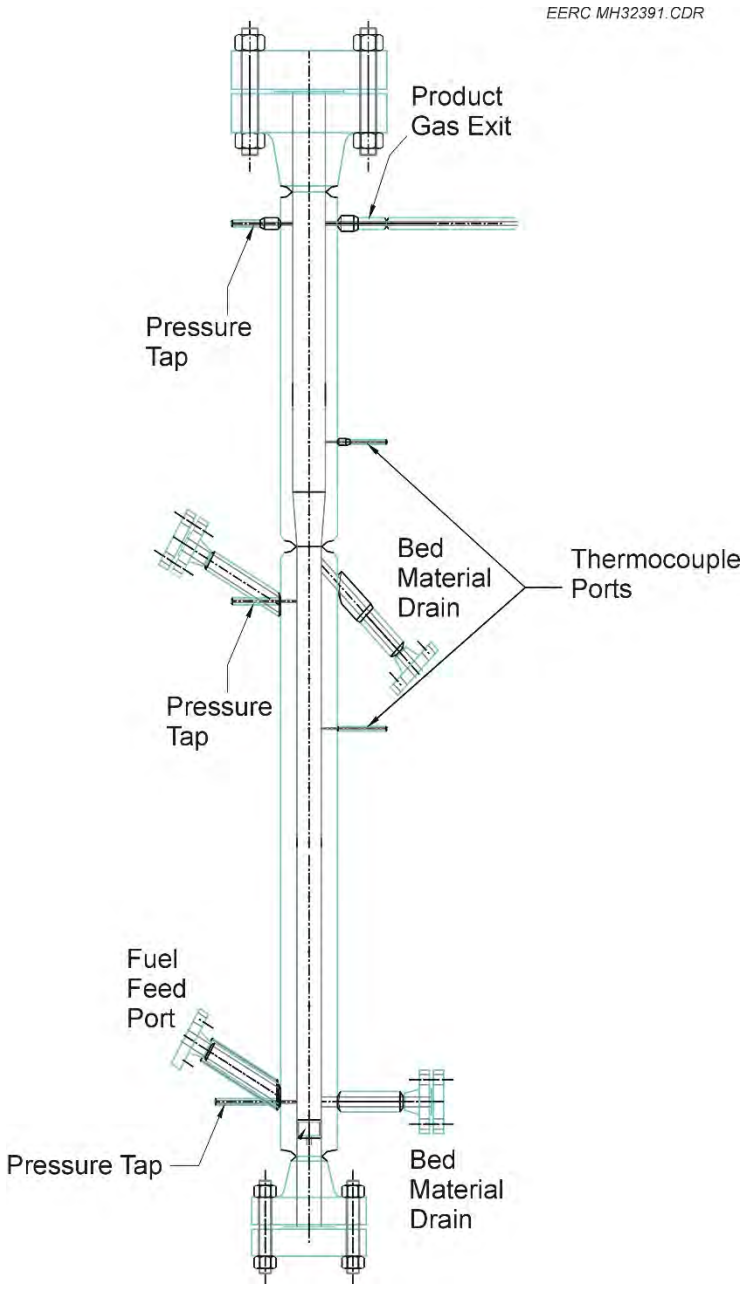

Figure 6-14. Design drawing of the pressurized, fluidized gasification reactor.

The reactor uses an auger in the inclined feed port to promote fuel feed into the gasifier at a location immediately above the distributor plate. The distributor plate functions to support the bed material and reacting fuel and allows introduction of the reactant gases (e.g., steam, oxygen, and nitrogen). Ancillary gasifier systems include steam generation (high-pressure pump and electric superheater) and separate electric preheaters for recycle syngas and oxygen/nitrogen.

A cyclone and associated standpipe are used to capture and return coarse entrained reactor solids (degraded bed material, unreacted fuel, and ash) back to the reactor to facilitate enhanced fuel carbon conversion and maintain bed inventory. The solids collecting at the bottom of the recycle standpipe are reintroduced just above the reactor distributor plate using a horizontal auger. Bed material samples can be collected through sample ports located on the standpipe or 5 ft above the distributor plate.

The reactor, cyclone, and standpipe are externally, electrically heated to negate heat losses associated with the high surface area/volume ratio of a typical pilot-scale reactor system. The system is highly instrumented with thermocouples, pressure transducers, and mass flow measurement devices to guide system operations and maintain the system within safe operating limits.

The FBG is capable of feeding up to 9.0 kg/hr (20 lb/hr) of pc or biomass at pressures up to 70 bar absolute (1000 psig). The externally heated bed is initially charged from an independent hopper with silica sand or, in the case of high-alkali fuels, an appropriate fluidization media. Independent mass flow controllers meter the flow of nitrogen, oxygen, steam, and recycled syngas into the bottom of the fluid bed. Various safety interlocks prevent the inadvertent flow of pure oxygen into the bed or of reverse flow into the coal feeder. Recycled syngas is injected several inches above the bottom distributor plate, which prevents direct combustion of syngas with oxygen entering at the bottom of the bed.

Coal is fed by a K-Tron® loss-in-weight, twin-screw feeder that provides instantaneous online measurement of the coal feed rate. The feeder is located in a pressure vessel and is capable of feeding at pressures up to 70 bar (1000 psig). The feed system's electronic controls are interfaced to a data acquisition system that allows for local or remote computer control of the fuel feed rate. Above the main feed hopper is the fuel charge lock hopper. The fuel charge hopper is manually charged with fuel through the top valve while at atmospheric pressure. It is then sealed and pressurized. Finally, the fuel feed material is transferred by gravity feed to the weigh hopper of the feeder. Metered coal from the feeder drops through a long section of vertical tubing and is then pushed quickly into the fluid bed through a downward-angled feed auger.

6.3.3 Warm-Gas Conditioning and Sampling Description

The product from the FBG flows through a warm-gas (230°–400°F) conditioning system, as seen in Figure 6-15, composed of a filter and fixed-bed reactors. The syngas passes through a hot candle filter to remove fine particulate. The filter has near-absolute filtration capability.

The warm-gas cleanup system was operated in a manner to achieve maximum H_2 and minimum CO concentration while maintaining acceptably low levels of H_2S. A train of up to seven fixed beds and an adsorbent transport reactor were available for conditioning of the syngas; however, only four fixed beds were necessary for this testing. All are externally heated and instrumented to facilitate accurate temperature monitoring and control. The beds can be loaded with WGS catalyst, heavy metal sorbent, chlorine sorbent, sulfur sorbent, and other materials, as

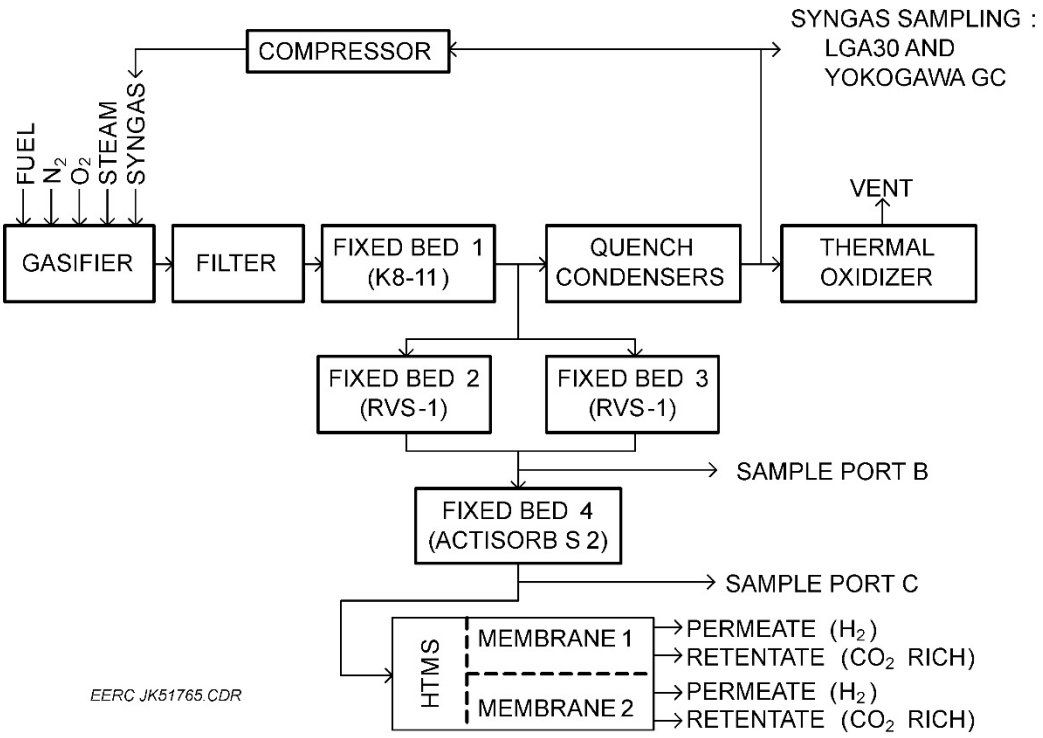

Figure 6-15. Gasification system process diagram.

needed. Referring to Figure 6-15, syngas flows through Fixed Beds 1–4. Slipstreams can be taken from any intermediate point between the filter and fixed beds, thereby promoting flexibility in the utilization of the warm-gas cleanup system.

The first fixed bed was used for WGS. WGS was achieved through the use of Johnson Matthey KATALCO K8-11 sour-gas shift catalyst to maximize hydrogen and minimize CO concentrations in the syngas. Observations during prior use of the K8-11 indicate that it may also crack tars. The K8-11 catalyst was reduced and conditioned prior to the start of the run. The first fixed bed operated at approximately 300°C. A slipstream to the HMTS was taken downstream from Fixed Bed 1 and further conditioned in Fixed Beds 2–4. Süd-Chemie RVS-1 solid sorbent was used in Fixed Beds 2 and 3 to remove sulfur. RVS-1 is a regenerable sorbent that was originally developed by DOE NETL. Fixed Beds 2 and 3 were used in an alternating manner. The RVS-1, with the space volumes of the fixed beds, has demonstrated H_2S <1 ppm operation. Once one became saturated and sulfur breakthrough was observed, the other fixed bed was brought online while the first was isolated for regeneration. Fixed Bed 4 was employed as a polishing bed and was loaded with new Actisorb S2 adsorbent. Actisorb S2 is produced by Süd-Chemie and is a nonregenerable ZnO-based adsorbent capable of removal of H_2S, mercaptans, and COS.

Feed gas to the HMTS is monitored through the use of continuous slipstream sampling at Port C, seen in Figure 6-15. Online analyzers are not capable of measuring high concentrations of water. Since the WGS reaction consumes some of the steam from the FBG's product gas, measurement of the actual water in the HMTS feed gas is necessary. The analyzer slipstream is dried through the use of high-pressure condensers. The syngas flow through the condensers is set

to approximately 0.57 scmh (20 scfh). Steam concentration in the feed gas is periodically quantified through the use of a dry gas meter to measure the slipstream's volumetric flow and measurements of condensed water. This technique permits the determination of the feed gas composition on a wet basis.

Dry gas is fed to a laser gas analyzer (LGA) and a gas chromatograph (GC) for online analysis of major gas components and for low-level (ppb) analysis of sulfur species. The EERC has two GCs and up to six Atmosphere Recovery, Inc., LGAs available for use with the gasifiers. The LGAs employ Ramen detectors to stimulate sample gas and emit distinct light spectra. Four LGAs were used for these tests. The LGAs use designations LGA35, LGA39, LGA105, and LGA106. The LGAs are each capable of measuring the real-time concentrations of eight gases at once. Seven of those gases are H_2, CO, CO_2, N_2, H_2S, CH_4, and total hydrocarbons. LGA39, LGA105, and LGA106 are capable of measuring O_2, in addition to the suite of aforementioned gases, and are normally dedicated to gasifier control and operation. LGA35 is capable of measuring H_2S instead of O_2. It is generally used to measure the gas compositions from various sample ports.

A Yokogawa GC is paired with LGA39. The Yokogawa GC is capable of measuring CO, CO_2, N_2, O_2, H_2S, COS, CH_4, ethane, ethene, propane, and propene. Referring to Table 6-2, the Yokogawa has high H_2S measurement capabilities and is better suited to syngas that has not had the H_2S removed. LGA35 is paired with a Varian 450 GC. The Varian GC is equipped with two thermal conductivity (TC) detectors and a pulsed-flame photometric detector for ultralow sulfur detection. The first TC detector is dedicated solely to analyzing hydrogen and provides three hydrogen measurements for each 15-min analysis cycle. The second detector analyzes the gas stream for CO, CO_2, N_2, O_2, H_2S, COS, CH_4, ethane, ethene, propane, and propene. One measurement is provided every 15 min for each of those gases. The third detector is capable of ultralow sulfur detection, down to 50 ppb. It provides three H_2S and COS measurements for each 15-min cycle. Table 6-2 summarizes the H_2S detection limits of the four analyzers used in this test.

Table 6-2. H_2S Detection Ranges

Analyzer	H_2S Detection Limits, ppm
LGA35	50–5000
LGA39	50–5000
LGA105	50–5000
LGA106	50–5000
Varian 450 GC	0.02–1 and 50–3000
Yokogawa	>50
Dräger Tubes	0.2–6, 1–200, 100–2000

The analyzers are calibrated prior to the start of and after each test program. Sample gas streams are manually switched via valves at the sample ports. LGA 39 and the Yokogawa GC were used to continuously monitor syngas produced by the FBG. LGA35 and the Varian are paired and are used after the fixed beds to continuously monitor the gas composition supplied to the HMTS. LGA105 and LGA106 were used to monitor the gas composition of the permeate and retentate flows exiting the membrane assemblies. Periodic samples are taken from one membrane assembly

at a time. The time duration for sampling is generally 1–2 hr. Sample gas tubing from sample ports to the analyzers is polyethylene, with no line longer than 25 m.

Sample gas transit times to the analyzers are estimated to be less than 1 min, depending on the individual sample gas flow rate. Gas is cooled and quenched before transport to the analyzers, so measurements are on a dry basis. Analyzer sample locations are indicated in Table 6-3. Since two membrane assemblies were tested simultaneously, LGA105 was calibrated for high hydrogen concentrations and used for measurement of the permeate streams. LGA106 was calibrated for measurement of retentate streams. Valves were employed to switch between the streams.

Table 6-3. Analyzer Sample Locations

Analyzer	Gas Stream	Location
LGA39	FBG product gas	Gasifier exit
LGA35	Feed	Port C
LGA105	Permeate	Port E
LGA106	Retentate	Port D
Varian 450 GC	Feed	Port C
Yokogawa	FBG product gas	Gasifier exit

In addition to analyzer sampling from various points throughout the system, Dräger tubes are used. H_2S, HCl, HCN, NH_3, and other trace gases can be checked to verify low-level chromatograph data. Dräger tube and gas bag samples may be drawn from each of the sample ports on the membrane skid as well as from several other ports on the gasifier system. Dräger tube sampling is typically performed most frequently at Sample Port B and other points downstream from the H_2S sorbent beds as a means of detecting the start of breakthrough and, thereby, maintaining appropriate H_2S exposures.

Because of the high temperature and pressure of the syngas supplied to the HTMS, direct measurement of H_2O is not feasible. A moisture-sampling system was employed to measure the fraction of water in the syngas supplied to the HMTS. A metering valve diverted a slipstream to a water-cooled indirect quench pot and a secondary ice bath to remove condensables from the syngas at sample Port C. Following the quench and ice bath, a gas regulator dropped the pressure to approximately 135 kPa (5 psig), and the dry syngas flow was measured with a dry gas meter. Syngas from the water balance system was sent to the Varian GC and LGA35 for real-time analysis. The condensing train was drained in 2- to 3-hr intervals, the recovered water was weighed, and total volume of syngas taken during the sample interval was recorded from the dry gas meter.

6.3.4 Hydrogen Membrane Test System

The HMTS is capable of simultaneously testing multiple hydrogen separation membranes. The HMTS is composed of controlled heaters; purge gas mass flow controllers; water-cooled quench pots for gas cooling; retentate flow control; and instrumentation for temperature, pressure,

flow measurement and a highly instrumented control system. Figure 6-16 provides an example of instrumentation graphing. The HMTS uses a reconfigurable, high-speed data acquisition and control system. User control and data logging are via a remotely located personal computer. The control computer utilizes a custom-written program with a graphical user interface. The control program is usually modified to meet the specific needs of the test. Figure 6-17 shows the main HMTS control window used for testing two membranes. Three membranes have been simultaneously tested with the HMTS.

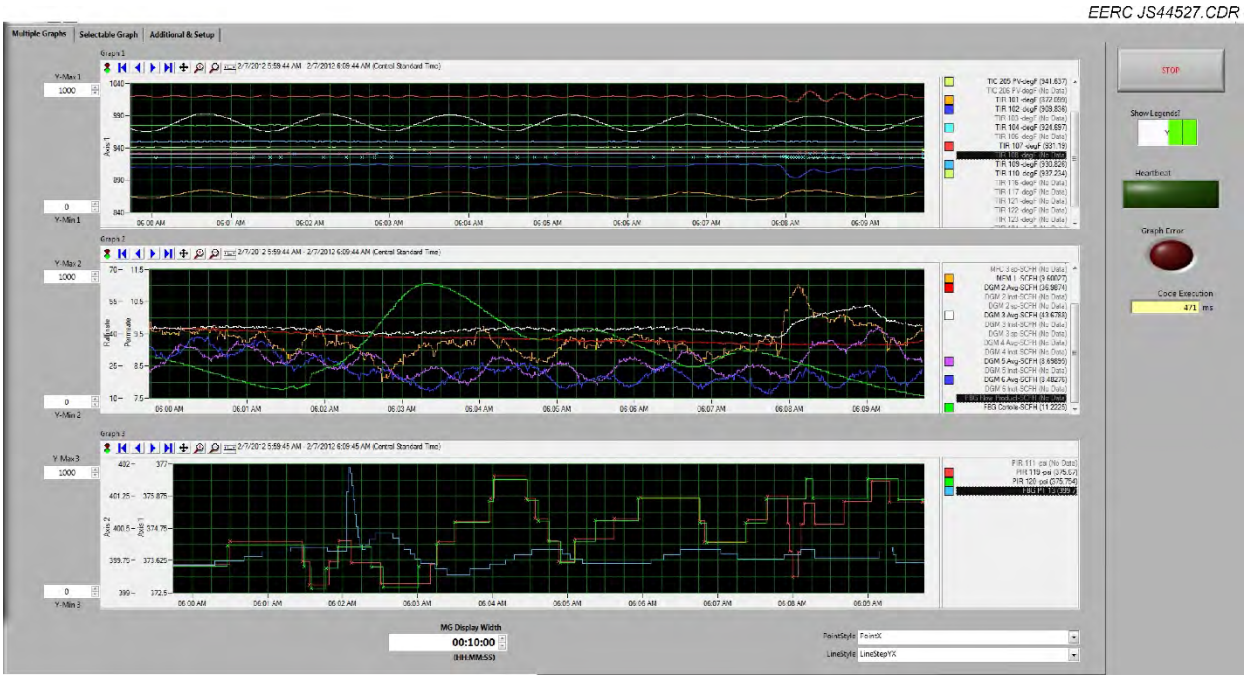

Figure 6-16. HMTS instrumentation trend graphing.

Flow measurement on the HMTS is done through the use of dry gas meters. The dry gas meters are rated for 200 scfh (5.66 scmh) at 0 psig (101 kPa). Full-scale accuracy is 1% with 1/100 ft^3 resolution on the dial face of the meters. The meter shaft on each dry gas meter is coupled to a high-resolution encoder, which is connected to the control system. Dry gas meter flows are averaged. Figure 6-17 shows two of the dry gas meter trend windows.

Figure 6-18 shows the P&ID of the HMTS. The design of the HMTS allows for individual controlled purge flows to each side of a membrane as well as custom supply gas blending and transitioning. Retentate flow control is done through the use of high-accuracy, pneumatically actuated flow control valves. The flow coefficient of the valves may be changed by changing seat and stem. Heater controllers feature both ramp-up and ramp-down control. Pressure transmitters use a digital sensor, providing stable and precise pressure measurement. The pressure transmitter's CPU (central processing unit) directly counts the sensor output frequencies without any additional A/D (analog/digital) conversion.

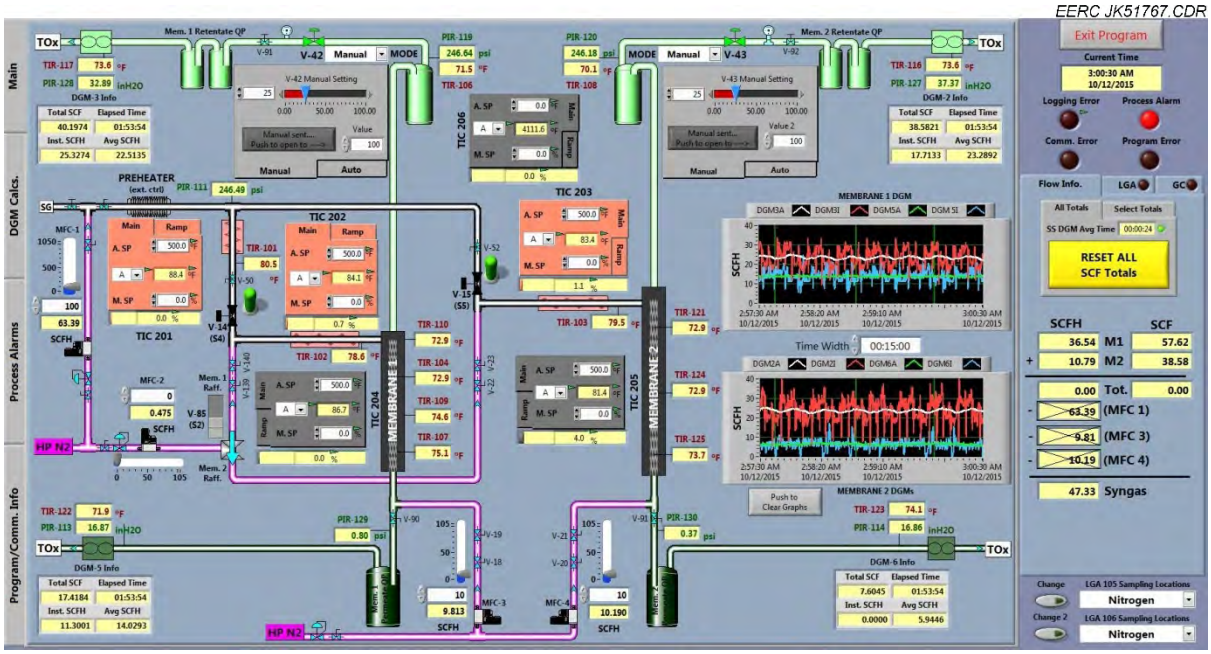

Figure 6-17. HMTS controls.

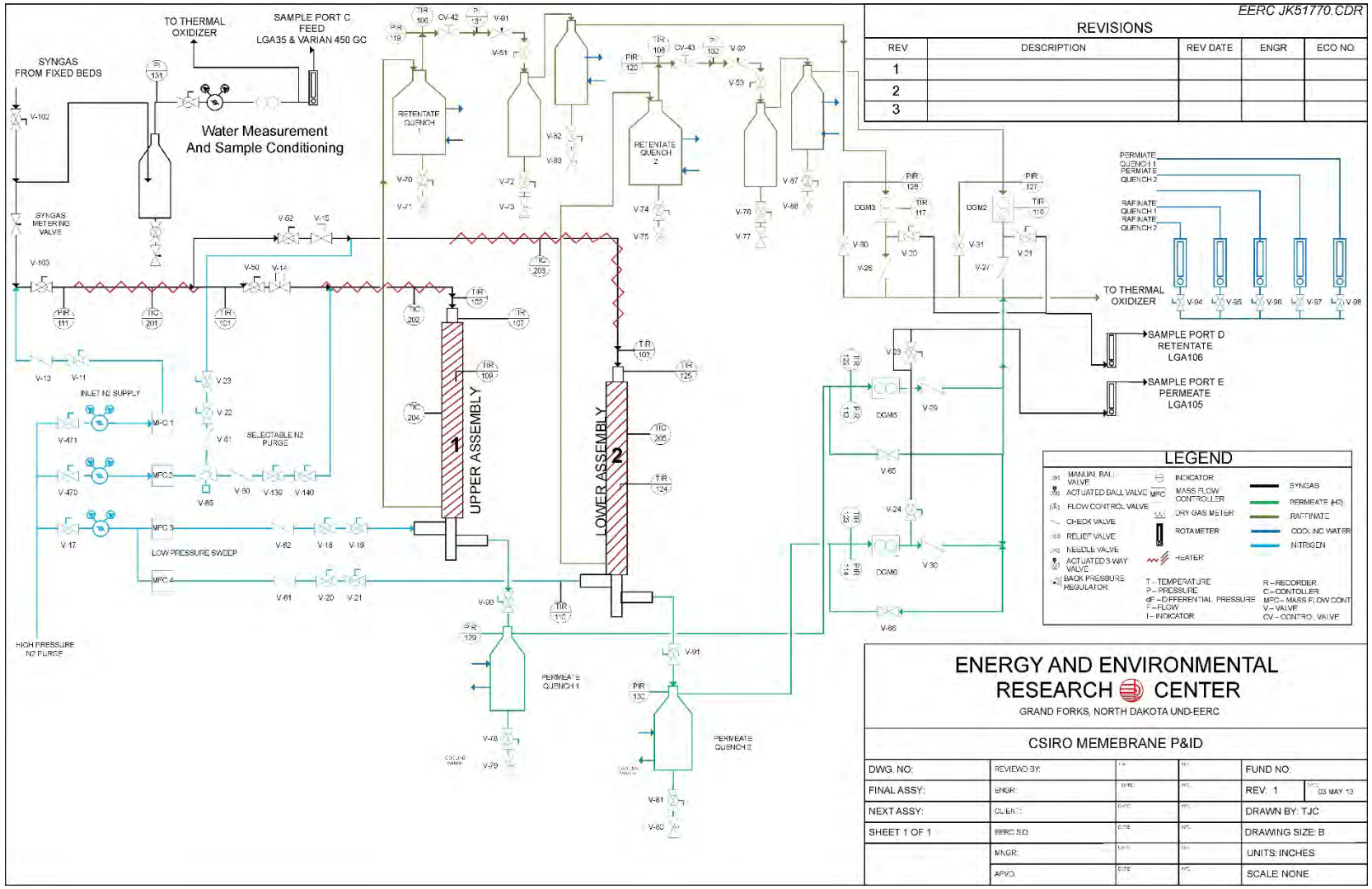

Figure 6-18. HMTS P&ID.

6.4 Testing Program

At the direction of CSIRO, a conservative approach was undertaken to observe the effects of coal-derived syngas on the membrane tubes since these were the first tests using coal-derived syngas. This conservative approach involved maintaining consistent pressures, temperatures, and flows. As a result, a parametric test matrix was not undertaken. Testing was conducted in two test programs, each 1 week long. The first test program, H2M-015, was conducted during the week of October 12–16, 2015, and the second test program, H2M-016, was conducted during the week of October 26–31, 2015.

The FBG was used to gasify lignite coal from the Falkirk Mine near Underwood, North Dakota. Originally, Australian brown coal from the Loy Yang Mine was discussed as the preferred feedstock. International transport issues prevented its use. Air-dried Falkirk Mine lignite was utilized as the feedstock for these tests as it was felt to be close in characteristics to the Loy Yang brown coal. This fuel was crushed to a –10-mesh particle-size distribution before air drying. A representative sample of this fuel was submitted for proximate, ultimate, heating value, and x-ray fluorescence (XRF) analyses, with the results shown in Table 6-4.

Table 6-4. Fuel Analysis

	As-Received Falkirk Lignite	Air-Dried Falkirk Lignite
Proximate Analysis, wt%		
Moisture	32.53	22.95
Volatile Matter	23.20	26.49
Fixed Carbon	32.63	37.26
Ash	11.63	13.28
Ultimate Analysis, wt%		
Hydrogen	6.25	5.55
Carbon	37.64	42.98
Nitrogen	0.63	0.72
Sulfur	0.68	0.78
Oxygen	43.17	36.69
Ash	11.63	13.28
Heating Value, Btu/lb	6290	7183
XRF Analysis, wt%		
SiO_2	ND[1]	45.18
Al_2O_3	ND	12.66
Fe_2O_3	ND	8.37
TiO_2	ND	0.50
P_2O_5	ND	0.20
CaO	ND	11.61
MgO	ND	4.42
Na_2O	ND	5.90
K_2O	ND	1.79
SO_3	ND	9.38

[1] Not detected.

During each test program, the gasifier was first brought online independent of the back-end syngas-conditioning systems. During gasifier start-up, there was a chance that high tar-pyrolyzing conditions or oxygen breakthrough could occur. Once the gasifier was at steady-state conditions, Fixed Bed 1 was brought online to promote WGS, as discussed previously. The WGS catalyst used was presulfided Johnson Matthey KATALCO K8-11 sour-shift catalyst. The full flow of product gas from the FBG was routed through Fixed Bed 1. Syngas was routed from the WGS to the quench train. Syngas was cooled and dried, with a portion being recycled back into the FBG using a syngas compressor. Excess syngas was vented through the FBG pressure control valves and then to the thermal oxidizer.

After the gasifier operation and WGS reactions were verified, a slipstream of syngas was sent through either Fixed Bed 2 or 3, with one online and the other on standby or regenerating. Each of these fixed beds contained regenerable, zinc-based RVS-1 sulfur adsorbent. Syngas was then sent through Fixed Bed 4, which was used as a polishing bed, and then to the HMTS. Fixed Bed 4 was loaded with SudChemie Actisorb-S_2, a nonregenerable sorbent capable of removing H_2S, mercaptans, and COS. In commercial operation, a polishing bed of nongenerable sorbent would most likely be operationally and cost prohibitive. However, for research purposes the polishing bed was used to reduce the potential of membrane poisoning in the interest of evaluating performance.

Syngas was allowed to flow through Sample Port C with a flow rate of approximately 0.57 scmh (20 scfm). The flow through Sample Port C went through high-pressure condensers which are used for bulk removal of water from the syngas. The steam component of the syngas was determined as a function of the totalizing dry gas meter, time duration, condensed water measurement, temperature measurement, pressure measurement, and LGA35 dry syngas composition measurement. Sample Port B was also used for Dräger tube measurements downstream from Fixed Beds 2 and 3. H_2S was the molecule of critical concern. Dräger Tube 8101991 was used for indications of H_2S concentrations. These tubes have a range of 0.2–6 ppm, using n = 1 pumps of the calibrated Accuro® sample pump. If no indication was obtained after one pump, multiple pumps were sometimes drawn until an indication was observed. The objective was to keep the H_2S level entering Fixed Bed 4 to less than 4 ppm. If the H_2S concentration was observed to be trending up, a switch between Fixed Beds 2 and 3 was made. The fixed bed coming offline was then regenerated.

Two membrane assemblies were loaded into the HMTS and tested simultaneously. The assemblies consist of the housing, external feed gas heat exchanger coil, thermocouples, membrane tube (separator), and compression fittings. The housings were disassembled for installation of the separator through the use of compression fittings. Personnel wore rubber gloves when handling the separator tube to reduce the risk of surface contamination. The HMTS assemblies were designated Membrane 1 and Membrane 2. Each membrane assembly was installed in a separate clam shell heater. An assembly could be removed from the HTMS independent of the other's operation for replacement of the separator tube, if needed. The membrane assemblies were slowly pressurized with N_2 and then checked for leaks. Nitrogen flow was established, with the retentate flow rates set to approximately 0.57–0.71 scmh (20–25 scfh). Nitrogen purge flows through the permeate side of each membrane assembly were set at approximately 0.14 scmh (5 scfh). The membrane assemblies were then heated to their operating temperatures using ramp control. Heat-

traced feed lines were adjusted to balance temperatures as the target temperatures were approached. Once stable target temperatures were achieved, the nitrogen purges to the permeate side of the assemblies were discontinued and baseline leak rates to the permeate side were determined. Adjustments were made to the N_2 feed pressure such that they were equal to the syngas pressure. Syngas was fed to the membranes while N_2 to the feed was discontinued. No attempts to gradually transition from N_2 to syngas were made. Retentate flows and temperatures were monitored and adjusted as necessary. Permeate flows and compositions were monitored for indications of membrane leaks and failures. Periodic calculations were performed as an approximate indication of performance.

Membranes were taken offline by supplying preheated N_2 feed while discontinuing syngas feed. No attempt was made to gradually transition to N_2. The N_2 feed flow rate was maintained at approximately 0.57–0.71 scmh (20–25 scfh). The permeate flow was monitored for an indication of leaking across the separator and seals. The permeate side of the membrane assembly was purged with preheated N_2 at approximately 0.14 scmh (5 scfh). Temperatures were ramped down to ambient followed by a gradual reduction in pressures. Once down to near-ambient temperature and pressure, N_2 flows were discontinued. It should be noted that standard conditions used were 15.6°C (60°F) and 101 kPa (14.7 psig).

6.4.1 Test Program H2M-015

The objective of testing during H2M-015 was to subject the separators to syngas for the maximum possible time and observe their performance characteristics. CSIRO specified 300°C (572°F) and 325°C (617°F) as the target temperatures for membrane assemblies. The target feed flow rate for the separators was 0.71–0.0.85 scmh (25–30 scfh). The target feed pressure was 2859 kPa (400 psig) throughout.

Overall, gasification with the lignite fuel produced syngas quality similar to those experienced in previous FBG tests with similar feedstocks, although maintaining consistent composition was a challenge. The carbon conversions were somewhat lower because of operation at lower O_2/fuel ratios. The lower O_2/fuel ratios were chosen based on the potential of generating bed agglomerations. The FBG developed a critical hot flange gasket leak which required gasifier shutdown and a cooldown period for repairs. Only 38.5 hr on coal were achieved, with approximately 12 hr of syngas flow to the HMTS. Some agglomeration of bed material was observed during postrun maintenance. This agglomeration also prevented the recycle of the cyclone ash back to the bottom of the FBG, resulting in higher dust loadings to the particulate control device (PCD) and more frequent backpulsing. Nitrogen is used for back pulsing the PCD. This high-frequency backpulsing led to more nitrogen dilution. Operating pressure for the first week of testing was 420 psig, as measured at the bottom of the bed, and average bed temperatures were approximately 1550°C. Average gasifier operating conditions for Test H2M-015 can be seen in Table 6-5.

Table 6-5. Average Gasifier Operating Conditions for H2M-015

Start Date:	10/15/2015	
Start Time:	13:00	
End Date:	10/16/2015	
End Time:	01:00	
FBG Temperature	°F	°C
O_2/Steam Inlet	560	293
Recycle Inlet	894	478
Lower Reactor Bed	1540	838
Upper Freeboard	1546	841
Reactor Extension	1316	713
Cyclone Exit	1157	625
Filer Vessel Average	751	399
Flow	lb/hr	kg/hr
Fuel Feed Rate	9.48	4.3
Steam	21.4	9.7
Recycle Syngas	63.9	29
	scfh	slph
Oxygen	63	1783
Syngas Purges	151	4273
Product Gas	127	3594
Pressure	psig	kPa
Gasifier	420	2997
Filter Vessel	414	2996
Quench Pot	399	2852
Recycle Gas Surge Tank	680	4790

The composition of the feed gas is shown in Figure 6-19. It can be seen that there were significant challenges in maintaining consistent feed gas composition because of operational issues associated with the gasifier. The analyzers utilize gas-conditioning condensers to avoid water saturation and tar fouling. As a result, the analyzers return values on a dry basis. To determine the water content in the feed gas, a high-flow slipstream of feed gas was routed through a pair of condensers. The volume of gas and mass of water were measured on a timed basis and logged. During postprocessing, the moisture content of the feed gas was determined and added back into the dry gas analyses to arrive at the wet gas compositions. The short time frames of syngas production severely limited the slipstream water sampling for the empirical determination of steam content in the feed gas. Based on mass balance calculations associated with the FBG, a steam concentration of approximately 30 vol% was assumed. Nitrogen spikes during the latter portion of the campaign are due to attempts to clear the gasifier of agglomerates and to clean the filter through aggressive backpulsing.

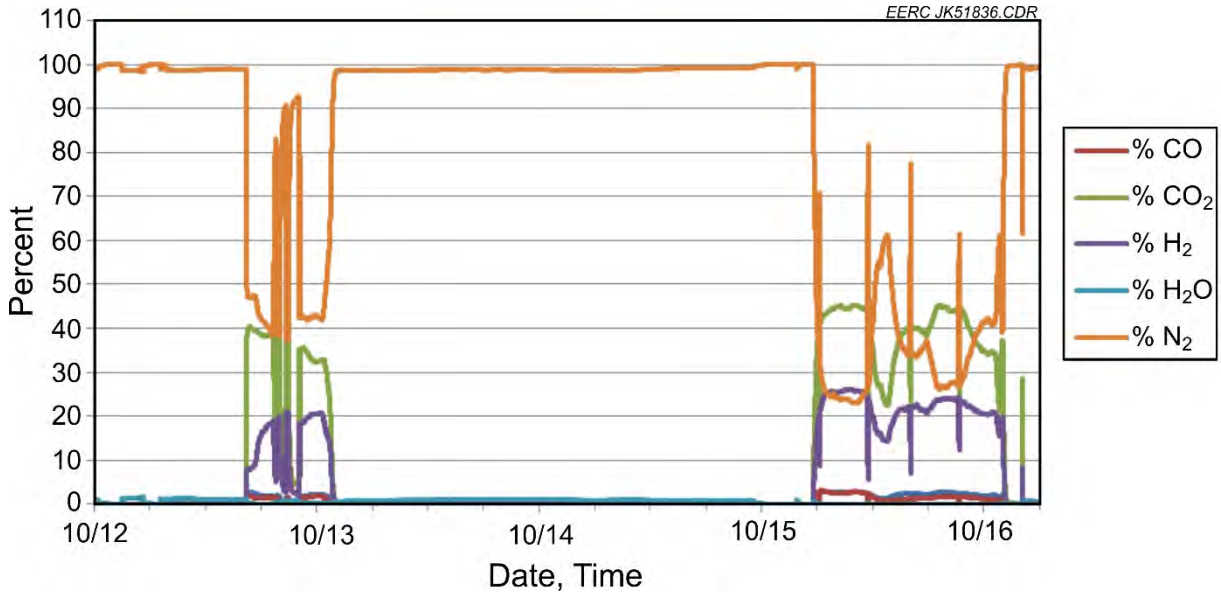

Figure 6-19. Feed gas composition, H2M-015.

Two membrane assemblies were installed in the HMTS on October 12, 2015. Table 6-6 summarizes the location on the HMTS, CSIRO separator numbers, feed gas type, and test periods. The Membrane 1 assembly contained Separator Tube 213, and the Membrane 2 assembly contained Separator Tube 212. The Membrane 1 assembly was operated at 300°C (572°F) and the Membrane 2 assembly at 325°C (617°F), with approximately 0.57 scmh (20 scfh) of nitrogen through each assembly. Fixed Beds 2 and 4 were brought online for sulfur control, and syngas flow was established to Sample Port C and the water balance system. H_2S levels were monitored with Dräger tubes, and levels were observed at less than 1 ppm. The membranes were adjusted to match the system pressure, N_2 flows were stopped and syngas flows started at 20:05. At 20:25, a leak was detected near Fixed Bed 2 so the HTMS was switched back to nitrogen. Flow was routed through Fixed Bed 3, and Fixed Bed 2 was taken off-line for repair of the tubing leak.

Table 6-6. H2M-015 Membrane Assemblies, Separator Numbers, Feed Gas, and Test Periods

Membrane Location	CSIRO Separator No.	Feed	Start Date	Start Time	End Date	End Time	Duration hh:mm
1	213[1]	Hydrogen	10/13/15	13:10	10/13/15	13:45	00:35
1	211[2]	Hydrogen	10/15/15	12:03	10/15/15	12:18	00:15
1	209	Syngas	10/15/15	16:43	10/16/15	01:35	08:52
2	212[1]	Hydrogen	10/13/15	13:10	10/13/15	13:45	00:35
2	210	Hydrogen	10/15/15	12:03	10/15/15	12:18	00:15
2	210[2]	Syngas	10/15/15	12:56	10/15/15	14:53	01:57
2	208	Syngas	10/15/15	16:43	10/16/15	01:35	08:52

[1] Developed leak after H_2 testing.
[2] Fractured during testing.

Syngas flow was reestablished to the HMTS at 20:38. Syngas flows to each membrane assembly were maintained between 25 to 30 scfh, and supply pressure and membrane temperatures remained constant. Operation continued until 00:41, October 13, 2015, when a gas leak was discovered in the FBG. The HMTS was taken off-line and switched to pressurized nitrogen.

While the FBG was down for repairs, H_2 bottle gas was connected to the HTMS to conduct testing on pure H_2. The N_2 feed pressure was reduced to 1150 kPa (152 psig). Temperatures were maintained at 300° (572°) and 325°C (617°F) for Membrane 1 and Membrane 2, respectively. H_2 was then supplied to both membrane assemblies containing Separators 213 and 212 at 13:10 on October 13, 2015. Flux rates were compared to historical data from prior CSIRO laboratory tests. A marked reduction in performance of Separator 213 was observed, and the membrane assemblies were switched back to N_2 at 13:36. It was decided to regenerate the membrane tubes by supplying them with low-pressure air. This would remove some impurities like sulfur or carbon coking from the tube surface and could restore performance. The system was prepared to supply low-pressure air to the membrane assemblies; however, shortly after H_2 was stopped and N_2 flows started, both membrane assemblies indicated a leak based on N_2 flows that were observed at the permeate gas meters.

Both membrane assemblies were depressurized and cooled then removed from the HMTS. Based on visual inspection, it was determined that the compression fittings on the ends of tubes were most likely at fault. Expansion of the membrane tube in a pure hydrogen environment had deformed the graphite compression ferrules. The membrane assemblies were depressurized and cooled and the membranes tubes replaced.

The FBG came back online during the early morning of October 15, 2015, and had achieved steady state at approximately 11:00. Separator Tube 211 was installed in the Membrane 1 assembly and Separator Tube 210 installed in the Membrane 2 assembly. At 11:51 on October 15, 2015, H_2 was delivered to Membrane 1 and Membrane 2 to baseline the separators. The H_2 feed pressure was gradually increased. At 12:20, Membrane 1 fractured at 494 kPa (57 psig) and was taken off line for replacement.

Membrane 2 was switched to N_2 at 12:27, and the pressure was increased to match the syngas feed pressure. At 12:56 the feed was switched from N_2 to syngas. At 14:50, Membrane 2 was taken off-line for replacement because of a very high leak rate. Figure 6-20 shows the fractures on Separator 211. Both separators exhibited a significant amount of radial and axial cracking. CSIRO retained all separators for its own investigations.

Separator 209 was installed in Membrane 1, and Separator 208 was installed in Membrane 2. Both were leak-checked with N_2 at 2880 kPa (403 psig) prior to and after heating. No attempt was made to conduct baseline testing using H_2 because of the failures observed with Separators 210 and 211 and the development of seal leaks on Separators 212 and 213. The feed gas was switched to syngas at 16:43 on October 15, 2015. Operating temperatures were 300° (572°) and 325°C (617°F), respectively, and syngas flow rates were approximately 0.71 scmh (25 scfh) for each membrane assembly. Figures 6-21 and 6-22 show the temperatures and pressures of the separators during this time. Figures 6-23 and 6-24 show the retentate and permeate flows during the same period.

Figure 6-20. Separator 211 fracture.

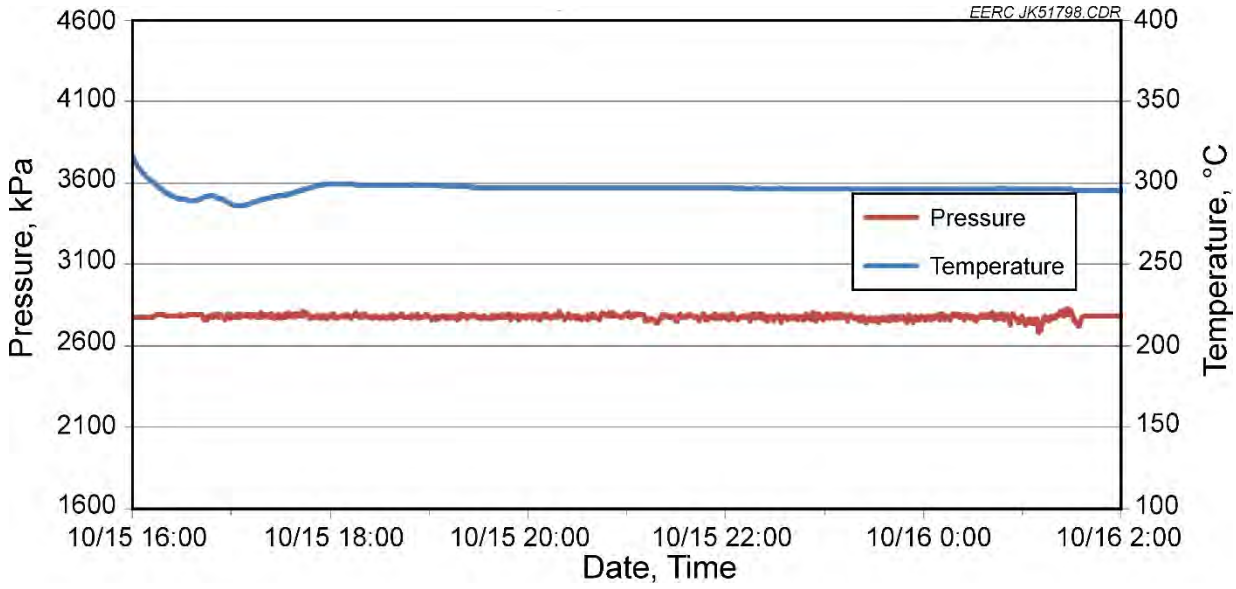

Figure 6-21. Temperature and pressure, Separator 209.

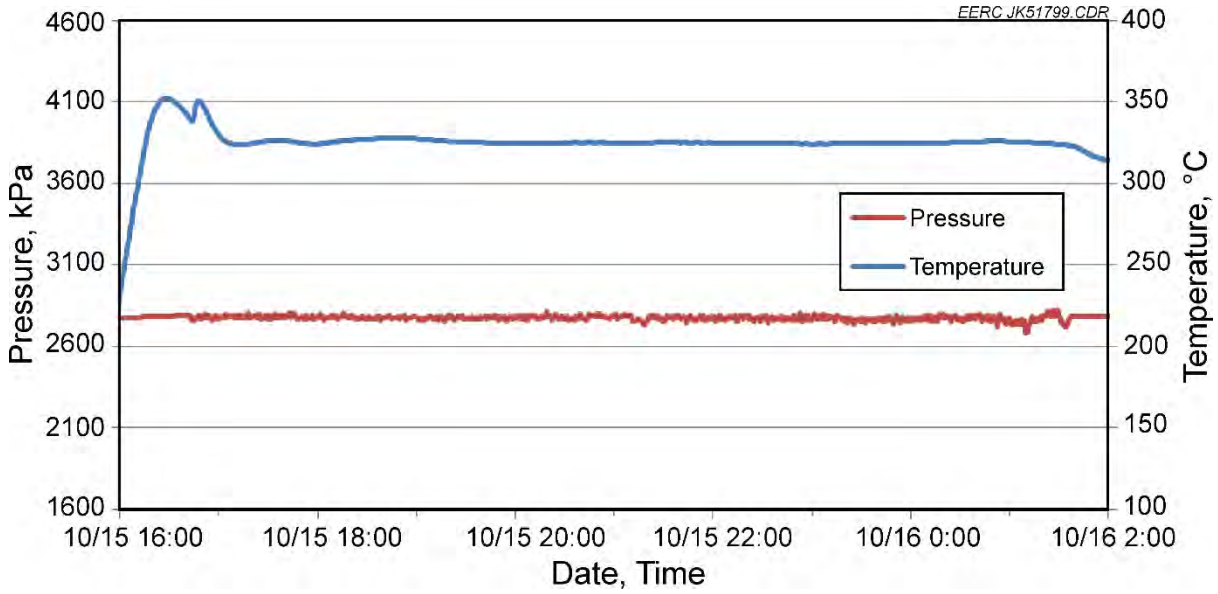

Figure 6-22. Temperature and pressure, Separator 208.

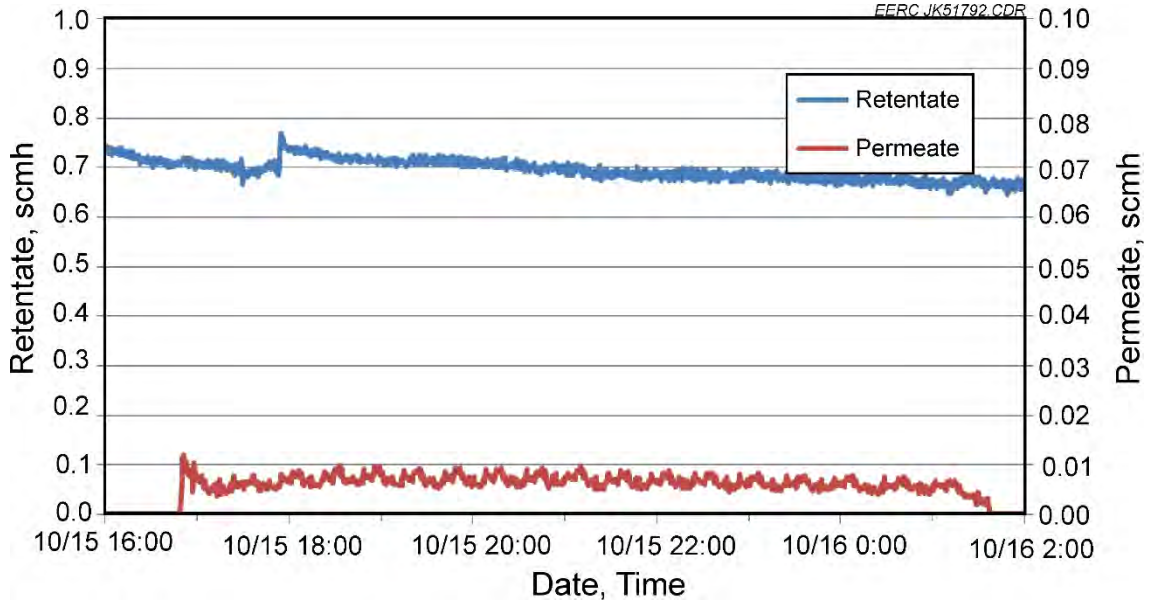

Figure 6-23. Flows, Separator 209.

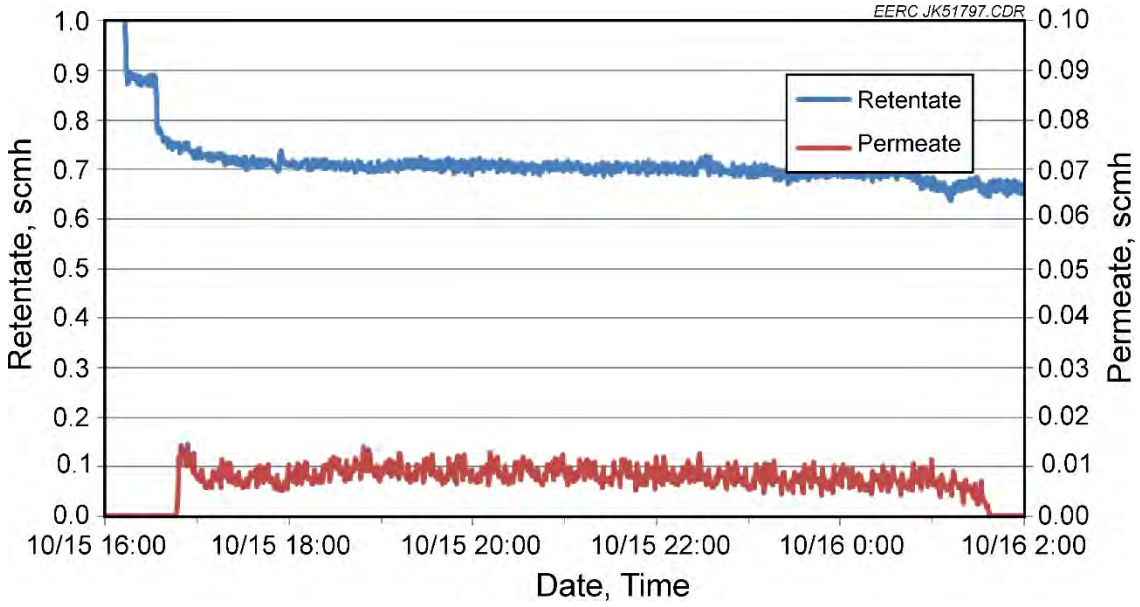

Figure 6-24. Flows, Separator 208.

The separators produced low-permeate flows. These low flows resulted in it taking a long time to flush nitrogen from the permeate quench pots. The time lag can be seen in Figure 6-25, showing the permeate composition for Separator 208. The low-permeate flow resulted in low-frequency cycling of the dry gas meter which, in turn, resulted in low flow to the analyzer. The oscillating H_2 and N_2 concentrations are due to a lack of consistent flow to LGA105. Figure 6-26 shows the retentate composition for Separator 208. The FBG started to build up agglomerations in the bed toward the end of the day, and the membranes were switched to N_2 at 01:35 on October 16, 2015, because of the need to shut down the gasifier. This shutdown prevented switching the analyzers over to Membrane 1 that held Separator 209. Therefore, no analyzer gas composition data were available for Separator 209 while operating on syngas. On October 16, 2015, from 08:21 to 09:33, both membrane assemblies were tested with pure hydrogen to observe flux performance. Table 6-7 summarizes the performance of separators tested during the H2M-015 campaign.

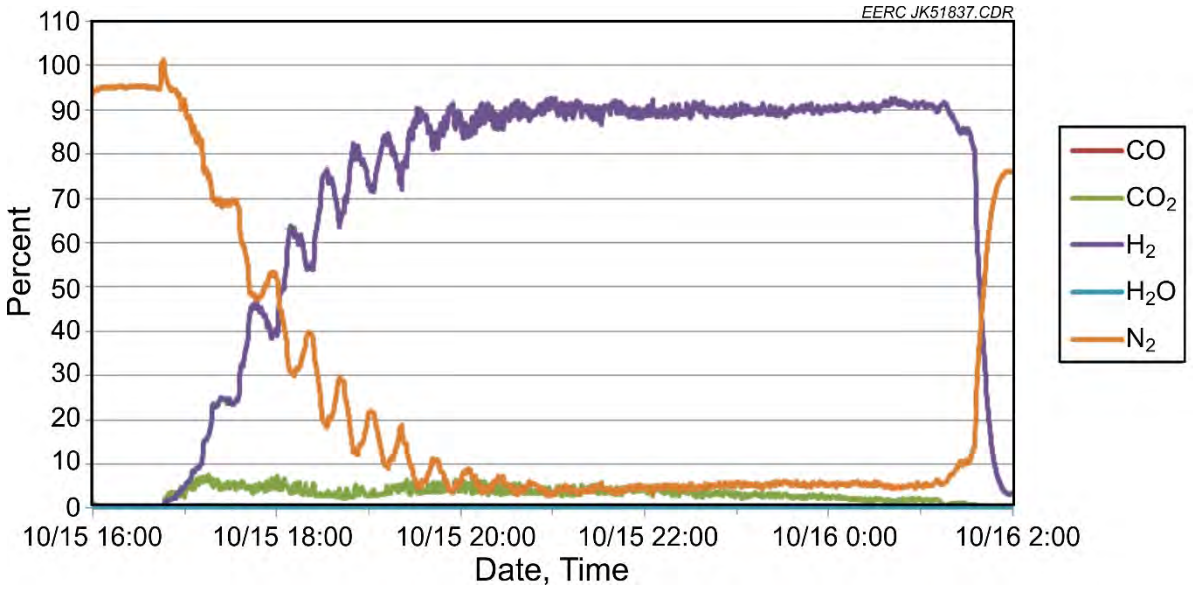

Figure 6-25. Permeate composition, Separator 208.

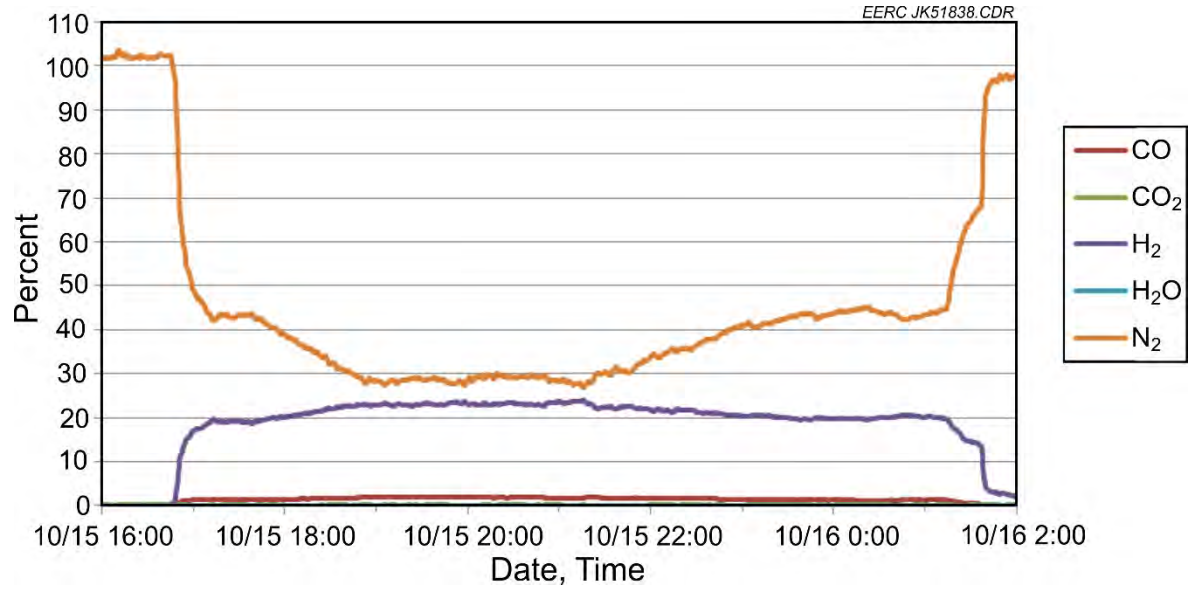

Figure 6-26. Retentate composition, Separator 208.

Table 6-7. H2M-015 Separator Performances

Test No.	Membrane Location	CSIRO Separator No.	Feed	Steady State Periods: Start Date	Start Time	End Date	End Time	Duration, hh:mm	Feed Pressure, kPa	Retentate Flow, scmh	Retentate H_2 Conc., %	Membrane Temp., °C	Permeate Flow, scmh	Permeate Pressure, kPa	Feed H_2 Conc. (Wet Basis), %	Permeate H_2 Conc. (Wet Basis), %	Augment H_2 Flow, scmh	Feed Flow, scmh	Leaking Gas Fraction, %
H2M-015 M1-1	1	213	Hydrogen	10/13/15	13:10	10/13/15	13:45	0:35	1058	0.000	0.0	315	0.057	1	100.0	100.0	0.212	0.269	ND
H2M-015 M1-2	1	211	Hydrogen	10/15/15	12:03	10/15/15	12:18	0:15	396	0.000	0.0	313	0.062	1	100.0	100.0	0.142	0.204	ND
H2M-015 M1-3	1	209	Syngas	10/15/15	16:43	10/16/15	1:35	8:52	2779	0.694	20.4	300	0.007	0	20.4	20.4	0.000	0.700	ND
H2M-015 M2-1	2	212	Hydrogen	10/13/15	13:10	10/13/15	13:45	0:35	1058	0.000	0.0	336	0.068	1	0.0	0.0	0.187	0.255	ND
H2M-015 M2-2	2	210	Hydrogen	10/15/15	12:03	10/15/15	12:51	0:48	396	0.000	0.0	344	0.062	1	0.0	0.0	0.130	0.193	ND
H2M-015 M2-3	2	210	Syngas	10/15/15	12:56	10/15/15	14:53	1:57	2770	0.739	25.0	326	0.099	2	25.0	25.0	0.000	0.838	97.5
H2M-015 M2-4	2	208	Syngas	10/15/15	16:43	10/16/15	1:35	8:52	2776	0.702	20.5	326	0.008	1	20.5	20.5	0.000	0.711	103.4

Test No.	Feed H_2 Partial, Pressure, kPa	Permeate H_2 Partial Pressure (leak-free basis), kPa	H_2 Partial Pressure Difference (leak-free basis), kPa	H_2 Flux Flow (leak-free basis), scmh	H_2 Flux Flow (leak-free basis), kmol/h	H_2 Flux (leak-free basis), $m^3/(m^2*s)$	H_2 Flux (leak-free basis), $kmol/(m^2*s)$	H_2 Permeance (leak-free basis), $m^3/(m^2*s*Pa)$	H_2 Permeance (leak-free basis), $kmol/(m^2*s*Pa)$	H_2 Flux at 700 kPa (leak-free basis), $m^3/(m^2*s)$	H_2 Flux at 700 kPa Seivert's Law (leak-free basis), $m^3/(m^2*s)$	H_2 Flux at 700 kPa (leak-free basis), $mol/(m^2*s)$	H_2 Flux at 700 kPa Seivert's Law (leak-free basis), $mol/(m^2*s)$	H_2 Recovery (leak-free basis), %
H2M-015 M1-1	1159	102	1057	0.057	0.002	0.002	7.2803E-05	1.6318E-06	6.8876E-08	0.0011	0.0013	4.7485E-05	5.4686E-05	21.05263
H2M-015 M1-2	498	102	396	0.062	0.003	0.002	8.0083E-05	4.7939E-06	2.0235E-07	0.0033	0.0028	1.3950E-04	1.1796E-04	30.55556
H2M-015 M1-3	524	ND	ND	ND	ND	ND	ND	ND	ND	ND	ND	ND	ND	ND
H2M-015 M2-1	1159	102	1057	0.068	0.003	0.002	8.7363E-05	1.9582E-06	8.2652E-08	0.0014	0.0016	5.6982E-05	6.5624E-05	26.66667
H2M-015 M2-2	498	102	396	0.062	0.003	0.002	8.0083E-05	4.7939E-06	2.0235E-07	0.0033	0.0028	1.3950E-04	1.1796E-04	32.35294
H2M-015 M2-3	523	39	484	0.037	0.002	0.001	4.7777E-05	2.3399E-06	9.8763E-08	0.0016	0.0012	6.8090E-05	5.1666E-05	16.74641
H2M-015 M2-4	595	89	505	0.007	0.000	0.000	9.2685E-06	4.3462E-07	1.8345E-08	0.0003	0.0003	1.2647E-05	1.1167E-05	4.778276

6.4.2 Test Program H2M-016

The objective of testing during H2M-016 was to subject the separators to syngas for the maximum possible time and observe their performance characteristics. CSIRO specified 325° (617°) and 350°C (662°F) as the target temperatures for membrane assemblies. The target feed flow rate for the separators was 0.71–0.0.85 scmh (25–30 scfh). The target feed pressure was 2170 kPa gauge (300 psig) throughout.

Operating conditions were held for 109 hours with over 100 hours of syngas flow to HTMS. No bed agglomeration was observed during the posttest maintenance. Table 6-8 shows the average gasifier operating conditions over the period when the gasifier was sending syngas to the membrane. Carbon conversions for these tests were somewhat lower than normal because of the lower-than-normal O_2/fuel ratios selected in order to ensure the gasifier would operate without agglomeration issues. Table 6-9 shows the average dry gas analysis for the two test campaigns. The higher nitrogen content for the first test campaign is indicative of the high PCD backpulse frequency used as compared to the second test campaign.

Table 6-8. Average Gasifier Operating Conditions for Test H2M-016

Start Date:	10/27/2015	
Start Time:	7:30	
End Date:	10/31/2015	
End Time:	12:00	
FBG Temperatures	°F	°C
O_2/Steam Inlet	803	428
Recycle Inlet	905	485
Lower Reactor Bed	1562	850
Upper Freeboard	1533	833
Reactor Extension	1265	685
Cyclone Exit	1157	625
Filter Vessel Temperatures		
Filter Vessel Average	729	387
Flows	lb/hr	kg/hr
Fuel Feed Rate	7.8	3.54
Steam	21.4	9.7
Recycle Syngas	33.8	15.3
	scfh	l/hr
Oxygen	48	1358
Syngas Purges	162	4585
Product Gas	79	2222
Pressures	psig	barg
Gasifier	314	21.7
Filter Vessel	309	21.3
Quench Pot	301	20.8
Recycle Gas Surge Tank	575	39.7
Calc. Carbon Conversion	88.6	

Table 6-9. Average Gasifier Exit Syngas Composition for Each Week of Testing

Test:	Week 1		Week 2	
Date:	10/15/2015		10/27/2015	
Start:	11:30		03:00	
End Date:	10/16/2015		10/31/2015	
End:	01:00		12:00	
Analyzer:	LGA	GC	LGA	GC
Average, mol%				
CO	1.68	1.3	2.63	2.1
H_2	21.58	17.6	37.64	33.8
O_2	0.03	0.0	0.12	0.0
N_2	31.53	36.8	11.96	10.3
CO_2	38.52	29.5	47.92	41.1
CH_4	1.47	1.2	2.83	4.1
Hydrocarbons	0.04	0.03	0.04	0.04
H_2S, ppm	2653	2100	4095	3191

Solid samples, representative of steady-state operations, were recovered from the HGFV on a regular interval. Bed material was only removed as needed to keep the bed level within normal operating ranges. Loss-on-ignition (LOI) determinations were made on each sample and are representative unconverted carbon in the sample. Filter ash sample LOIs were fairly consistent, averaging approximately 33%, while ranging from 31% to 40%. Bed material was only drained to maintain bed inventory within a desired operating range. These bed material samples averaged approximately 6.76 wt% and ranged from 1.3 wt% up to 18 wt% carbon.

The objective of testing during H2M-016 was to subject the separators to syngas for the maximum possible time and observe their performance characteristics. CSIRO specified 325° (617°) and 300°C (572°F) as the target temperatures for Membrane Assemblies 1 and 2, respectively. The temperatures were later increased to 350°C (662°F) to effect an increase in separator performance. On the last day, the temperatures were increased to 375°C (704°F) for both. The target feed flow rate for the separators was 0.71–0.85 scmh (25–30 scfh). The target feed pressure was 2170 kPa (300 psig) throughout.

Hydrogen membrane Separators 206, 207, and 218 were evaluated during the H2M-016 test period. Separators 206 and 207 were on hand at the start of testing, with Separator 218 arriving from CSIRO 2 days after testing was started. Testing was initiated with Separator 207 installed in the HMTS and with Separator 206 held in reserve if Separator 207 failed. After Separator 218 was delivered, Separator 206 was installed and tested. Table 6-10 shows the CSIRO serialized separators and their installed locations along with the period they were tested. Many of the graphs for Separators 206 and 218 show both separators plotted during a 5-day period. This was done to maintain a consistent time base for comparison of the data with Separator 207, which was in operation over the entire testing period.

Table 6-10. H2M-016 Membrane Assemblies, Separator Numbers, Feed Gas, and Test Periods

Membrane Location	CSIRO Separator No.	Feed	Start Date	Start Time	End Date	End Time	Duration hh:mm
1	207	Syngas	10/27/15	14:38	10/28/15	11:08	20:30
1	207	Syngas	10/28/15	16:07	10/30/15	06:58	38:51
1	207	Syngas	10/30/15	09:51	10/31/15	08:10	22:19
1	207	Syngas	10/31/15	10:36	10/31/15	12:08	01:32
2	206	Syngas	10/28/15	19:48	10/29/15	11:55	16:07
2	206	Syngas	10/29/15	14:18	10/30/15	06:28	16:10
2	218	Syngas	10/30/15	12:48	10/31/15	00:10	11:22
2	218	Syngas	10/31/15	00:15	10/31/15	09:01	08:46

The analyzers utilize gas-conditioning condensers to avoid water saturation and tar fouling. As a result, the analyzers return values on a dry basis. To determine the water content in the feed gas, a high-flow slipstream of feed gas was routed through a pair of condensers. The volume of gas and mass of water were measured on a timed basis and logged. During postprocessing, the moisture content of the feed gas was determined and added back into the dry gas analyses to arrive at the wet gas compositions. Because of the periodic sampling, water content of the feed gas appears to stair step. Figure 6-27 shows the feed gas composition for H2M-016. Small periodic bumps in the nitrogen are evidence of nitrogen backpulsing to clean the filter, located upstream of the HMTS. At about 10:25 on October 28, 2015, the gasifier developed a feed plug. The feeder

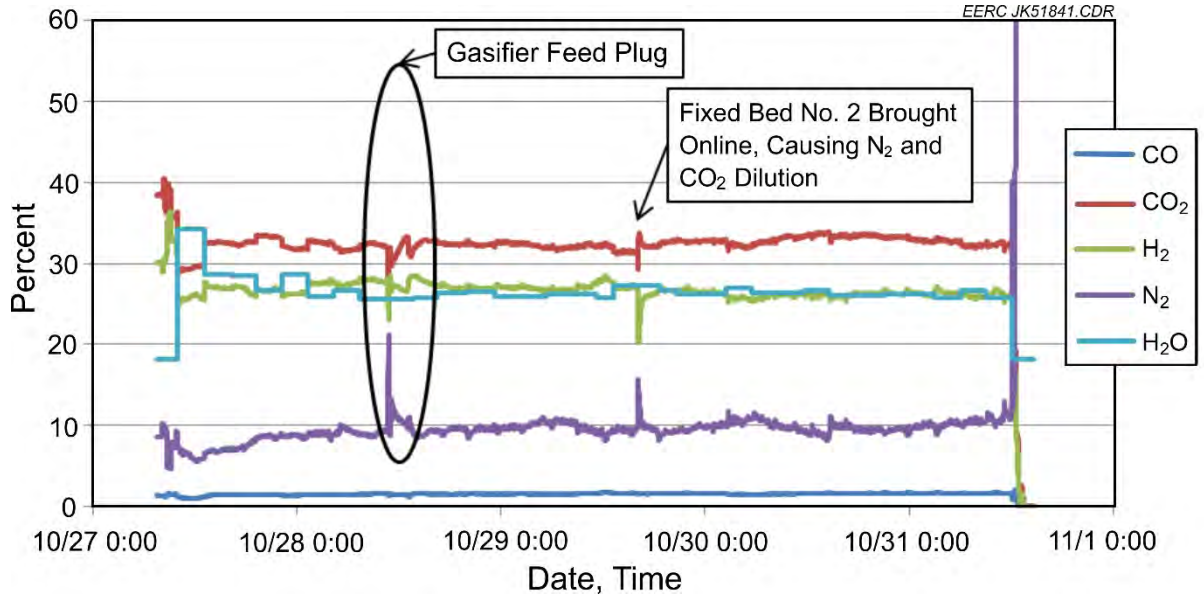

Figure 6-27. Feed gas composition, H2M-016.

was turned off for a short period, and efforts to clear it with high-pressure nitrogen resulted in nitrogen dilution. Since the gasifier was recycling syngas into its bed and it was also using syngas for its purges, it took about 2 hr for the excess nitrogen to work its way out of the system.

Initially, Fixed Bed 3 was placed online. At about 16:00 on October 29, Fixed Bed 2 was brought online and Fixed Bed 3 was taken offline and regenerated. A nitrogen spike can be seen in Figure 6-27 due to the volume of nitrogen in Fixed Bed 2 when it was brought online. The CO_2 also appeared to spike. It is believed that there was some residual oxygen deep within the pore structure of the sorbent that did not get removed during the nitrogen pressure purge cycling of the fixed bed following its previous regeneration. Fixed Bed 4 was loaded with SudChemie Actisorb-S2 and functioned as a guard bed. Feed gas levels of hydrogen sulfide were monitored at Sample Port C. Dräger tubes with a range of 0.2–6 ppm were used. At no time did the H_2S concentration of the feed gas exceed 2 ppm.

Prior to exposing to syngas, Separator 207 was brought up to pressure and purged with nitrogen on both the retentate and permeate sides. A cold leak test was performed. It was then brought up to operating temperature with nitrogen purges flowing while steady-state gasifier conditions were achieved. The assembly was leak-checked at temperature using 300 psig nitrogen. No effort was made to gradually transition from nitrogen to syngas when bringing the separator online. Separators 206 and 218 were later brought online in a similar manner to that described for Separator 207. Each of the separators exhibited strong exotherm upon initial exposure to syngas, which increased the internal assembly temperature by approximately 28°C (50°F). An example of the temperature spike associated with Separator 207 is shown in Figure 6-28. The temperature rise rate and duration were similar for all three.

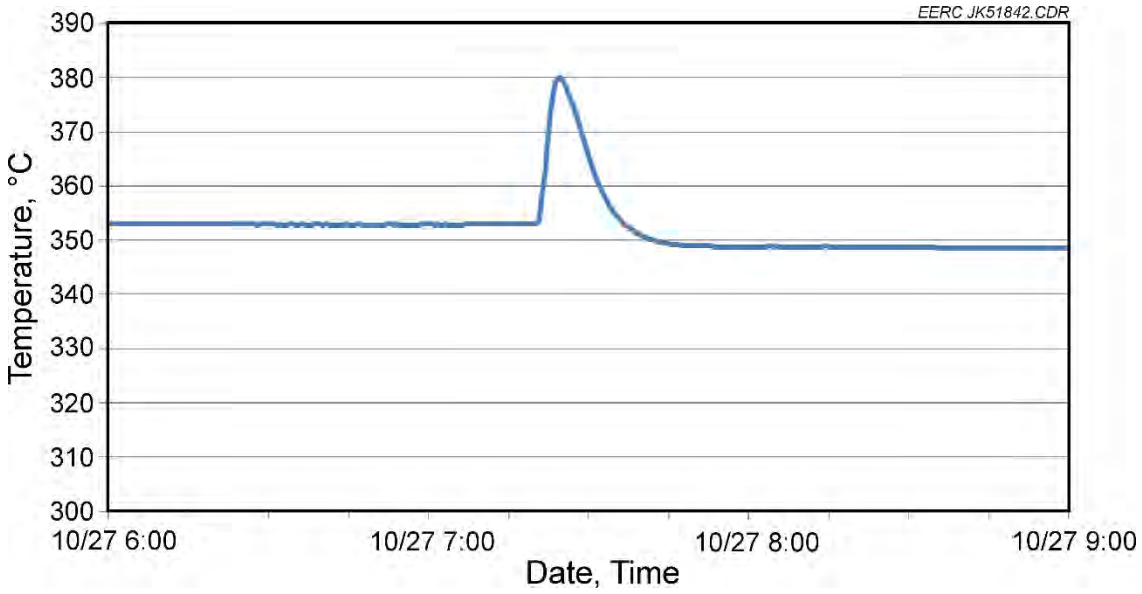

Figure 6-28. Start-up temperature spike, Separator 207.

LGA105 was used to measure permeates, and LGA106 was used to measure retentates. The two analyzers were switched back and forth between the two membrane assemblies. This resulted in gaps in the analyzer data seen in Figures 6-29–6-32. It should be noted that Separator 206 started out with a significant leak immediately after its first exposure to syngas. The leak rate was in the 60% range, seen in Figure 6-30. Figure 6-29 shows a very noisy permeate signal through 13:00 on October 29. The apparent cause of the noise was pressure pulses produced by the permeate dry gas meter that were transferred to LGA105. The sample flow through LGA105 was reduced to eliminate the pressure pulses and stabilize the analyzer readings. During postprocessing, it was observed that the hydrogen concentration roughly followed the indicated maximums. The other constituent gases tended to follow their respective minimums. Since the leak rate was derived from the gas concentrations, it too appeared very noisy. The apparent leak of Separator 207, seen in Figure 6-29, may be an artifact of analyzer noise since the reduction in the calculated leak rate correlated well with the resolution of the analyzer noise.

Although the target feed flows were 0.71–0.85 scmh (25–30 scfh), maintaining a consistent flow rate became more challenging during the last day of operation for Separator 207. This is most likely due to condensing tars on the retentate flow control valve. Since Separator 207 was in operation during the full week, it collected more tar in the valve. Separator 218 was affected to a lesser degree until during the final 6 hr of operation. The permeate and retentate flows are represented in Figures 6-33 and 6-34.

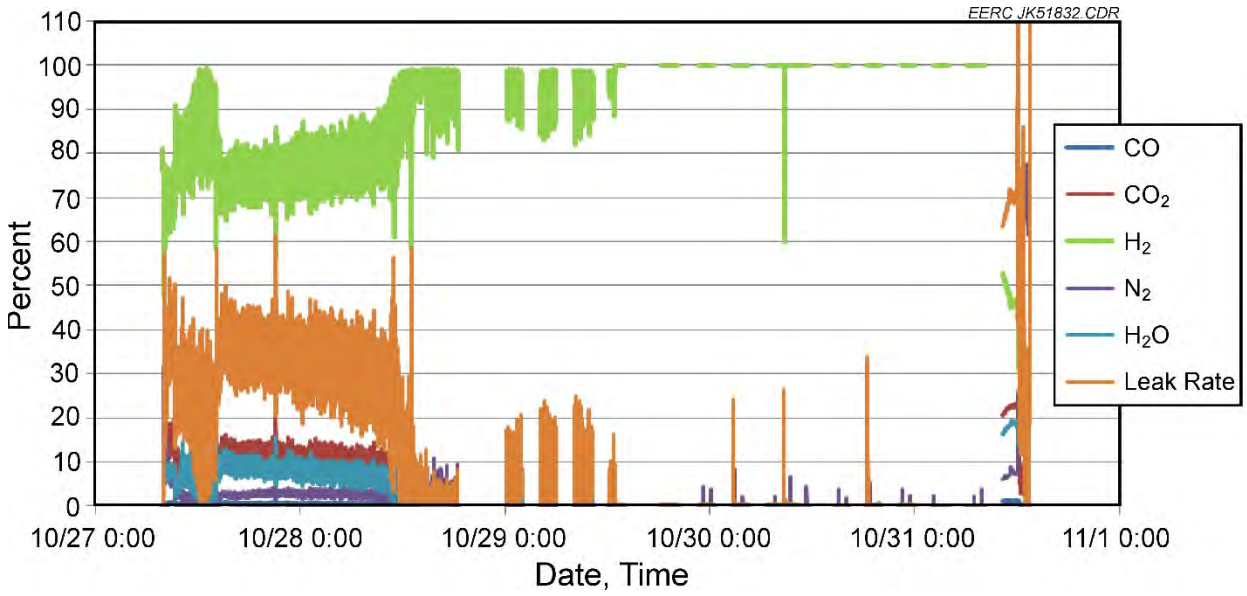

Figure 6-29. Permeate concentrations and leak rate, Separator 207.

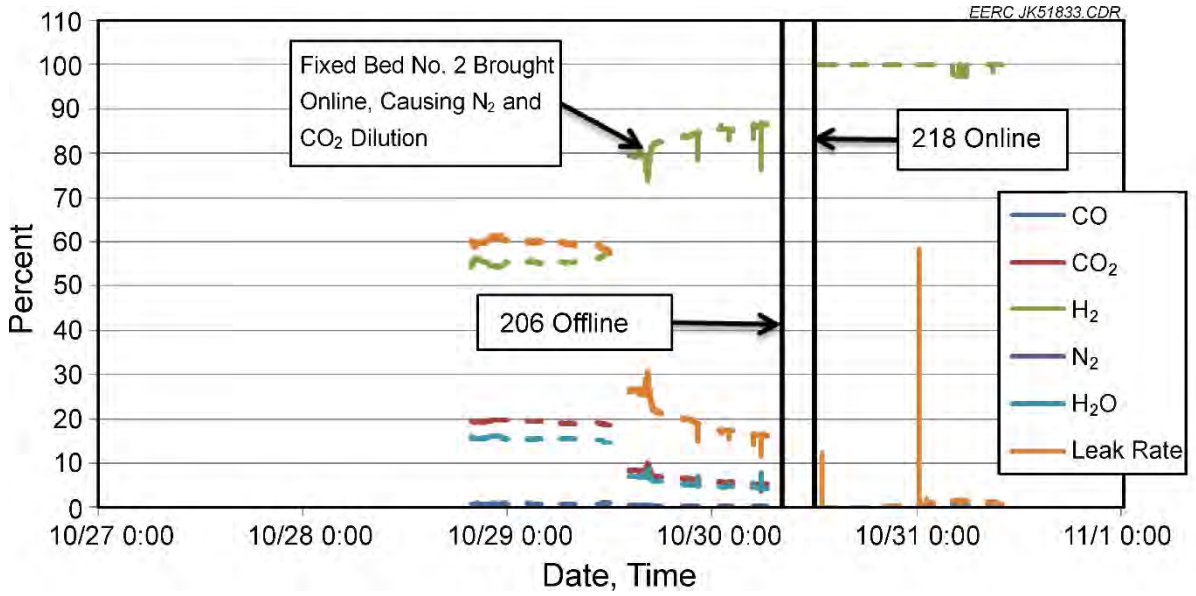

Figure 6-30. Permeate concentrations and leak rates, Separators 206 and 218.

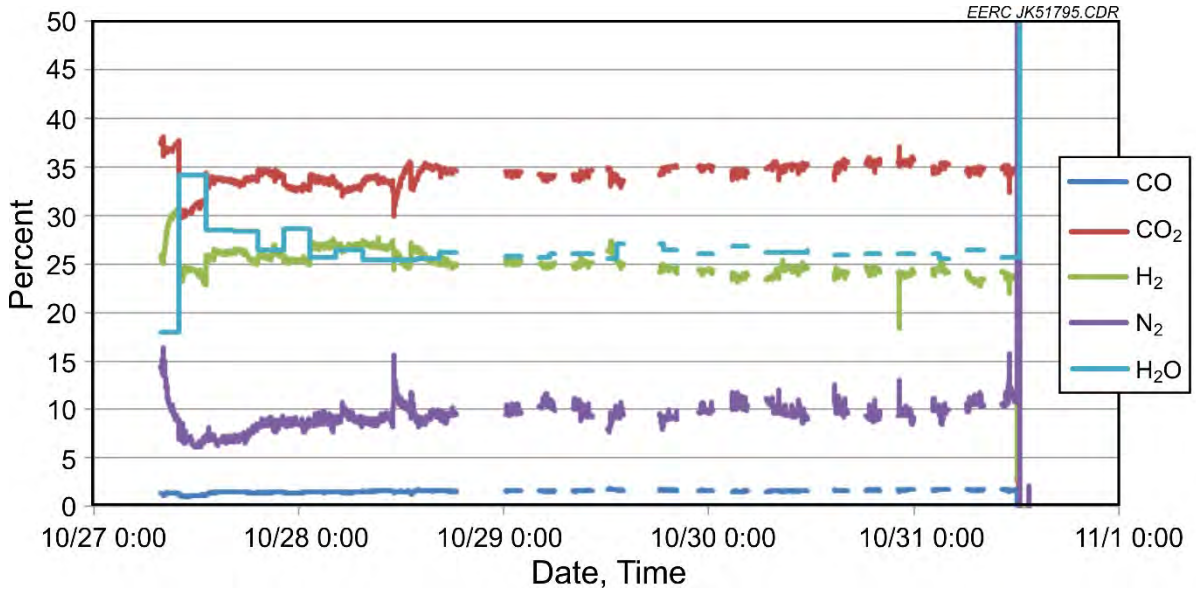

Figure 6-31. Retentate concentrations, Separator 207.

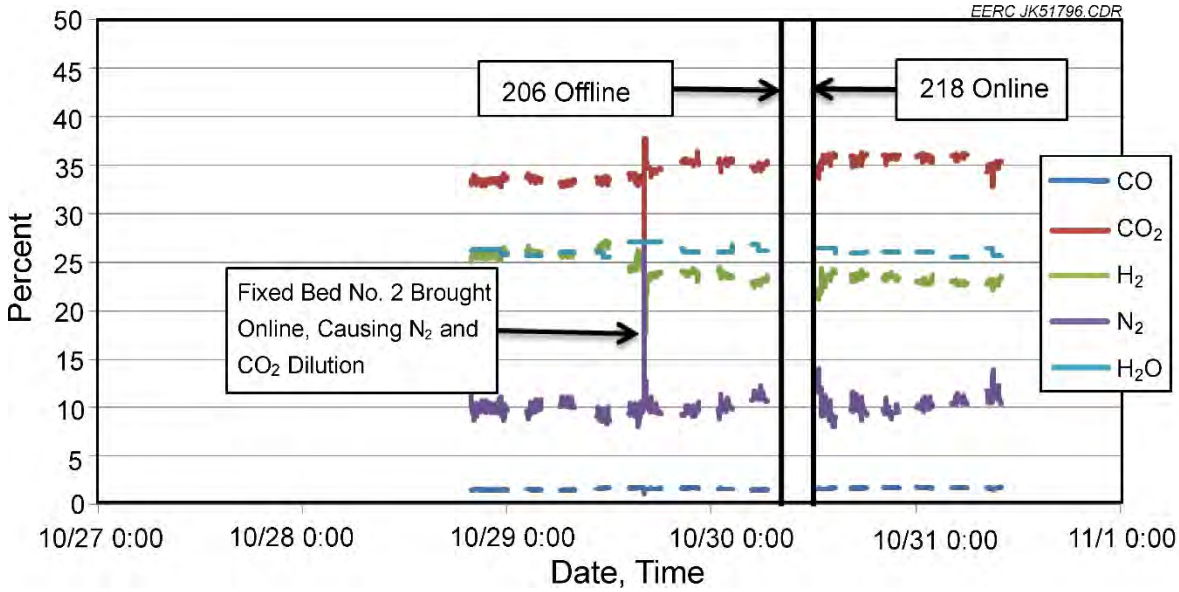

Figure 6-32. Retentate concentrations, Separators 206 and 218.

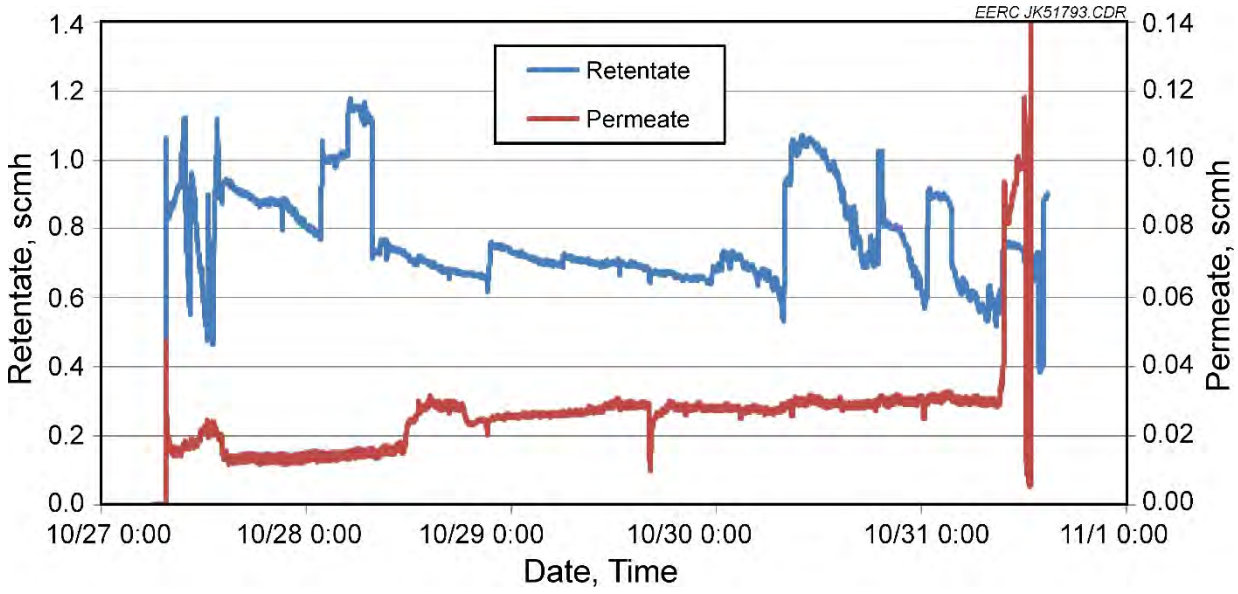

Figure 6-33. Flows, Separator 207.

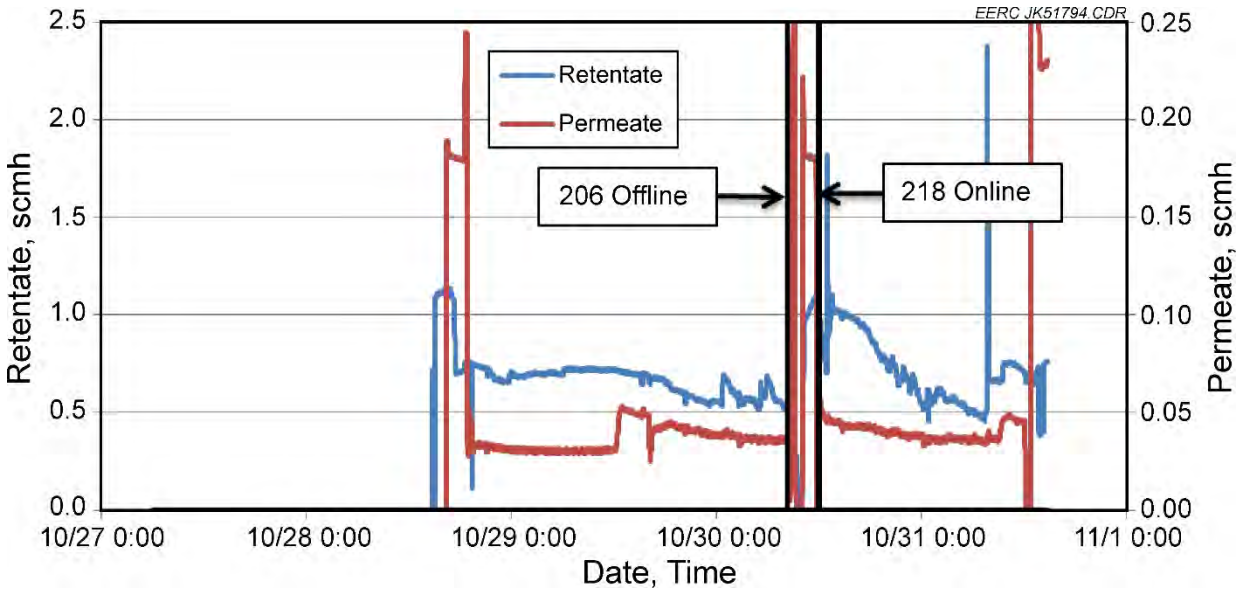

Figure 6-34. Flows, Separators 206 and 218.

The feed pressure was well maintained at 2200 kPa (304 psig), as seen in Figures 6-35 and 6-36. The H_2 partial differential pressures for all three separators ranged between about 414 (60) and 551 kPa (80 psi). Figure 6-35 shows the temperature of Separator 207 starting at about 356°C (673°F), which was above the target temperature of 325°C (617°F). The temperature was reduced to the 325°C (617°F) target at 14:00 on October 27. The temperature was raised at 10:00 on October 28 to 350°C (662°F) in an attempt to increase the flux of the separator. Figure 6-36 shows the temperature of Separator 206 starting at 300°C (572°F) and then being increased to 350°C (662°F) at 11:20 on October 29. It is interesting to note, in Figure 6-37, the leak rate of Separator 206 appears to decline with the increase in temperature. Separator 218 was brought online at a temperature of 350°C (662°F). The temperature of Separators 207 and 218 were increased to 375°C (707°F) in the final hours of the campaign to observe the effects on performance. Separator 207 developed a severe leak with this increase in temperature, which can be seen on the permeate trend line in Figure 6-33. Postrun inspection of the separator indicated that a graphite compression seal may have failed.

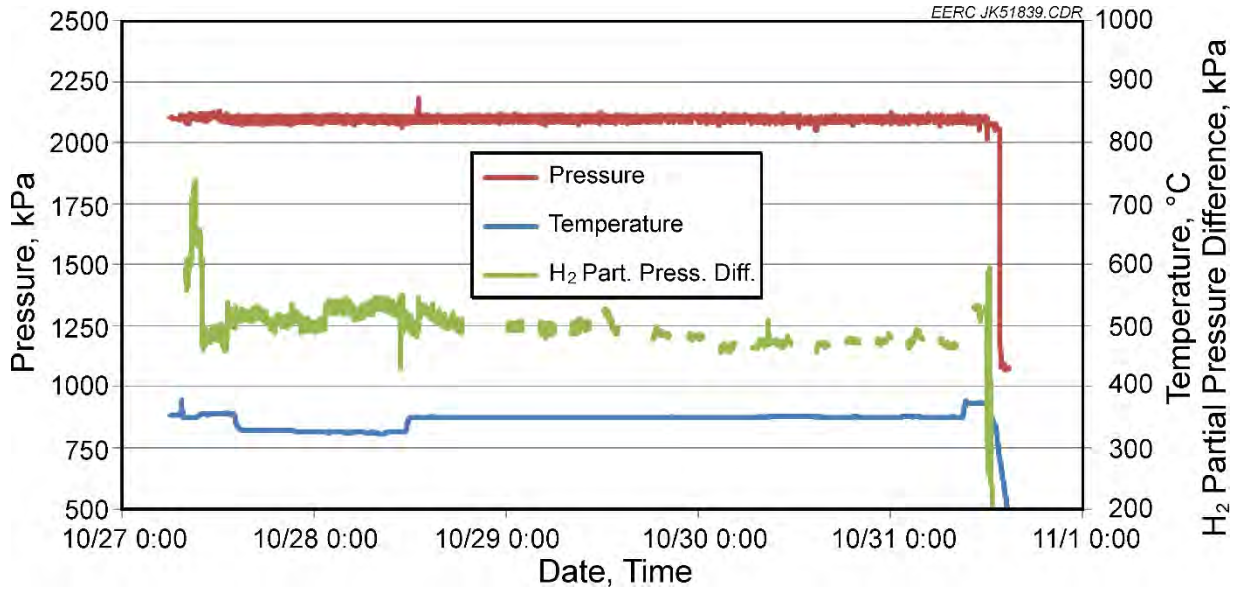

Figure 6-35. Temperature, pressure, and H_2 partial pressure difference, Separator 207.

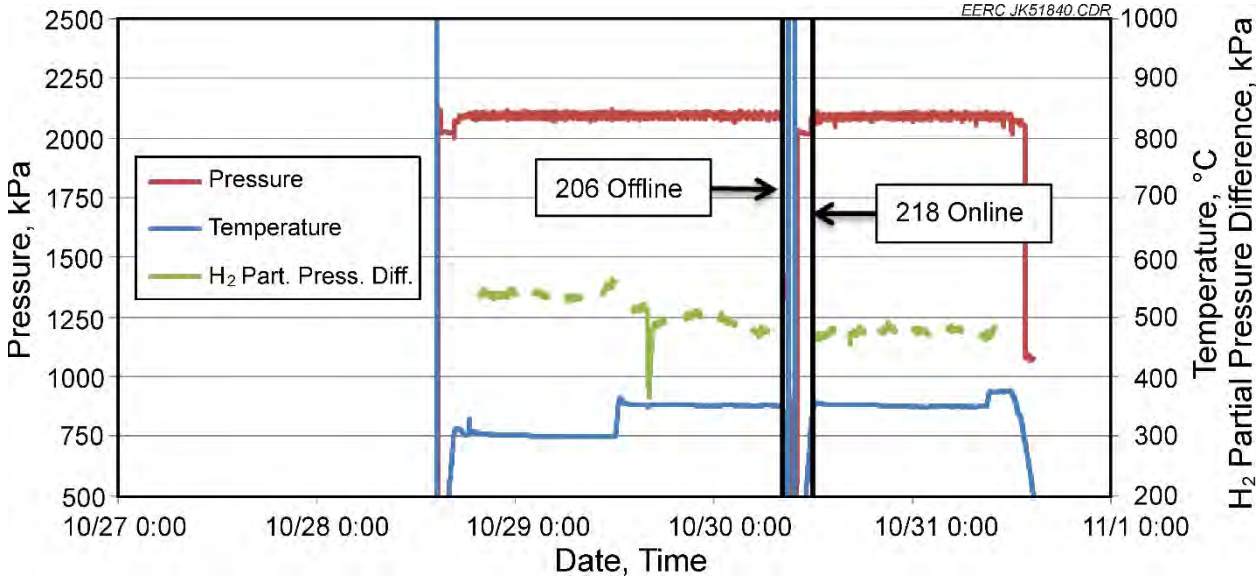

Figure 6-36. Temperature, pressure, and H_2 partial pressure difference, Separators 206 and 218.

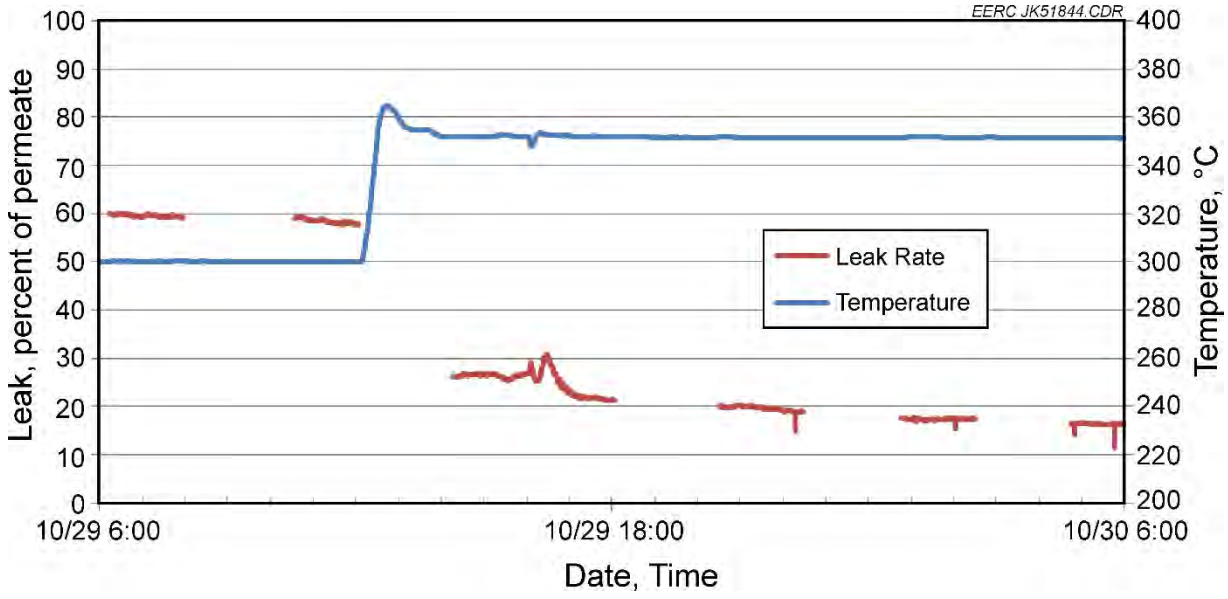

Figure 6-37. Leak rate and temperature, Separator 206.

The hydrogen recovery and flux of the separators are shown in Figures 6-38 and 6-39. Flux values are reported on a leak-free, 100 psi H_2 partial pressure difference basis. A leak-free basis was used to ascertain the performance of the separator materials and their ability to transport hydrogen. Two methods were used to calculate the flux with a transmembrane partial pressure difference of 689 kPa (100 psid). The first was based on the H_2 partial pressure differences. The second method for calculating the flux is based on Sievert's law using the difference between the square roots of the H_2 partial pressures (pressure exponent n = 0.5). Figure 6-40 shows the flux of the three separators using SI units.

Since hydrogen separation from the syngas stream affords some degree of CO_2 concentrating, the concentration factor of CO_2 leaving the separators is shown in Figure 6-41. It should be noted that the system was not operated to optimize CO_2 concentration; however, it does demonstrate some degree of concentrating capability. The advantage of concentrating CO_2 through the use of hydrogen separation membrane technologies is that the CO_2 leaves the separator at near the feed pressure.

For ease of comparison, Table 6-11 summarizes the average operating conditions and performance data for all CSIRO separators used during both 1-week campaigns. For test number designations, H2M-015 was used for the first week and H2M-016 for the second. The M1 and M2 designations reflect the location where a separator was installed in the HMTS. The final digit in the test number sequence represents the steady-state period for the separator. As a point of comparison, a set of typical conditions and performance data from a prior hydrogen separation membrane campaign at the EERC is shown at the bottom. The CSIRO separators performed better than the comparison case.

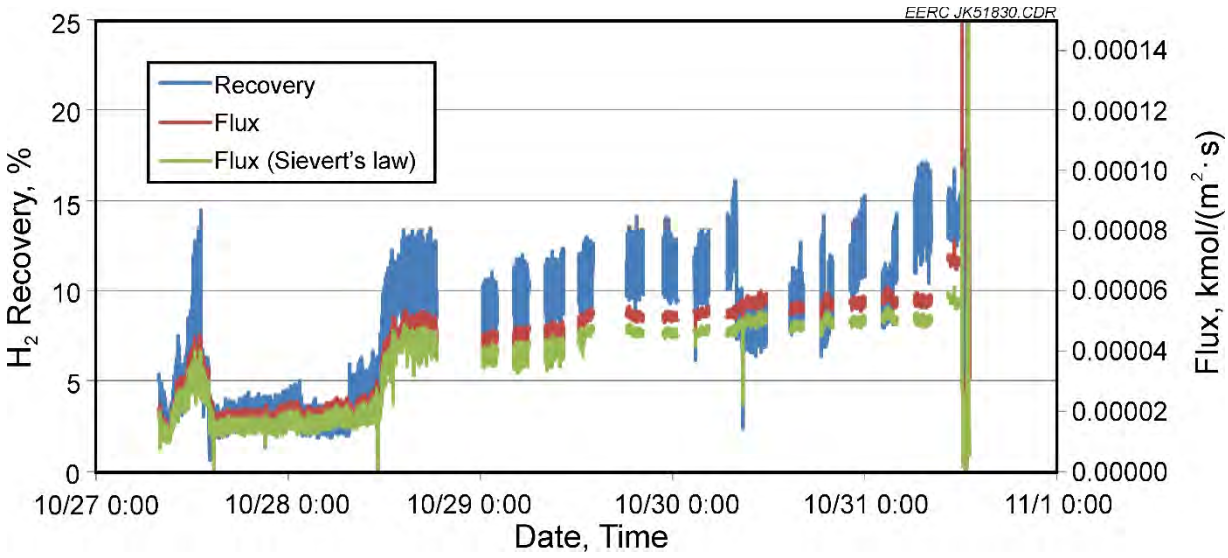

Figure 6-38. H_2 recovery and flux, Separator 207.

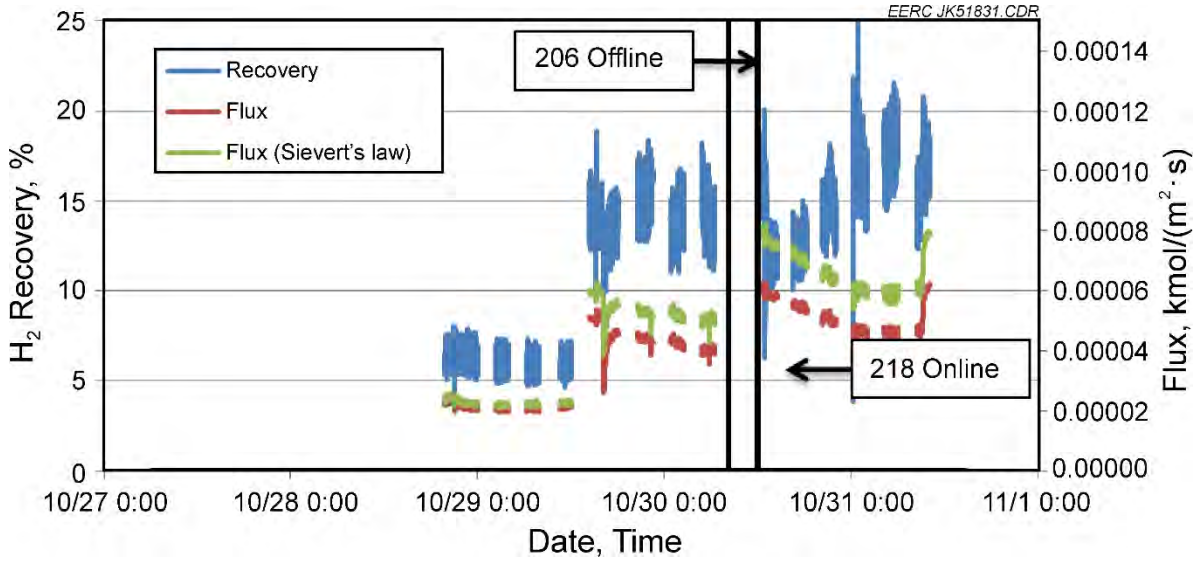

Figure 6-39. H_2 recovery and flux, Separator 206 and 218.

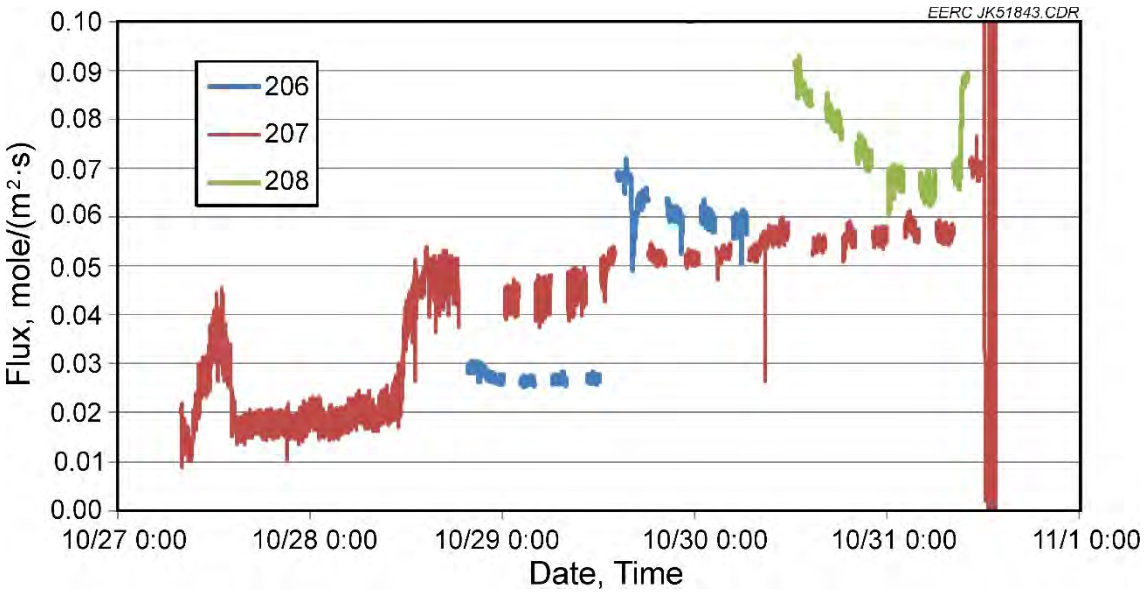

Figure 6-40. H_2 flux, Separators 206, 207, and 218 using SI units.

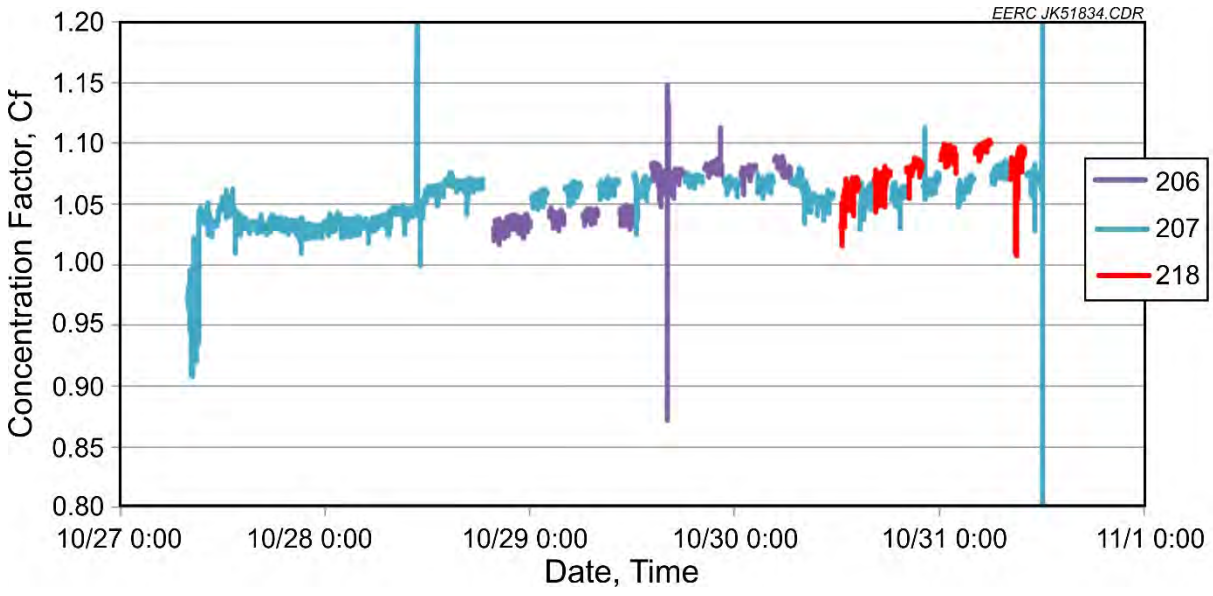

Figure 6-41. CO_2 concentration factors.

Table 6-11. H2M-015 and H2M-016 Separator Performance

Test No.	Membrane Location	CSIRO Separator No.	Feed	Steady State Periods: Start Date	Start Time	End Date	End Time	Duration, hh:mm	Feed Pressure, kPa	Retentate Flow, scmh	Retentate H_2 Conc., %	Membrane Temp, °C	Permeate Flow, scmh	Permeate Pressure, kPa	Feed H_2 Conc. (wet basis), %
H2M-015 M1-1	1	213	Hydrogen	10/13/15	13:10	10/13/15	13:45	0:35	1058	0.000	0.0	315	0.057	0.69	100.0
H2M-015 M1-2	1	211	Hydrogen	10/15/15	12:03	10/15/15	12:18	0:15	396	0.000	0.0	313	0.062	0.69	100.0
H2M-015 M1-3	1	209	Syngas	10/15/15	16:43	10/16/15	1:35	8:52	2779	0.694	20.4	300	0.007	0.05	20.4
H2M-015 M2-1	2	212	Hydrogen	10/13/15	13:10	10/13/15	13:45	0:35	1058	0.000	0.0	336	0.068	0.69	0.0
H2M-015 M2-2	2	210	Hydrogen	10/15/15	12:03	10/15/15	12:51	0:48	396	0.000	0.0	344	0.062	0.69	0.0
H2M-015 M2-3	2	210	Syngas	10/15/15	12:56	10/15/15	14:53	1:57	2770	0.739	25.0	326	0.099	2.07	25.0
H2M-015 M2-4	2	208	Syngas	10/15/15	16:43	10/16/15	1:35	8:52	2776	0.702	20.5	326	0.008	0.57	20.5
H2M-016 M1-1	1	207	Syngas	10/27/15	14:38	10/28/15	11:08	20:30	2098	0.903	26.3	327	0.014	0.83	27.1
H2M-016 M1-2	1	207	Syngas	10/28/15	16:07	10/30/15	6:58	38:51	2099	0.691	24.8	350	0.027	0.98	26.7
H2M-016 M1-3	1	207	Syngas	10/30/15	9:51	10/31/15	8:10	22:19	2096	0.802	24.2	350	0.030	0.85	26.2
H2M-016 M1-4	1	207	Syngas	10/31/15	10:36	10/31/15	12:08	1:32	2093	0.745	23.4	373	0.097	1.29	25.8
H2M-016 M2-1	2	206	Syngas	10/28/15	19:48	10/29/15	11:55	16:07	2100	0.705	26.0	301	0.031	0.34	27.0
H2M-016 M2-2	2	206	Syngas	10/29/15	14:18	10/30/15	6:28	16:10	2099	0.610	23.7	352	0.040	0.07	26.3
H2M-016 M2-3	2	218	Syngas	10/30/15	12:48	10/31/15	0:10	11:22	2096	0.839	23.5	352	0.041	−0.97	26.2
H2M-016 M2-4	2	218	Syngas	10/31/15	0:15	10/31/15	9:01	8:46	2097	0.577	22.9	349	0.036	−1.00	26.2
Example of Previously Tested Separator Assembly at the EERC									3075	120.700	15.0	403	4.577	34	15.0

Continued…

Table 6-11. H2M-015 and H2M-016 Separator Performance (continued)

Test No.	Perm. H_2 Conc. (wet basis), %	Augment H_2 Flow, scmh	Feed Flow, scmh	Leaking Gas Fraction, %	Feed H_2 Partial Pressure, kPa	Perm. H_2 Partial Pressure (leak-free basis), kPa	H_2 Partial Pressure Difference (leak-free basis), kPa	H_2 Flux Flow (leak-free basis), kmol/h	H_2 Flux (leak-free basis), kmol/(m^2*s)	H_2 Permeance (leak-free basis), kmol/(m^2*s*Pa)	H_2 Flux at 700 kPa (leak-free basis), mol/(m^2*s)	H_2 Flux at 700 kPa Seivert's Law (leak-free basis), mol/(m^2*s)	H_2 Recovery (leak-free basis), %
H2M-015 M1-1	100.0	0.212	0.269	ND	1159	102	1057	0.0024	7.3E-05	6.9E-08	4.7E-05	5.5E-05	2.1E+01
H2M-015 M1-2	100.0	0.142	0.204	ND	498	102	396	0.0026	8.0E-05	2.0E-07	1.4E-04	1.2E-04	3.1E+01
H2M-015 M1-3	20.4	0.000	0.700	ND	524	ND	ND	ND	ND	ND	ND	ND	ND
H2M-015 M2-1	0.0	0.187	0.255	ND	1159	102	1057	0.0029	8.7E-05	8.3E-08	5.7E-05	6.6E-05	2.7E+01
H2M-015 M2-2	0.0	0.130	0.193	ND	498	102	396	0.0026	8.0E-05	2.0E-07	1.4E-04	1.2E-04	3.2E+01
H2M-015 M2-3	25.0	0.000	0.838	97.5	523	39	484	0.0016	4.8E-05	9.9E-08	6.8E-05	5.2E-05	1.7E+01
H2M-015 M2-4	20.5	0.000	0.711	103.4	595	89	505	0.0003	9.3E-06	1.8E-08	1.3E-05	1.1E-05	4.8E+00
H2M-016 M1-1	76.7	0.000	0.917	33.1	597	78	518	0.0005	1.4E-05	2.7E-08	1.8E-05	1.6E-05	3.3E+00
H2M-016 M1-2	97.4	0.000	0.718	3.1	588	100	489	0.0011	3.4E-05	6.9E-08	4.8E-05	4.3E-05	1.0E+01
H2M-016 M1-3	100.0	0.000	0.832	0.2	576	102	474	0.0013	3.8E-05	8.1E-08	5.6E-05	5.0E-05	1.1E+01
H2M-016 M1-4	47.2	0.000	0.842	70.9	567	48	518	0.0019	5.9E-05	1.1E-07	7.8E-05	6.3E-05	1.4E+01
H2M-016 M2-1	55.5	0.000	0.735	59.8	595	56	538	0.0007	2.2E-05	4.1E-08	2.8E-05	2.3E-05	6.2E+00
H2M-016 M2-2	83.1	0.000	0.651	20.9	578	84	494	0.0014	4.3E-05	8.7E-08	6.0E-05	5.2E-05	1.4E+01
H2M-016 M2-3	100.0	0.000	0.881	0.1	576	100	476	0.0017	5.3E-05	1.1E-07	7.7E-05	6.8E-05	1.3E+01
H2M-016 M2-4	99.2	0.000	0.613	1.4	577	100	477	0.0015	4.6E-05	9.7E-08	6.7E-05	5.9E-05	1.7E+01
Example of Previously Tested Separator Assembly at the EERC	15.0	0.000	125	15.0	476	86	391	0.1219	3.7E-03	9.5E-06	3.6E-05	2.9E-05	1.1E+01

6.5 Conclusions and Recommendations

Efficient and cost-effective membranes for the separation of hydrogen and CO_2 represent a potentially cost-effective method for simultaneously producing power, hydrogen, and/or chemicals while CO_2 is sequestered. Significant progress has been made over the past decade in producing membranes that can effectively separate hydrogen from the syngas stream, leaving a relatively pure stream of CO_2 available at high pressure for sequestration. Cost-effective CO_2 separation is a significant technical hurdle, with a significant increase in COE produced for existing pc power plants with retrofit carbon capture. Therefore, novel approaches to the problem are required, including hydrogen and CO_2 separation membranes.

The CSIRO hydrogen separation membranes were a novel design constructed of extruded vanadium alloy. Vanadium is highly permeable to hydrogen and a much lower cost to manufacture compared to palladium alloys. The hydrogen permeability of vanadium is tens of times greater than that of palladium, making vanadium of particular interest for use in hydrogen-selective metal membranes. Self-supporting vanadium-based metal membranes, comprising a vanadium core overlaid with hydrogen dissociation and recombination catalysts, are a potentially low-cost alternative to the current benchmark Pd-based membranes.

Twelve dense metallic hydrogen separation membranes were provided by CSIRO for testing during the 2-week campaign. Nine of those separation membranes were used. Performance was comparable to others tested at the EERC. The second week of testing provided the most meaningful performance data. Degradation of the separator that operated the full week was not observed. Of particular concern is the brittle fractures observed on two of the separators and the long-term separator tolerance to syngas impurities. The root cause of these failures was not determined during these tests.

The performance of the membranes increased as the temperature was increased. Higher-temperature operation should be the objective of future testing to take advantage of the increased performance. Additionally, the higher temperatures would most likely accelerate membrane material degradation thereby facilitating the materials research that CSIRO was interested in. The compression seals used in the assemblies were problematic because of expansion issues; however, in large-scale operation, the separators would use welds to transition to conventional piping.

Novel separator technologies, such as those supplied by CSIRO and demonstrated at the EERC, using gasifier-generated syngas highlight a number of key issues for further evaluation. Temperature, pressure, and flow parametric evaluation is necessary to further understand the baseline performance characteristics. Additionally, long-term evaluation of the membrane technology is needed to understand the effects of specific impurities on performance and integrity as well as the adverse effects of transient operation that would be encountered in commercial operations. Welding or bonding techniques of the separator to standard metals are also required. The unique metallurgy in the heat-affected weld zone may produce vulnerabilities that are not readily apparent and need to be evaluated in the same manner as the separator materials.

7.0 CAPTURE TECHNOLOGY MODELING AND TECHNO-ECONOMIC ASSESSMENT

7.1 Postcombustion Capture Modeling

7.1.1 Introduction

A detailed process-modeling effort was undertaken to develop the basis for determining the cost of CO_2 capture using advanced postcombustion capture technologies and techniques, including solvents from KCRC and CSES, and a technique for partial capture with MEA. The model was developed using Aspen Plus software and mimics the boiler and steam cycle for Cases 11 and 12 from the DOE report entitled "Cost and Performance Baseline for Fossil Energy Plants, Volume 1: Bituminous Coal and Natural Gas to Electricity" (Black, 2013a). Case 11 represents a 550-MW-net pc-fired power plant with a supercritical steam cycle operating at 39.3% efficiency. Case 12 represents a 550-MW-net pc-fired supercritical power plant with 90% CO_2 capture. The overall plant size is increased in Case 12 to account for the significant parasitic load of the CO_2 capture process, and the overall efficiency is 28.4%. The models developed in the DOE report serve as the basis for which the advanced postcombustion technologies are analyzed. Assumptions used in developing the model are provided in Appendix A.

7.1.2 Experimental Methods and Software Description

7.1.2.1 Aspen Plus Modeling Software

The power plant, including the CO_2 capture unit, was modeled using Aspen Plus, licensed and distributed by AspenTech. The software has the capability of modeling the mass and energy balance for an entire power plant, from coal feed and combustion to CO_2 capture. The program allows the user to set up unit operations in a block flow diagram and then enter the specific details for each process and input stream. Detailed physical and chemical property data are utilized to develop rigorous reaction-based equilibrium and kinetic models. Aspen Plus has built-in property packages for handling coal solids and also for CO_2 reaction kinetics with various solvents. The mass and energy balances developed in Aspen Plus can be exported directly to APEA for sizing and costing of equipment and materials, enhancing the capabilities and value of Aspen Plus.

7.1.2.2 Model Basis and Assumptions

The strategy for the modeling effort was to develop the overall mass and energy balance for the coal-fired system using Aspen Plus. The power plant boundaries for the techno-economic study included the entire power plant system. Because of the time constraints put on the modeling effort, it was not possible to model every system and subsystem of the power plant in detail. Detailed mass and energy balance modeling was performed for the boiler, flue gas cleanup, and steam cycle, but not all subsystems were modeled. Therefore, the results from Cases 11 and 12 were used to determine the cost and energy requirements of many of the subsystems in the power plant.

The boundaries for the system model as determined by DOE are given as follows:

- Delivered coal entering the pc plant through high-pressure, high-purity CO_2 stream crossing plant fence
- Net electricity conditioned and sent to electric grid
- Raw makeup water

Waste streams generated by the pc plant, including the CO_2 capture system, should be adequately treated on-site prior to disposal either by landfill or other commercial disposal options.

A schematic identifying system boundaries is shown in Figure 7-1.

The process design assumptions were also called out in detail and are expected to be identical to Cases 11 and 12 of the DOE report.

7.1.2.3 Combustion Model

The combustion system with steam heat exchangers and flue gas cleanup was modeled in Aspen Plus to mimic the mass and energy balance presented in Cases 11 and 12 of the DOE report. The Aspen model built is shown in Figure 7-2. The Aspen model does not represent all of the components of the power plant but, rather, the main components necessary to produce an accurate mass and energy balance around the major pieces of equipment. Separation of the steam cycle and

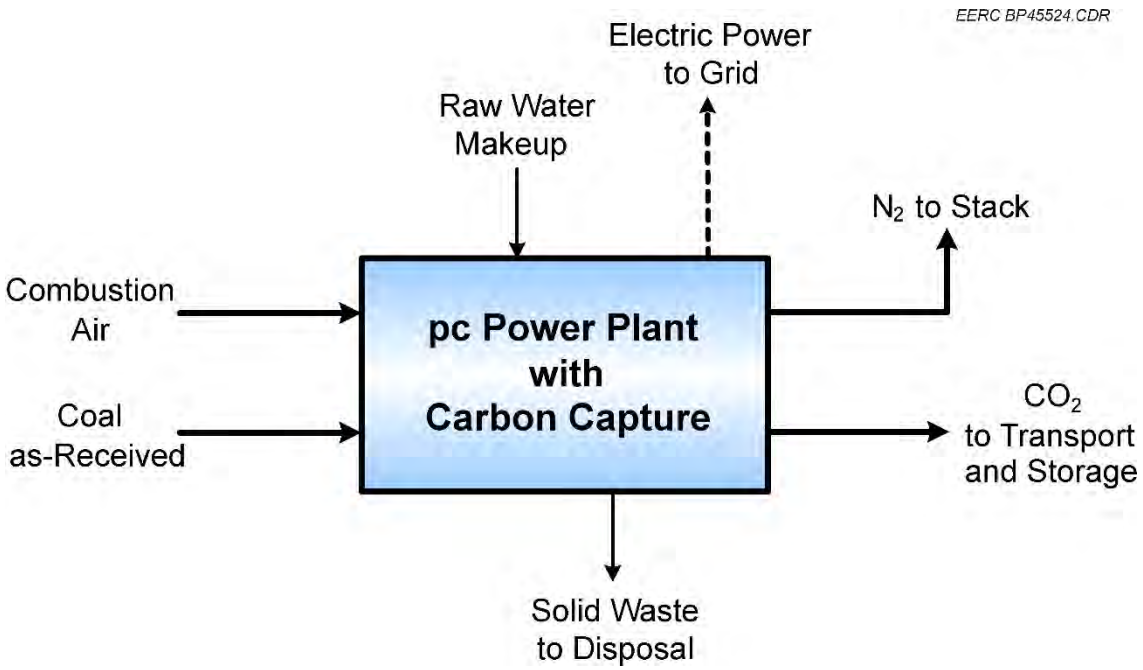

Figure 7-1. Power plant modeling system boundaries.

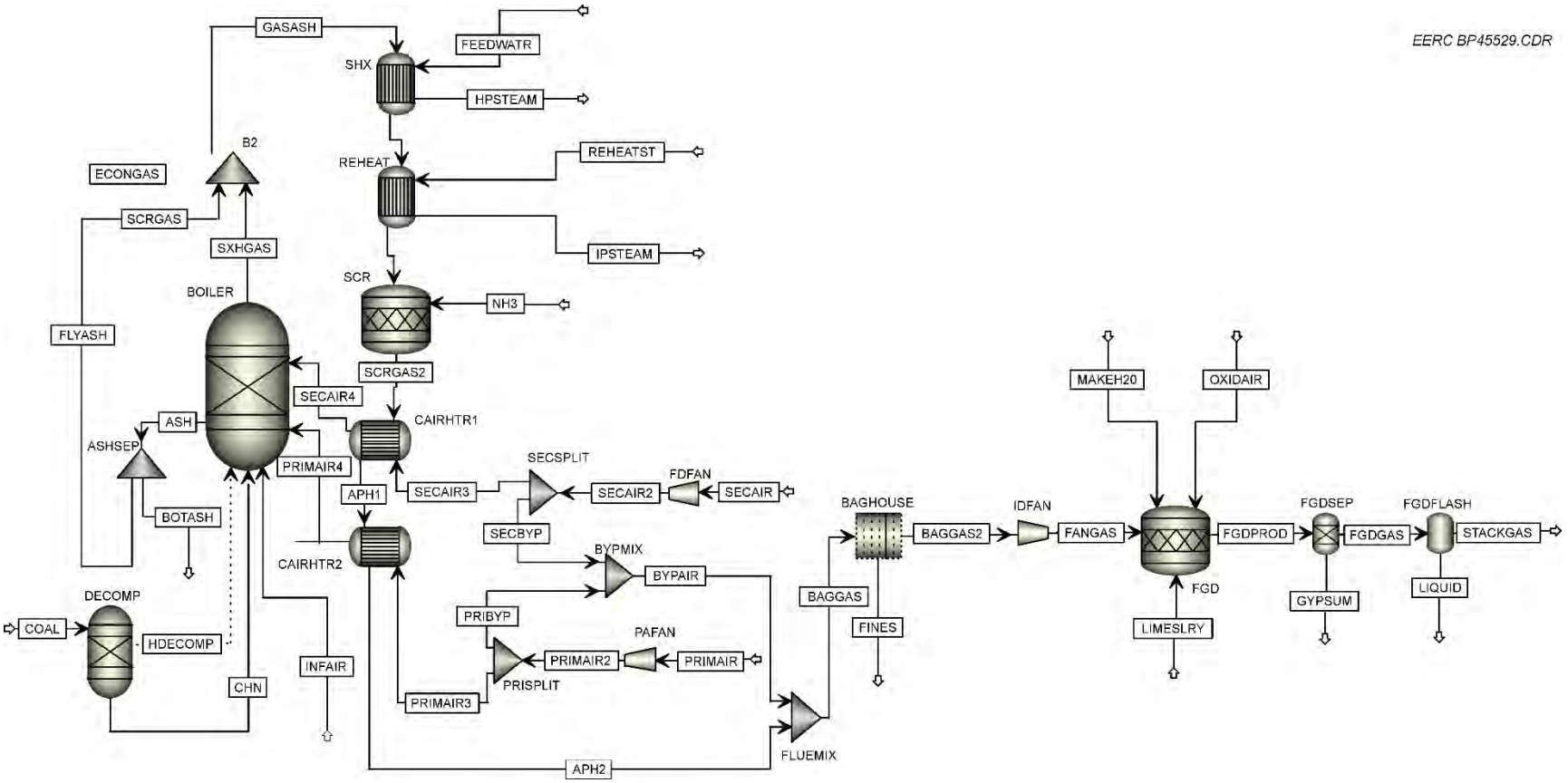

Figure 7-2. Aspen model representing the coal combustion portion of Case 12.

the CO_2 capture system resulted in the most efficient modeling strategy for the different process areas. Integration of each area and the use of recycle streams become very difficult and can result in unstable models when small changes are made. The separation of the systems still allowed for rapid evaluation of changing process conditions by using built-in tools such as transfer blocks to move information to different model segments.

The overall property method chosen for the coal and flue gas handling was the Peng–Robinson method with Boston–Mathais modifications. Areas of pure water or steam use the National Bureau of Standards/National Research Council (NBS/NRC) steam tables for physical properties. The model was originally built and calibrated based on Case 11 from the DOE report. Coal feed enters into a decomposition block that uses the user-entered proximate and ultimate analysis to break the coal down into base components that can be modeled in the combustion unit. A portion of the primary and secondary air bypasses the combustor and joins the flue gas stream after the SCR unit. The remaining air is preheated and enters the boiler along with an infiltration airstream that represents air leaks into the slightly negatively pressured boiler. The Gibbs free energy minimization equilibrium model is used to model the coal combustion step. Flue gas exit temperature is calculated based on the enthalpies of the streams entering and leaving the system. Solid ash exits the combustor in a separate stream and is then separated into fly ash and bottom ash. The fly ash is rejoined with the flue gas in a mixing block. Heat exchangers are used to heat the steam entering the boiler. The heat exchange process is not rigorously modeled to match the exact configuration of the boiler but is detailed enough to produce an accurate mass and energy balance around the system. The flue gas passes through an SCR with ammonia injection for NO_x control, which is simply modeled using a stoichiometric reactor with specifications for reaction extents. The flue gas passes through a set of air preheaters prior to the remaining control equipment.

A baghouse is used for particulate control and is specified with a built-in baghouse model in Aspen Plus. The fines collected are shown as an output stream, and then the gas pressure is boosted with an ID fan prior to entering the WFGD unit. Limestone, water, and oxygen all enter into the WFGD where the sulfur reaction takes place, producing gypsum and additional CO_2. A separation block removes the solids, and a flash step separates the saturated water from the flue gas at the given temperature and pressure. The gas exiting the flash represents the composition of the flue gas entering the CO_2 capture system.

7.1.2.4 Steam Cycle

The supercritical steam cycle was first built and calibrated in Aspen Plus to mimic Cases 11 and 12 from the DOE report. The model is shown in Figure 7-3. The NBS/NRC steam table property method was used for all unit operations in the steam cycle. The high-pressure, intermediate-pressure, and low-pressure turbine were modeled in Aspen, with some cases using multiple turbine blocks to represent intermediate steam draws. The steam passes into a condenser unit and then is pumped to a midrange pressure for passage through the boiler feedwater heaters. The steam drawn from the turbines is used to preheat the boiler feedwater and help maximize efficiency for the cycle. The high-pressure water for the supercritical cycle reaches a pressure of 28.85 MPa (4185 psia) and is expanded to 6.89 kPa (1 psia) in the low-pressure turbine, maximizing efficiency and energy extraction potential.

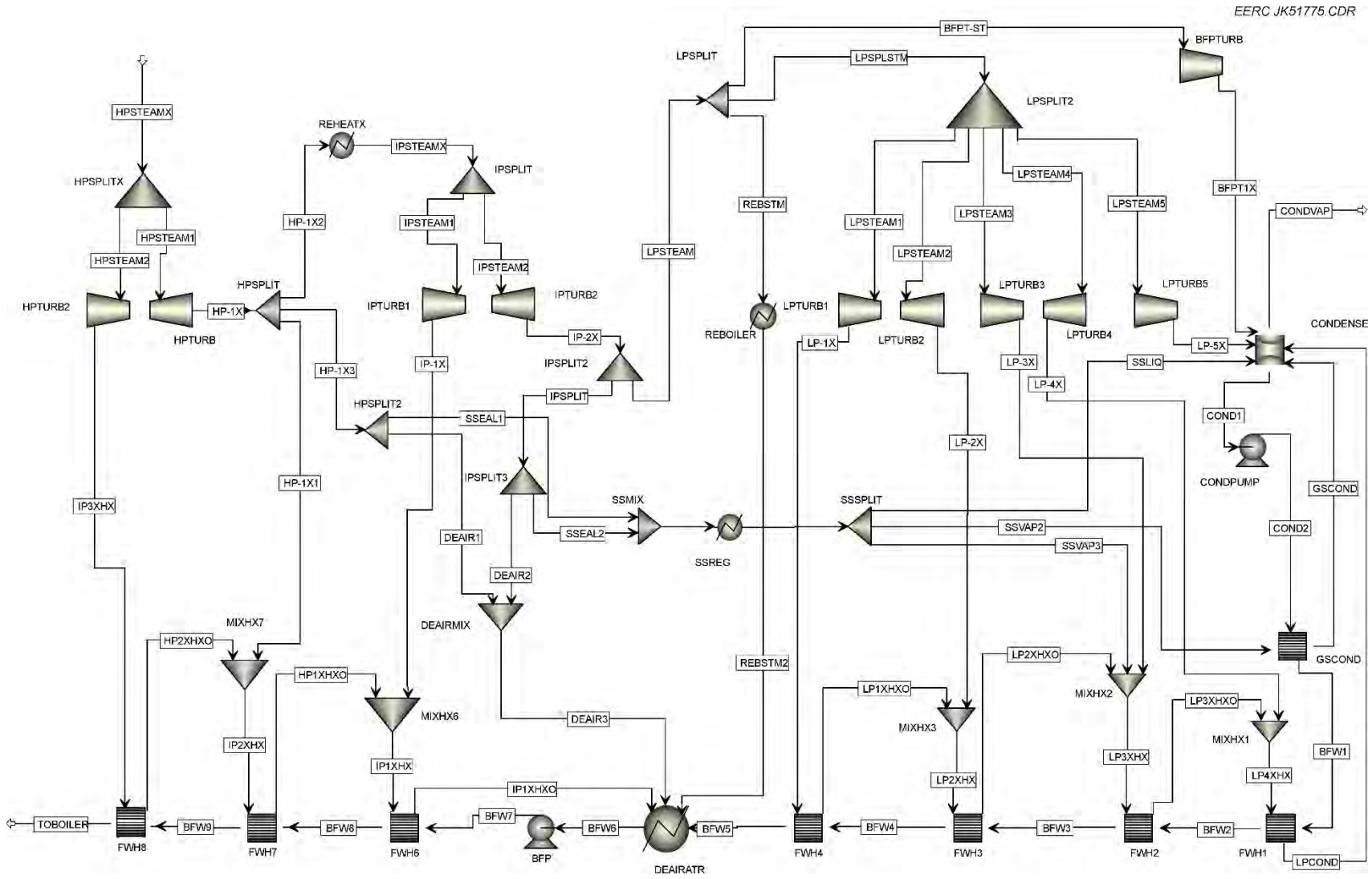

Figure 7-3. Aspen model representing the steam cycle of Case 12.

The NBS/NRC steam tables were used for the steam cycle model property method. Throttle steam enters the model at the conditions given by the combustion model. After passing through the high-pressure turbine, the steam is reheated in a reheater that represents the reheat section of the boiler. The duty available for this reheater is also calculated from the combustion model. Portions of the steam are used for boiler feedwater preheating and get spent through the steam seal regulator. The majority of the steam continues to the intermediate-pressure turbine. The exiting steam from the intermediate-pressure turbine is again separated for boiler feedwater preheating and for the steam seal regulator, and the majority of the steam leaving the intermediate-pressure turbine passes on to the low-pressure turbines. A portion of the steam is also sent to the boiler feed pump turbine to provide power for pumping the water back to the pressure required for the high-pressure turbine.

Several extraction points from the low-pressure turbines are used for boiler feedwater preheating. All of the steam extracted eventually makes its way back to the condenser where it is condensed to water. The water is pumped to a higher pressure for the first set of boiler feedwater heaters and then pumped to boiler tube pressure for the last set of heat exchangers. A deaerator prevents oxygen buildup in the system. Makeup water is brought in at the condenser location and represents evaporative losses. Water is drawn off at the deaerator location to enable a steady-state model.

The main output from the model is the work produced in each of the turbines. This work was summated and used to calibrate the steam cycle to Case 11 of the DOE report. Turbine efficiencies were adjusted to match the conditions presented in the DOE model and were within typical values. The steam cycle model was used to calculate the gross power generation of the plant for the base model and for various CO_2 capture scenarios.

7.1.2.5 Solvent-Based Absorber–Stripper System

The advanced solvents have proprietary formulations, and the compositions are unknown to the EERC. Therefore, in the absence of complete chemical and kinetic data, MEA was used in Aspen Plus to simulate the performance of the solvents. Flue gas generated by the coal combustion model was sent to a CO_2 capture system that used a rigorous rate-based model to estimate capture performance (Figure 7-4). Flue gas from the combustor and lean solvent were contacted in an absorber system, using a standard absorber tower. CO_2 absorption is exothermic in nature, so the flue gas was heated during absorption, and cooling was used to control the temperature exotherm. The flow rate of lean MEA solvent was adjusted so that 90% of the CO_2 in the flue gas was captured. During absorption, the flue gas evaporates a small portion of MEA, so it was sent to a wash tower where water removed most of the MEA from the flue gas. The water and MEA were recycled to the absorber system. A small fraction of MEA was still lost through evaporation in the flue gas stream and also through a wastewater purge operation; therefore, a fresh MEA makeup stream was included in the model. Any MEA that would be lost to degradation through HSS formation was also estimated in the model.

A rate-based add-on package to Aspen Plus called RateSep was used to calculate the rate of CO_2 absorption and desorption in the system. Aspen Plus used the following electrolyte reaction

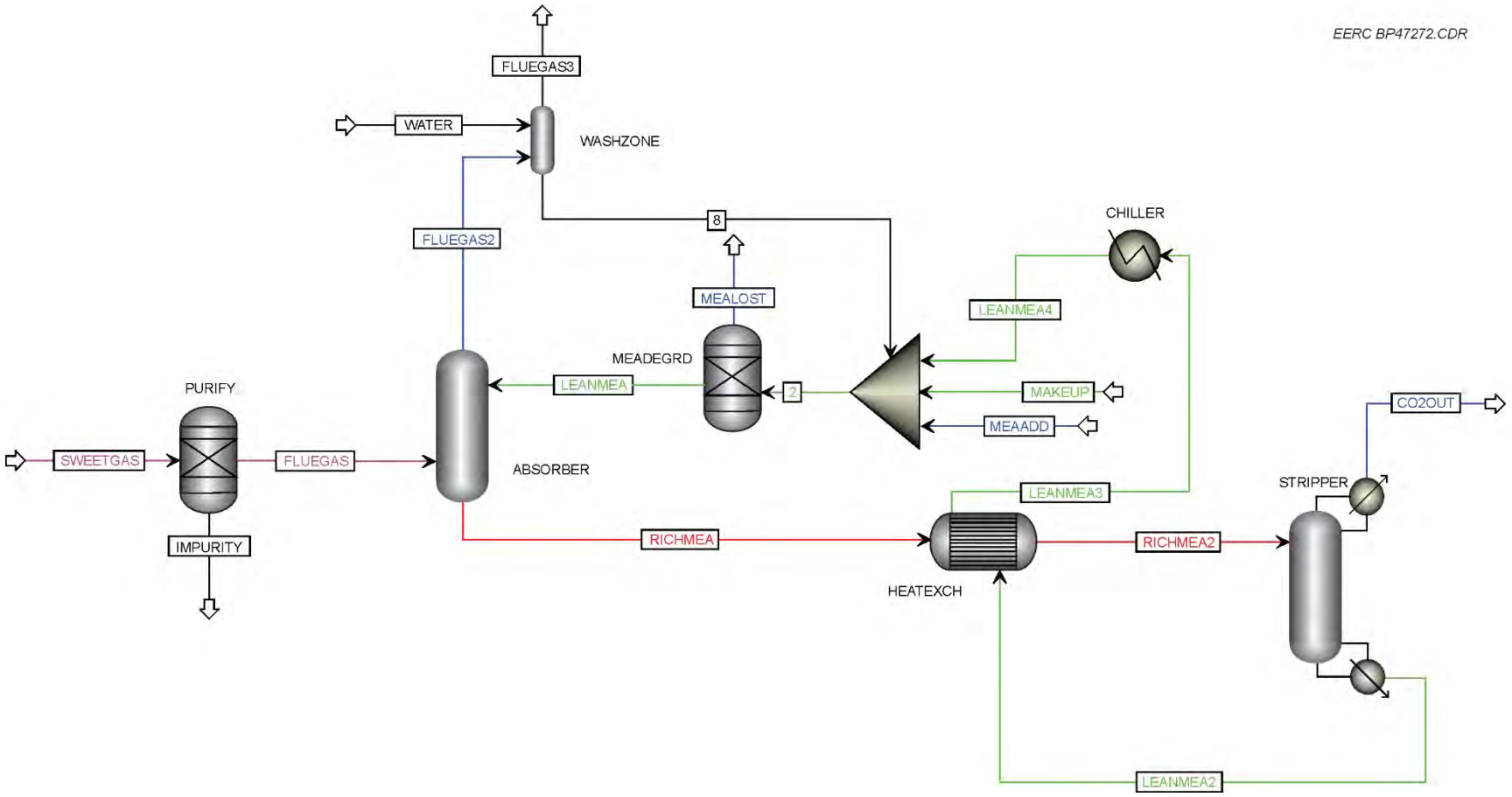

Figure 7-4. Aspen Plus model for CO_2 absorber–stripper system.

chemistry for CO_2 capture with MEA to determine the rates of absorption and other chemical reaction properties:

$$H_2O + MEACOO- \leftrightarrow MEA + H_3O + \quad \text{[Eq. 7.1]}$$

$$H_2O + MEA + \leftrightarrow MEA + H_3O + \quad \text{[Eq. 7.2]}$$

$$NH_3 + HCO_3- \leftrightarrow H_2O + NH_2COO- \quad \text{[Eq. 7.3]}$$

$$H_2O + NH_3- \leftrightarrow OH- + NH_4 + \quad \text{[Eq. 7.4]}$$

$$H_2O + HCO_3- \leftrightarrow CO_3- - + H_3O + \quad \text{[Eq. 7.5]}$$

$$2\,H_2O + CO_2 \leftrightarrow HCO_3- + H_3O + \quad \text{[Eq. 7.6]}$$

$$2\,H_2O \leftrightarrow OH- + H_3O + \quad \text{[Eq. 7.7]}$$

The rich MEA solvent exiting the absorber was heated by lean solvent in a cross-heat exchanger up to 200°F. The rich solvent then entered a stripping column to drive the CO_2 from the solvent. A reboiler at the bottom of the stripper column provided the energy for regeneration. A condenser at the top of the column condensed water from the CO_2-rich stream and returned it to the column. High-purity CO_2 saturated with water exited the top of the absorber column before proceeding to the condensation and compression step. The temperature of the stripper column was set to control the loading of the MEA solvent and, ultimately, the CO_2 capture rate. The lean solvent exiting the bottom of the stripper was sent to the cross-heat exchanger for cooling, and it was recycled to the absorber tower.

Case 12 was modeled with 30 wt% MEA as an approximation for the advanced solvents. A baseline CO_2 capture rate was established using the reduced L/G and regeneration steam usage requirements. That baseline capture rate was then used as the target for subsequent model iterations. Compression was not modeled in detail in this effort, and NETL estimates for compressor cost and power were used to guide the overall plant mass and energy balance.

7.1.2.6 Model Iterations

The three models were used together in an iterative process to determine the size of the plant necessary to capture CO_2 and generate 550 MW net power. The original steam cycle and combustion models were calibrated to Case 11 of the DOE report. Then the auxiliary power requirements for running the CO_2 capture system and CO_2 compression were considered, and the entire plant was resized to compensate for the loss in generation from the auxiliary equipment. The increase in plant size resulted in higher production rates of CO_2; therefore, the CO_2 capture system had to be increased in size to accommodate for additional CO_2. The larger CO_2 capture system then required more auxiliary power for pumping and compression. This process continued in an iterative manner until all three models converged at the same steam generation and power usage rates, and the net power output was 550 MW from the plant.

7.1.3 KCRC Performance/Model Results and Discussion

The results of the Aspen Plus process modeling effort were used to develop the mass and energy balance for utilization of the KCRC solvent in a 550-MWe power facility. The results of the study are presented in similar format to the DOE report for rapid comparison of the differences. A complete mass and energy balance around the system is presented along with overall efficiency calculations.

7.1.3.1 Block Flow Diagram and Stream Table, Supercritical Unit with CO_2 Capture

Figure 7-5 shows the overall block diagram for the supercritical pc combustion plant with CO_2 capture using the KCRC solvent. Table 7-1 follows the figure to give detailed information about the composition, temperature, and pressure of each stream in the system. The block flow diagram does not represent a complete mass balance of the system and is intended as a visual aid for understanding the layout of the power plant.

The system modeled represents a pc power plant with a supercritical steam cycle and a CO_2 capture system. The boiler is wall-fired with primary air and secondary air that represents overfire air (OFA) staging used to control NO_x emissions. SCR with ammonia injection is used to control NO_x emissions at the boiler exit. A standard pulse-jet baghouse is used for flue gas particulate control. A WFGD with limestone injection is used to control sulfur levels entering the CO_2 capture system. Case 12 uses a standard absorber tower and stripper column.

7.1.3.2 Heat and Mass Balance Diagrams

Diagrams showing the overall heat and mass balance for the power plant are shown in Figures 7-6 and 7-7. The heat and mass balance diagrams follow Case 11 of the DOE report very closely, and the flow, temperature, pressure, and enthalpy values were derived from the models developed in Aspen Plus.

7.1.3.3 Plant Performance Summary Table

The addition of CO_2 capture technology to the base plant increases the auxiliary power load; therefore, a bigger overall power plant is needed to produce the 550 MW net of power required for the study. Table 7-2 shows the overall power plant performance summary for KCRC; Cases 11 and 12 from the DOE report are also included for comparison. The overall plant performance in the KCRC case is significantly improved over Case 12. The main reason for this improvement is the reduced steam withdrawal from the steam cycle for regeneration, which results in a much lower coal feed rate and smaller overall plant size. The auxiliary load for CO_2 capture and compression is also lower than Case 12. It should be noted that the baseline MEA model uses five CO_2 capture trains. The reduced L/G for the KCRC solvent enabled the same amount of CO_2 capture in three trains instead of five trains. This reduces the overall auxiliary load on the plant and also results in economic advantages that will be discussed later. The overall efficiency of the plant was improved from 28.4% to 30.8% as compared to Case 12.

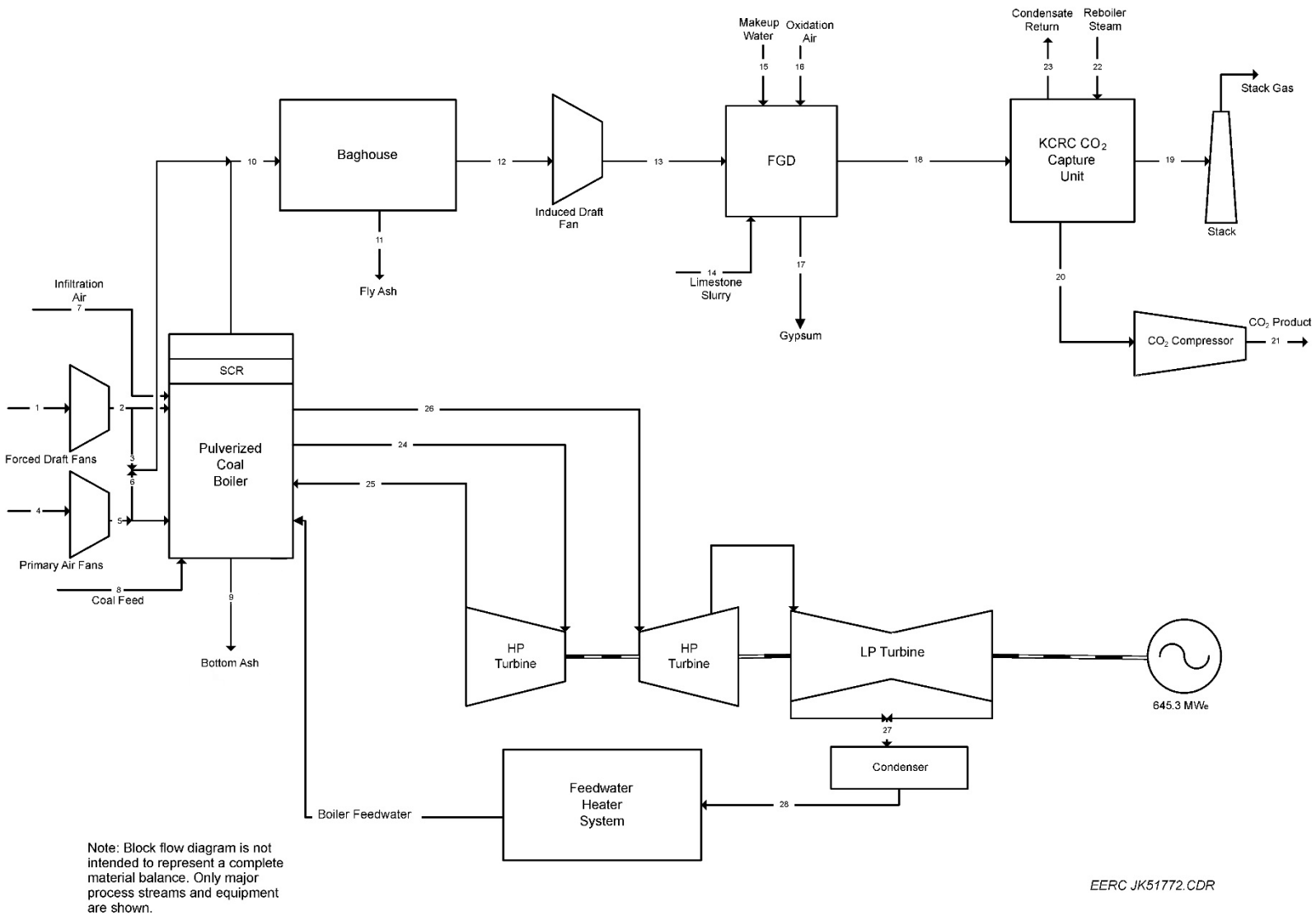

Figure 7-5. Block flow diagram for the supercritical pc combustion plant with CO_2 capture.

Table 7-1. KCRC Stream Table, Supercritical Unit with CO_2 Capture

	1	2	3	4	5	6	7	8	9	10	11	12	13	14
Vapor–Liquid (V-L) Mole Fraction														
Ar	0.0092	0.0092	0.0092	0.0092	0.0092	0.0092	0.0092	0.0000	0.0000	0.0087	0.0000	0.0087	0.0087	0.0000
CO_2	0.0003	0.0003	0.0003	0.0003	0.0003	0.0003	0.0003	0.0000	0.0000	0.1446	0.0000	0.1446	0.1446	0.0000
H_2	0.0000	0.0000	0.0000	0.0000	0.0000	0.0000	0.0000	0.0000	0.0000	0.0000	0.0000	0.0000	0.0000	0.0000
H_2O	0.0099	0.0099	0.0099	0.0099	0.0099	0.0099	0.0099	0.0000	0.0000	0.0892	0.0000	0.0892	0.0892	1.0000
N_2	0.7732	0.7732	0.7732	0.7732	0.7732	0.7732	0.7732	0.0000	0.0000	0.7305	0.0000	0.7305	0.7305	0.0000
O_2	0.2074	0.2074	0.2074	0.2074	0.2074	0.2074	0.2074	0.0000	0.0000	0.0244	0.0000	0.0244	0.0244	0.0000
SO_2	0.0000	0.0000	0.0000	0.0000	0.0000	0.0000	0.0000	0.0000	0.0000	0.0021	0.0000	0.0021	0.0021	0.0000
Total	1.0	1.0	1.0	1.0	1.0	1.0	1.0	0.0	0.0	1.0	0.0	1.0	1.0	1.0
V-L Flow Rate, kg-mol/hr	61,635	61,635	1825	18,934	18,934	2606	1425	0	0	86,956	0	86,956	86,956	3370
V-L Flow Rate, kg/hr	1,778,518	1,778,518	52,676	546,343	546,343	75,191	41,108	0	0	2,583,413	0	2,583,413	2,583,413	60,709
Solids Flow Rate, kg/hr	0	0	0	0	0	0	0	236,526	4588	18,347	18,347	0	0	26,231
Temperature, °C	15	19	19	15	26	26	15	15	15	169	15	169	182	15
Pressure, MPa, abs	0.10	0.11	0.11	0.10	0.11	0.11	0.10	0.10	0.10	0.10	0.10	0.10	0.11	0.10
Enthalpy, kJ/kgA	−97.5	−92.8	−92.8	−97.5	−86.8	−86.8	−97.5	–	–	−2511.6	–	−2511.6	−2498.6	–
Density, kg/m^3	1.2	1.2	1.2	1.2	1.3	1.3	1.2	–	–	0.8	–	0.8	0.8	–
V-L Molecular Weight	28.856	28.856	28.856	28.856	28.856	28.856	28.856	–	–	29.709	–	29.709	29.709	–
V-L Flow Rate, lb-mol/hr	135,882	135,882	4024	41,742	41,742	5745	3141	0	0	191,706	0	191,706	191,706	7429
V-L Flow Rate, lb/hr	3,920,960	3,920,960	116,131	1,204,480	1,204,480	165,768	90,627	0	0	5,695,450	0	5,695,450	5,695,450	133,841
Solids Flow Rate, lb/hr	0	0	0	0	0	0	0	521,450	10,115	40,449	40,449	0	0	57,830
Temperature, °F	59	67	67	59	78	78	59	59	59	337	59	337	359	59
Pressure, psia	14.7	15.3	15.3	14.7	16.1	16.1	14.7	14.7	14.7	14.4	14.7	14.2	15.3	15.0
Enthalpy, Btu/lb[1]	−41.9	−39.9	−39.9	−41.9	−37.3	−37.3	−41.9	–	–	−1079.8	–	−1079.8	−1074.2	–
Density, lb/ft^3	0.076	0.078	0.078	0.076	0.081	0.081	0.076	–	–	0.05	–	0.049	0.052	–

[1] Reference conditions are 77°F and 14.696 psia.

Continued. . .

Table 7-1. KCRC Stream Table, Supercritical Unit with CO_2 Capture (continued)

	15	16	17	18	19	20	21	22	23	24	25	26	27	28
V-L Mole Fraction														
Ar	0.0000	0.0128	0.0000	0.0081	0.0106	0.0004	0.0004	0.0000	0.0000	0.0000	0.0000	0.0000	0.0000	0.0000
CO_2	0.0000	0.0005	0.0001	0.1349	0.1760	0.9957	0.9957	0.0000	0.0000	0.0000	0.0000	0.0000	0.0000	0.0000
H_2	0.0000	0.0000	0.0000	0.0000	0.0000	0.0000	0.0000	0.0000	0.0000	0.0000	0.0000	0.0000	0.0000	0.0000
H_2O	1.0000	0.0062	0.9999	0.1535	0.0466	0.0038	0.0037	1.0000	1.0000	1.0000	1.0000	1.0000	1.0000	1.0000
N_2	0.0000	0.7505	0.0000	0.6792	0.8940	0.0001	0.0001	0.0000	0.0000	0.0000	0.0000	0.0000	0.0000	0.0000
O_2	0.0000	0.2300	0.0000	0.0238	0.0311	0.0000	0.0000	0.0000	0.0000	0.0000	0.0000	0.0000	0.0000	0.0000
SO_2	0.0000	0.0000	0.0000	0.0000	0.0000	0.0000	0.0000	0.0000	0.0000	0.0000	0.0000	0.0000	0.0000	0.0000
Total	1.0	1.0	1.0	1.0	1.0	1.0	1.0	1.0	1.0	1.0	1.0	1.0	1.0	1.0
V-L Flow Rate, kg-mol/hr	13,485	974	9737	94,596	71,886	11,557	12,588	28,913	28,913	116,590	95,141	95,141	41,644	57,924
V-L Flow Rate, kg/hr	242,940	28,290	175,415	2,726,884	2,018,563	507,426	552,664	520,883	520,883	2,100,409	1,713,985	1,713,985	750,224	1,043,521
Solids Flow Rate, kg/hr	0	0	39285	0	0	0	0	0	0	0	0	0	0	0
Temperature, °C	15	181	57	57	32	21	35	291	151	593	354	593	39	39
Pressure, MPa, abs	0.10	0.31	0.10	0.10	0.10	0.16	15.27	0.51	0.92	24.23	4.90	4.52	0.01	1.69
Enthalpy, kJ/kgA	−16,007.1	−98.6	–	−3095.3	−642.0	−8955.6	−9184.9	−12,935.6	−15,83.0	−12,502.3	−12,900.0	−12,325.7	−13,520.6	−15,814.5
Density, kg/m^3	1003.1	2.4	–	1.1	1.1	2.9	560.5	2.0	759.3	69.2	18.6	11.6	0.0	993.2
V-L Molecular Weight	18.015	29.029	–	28.83	28.08	43.91	43.91	18.015	18.015	18.015	18.015	18.015	18.015	18.015
V-L Flow Rate, lb-mol/hr	29,730	2148	21,466	208,549	158,481	25,478	25,476	63,743	63,743	257,038	209,749	209,749	91,809	127,701
V-L Flow Rate, lb/hr	535,592	62,368	386,723	6,011,750	4,450,170	1,118,682	1,118,682	1,148,350	1,148,350	4,630,610	3,778,690	3,778,690	1,653,960	2,300,570
Solids Flow Rate, lb/hr	0	0	86,609	0	0	0	0	0	0	0	0	0	0	0
Temperature, °F	59	357	135	135	89	69	95	556	304	1,100	669	1,100	102	103
Pressure, psia	14.7	45	14.8	14.9	14.7	23.5	2214.5	73.5	133.6	3,514.7	710.8	655.8	1.0	245.0
Enthalpy, Btu/lb[1]	−6881.8	−42.4	–	−1330.75	−276.0	−3850.2	−3948.8	−5561.3	−6613.5	−5375.0	−5546.0	−5299.1	−5812.8	−6799.0
Density, lb/ft^3	62.622	0.149	–	0.067	0.070	0.183	34.993	0.123	47.4	4.319	1.16	0.722	0.003	62.004

[1] Reference conditions are 77°F and 14.696 psia.

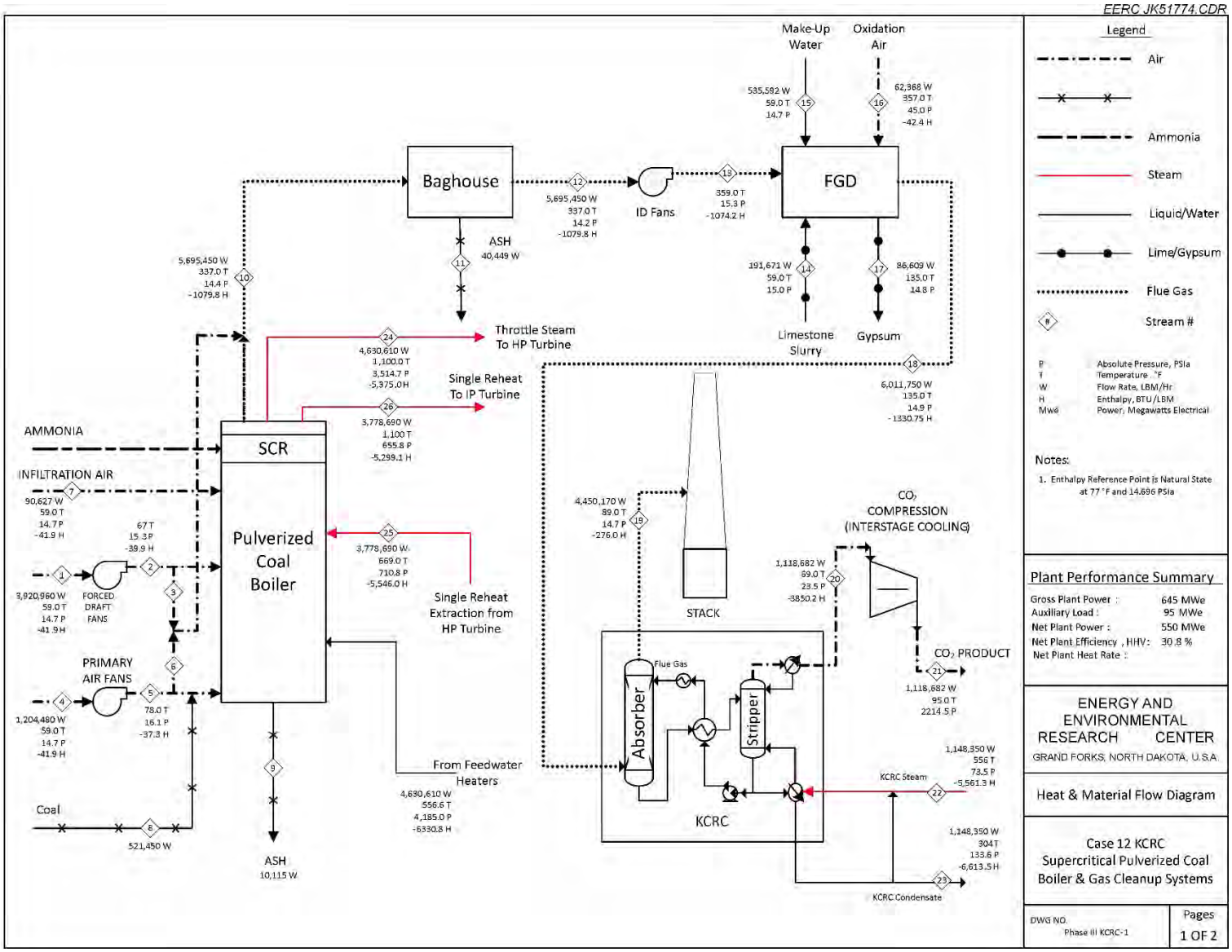

Figure 7-6. Combustor heat and material flow diagram for KCRC.

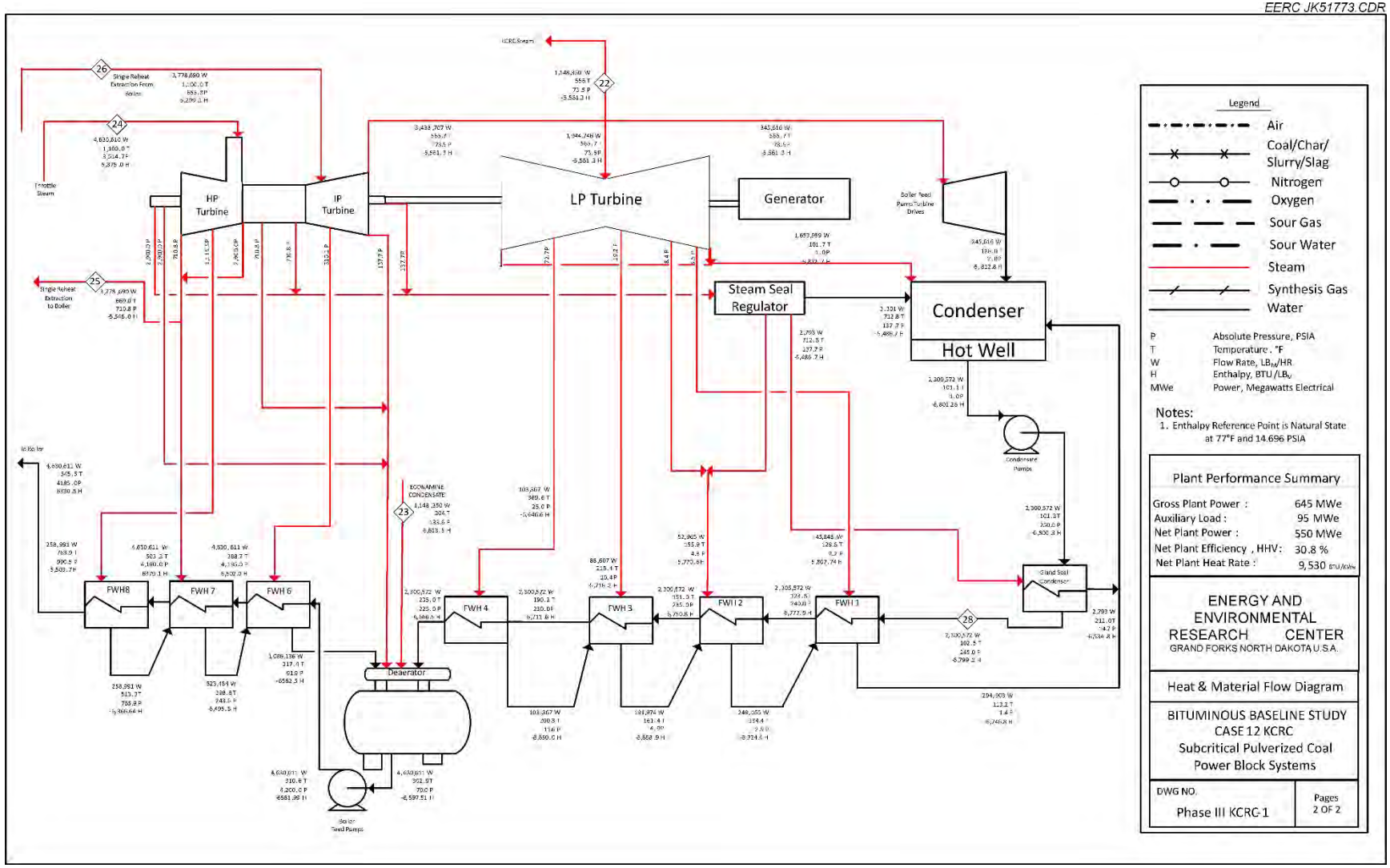

Figure 7-7. Steam cycle heat and material flow for KCRC.

Table 7-2. Overall Plant Performance

Steam Turbine Power:	Case 11 580,400	Case 12 662,800	KCRC 645,269
Coal Handling and Conveying	440	510	490
Pulverizers	2780	3850	3546
Sorbent Handling and Reagent Preparation	890	1250	1148
Ash Handling	530	740	680
Primary Air Fans	1300	1800	1658
Forced-Draft Fans	1660	2300	2118
ID Fans	7050	11,120	9965
SCR	50	70	64
Baghouse	70	100	91
WFGD	2970	4110	3786
CSES Auxiliaries	–	20,600	11,391
CO_2 Compression	–	44,890	41,370
Miscellaneous BOP	2000	2000	2000
Steam Turbine Auxiliaries	400	400	400
Condensate Pumps	800	560	628
Circulating Water Pump	4730	10,100	8576
Groundwater Pumps	480	910	788
Cooling Tower Fans	2440	5230	4438
Transformer Losses	1820	2290	2157
Total Auxiliaries, kW_e	30,410	112,830	95,294
Net Power, kW_e	549,990	549,970	549,975
Net Plant Efficiency (HHV[1])	39.3%	28.4%	30.8%
Net Plant Heat Rate, Btu/kWh	8687	12,002	9530
Condenser Cooling Duty, 10^6 Btu/hr	2178	1646	1997
Consumables			
As-Received Coal Feed, lb/hr	409,528	565,820	521,450
Limestone Sorbent Feed, lb/hr	40,646	57,245	52,533
Thermal Input, kW_{th}	1,400,163	1,934,520	1,782,820
Raw Water Withdrawal, gpm	5321	10,071	8723
Raw Water Consumption, gpm	4227	7733	6738

[1] Higher heating value.

The total steam turbine power output for KCRC is 645.3 MW, which represents a reduction of 17.5 MW over Case 12, with the same net power production of 550 MW. Auxiliary power requirements for the CO_2 capture system and the total output of the steam turbines were modeled in detail using Aspen Plus. The power requirements for some of the smaller systems were estimated based on the information provided in the DOE report. The coal feed rate for KCRC is reduced by 44,370 lb/hr over Case 12, and this reduction contributes to the overall efficiency increase of the system. Overall, it is shown that utilization of the KCRC solvent can improve the efficiency of CO_2 capture versus MEA.

7.1.4 CSES Performance/Model Results and Discussion

The results of the Aspen process modeling were used to develop the mass and energy balance for utilization of the CSES on a 550-MW power facility. The results of the study are presented in similar format to the DOE report for rapid comparison of the differences. A complete mass and energy balance around the system is presented along with overall efficiency calculations.

7.1.4.1 Block Flow Diagram and Stream Table, Subcritical Unit with CO_2 Capture

Figure 7-8 shows the overall block diagram for the supercritical pc combustion plant with CO_2 capture using CSES. Table 7-3 follows the figure to give detailed information about the composition, temperature, and pressure of each stream in the system. The block flow diagram does not represent a complete mass balance of the system and is intended as a visual aid for understanding the layout of the power plant.

The system modeled represents a pc power plant with a supercritical steam cycle and a CO_2 capture system. The boiler is wall-fired with primary air and secondary air that represents OFA staging used to control NO_x emissions. SCR with ammonia injection is used to control NO_x emissions at the boiler exit. A standard pulse-jet baghouse is used for flue gas particulate control. A WFGD with limestone injection is used to control sulfur levels entering the CO_2 capture system. CO_2 capture is simulated by assuming CSES performance similar to MEA.

7.1.4.2 Heat and Mass Balance Diagrams

Diagrams showing the overall heat and mass balance for the power plant are shown in Figures 7-9 and 7-10. The heat and mass balance diagrams follow Case 11 of the DOE report very closely, and the flow, temperature, pressure, and enthalpy values were derived from the models developed in Aspen Plus.

7.1.4.3 Plant Performance Summary Table

The addition of CO_2 capture technology to the base plant increases the auxiliary power load; therefore, a bigger overall power plant is needed to produce the 550 MW net of power required for the study. Table 7-4 shows the overall power plant performance summary for CSES; Cases 11 and 12 from the DOE report are also included for comparison. The overall plant performance in the CSES case is significantly improved over Case 12. The main reason for this improvement is the lack of steam withdrawal from the steam cycle for regeneration, which results in a much lower coal feed rate and smaller overall plant size. The auxiliary load for CO_2 capture and compression is comparable to Case 12, although slightly less because of the lower coal feed rate and, therefore, less CO_2 that is required to be captured. The overall efficiency of the plant was improved from 28.4% to 35.8% as compared to Case 12.

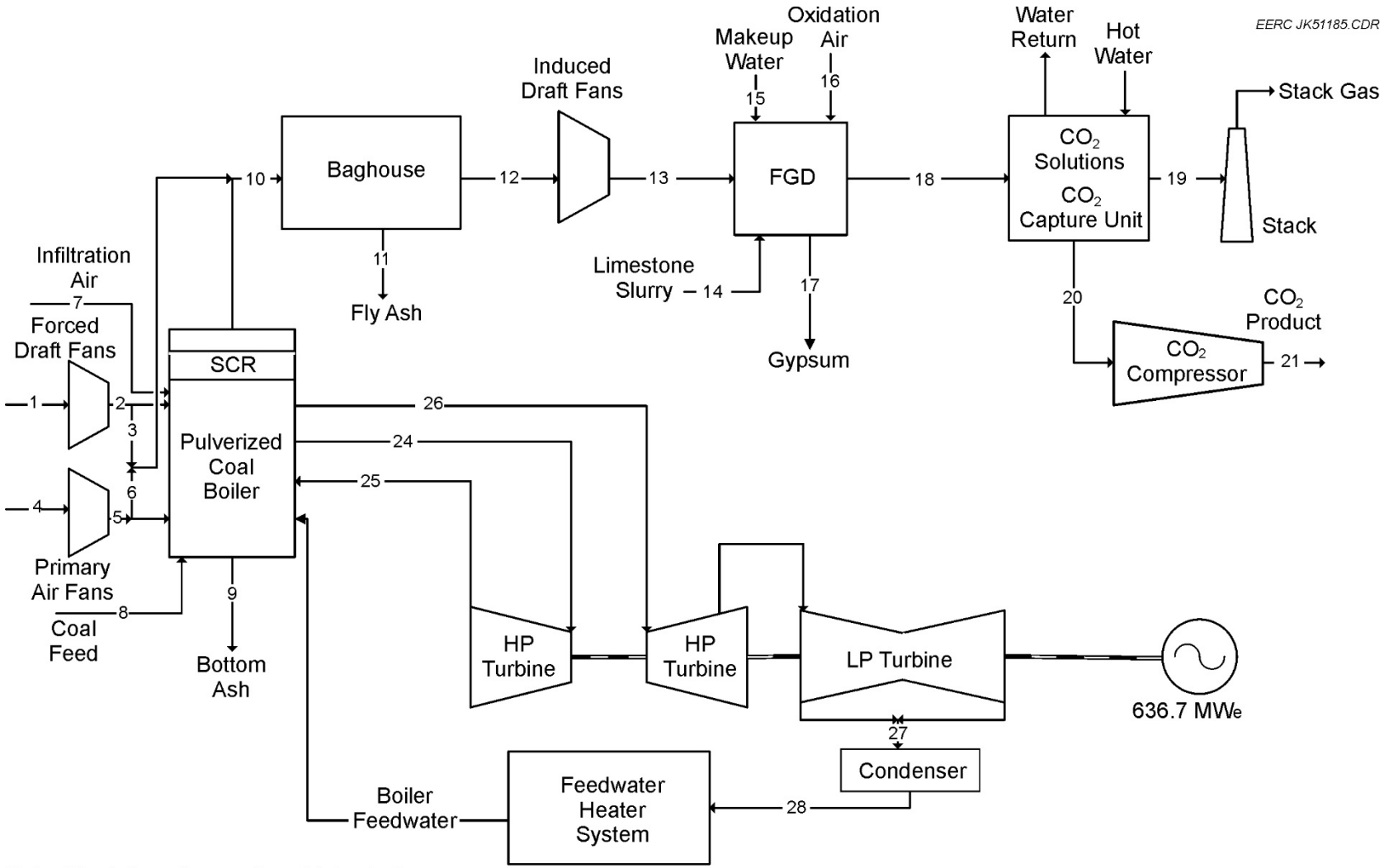

Figure 7-8. Block flow diagram for the supercritical pc combustion plant with CO_2 capture.

Table 7-3. CSES Stream Table, Supercritical Unit with CO_2 Capture

	1	2	3	4	5	6	7	8	9	10	11	12	13
V-L Mole Fraction													
Ar	0.0092	0.0092	0.0092	0.0092	0.0092	0.0092	0.0092	0.0000	0.0000	0.0087	0.0000	0.0087	0.0087
CO_2	0.0003	0.0003	0.0003	0.0003	0.0003	0.0003	0.0003	0.0000	0.0000	0.1446	0.0000	0.1446	0.1446
H_2	0.0000	0.0000	0.0000	0.0000	0.0000	0.0000	0.0000	0.0000	0.0000	0.0000	0.0000	0.0000	0.0000
H_2O	0.0099	0.0099	0.0099	0.0099	0.0099	0.0099	0.0099	0.0000	0.0000	0.0884	0.0000	0.0884	0.0884
N_2	0.7732	0.7732	0.7732	0.7732	0.7732	0.7732	0.7732	0.0000	0.0000	0.7305	0.0000	0.7305	0.7305
O_2	0.2074	0.2074	0.2074	0.2074	0.2074	0.2074	0.2074	0.0000	0.0000	0.0247	0.0000	0.0247	0.0247
SO_2	0.0000	0.0000	0.0000	0.0000	0.0000	0.0000	0.0000	0.0000	0.0000	0.0021	0.0000	0.0021	0.0021
Total	1.0	1.0	1.0	1.0	1.0	1.0	1.0	0.0	0.0	1.0	0.0	1.0	1.0
V-L Flow Rate, kg-mol/hr	53,113	53,113	1573	16,316	16,316	2245	1227	0	0	74,930	0	74,930	74,930
V-L Flow Rate, kg/hr	1,532,621	1,532,621	45,393	470,802	470,802	64,795	35,417	0	0	2,225,810	0	2,225,810	2,225,810
Solids Flow Rate, kg/hr	0	0	0	0	0	0	0	203,782	3953	15,808	15,808	0	0
Temperature, °C	15	19	19	15	26	26	15	15	15	169	15	169	182
Pressure, MPa, abs	0.10	0.11	0.11	0.10	0.11	0.11	0.10	0.10	0.10	0.10	0.10	0.10	0.11
Enthalpy, kJ/kg A	–97.5	–92.8	–92.8	–97.5	–6.8	–86.8	–97.5	–	–	–2504.6	–	–2504.9	–2491.1
Density, kg/m^3	1.2	1.2	1.2	1.2	1.3	1.3	1.2	–	–	0.8	–	0.8	0.8
V-L Molecular Weight	28.856	28.856	28.856	28.856	28.856	28.856	28.856	–	–	29.705	–	29.705	29.705
V-L Flow Rate, lb-mol/hr	117,095	117,095	3468	35,970	35,970	4950	2706	0	0	165,193	0	165,193	165,193
V-L Flow Rate, lb/hr	3,378,850	3,378,850	100,075	1,037,940	1,037,940	142,848	78,081	0	0	4,907,070	0	4,907,070	4,907,070
Solids Flow Rate, lb/hr	0	0	0	0	0	0	0	449,263	8715	34,850	34,850	0	0
Temperature, °F	59	67	67	59	78	78	59	59	59	337	59	337	359
Pressure, psia	14.7	15.3	15.3	14.7	16.1	16.1	14.7	14.7	14.7	14.4	14.7	14.2	15.3
Enthalpy, Btu/lb[1]	–41.9	–39.9	–39.9	–41.9	–37.3	–37.3	–41.9	–	–	–1076.8	–	–1076.9	–1071
Density, lb/ft^3	0.076	0.078	0.078	0.076	0.081	0.081	0.076	–	–	0.050	–	0.049	0.052

[1] Reference conditions are 77°F and 14.696 psia.

Continued. . .

Table 7-3. CSES Stream Table, Supercritical Unit with CO_2 Capture (continued)

	14	15	16	17	18	19	20	21	24	25	26	27	28
V-L Mole Fraction													
Ar	0.0000	0.0000	0.0128	0.0000	0.0081	0.0097	0.0004	0.0004	0.0000	0.0000	0.0000	0.0000	0.0000
CO_2	0.0000	0.0000	0.0005	0.0004	0.1342	0.0160	0.9958	0.9994	0.0000	0.0000	0.0000	0.0000	0.0000
H_2	0.0000	0.0000	0.0000	0.0000	0.0000	0.0000	0.0000	0.0000	0.0000	0.0000	0.0000	0.0000	0.0000
H_2O	1.0000	1.0000	0.0062	0.9996	0.1550	0.1264	0.0038	0.0001	1.0000	1.0000	1.0000	1.0000	1.0000
N_2	0.0000	0.0000	0.7505	0.0000	0.6774	0.8183	0.0001	0.0001	0.0000	0.0000	0.0000	0.0000	0.0000
O_2	0.0000	0.0000	0.2300	0.0000	0.0244	0.0294	0.0000	0.0000	0.0000	0.0000	0.0000	0.0000	0.0000
SO_2	0.0000	0.0000	0.0000	0.0000	0.0000	0.0000	0.0000	0.0000	0.0000	0.0000	0.0000	0.0000	0.0000
Total	1.0	1.0	1.0	1.0	1.0	1.0	1.0	1.0	1.0	1.0	1.0	1.0	1.0
V-L Flow Rate, kg-mol/hr	3928	13,485	975	10,483	81,887	67,702	10,012	12,588	101,354	84,022	84,022	57,050	76,672
V-L Flow Rate, kg/hr	60,709	242,940	28,290	188,847	2,357,655	1,844,161	439,945	552,664	1,825,913	1,513,679	1,513,679	1,027,772	1,381,266
Solids Flow Rate, kg/hr	26,231	0	0	37,478	0	0	0	0	0	0	0	0	0
Temperature, °C	15	15	181	57	57	52	21	29	593	364	604	39	39
Pressure, MPa, abs	0.10	0.10	0.31	0.10	0.10	0.11	0.16	15.27	24.23	4.90	4.52	0.01	1.69
Enthalpy, kJ/kg A	–	–16,007.1	98.6	–	–3102.4	–1326.8	–8955.1	–9185.4	–12,502.3	–12,874.2	–12,299.9	–13,586.9	–15,814.7
Density, kg/m^3	–	1003.1	2.4	–	1.1	1.1	2.9	838.3	69.2	18.2	11.4	0.0	993.2
V-L Molecular Weight	–	18.015	29.029	–	28.79	27.24	43.91	43.91	18.015	18.015	18.015	18.015	18.015
V-L Flow Rate, lb-mol/hr	8660	29,730	2150	23,110	180,531	149,258	22,073	27,752	223,447	185,237	185,237	125,774	169,033
V-L Flow Rate, lb/hr	133841	535,592	62,368	416,336	5,197,740	4,065,680	969,912	1,218,416	4,025,450	3,337,090	3,337,090	2,265,850	3,045,170
Solids Flow Rate, lb/hr	57830	0	0	82,625	0	0	0	0	0	0	0	0	0
Temperature, °F	59	59	357	135	135	125	69	85	1100	687	1120	102	103
Pressure, psia	15.0	14.7	45	14.8	14.8	15.5	23.5	2215	3514.7	710.8	655.8	1.0	245
Enthalpy, Btu/lb[1]	–	–6881.8	42.39	–	–1333.8	–570.4	–3850	–3949	–5375.0	–5534.9	–5288.0	–5841.3	–6799
Density, lb/ft^3	–	62.622	0.149	–	0.067	0.067	0.183	52.332	4.319	1.139	0.712	0.003	62.005

[1] Reference conditions are 77°F and 14.696 psia.

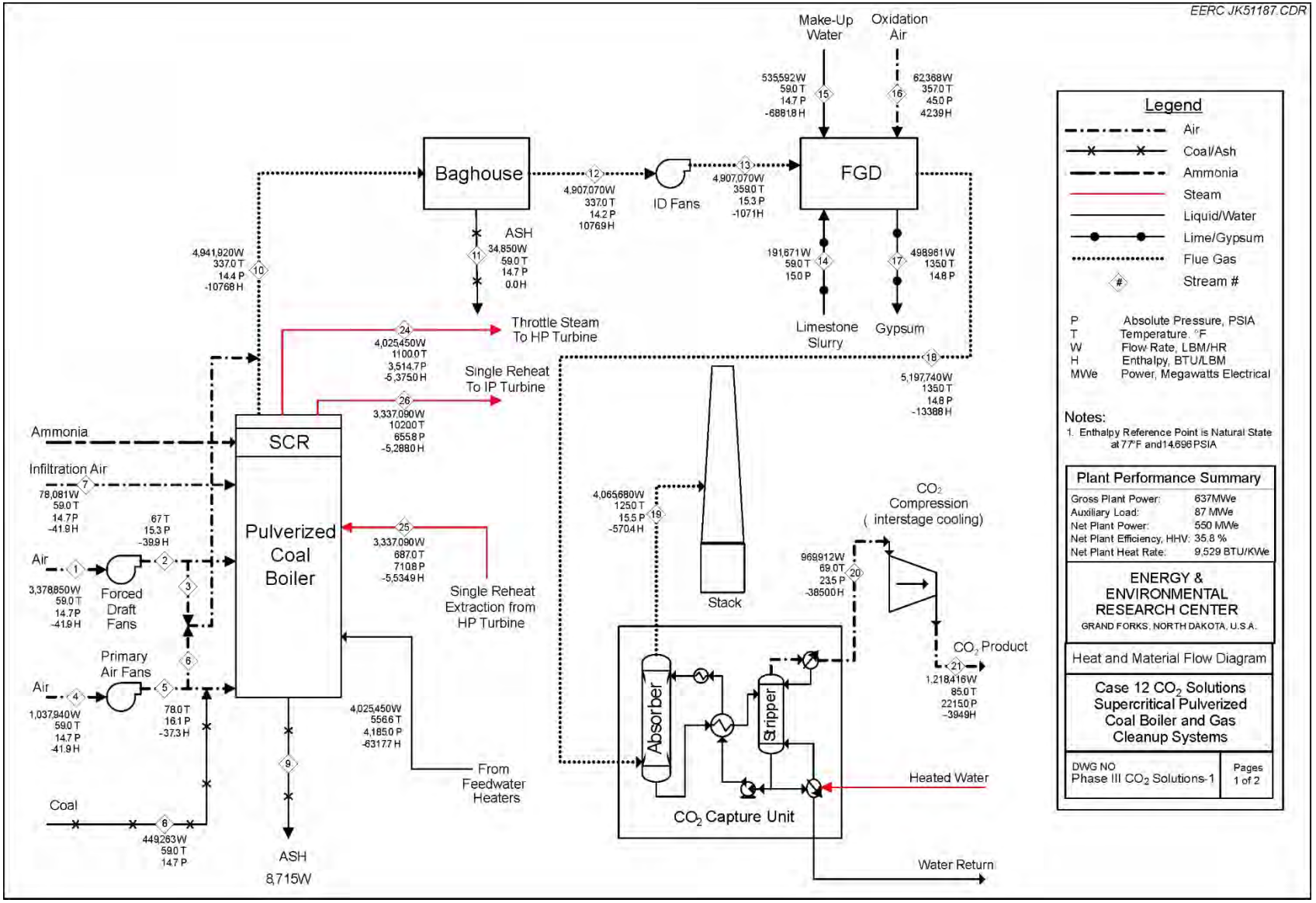

Figure 7-9. Combustor heat and material flow diagram for CSES.

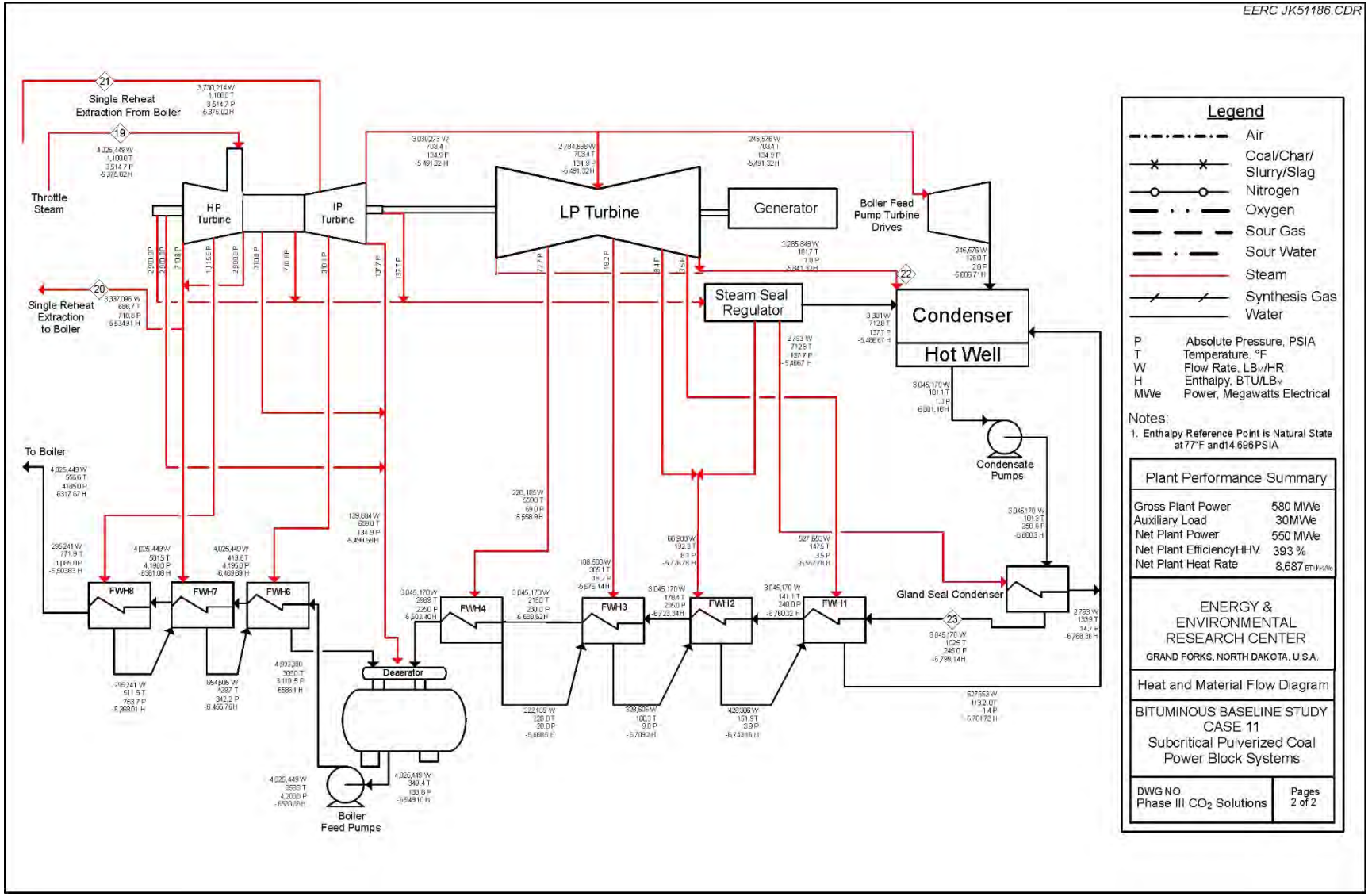

Figure 7-10. Steam cycle heat and material flow for CSES.

Table 7-4. Overall Plant Performance

Steam Turbine Power:	Case 11 580,400	Case 12 662,800	CSES 636,714
Coal Handling and Conveying	440	510	458
Pulverizers	2780	3850	3052
Sorbent Handling and Reagent Preparation	890	1250	982
Ash Handling	530	740	583
Primary Air Fans	1300	1800	1427
Forced-Draft Fans	1660	2300	1823
ID Fans	7050	11,120	8085
SCR	50	70	55
Baghouse	70	100	78
WFGD	2970	4110	3260
CSES Auxiliaries	–	20,600	16,356
CO_2 Compression	–	44,890	35,643
Miscellaneous BOP	2000	2000	2000
Steam Turbine Auxiliaries	400	400	400
Condensate Pumps	800	560	739
Circulating Water Pump	4730	10,100	6095
Groundwater Pumps	480	910	589
Cooling Tower Fans	2440	5230	3149
Transformer Losses	1820	2290	1939
Total Auxiliaries, kW_e	30,410	112,830	86,713
Net Power, kW_e	549,990	549,970	550,001
Net Plant Efficiency (HHV)	39.3%	28.4%	35.8%
Net Plant Heat Rate, Btu/kWh	8687	12,002	9529
Condenser Cooling Duty, 10^6 Btu/hr	2178	1646	2434
Consumables			
As-Received Coal Feed, lb/hr	409,528	565,820	449,263
Limestone Sorbent Feed, lb/hr	40,646	57,245	44,866
Thermal Input, kW_{th}	1,400,163	1,934,520	1,536,015
Raw Water Withdrawal, gpm	5321	10,071	6529
Raw Water Consumption, gpm	4227	7733	5118

The total steam turbine power output for CSES is 636.7 MW, which represents a reduction of 26.1 MW over Case 12, with the same net power production of 550 MW. Auxiliary power requirements for the CO_2 capture system and the total output of the steam turbines were modeled in detail using Aspen Plus. The power requirements for some of the smaller systems were estimated based on the information provided in the DOE report. The coal feed rate for CSES is reduced by 116,557 lb/hr over Case 12, and this reduction contributes to the overall efficiency increase of the system. Overall, it is shown that if waste heat alone can be utilized to regenerate the solvent, the utilization of CSES can greatly improve the efficiency of CO_2 capture.

7.1.4.4 Modeling Results Summary and Next Steps

For the analysis contained herein, it was assumed that adequate waste heat could be gathered from the power plant to regenerate the solvent, and that the solvent will perform in a comparable manner to MEA. The results indicate that if these two assumptions can be met, significant increases in overall plant efficiency and reductions in coal feed rate versus Case 12 can be realized. Even if all of the heat required for 90% capture cannot be obtained, the result holds promise for systems that could require partial capture of CO_2. The solvent holds significant potential in this situation to provide low levels of capture with no impact to the overall steam cycle. Additional studies are needed to verify potential sources of waste heat as well as heat sources that could have less impact on the overall plant efficiency such as hot-water withdrawal. Additional testing will also be needed on the solvent to verify the performance and determine if it can perform as well as or better than MEA. Any improvement in performance over MEA will reduce the amount of waste heat that is needed for regeneration.

Another important factor is the use of vacuum in the stripping column for solvent regeneration. Vacuum is an important component for the performance of CSES but was not included in the projections made here. More investigation of the components necessary and the appropriate sizing are needed to arrive at energy demands and costs. The results presented here are a very conservative first step in the economic projection process for this technology.

7.1.5 Partial Capture Performance/Model Results and Discussion

7.1.5.1 Introduction

EPA has recently released new rules for each state regarding the emissions of CO_2 from stationary power sources. The reduction targets for most states fall within the 25%–45% range. The cost of CO_2 capture is expected to be significantly lower for a partial capture solvent system as compared to a system targeting 90% total capture, making partial CO_2 capture a potentially attractive strategy. In order to estimate this cost, the EERC has undertaken a detailed techno-economic analysis focused on modeling the mass and energy balance and equipment needs associated with partial capture of CO_2. Several capture targets could be evaluated, but it was decided that 45% capture will be the basis for modeling in this initial study since that represents the potential high end of CO_2 capture requirements for plants. The standard models use five capture trains to achieve 90% CO_2 capture from the base cases; therefore, several options exist to achieve lower levels of CO_2 separation. These options could include 45% capture from five trains, 75% capture from three trains, or 90% capture from two trains, with a third smaller train still required. As a starting point, it was decided to model 75% capture from three trains using a standard MEA solvent, resulting in 45% overall CO_2 capture.

The EERC-developed Aspen Plus model was resized and calibrated based on the liquid flow and steam usage requirements for 45% capture. A complete mass and energy balance was developed around the major process areas of a coal-fired power plant, and guidance from Cases 11 and 12 of the report was used to size minor equipment and determine auxiliary power loads. The CO_2 capture portion of the process was modeled in detail and integrated with the steam cycle model. The partial capture case results in less parasitic load than the baseline MEA case;

therefore, the overall plant efficiency achieved when using the advanced technology was higher than Case 12 of the DOE report. This section presents the detailed mass and energy balance resulting from partial capture of CO_2 and compares it to the performance of Cases 11 and 12. This subsection concludes with an overall plant efficiency calculation based on the reduced parasitic loads for partial capture.

7.1.5.2 Block Flow Diagram and Stream Table, Supercritical Unit with CO_2 Capture

Figure 7-11 shows the overall block diagram for the supercritical pc combustion plant with partial CO_2 capture using MEA solvent. Table 7-5 follows the figure to give detailed information about the composition, temperature, and pressure of each stream in the system. The block flow diagram does not represent a complete mass balance of the system and is intended as a visual aid for understanding the layout of the power plant.

The system modeled represents a pc power plant with a supercritical steam cycle and a partial CO_2 capture system. The boiler is wall-fired with primary air and secondary air that represents OFA staging used to control NO_x emissions. SCR with ammonia injection is used to control NO_x emissions at the boiler exit. A standard pulse-jet baghouse is used for flue gas particulate control. A WFGD with limestone injection is used to control sulfur levels entering the CO_2 capture system. Case 12 uses a standard absorber tower and stripper column.

7.1.5.3 Heat and Mass Balance Diagrams

Diagrams showing the overall heat and mass balance for the power plant are shown in Figures 7-12 and 7-13. The heat and mass balance diagrams closely follow Case 12 of the DOE report, and the flow, temperature, pressure, and enthalpy values were derived from the models developed in Aspen Plus.

7.1.5.4 Plant Performance Summary Table

The addition of CO_2 capture technology to the base plant increases the auxiliary power load; therefore, a bigger overall power plant is needed to produce the 550 MW net of power required for the study. Table 7-6 shows the overall power plant performance summary for 45% capture of CO_2 using three trains at 75% capture each. Cases 11 and 12 from the DOE report are also included for comparison. As expected, the overall plant performance in the partial capture case is significantly improved over Case 12. Performance improvements were noted in the model, which were directly related to a reduced capture requirement in each train. At 90% capture, mass transfer limitations and slower chemical reaction kinetics increase the amount of solvent needed to reach the final increment of CO_2 removal. However, at 75% capture, these kinetic and mass transfer limitations are significantly reduced; therefore, less than half of the parasitic steam load required for 90% overall capture is required for 45% overall capture. The overall efficiency of the plant was improved from 28.4% to 33.6% as compared to Case 12.

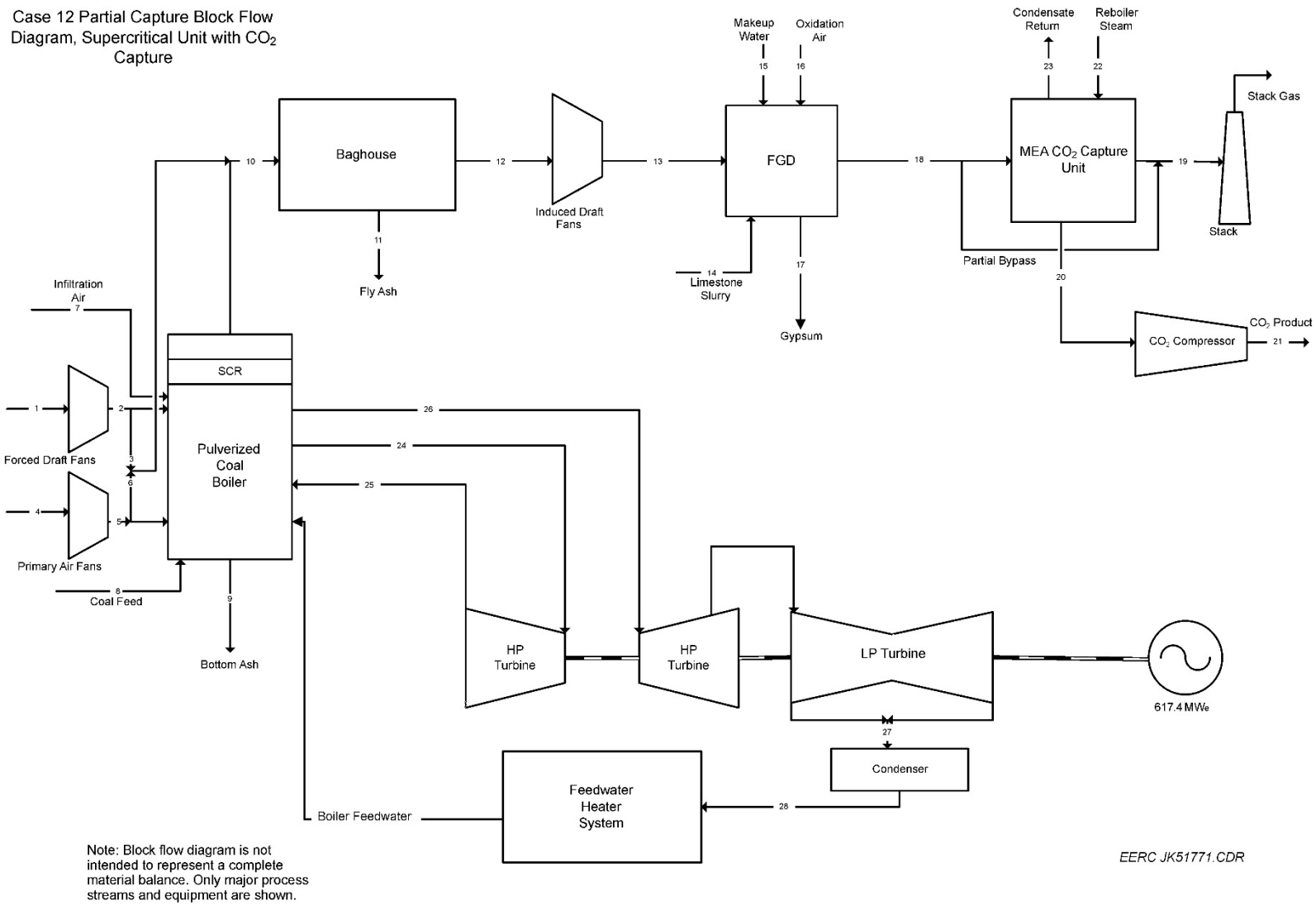

Figure 7-11. Block flow diagram for the supercritical pc combustion plant with partial CO_2 capture.

Table 7-5. Stream Table, Supercritical Unit with 45% CO_2 Capture

	1	2	3	4	5	6	7	8	9	10	11	12	13	14
V-L Mole Fraction														
Ar	0.0092	0.0092	0.0092	0.0092	0.0092	0.0092	0.0092	0.0000	0.0000	0.0087	0.0000	0.0087	0.0087	0.0000
CO_2	0.0003	0.0003	0.0003	0.0003	0.0003	0.0003	0.0003	0.0000	0.0000	0.1446	0.0000	0.1446	0.1446	0.0000
H_2	0.0000	0.0000	0.0000	0.0000	0.0000	0.0000	0.0000	0.0000	0.0000	0.0000	0.0000	0.0000	0.0000	0.0000
H_2O	0.0099	0.0099	0.0099	0.0099	0.0099	0.0099	0.0099	0.0000	0.0000	0.0895	0.0000	0.0895	0.0895	1.0000
N_2	0.7732	0.7732	0.7732	0.7732	0.7732	0.7732	0.7732	0.0000	0.0000	0.7304	0.0000	0.7304	0.7304	0.0000
O_2	0.2074	0.2074	0.2074	0.2074	0.2074	0.2074	0.2074	0.0000	0.0000	0.0243	0.0000	0.0243	0.0243	0.0000
SO_2	0.0000	0.0000	0.0000	0.0000	0.0000	0.0000	0.0000	0.0000	0.0000	0.0021	0.0000	0.0021	0.0021	0.0000
Total	1.0	1.0	1.0	1.0	1.0	1.0	1.0	0.0	0.0	1.0	0.0	1.0	1.0	1.0
V-L Flow Rate, kg-mol/hr	56,615	56,615	1677	17,392	17,392	2394	1309	0	0	79,892	0	79,892	79,892	3370
V-L Flow Rate, kg/hr	1,633,655	1,633,655	48,386	501,844	501,844	69,067	37,759	0	0	2,373,304	0	2,373,304	2,373,304	60,709
Solids Flow Rate, kg/hr	0	0	0	0	0	0	0	217,260	4214	16,853	16,853	0	0	26,231
Temperature, °C	15	19	19	15	26	26	15	15	15	169	15	169	182	15
Pressure, MPa, abs	0.10	0.11	0.11	0.10	0.11	0.11	0.10	0.10	0.10	0.10	0.10	0.10	0.11	0.10
Enthalpy, kJ/kg[a]	−97.5	−92.8	−92.8	−97.5	−86.8	−86.8	−97.5	–	–	−2513.2	–	-2513.2	−2500.2	–
Density, kg/m^3	1.2	1.2	1.2	1.2	1.3	1.3	1.2	–	–	0.8	–	0.8	0.8	–
V-L Molecular Weight	28.856	28.856	28.856	28.856	28.856	28.856	28.856	–	–	29.706	–	29.706	29.706	–
V-L Flow Rate, lb-mol/hr	124,814	124,814	3697	38,342	38,342	5277	2885	0	0	176,132	0	176,132	176,132	7429
V-L Flow Rate, lb/hr	3,601,592	3,601,592	106,672	1,106,376	1,106,376	152,266	83,245	0	0	5,232,239	0	5,232,239	5,232,239	133,841
Solids Flow Rate, lb/hr	0	0	0	0	0	0	0	478,977	9291	37,154	37,154	0	0	57,830
Temperature, °F	59	67	67	59	78	78	59	59	59	337	59	337	359	59
Pressure, psia	14.7	15.3	15.3	14.7	16.1	16.1	14.7	14.7	14.7	14.4	14.7	14.2	15.3	15.0
Enthalpy, Btu/lb[a]	−41.9	−39.9	−39.9	−41.9	−37.3	−37.3	−41.9	–	–	−1080.5	–	−1080.5	−1074.9	–
Density, lb/ft^3	0.076	0.078	0.078	0.076	0.081	0.081	0.076	–	–	0.05	–	0.049	0.052	–

[a] Reference conditions are 77°F and 14.696 psia.

Continued. . .

Table 7-5. Stream Table, Supercritical Unit with 45% CO_2 Capture (continued)

	15	16	17	18	19	20	21	22	23	24	25	26	27	28
V-L Mole Fraction														
Ar	0.0000	0.0128	0.0000	0.0081	0.0091	0.0004	0.0004	0.0000	0.0000	0.0000	0.0000	0.0000	0.0000	0.0000
CO_2	0.0000	0.0005	0.0001	0.1347	0.0834	0.9957	0.9957	0.0000	0.0000	0.0000	0.0000	0.0000	0.0000	0.0000
H_2	0.0000	0.0000	0.0000	0.0000	0.0000	0.0000	0.0000	0.0000	0.0000	0.0000	0.0000	0.0000	0.0000	0.0000
H_2O	1.0000	0.0062	0.9999	0.1535	0.1181	0.0038	0.0037	1.0000	1.0000	1.0000	1.0000	1.0000	1.0000	1.0000
N_2	0.0000	0.7505	0.0000	0.6792	0.7628	0.0001	0.0001	0.0000	0.0000	0.0000	0.0000	0.0000	0.0000	0.0000
O_2	0.0000	0.2300	0.0000	0.0239	0.0266	0.0000	0.0000	0.0000	0.0000	0.0000	0.0000	0.0000	0.0000	0.0000
SO_2	0.0000	0.0000	0.0000	0.0000	0.0000	0.0000	0.0000	0.0000	0.0000	0.0000	0.0000	0.0000	0.0000	0.0000
Total	1.0	1.0	1.0	1.0	1.0	1.0	1.0	1.0	1.0	1.0	1.0	1.0	1.0	1.0
V-L Flow Rate, kg-mol/hr	13,485	974	10,322	86,984	77,470	5308	12,588	17,607	17,607	107,093	87,391	87,391	45,865	62,157
V-L Flow Rate, kg/hr	242,940	28,290	185,961	2,507,292	2,198,664	233,077	552,664	317,189	317,189	1,929,316	1,574,377	1,574,377	826,261	1,119,780
Solids Flow Rate, kg/hr	0	0	38,222	0	0	0	0	0	0	0	0	0	0	0
Temperature, °C	15	181	57	57	49	21	35	291	151	593	354	593	39	39
Pressure, MPa, abs	0.10	0.31	0.10	0.10	0.10	0.16	15.27	0.51	0.92	24.23	4.90	4.52	0.01	1.69
Enthalpy, kJ/kg[a]	−16,007.1	−98.6	–	−3093.6	−2138.5	−8955.3	−9184.7	−12,935.6	−15,383.0	−12,502.3	−12,900.0	−12,325.7	−13,520.6	−15,814.5
Density, kg/m^3	1003.1	2.4	–	1.1	1.1	2.9	560.5	2.0	758.9	69.2	18.6	11.6	0.0	993.2
V-L Molecular Weight	18.015	29.029	–	28.83	28.08	43.91	43.91	18.015	18.015	18.015	18.015	18.015	18.015	18.015
V-L Flow Rate, lb-mol/hr	29,730	2148	22,757	191,766	170,792	11,702	11,702	38,816	38,816	236,100	192,665	192,665	101,114	137,033
V-L Flow Rate, lb/hr	535,592	62,368	409,974	5,527,633	4,847,224	513,846	513,846	699,281	699,281	4,253,413	3,470,908	3,470,908	1,821,594	2,468,692
Solids Flow Rate, lb/hr	0	0	84,265	0	0	0	0	0	0	0	0	0	0	0
Temperature, °F	59	357	135	135	121	69	95	556	304	1100	669	1100	102	103
Pressure, psia	14.7	45	14.9	14.9	14.9	23.5	2214.5	73.5	133.6	3,514.7	710.8	655.8	1.0	245.0
Enthalpy, Btu/lb[a]	−6881.8	−42.4	–	−1330.0	−919.4	−3850.1	−3948.7	−5561.3	−6613.5	−5375.0	−5546.0	−5299.1	−5812.8	−6799.0
Density, lb/ft^3	62.622	0.149	–	0.067	0.068	0.183	34.990	0.123	47.377	4.319	1.16	0.722	0.003	62.004

[a] Reference conditions are 77°F and 14.696 psia.

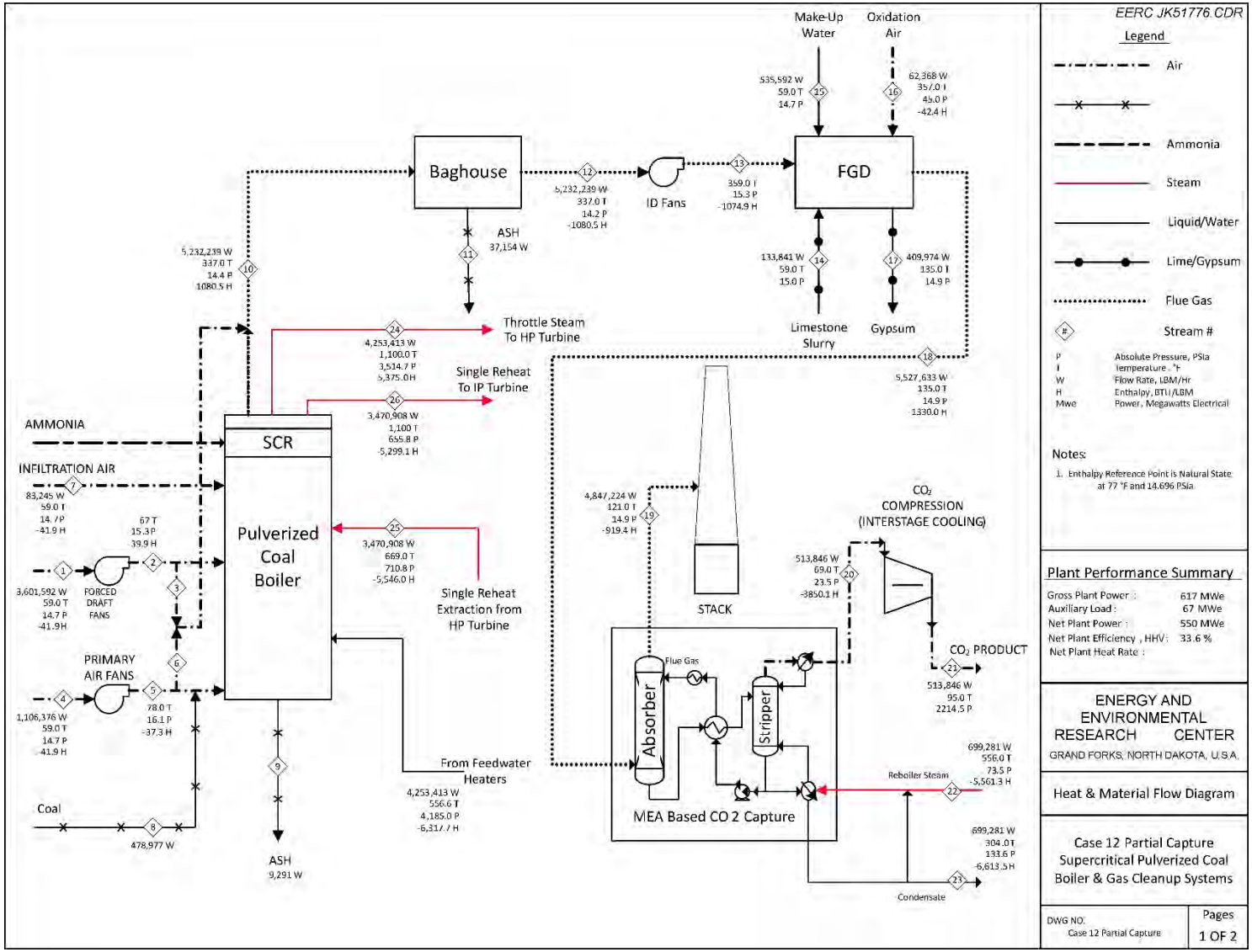

Figure 7-12. Combustor heat and material flow diagram for 45% capture of CO_2.

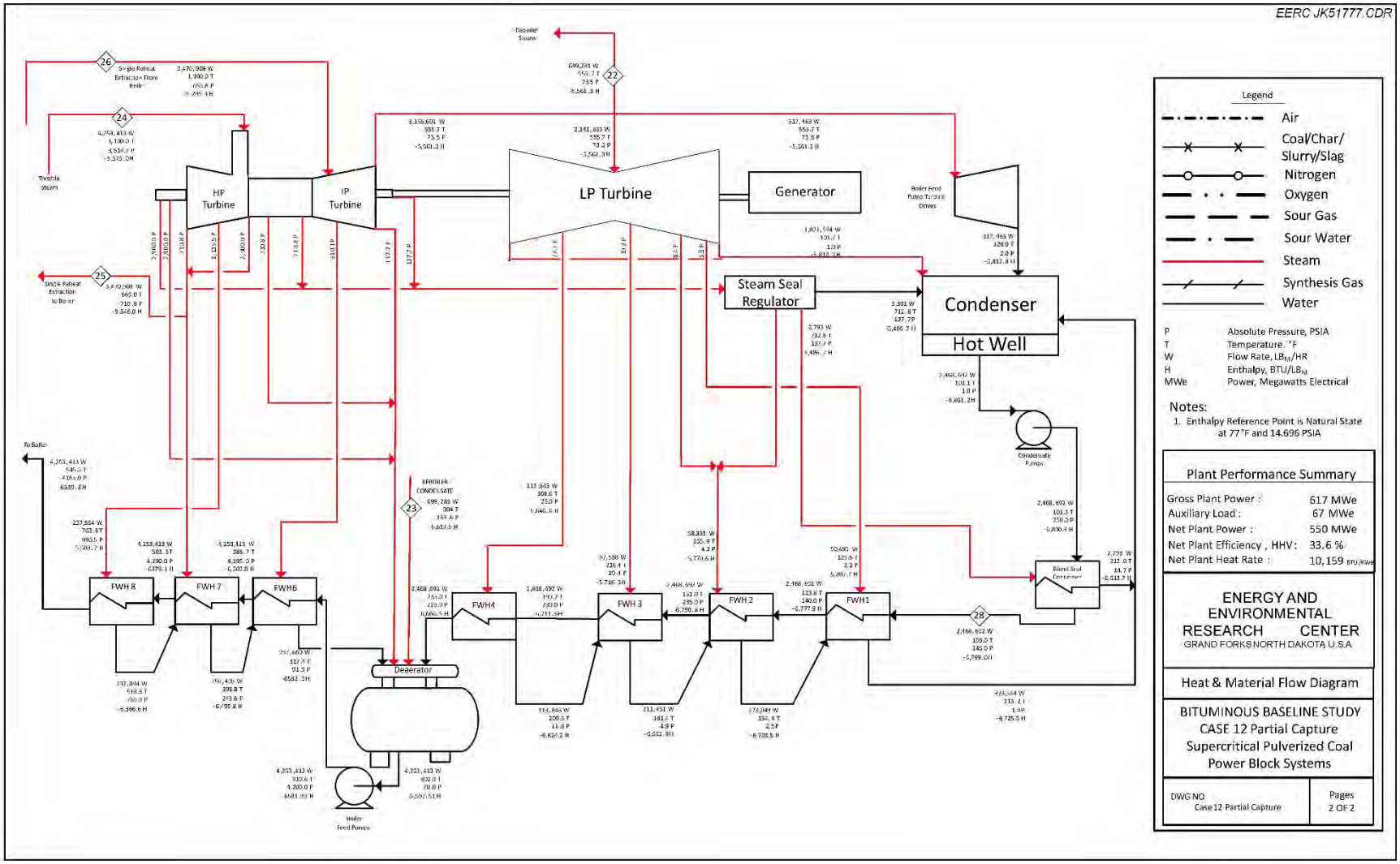

Figure 7-13. Steam cycle heat and material flow for partial capture of CO_2.

Table 7-6. Overall Plant Performance

Steam Turbine Power:	Case 11 580,400	Case 12 662,800	45% Capture 617,400
Coal Handling and Conveying	440	510	471
Pulverizers	2780	3850	3255
Sorbent Handling and Reagent Preparation	890	1250	1050
Ash Handling	530	740	623
Primary Air Fans	1300	1800	1522
Forced-Draft Fans	1660	2300	1944
ID Fans	7050	11,120	8859
SCR	50	70	59
Baghouse	70	100	83
WFGD	2970	4110	3477
CO_2 Capture Auxiliaries	–	20,600	10,463
CO_2 Compression	–	44,890	19,000
Miscellaneous BOP	2000	2000	2000
Steam Turbine Auxiliaries	400	400	400
Condensate Pumps	800	560	693
Circulating Water Pump	4730	10,100	7116
Ground Water Pumps	480	910	671
Cooling Tower Fans	2440	5230	3680
Transformer Losses	1820	2290	2029
Total Auxiliaries, kW_e	30,410	112,830	67,396
Net Power, kW_e	549,990	549,970	550,004
Net Plant Efficiency (HHV)	39.3%	28.4%	33.6%
Net Plant Heat Rate, Btu/kWh	8687	12,002	10,159
Condenser Cooling Duty, 10^6 Btu/hr	2178	1646	2144
Consumables			
As-Received Coal Feed, lb/hr	409,528	565,820	478,977
Limestone Sorbent Feed, lb/hr	40,646	57,245	48,022
Thermal Input, kW_{th}	1,400,163	1,934,520	1,637,607
Raw Water Withdrawal, gpm	5321	10,071	7432
Raw Water Consumption, gpm	4227	7733	5785

The total steam turbine power output for the partial capture case is 617.4 MW, which represents a reduction of 45.4 MW over Case 12, with the same net power production of 550 MW. Auxiliary power requirements for the CO_2 capture system and the total output of the steam turbines were modeled in detail using Aspen Plus. The power requirements for some of the smaller systems were estimated based on the information provided in the DOE report. The coal feed rate for partial capture is reduced by 86,843 lb/hr over the 90% capture Case 12 scenario. As compared to Case 11, the system still experiences significant auxiliary load impacts due to the power requirements for the capture and compression systems and the steam for regeneration of the solvent. Overall, it is shown that a supercritical coal-fired power plant operating with 45% CO_2 capture can achieve net plant efficiencies of over 33%.

7.2 Techno-Economic Performance

7.2.1 Experimental Methods and Software Description

7.2.1.1 Description of APEA

In order to estimate the impact that process improvements in CO_2 capture technology can have on the economics of a power plant, the APEA software package was used. It is a project-scoping tool that enables engineers to evaluate the economic impact of their process designs. APEA is most valuable in the early phases of conceptual design to compare competing technologies and evaluate alternative process configurations. Models constructed in Aspen Plus for calculating mass and energy balances were imported into APEA for economic analysis.

Once imported, APEA assigned specific equipment types to each process block from a large database of various real-world components. For example, APEA assigned a floating-head shell-and-tube heat exchanger for the cross-heat exchanger in the CO_2 capture model. APEA determined from its database of equipment that this was the most appropriate type based on flow rates, materials, heat-transfer area, and other factors. The software package also estimates the size of the process equipment. For the heat exchanger discussed, dimensions of the tubes and shell were calculated, which included the required thickness of the materials in order to withstand the temperatures and pressure that the heat exchanger would be required to endure. When necessary, the user had the ability to manually revise specific types of equipment, materials of construction, sizes of equipment, and costs.

At this initial level of estimation, the components assigned by APEA are accepted as the basis for the equipment makeup of the plant and CO_2 capture system even though they may not be the optimal choice for a particular CO_2 capture technology. For the evaluation being conducted at this scale, it is the belief of the EERC that this is acceptable in light of the limited data that are obtained upon which the assessment is based. It is expected that as data from scale-up are collected and further refinements are made to the physical equipment requirements, the specific components will be more tightly constrained. This also is an attempt to remove some factors of performance that are only attributable to efficiency of the equipment and are not the result of the solvent being used in the process. Therefore, the EERC believes that the results yield a conservative assessment of performance.

7.2.1.2 Key Economic Assumptions

Because of constraints on resources and time, the entire power plant was not modeled and economically analyzed from scratch. A thorough NETL report, Cost and Performance Baseline for Fossil Energy Plants (Black, 2013a), was referenced to estimate the costs for the majority of the power plant. The cost estimates in the report had a base year of 2007. Case 11, supercritical pc power plant without CO_2 capture, and Case 12, supercritical pc power plant with Econamine-based CO_2 capture, were used as a baseline for comparisons. These case studies use Illinois No. 6 bituminous coal as the fuel. Under this process, the assumption is made that the plant being assessed is a Greenfield plant with a net power output of 550 MWe. A list of the assumptions made in the assessment is provided in Appendix B.

DOE strongly urges, and in large slipstream programs requires, strict application of the information contained in the report from which Case 11 and Case 12 is referenced. The concept used is to create a generic plant comprising basic equipment and to include a basic CO_2 capture system that the solvent can operate within. It is recognized that there will be specific situations that could allow for differing components (pumps, heat exchanger, piping, controls, etc.), but these changes can result in calculated improvements in the cost of CO_2 capture that are not directly related to the performance of a particular solvent. Therefore, the DOE mandate was followed for this initial economic assessment. Cost estimations in DOE studies are considered to be an Advancement of Cost Engineering International (AACE International) Class 4 "feasibility study" with an accuracy range of –15%/+30%. If an assessment is to be more specific, then it is conducted during the front-end engineering design (FEED) study. This assessment is intended to serve as proof-of-concept-level information.

For the advanced solvents developed for the CO_2 capture plant, APEA was used to estimate the capital and operating costs for the capture portion of the plant. Values for cost were adjusted from values given for Case 12 by utilizing information from Aspen modeling and derived adjustment factors as described in the NETL document "Capital Cost Scaling Methodology" (Black, 2013b). The methodology provides a system to modify costs from a base case utilizing parameters that directly affect those costs.

Case 12 is used for the economic portion of the assessment as it contains the equipment necessary to conduct CO_2 capture from the Greenfield plant. The only modification is that the assumption is made that the steam cycle of the plant will not be touched.

To estimate COE, a simplified equation that was a function of total overnight capital (TOC), fixed and variable operating and maintenance (O&M) costs, capacity factor, and net output was given by the NETL report (U.S. Department of Energy National Energy Technology Laboratory, 2011).

$$COE = \frac{\substack{first-year \\ capital\ charge} + \substack{first-year \\ fixed\ operating \\ costs} + \substack{first-year \\ variable\ operating \\ costs}}{\substack{annual\ net\ megawatt\ hours \\ of\ power\ generated}} \quad \text{[Eq. 7.8]}$$

$$COE = \frac{(CCF)(TOC) + OC_{FIX} + (CF)(OC_{VAR})}{(CF)(MWH)} \quad \text{[Eq. 7.9]}$$

where:

COE = Revenue received by the generator (US$/MWh) during the power plant's first year of operation (expressed in base-year dollars)

CCF = Capital charge factor

TOC = Expressed in base-year dollars

OC_{FIX} = The sum of all fixed annual operating costs

OCVAR = The sum of all variable annual operating costs, including fuel at 100% capacity factor

CF = Plant capacity factor (85%)

MWh = Annual net megawatt-hours of power generated at 100% capacity factor

Other details for the cost-estimating methodology can be found in the NETL report "Cost Estimation Methodology for NETL Assessments of Power Plant Performance" (U.S. Department of Energy National Energy Technology Laboratory, 2011).

7.2.1.3 Major Equipment List

Cost estimates were provided for each section of the power plant and categorized by account code (Table 7-7). Details for the major equipment in each account can be referenced in the NETL report. DOE scaling factors are applied to the account numbers based on parameter outputs given in the Aspen model. For example, Account 1 factors are based on the coal feed rate of the plant whereas Account 3 factors are based on parameters such as raw water makeup and water load to treatment. Account 9 factors are adjusted based on circulating water flow rate and cooling tower duty. Details for every account can be found in the NETL report.

Table 7-7. Plant Sections by Account Number

Account No.	Section Description
1	Coal and sorbent handling
2	Coal and sorbent preparation and feed
3	Feedwater and miscellaneous systems and equipment
4	Boiler and accessories
5	Flue gas cleanup
5B	CO_2 recovery
6	Combustion turbine/accessories
7	HRSG,[1] ducting, and stack
8	Steam turbine generator and auxiliaries
9	Cooling water system
10	Ash/spent sorbent recovery and handling
11	Accessory electric plant
12	Instrumentation and control
13	Improvement to site
14	Building structures

[1] Heat recovery steam generator.

7.2.2 KCRC Economic Results and Discussion

The cost-estimating methodology described was used to calculate the total plant capital costs and was compared to Case 11 and Case 12. Table 7-8 shows the total plant cost (TPC) results, organized by cost account. Further results of the economic evaluation are given in Table 7-9.

Table 7-8. TPC Results for Each Case Organized by Account Code, costs in US$1000 (2007 $)

Acct. No.	Description	Case 11	Case 12	KCRC
1	Coal and sorbent handling	38,365	47,015	44,566
2	Coal and sorbent preparation and feed	18,059	22,441	21,182
3	Feedwater and miscellaneous systems and equipment	79,149	102,552	98,725
4	Boiler and accessories	296,317	369,144	347,916
5	Flue gas cleanup	128,593	163,337	153,472
5B	CO_2 recovery	0	468,782	311,966
6	Combustion turbine/accessories	0	0	0
7	HRSG, ducting, and stack	37,291	37,525	39,686
8	Steam turbine generator and auxiliaries	115,947	132,111	126,140
9	Cooling water system	37,370	60,964	54,245
10	Ash/spent sorbent recovery and handling	12,626	15,109	14,404
11	Accessory electric plant	51,068	80,932	72,479
12	Instrumentation and control	21,555	25,838	23,810
13	Improvements to site	14,054	15,717	15,527
14	Buildings and structures	55,506	60,557	59,056
TPC		905,900	1,602,024	1,383,195
TOC		1,113,444	1,963,646	1,697,214

Table 7-9. Estimated Costs for Case 11, Case 12, and CO_2 Solutions (KCRC) Case

	Case 11	Case 12	KCRC
TPC, US$ (2007)/kW	1647	2913	2515
TOC, US$ (2007)/kW	2024	3570	3086
Total As-Spent Capital, US$ (2007)/kW	2296	4070	3518
COE, US$ (2007)/MWh	58.9	100.9	89.1
Levelized COE, US$ (2007)/MWh	74.7	127.8	113.0
CO_2 Capture Cost, US$ (2007)/tonne	N/A	47.7	44.0

To further illustrate the results of the KCRC case over the DOE Case 12, Figure 7-14 presents the COE, with the fuel costs, variable costs, fixed costs, and capital costs shown separately. Additional cost breakdown is given in Table 7-10. Further detail is not given as each section for the KCRC case is determined by scale factors applied to the DOE Case 11 from the document previously described and is not calculated individually based on acquired information about the specifics of a particular item cost.

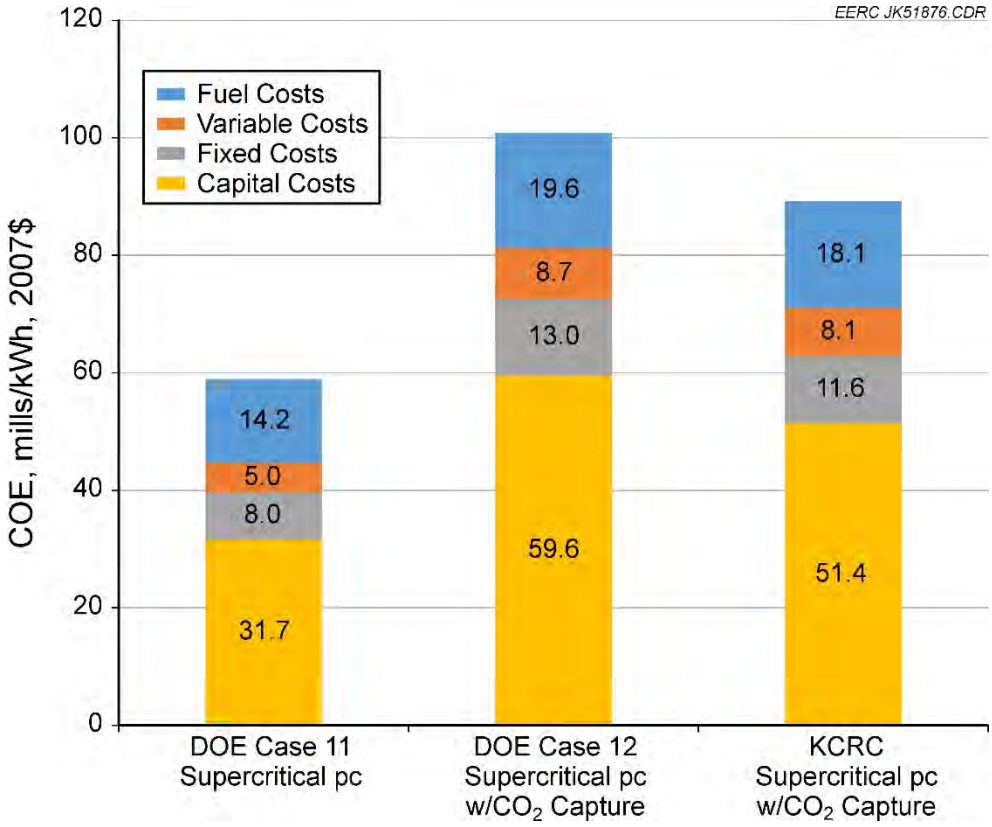

Figure 7-14. COE breakdown between DOE cases and KCRC case.

Table 7-10. Additional Cost Estimations for DOE Cases 11 and 12 and KCRC, costs in US$1000 (2007 $)

Description	Case 11	Case 12	KCRC
Preproduction Costs	28,826	48,094	43,327
Inventory Capital	17,474	26,573	22,612
Land	900	900	900
Other Owner's Costs	135,885	240,304	207,479
Financing Costs	24,459	43,255	37,346
TOC	1,113,445	1,963,644	1,697,214
Total As-Spent Cost (TASC)	1,262,647	2,238,554	1,934,824
Total Fixed Operating Costs	32,635	53,198	47,360
Variable Operating Costs	20,633	35,730	33,314
Fuel Cost	58,218	80,435	74,170

7.2.2.1 KCRC Economic Conclusions

KCRC Solvent-B demonstrated improved performance over MEA at the pilot scale. Projecting that performance to full scale indicated that the overall efficiency of a plant utilizing the solvent would be increased over MEA. The reduced L/G for the solvent enabled the size of the

capture system to be reduced. Initial modeling indicated that the five-train system could be reduced to three trains. These improvements benefit the overall economic assessment of performance at full scale.

The solvent is still in the development stage; therefore, estimates of solvent cost and usage were kept equivalent to those provided for MEA in the DOE Case 12 evaluation. As development of the solvent advances, this basic assumption must be corrected. This first-time economic projection indicates that Solvent-B improves the cost of carbon capture over MEA (DOE Case 12) because of the reduced equipment requirements and improved solvent performance. As development continues to larger demonstrations, it is anticipated that the costs will improve even more.

7.2.3 CSES Economic Results and Discussion

The cost-estimating methodology described was used to calculate the total plant capital costs and was compared to Case 11 and Case 12. Table 7-11 shows the TPC results, organized by cost account. Further results of the economic evaluation are given in Table 7-12.

To further illustrate the results of the CSES case over the DOE Case 12, Figure 7-15 presents the COE, with the fuel costs, variable costs, fixed costs, and capital costs shown separately. Additional cost breakdown is given in Table 7-13. Further detail is not given as each section for the CSES case is determined by scale factors applied to the DOE Case 11 from the document previously described and is not calculated individually based on acquired information about the specifics of a particular item cost.

Table 7-11. TPC Results for Each Case Organized by Account Code, costs in US$1000 (2007 $)

Acct. No.	Description	Case 11	Case 12	CSES
1	Coal and sorbent handling	38,365	47,015	40,633
2	Coal and sorbent preparation and feed	18,059	22,441	19,198
3	Feedwater and miscellaneous systems and equipment	79,149	102,552	92,134
4	Boiler and accessories	296,317	369,144	315,868
5	Flue gas cleanup	128,593	163,337	137,425
5B	CO_2 recovery	0	468,782	384,476
6	Combustion turbine/accessories	0	0	0
7	HRSG, ducting, and stack	37,291	37,525	38,168
8	Steam turbine generator and auxiliaries	115,947	132,111	122,543
9	Cooling water system	37,370	60,964	43,366
10	Ash/spent sorbent recovery and handling	12,626	15,109	13,257
11	Accessory electric plant	51,068	80,932	58,835
12	Instrumentation and control	21,555	25,838	22,356
13	Improvements to site	14,054	15,717	15,517
14	Buildings and structures	55,506	60,557	58,581
TPC		905,900	1,602,024	1,362,358
TOC		1,113,444	1,963,646	1,667,685

Table 7-12. Estimated Costs for Case 11, Case 12, and CO_2 Solutions (CSES) Case

	Case 11	Case 12	CSES
TPC, US$ (2007)/kW	1647	2913	2477
TOC, US$ (2007)/kW	2024	3570	3032
Total As-Spent Capital, US$ (2007)/kW	2296	4070	3457
COE, US$ (2007)/MWh	58.9	100.9	82.3
Levelized COE, US$ (2007)/MWh	74.7	127.8	104.4
CO_2 Capture Cost, US$ (2007)/tonne	NA	47.7	39.3

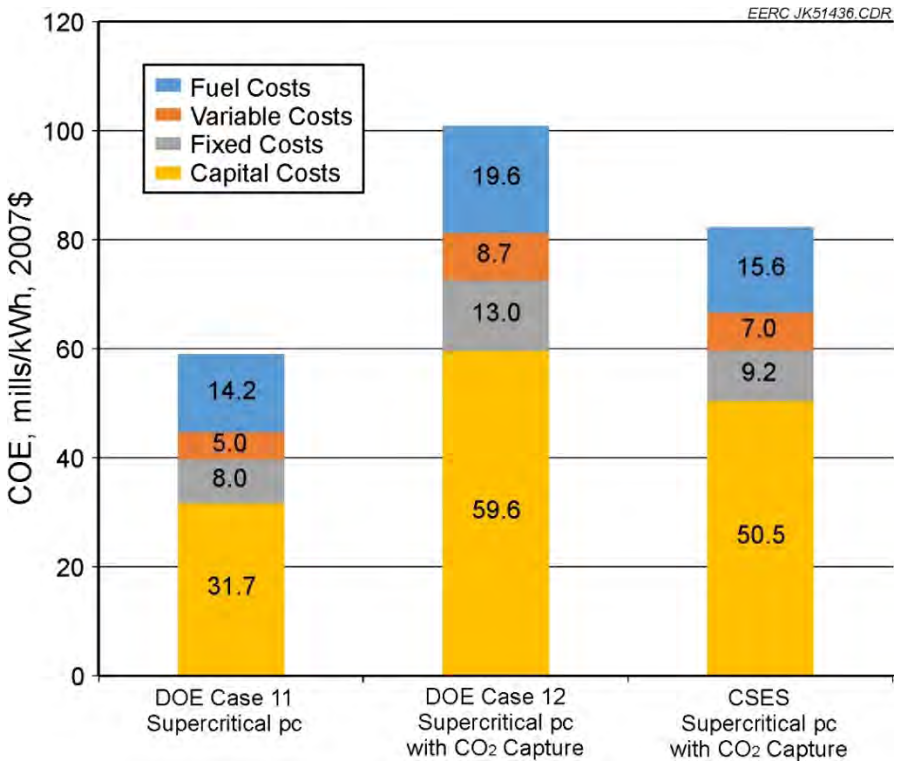

Figure 7-15. COE breakdown between DOE cases and CSES case.

Table 7-13. Additional Cost Estimations for DOE Cases 11 and 12 and CSES, costs in US$1000 (2007 $)

Description	Case 11	Case 12	CSES
Preproduction Costs	28,826	48,094	42,273
Inventory Capital	17,474	26,573	20,153
Land	900	900	900
Other Owners' Costs	135,885	240,304	204,354
Financing Costs	24,459	43,255	36,784
TOC	1,113,445	1,963,644	1,667,685
TASC	1,262,647	2,238,554	1,901,161
Total Fixed Operating Costs	32,635	53,198	44,544
Variable Operating Costs	20,633	35,730	33,762
Fuel Cost	58,218	80,435	75,179

7.2.3.1 Closer Simulation of Capture System

It is recognized that there are components of the carbon capture system that truly do not apply to the CO_2 Solutions capture system. These are components that are not needed for the CO_2 Solutions solvent but are in the Econamine basis for the DOE case studies. These systems include the water wash tower and associated subsystems and the solvent reclaimer and associated subsystems. Exact detail on the precise components cannot be derived as that information is held as proprietary by Fluor and cannot be released by DOE. Nonetheless, an attempt was made to remove those components from the system and the costs estimated by their removal from the case study. The resultant changes to the cost breakdown are given in Table 7-14, showing the modified system as CSESmod. A graphical breakdown is provided in Figure 7-16.

Table 7-14. Comparison Chart of Costs Associated with the DOE Cases, CSES, and the Modified CSES Case (costs in US$1000 [2007 $] unless otherwise noted)

Description	Case 11	Case 12	CSES	CSESmod
Coal and Sorbent Handling	38,365	47,015	40,633	40,633
Coal and Sorbent Preparation and Feed	18,059	22,441	19,198	19,198
Feedwater and Miscellaneous Systems and Equipment	79,149	102,552	92,134	92,134
Boiler and Accessories	296,317	369,144	315,868	315,868
Flue Gas Cleanup	128,593	163,337	137,425	137,425
CO_2 Recovery	0	468,782	384,476	351,790
Combustion Turbine/Accessories	0	0	0	0
HRSG, Ducting, and Stack	37,291	37,525	38,168	38,168
Steam Turbine Generator and Auxiliaries	115,947	132,111	122,543	122,543
Cooling Water System	37,370	60,964	43,366	43,366
Ash/Spent Sorbent Recovery and Handling	12,626	15,109	13,257	13,257
Accessory Electric Plant	51,068	80,932	58,835	58,835
Instrumentation and Control	21,555	25,838	22,356	22,356
Improvements to Site	14,054	15,717	15,517	15,426
Buildings and Structures	55,506	60,557	58,581	58,409
TPC	905,900	1,602,024	1,362,358	1,329,408
Preproduction Costs	28,826	48,094	42,273	41,614
Inventory Capital	17,474	26,573	20,153	19,968
Land	900	900	900	900
Other Owner's Costs	135,885	240,304	204,354	199,411
Financing Costs	24,459	43,255	36,784	35,894
TOC	1,113,445	1,963,644	1,667,685	1,628,035
TASC	1,262,647	2,238,554	1,901,161	1,855,960
Total Fixed Operating Costs	32,635	53,198	44,544	44,544
Variable Operating Costs	20,633	35,730	33,762	33,470
Fuel Cost	58,218	80,435	75,179	75,179
COE, US$ (2007)/MWh	58.9	100.9	82.3	81.0
Levelized COE, US$ (2007)/MWh	74.7	127.8	104.4	102.8
CO_2 Capture Cost, US$ (2007)/tonne	NA	47.7	39.3	37.2

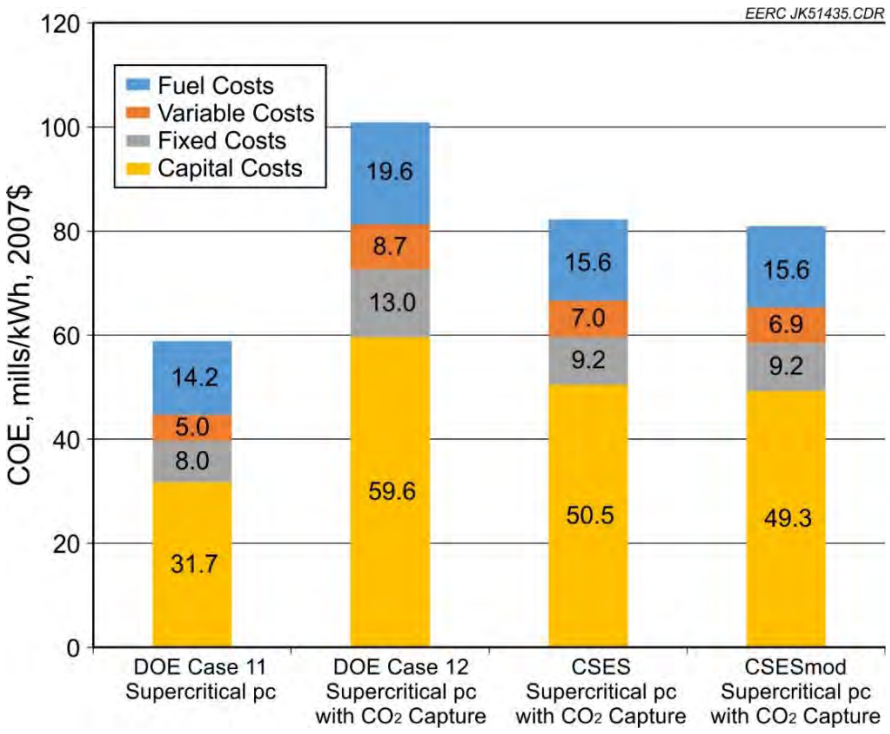

Figure 7-16. COE breakdown between DOE cases, CSES case, and CSESmod case.

The estimated reduction in costs associated with removal of the subsystems not needed to operate with the CO_2 Solutions solvent results in an approximate reduction of the capture cost by 5%. In this exercise, the cost of the stripper vacuum has not been included in the CSES and CSESmod cases. The associated vacuum costs need to be explored further.

7.2.3.2 CSES Economic Conclusions

Expected capture rates were not achieved because of two main limitations: 1) the flow rate of hot water to regenerate the solvent was very weak and below what was required for capture at the 90% level and 2) solvent flow between the absorber and stripping columns could not be increased to sufficient levels to meet target L/Gs. Additionally, the reboiler was not of an optimum design to meet the requirements of this solvent. All test data and solvent samples taken were sent to CO_2 Solutions at the conclusion of testing. Although challenges existed, the solvent was still shown to perform well under the conditions of the tests, and regeneration was achieved at low regeneration temperature. Because of inconsistent gas analyzer data from Weeks 1 and 2 as compared to Week 3, it is very difficult to directly compare results between the two sets, and caution must be taken when doing so. Unfortunately, additional testing will be needed to generate more consistent data sets for direct comparison.

Initial modeling to project performance of full-scale operation was based on DOE Case 11 (plant with no capture) and Case 12 (plant with capture). Because of the nature of this technology not requiring steam for regeneration, a hybrid process of utilizing information from both DOE case studies was needed, and results indicated increased benefit to a coal-fired utility utilizing this

technology over MEA for CO_2 capture. Much of the benefit resides in the low heat requirements for regeneration. If ample low-quality heat sources can be identified at the full scale to provide the regeneration energy required, then the steam cycle can remain unaltered. This concept alone can be the driving factor for a utility to utilize this technology and results in lower cost as compared to the DOE Case 12 scenario for a plant with carbon capture. Results of this beginning work indicate the strong potential to meet the DOE goal of $40/tonne of CO_2 captured.

Beyond the more intensive study of the potential of low-quality heat sources, a more in-depth examination of the stripper vacuum requirement needs to be undertaken and incorporated into the technical and economic evaluations of the technology. Additionally, at the FEED study level it is assumed that many system components will be customized to better suit the unique characteristics of this technology and provide additional projected cost savings. An example of this was shown in removing components not needed to operate the CO_2 Solutions technology. As the technology undergoes testing at larger scales, the expectation is that the projections provided here will improve in accuracy, and the costs and benefits will become more positive.

8.0 PLANT-SPECIFIC CAPTURE EVALUATION

8.1 Introduction

The EPA CPP aims to reduce CO_2 emissions from power plants to 32% below 2005 levels by 2030. The CPP establishes CO_2 emission targets for each state, which range from 7% to 47%. These percentages represent how much states must reduce their power fleet emission rates below 2012 levels.

One approach that could be used to meet the required emission reductions is CCS. The actual impact of capture of CO_2 on a power plant will not be known until data from the only existing full-scale capture project at the SaskPower Boundary Dam facility become available. At this time, the impacts of CO_2 capture on a power plant must be estimated, generally through some sort of modeling. This report describes the results of a modeling effort that was undertaken at the EERC to provide decision makers with a tool to enable them to assess possible CO_2 emission reduction strategies. The work also highlights potential challenges that may exist for some power plants at which CO_2 capture is being considered.

8.2 Experimental Methods and Software Description

8.2.1 Model Used for the Estimates

The EERC used the Carnegie Mellon IECM Version 9.1 to model three existing coal-fired power plant units. Funded by DOE NETL, the IECM allows different technology options to be evaluated systematically at the level of an individual plant or facility and takes into account not only avoided carbon emissions, but the impacts on multipollutant emissions as well; plant-level resource requirements; capital, operating, and maintenance costs; and net plant efficiency. Uncertainties and technological risks also can be defined. The modeling framework is designed to support a variety of technology assessment and strategic planning activities.

The IECM allows the user to input specific values or built-in default values when modeling a utility. For this study, values for several of the model inputs were provided for three separate power plant units by plant engineers. A combination of plant-specific input values and default values were used to build a baseline model for each unit. Each baseline model was then retrofitted with CO_2 capture technologies as well as any other devices required in order to facilitate CO_2 capture.

8.2.2 Facilities Modeled

Plant A is a coal-fired unit that burns subbituminous coal. Because the use of the subbituminous coal allows the plant to meet air pollution regulations, it does not employ any pollution control devices other than a baghouse for particulate capture and a sorbent injection system for mercury control. CO_2 capture using chemical absorption requires that the level of SO_x emissions be less than 20 ppm and preferably in the 10-ppm range so as to minimize the formation of HSS. HSS are formed by the reaction of nitrogen and sulfur oxides with the solvent. Because they cannot be removed during the regeneration process, they take a portion of the amine out of service. Recovery of some of the amine is possible in a reclaiming process, but the waste from this process must be shipped to a specialized waste collection facility. To minimize the formation of HSS, a WFGD was included during the modeling effort of Plant A. The SO_2 removal efficiency of the modeled WFGD was set at 98% to eliminate the need for additional flue gas scrubbing prior to CO_2 capture.

Plant B is a coal-fired unit that burns low-sulfur subbituminous coal. The plant contains state-of-the-art scrubbers that allow it to both meet the Clean Air Act regulations for SO_2 emissions and low-NO_x burners to reduce its NO_x emissions. The unit has a sorbent injection system for mercury control. To meet the low SO_x levels required by most CO_2 capture solvents, the model of this unit included a WFGD.

Plant C is also a coal-fired unit that burns a low-sulfur subbituminous coal. It currently does not have any pollution control devices except for particulate capture and a sorbent injection system for mercury control. The unit was modeled with a WFGD capable of removing 98% of the SO_2 in the flue gas.

8.2.3 CO_2 Capture Technologies Modeled

Three postcombustion CO_2 capture processes that employ solvents were applied to the power plant units modeled in this study: MEA, Fluor's Econamine FG Plus^{SM} process, and ALSTOM's chilled ammonia process.

- MEA was developed over 60 years ago as a nonselective solvent to remove acid gas impurities such as CO_2 and H_2S from natural gas streams. It was adapted to capture CO_2 from flue gas streams. Typically, 75%–90% of the CO_2 can be captured using MEA, producing a CO_2 product stream with a purity in excess of 99% (Rao and Rubin, 2002). It is used in other applications besides gas treating, including cement, metalworking fluids, personal care products, pharmaceuticals, printing inks, and textiles/textile additives (DOW Specialty Amines, 2016). For many years, MEA was used as the

benchmark technology for CO_2 capture demonstration against which other technologies were compared.

- The Econamine FG Plus process is a Fluor proprietary, amine-based technology for large-scale CO_2 capture. The primary ingredient is MEA, although additives increase its ability to capture CO_2 from oxygen-containing systems without the degradation that usually occurs when an amine is exposed to oxygen (Reddy and others, 2008).

- The ALSTOM chilled ammonia process utilizes the low-temperature, low-energy reaction of an aqueous ammonium carbonate solution with CO_2. The flue gas is cooled prior to its reaction with the ammonium carbonate solution. A refrigeration system is needed to chill the flue gas and keep the absorber operating temperature below 50°F (Rhudy, 2006). The process can capture nearly 90% of the CO_2 with a product quality in excess of 99% (Kozak and others, 2010).

8.2.4 Model Run Matrix

Each power plant unit was modeled for the three different CO_2 capture processes and three different levels of capture: 90% of the full flue gas stream, 65% of the full flue gas stream, and 90% of a portion of the flue gas, with the remaining flue gas bypassing the capture system. In this case, 65% of the entire CO_2 emission for the unit was captured. The capture of CO_2 requires the removal of low-pressure steam from the power plant unit in order to regenerate the solvent, effectively derating the unit. Therefore, each model run was repeated assuming that an auxiliary natural gas boiler was added to the capture plant such that all of the low-pressure steam was provided by the auxiliary boiler. This approach maintained most of the unit's electric output, although it increased the total CO_2 emission from the unit (original CO_2 emission plus the CO_2 generated by the auxiliary boiler). To compensate, the modeled capture level from the coal-derived flue gas was increased so as to maintain 65% capture for the entire unit including the auxiliary boiler.

Table 8-1 presents a grid showing the matrix of model runs that was performed for each power plant unit during this study.

Table 8-1. Model Runs Performed During the Study

Capture Level	90%	65%	65% with a Bypass	Level Needed to Reach 65%	Level Needed to Reach 65% with a Bypass
Baseline (no capture)	NA	NA	NA	NA	NA
Without Auxiliary Boiler					
MEA	X	X	X	NA	NA
Econamine FG Plus	X	X	X	NA	NA
Chilled Ammonia	X	X	X	NA	NA
With Auxiliary Boiler					
MEA	X	X	X	X	X
Econamine FG Plus	X	X	X	X	X
Chilled Ammonia	X	X	X	X	X

8.2.5 Assumptions Made During Modeling

8.2.5.1 Base Plant Assumptions

Operation data from each utility were collected and used to build a model representative of the existing utilities. Although each plant in this study was modeled independently to match the real-world facility as closely as possible, data for all variables and plant conditions could not be acquired under the scope of the project, so several assumptions were made in setting up the model. IECM Version 9.1 default values were used for plant variables when actual values were not available.

The capital costs for the existing plants were assumed to be paid in full and do not contribute to the calculated required revenue, or COE, for plant operations.

8.2.5.2 CO_2 Capture System Assumptions

All CO_2 capture models were assumed to be retrofitted to the existing facility while maintaining the same fuel input rate. No retrofitting of the existing boilers was considered. The CO_2 capture models assume that the system is online at all times the plant is producing flue gas.

The IECM interface has an option to input a cost factor (retrofit$/new$) for retrofit equipment. For this study, the cost factor for the CO_2 capture equipment was entered as 1.0, which assumed that all retrofit costs are equal to new build costs of the same CO_2 capture equipment. This assumption is made because retrofit factors will be case-specific, depending on plant layout, proximity of the plant to vendors and resources, labor availability, etc.

The IECM allows for some of the flue gas to bypass the capture system. This enables smaller, more efficient absorber(s) to be used, which reduces the capital cost of the absorber tower(s). However, additional costs are incurred that are associated with the bypass, such as additional ductwork and fans.

The CO_2 product stream in all cases is assumed to be compressed to 2000 psia and transported via pipeline, with a product purity of 99.5 vol%.

8.3 Results and Discussion

The modeled results for a few important outputs were plotted to better show trends in the data and allow conclusions regarding the most likely scenario for a given plant to be determined.

8.3.1 Plant A

8.3.1.1 Net Power Output

Figure 8-1 shows the fraction of Plant A's baseline net power output that is achieved when capture is installed. As the plot shows, the addition of capture to Plant A reduces the net power

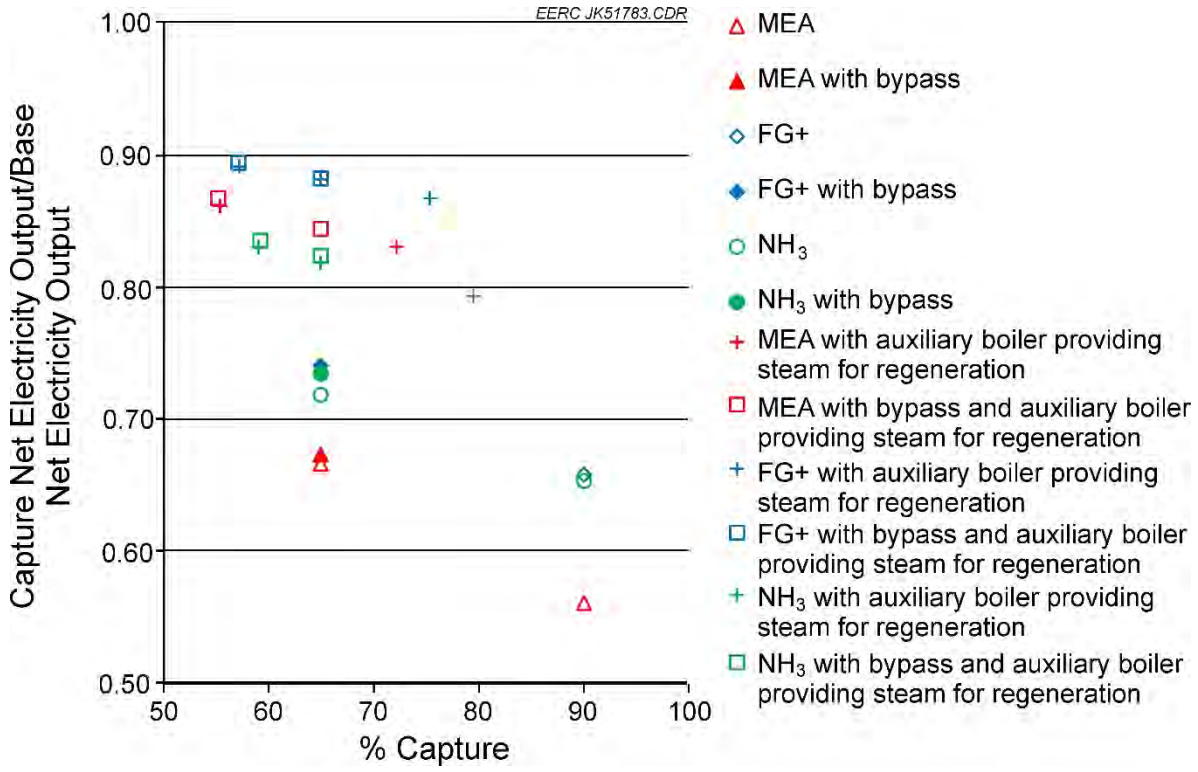

Figure 8-1. Net power output of Plant A with capture as a fraction of the net power output of the baseline for Plant A.

output by roughly 10% to 45%, depending upon the capture technology chosen, the level of CO_2 emission reduction that is targeted, whether or not some of the flue gas is allowed to bypass the capture system, and if an auxiliary boiler is employed. The use of an auxiliary boiler maintains roughly 80% or more of the plant's power output, with lower levels of capture maintaining the highest power output. It can be seen that, in general, the Econamine FG Plus process requires less of the power produced by the plant for capture, whether additional steam is provided by an auxiliary boiler or not. The MEA process seems to require more steam than the chilled ammonia process. This is illustrated by the fact that the MEA process results in a higher power output than the ammonia process when the steam is provided by an auxiliary boiler, yet the fraction of the power output is higher for the chilled ammonia process than for the MEA process when auxiliary steam is not provided.

8.3.1.2 Revenue Required

The revenue required to operate Plant A is the levelized annual cost and includes both the amortized capital costs and the operating and maintenance costs. For Plant A, the ratio of the revenue required for the plant with capture to the baseline plant shows that the least expensive approach is to employ the Econamine FG Plus process without an auxiliary boiler for steam production. This can be seen in Figure 8-2.

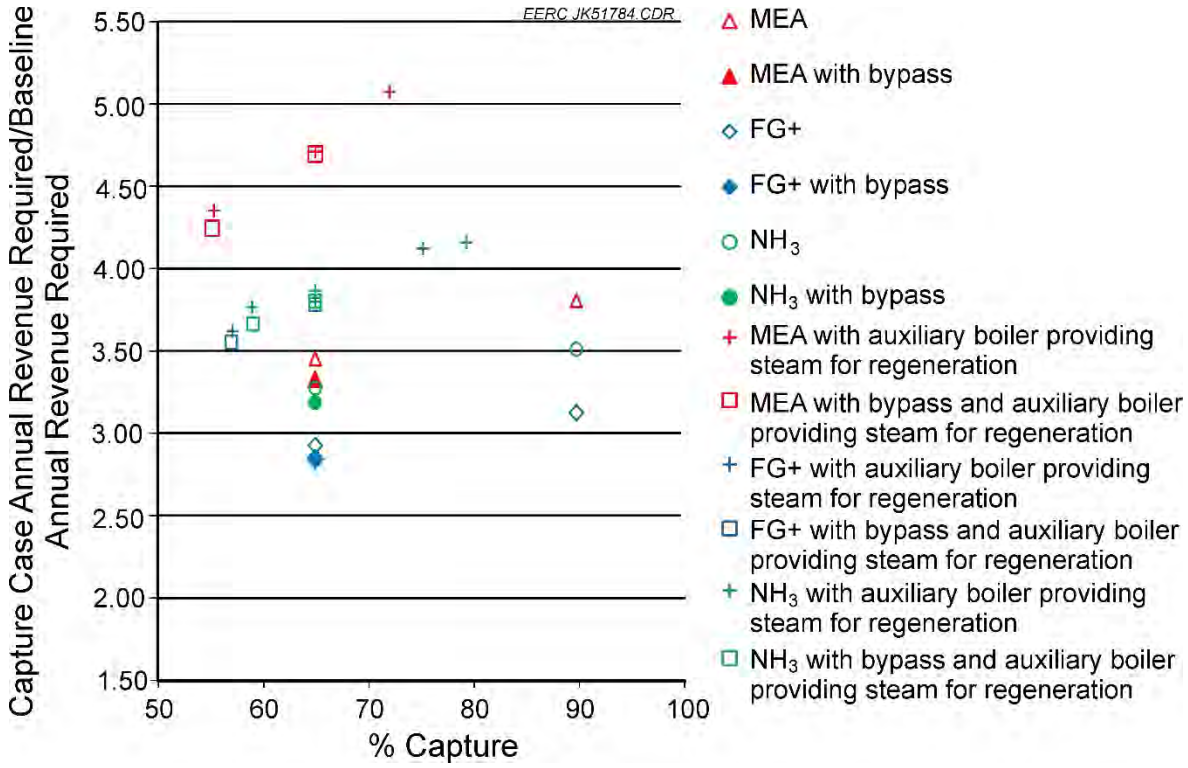

Figure 8-2. Ratio of the annual revenue required to operate Plant A with capture to the baseline revenue required for various capture levels and processes.

The use of a capture system reduces the amount of power produced by the plant, irrespective of whether a bypass is present or not. It is of interest to estimate the annual revenue requirement per MW power produced. In Figure 8-3, the revenue required per MW produced for the various capture cases is shown as a fraction of the equivalent value for the baseline plant. Figure 8-3 clearly shows that the Econamine FG Plus process requires less annual revenue on a per-MW basis than either the MEA process or the chilled ammonia process.

8.3.1.3 Water Use

The total water withdrawal requirement for Plant A was plotted as a fraction of the total water withdrawal requirement of the baseline plant for each of the three capture processes and at various capture levels. This is shown in Figure 8-4. The plot shows that less water is required for lower capture levels and that the chilled ammonia process requires considerably more water than does either the MEA or Econamine FG Plus process. The chilled ammonia process needs less steam to regenerate the solvent than does either the MEA or Econamine FG Plus process. Therefore, when an auxiliary boiler is added to the system, the additional water required is less for the chilled ammonia process than for the MEA or the Econamine FG Plus processes.

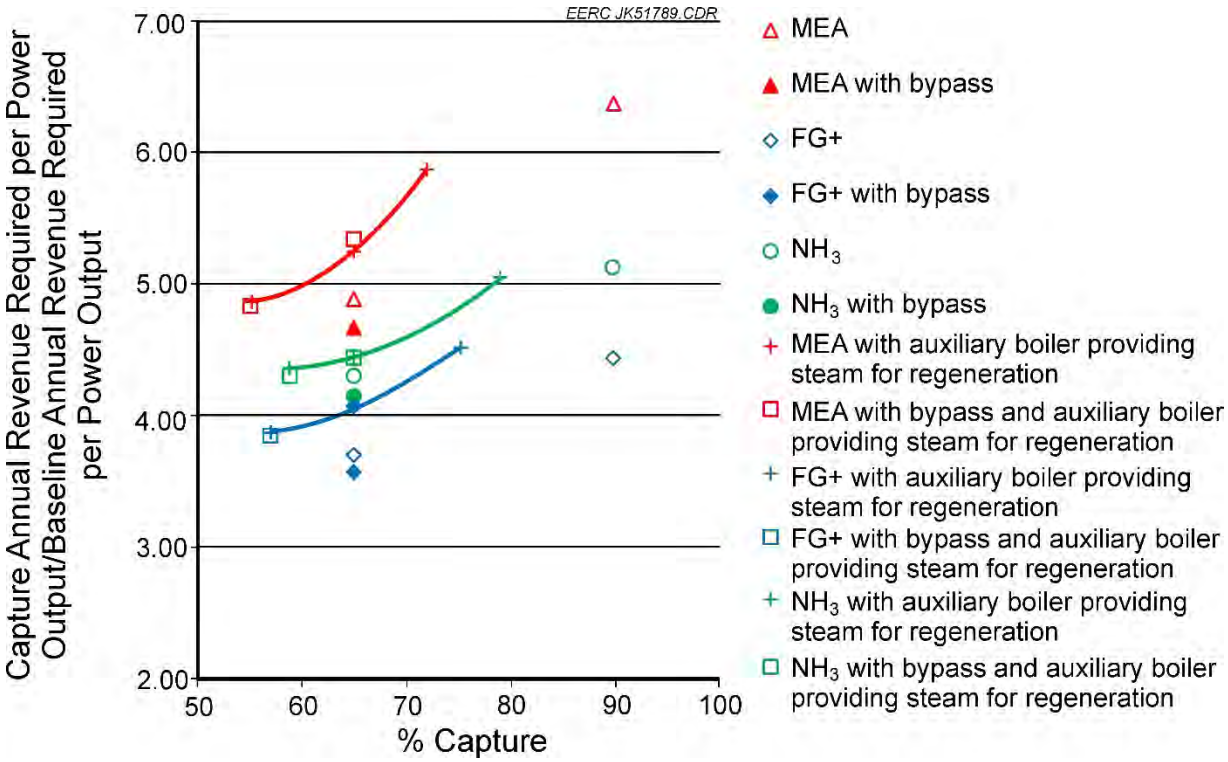

Figure 8-3. The revenue required on a per-MW-produced basis for Plant A as a fraction of the revenue required per MW produced for the baseline plant for various capture levels.

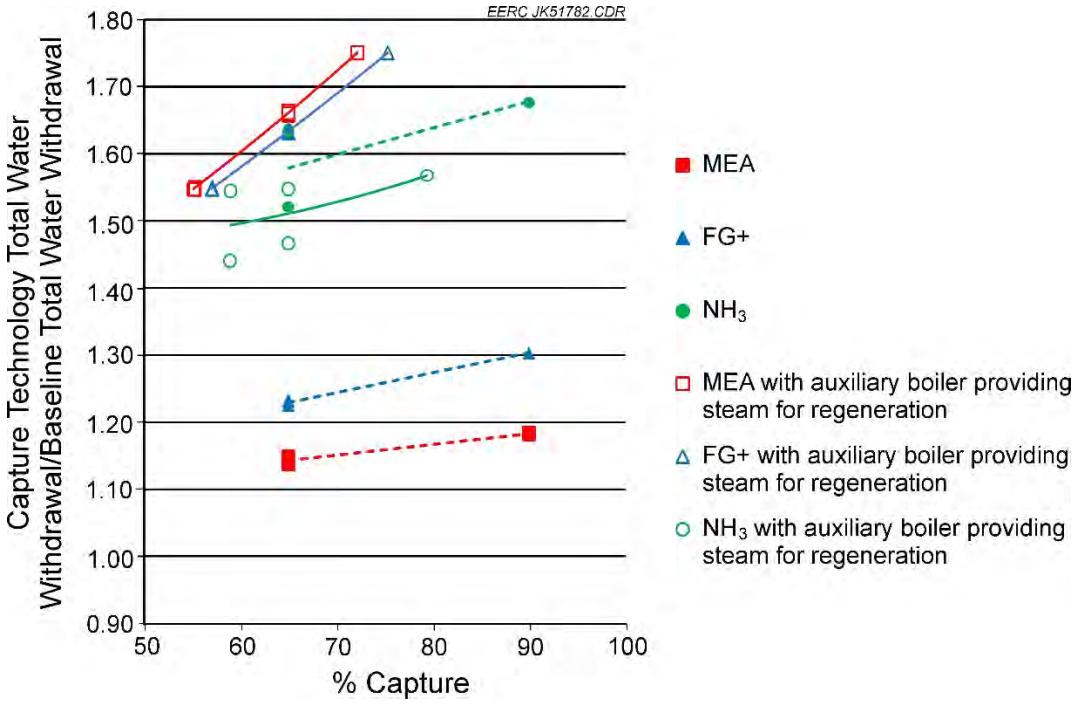

Figure 8-4. Total water withdrawal of various capture processes as a fraction of the total water withdrawal of baseline Plant A for various levels of capture.

8.3.2 Plant B

8.3.2.1 Net Power Output

Figure 8-5 presents the fraction of Plant B's baseline net power output that is achieved when capture is installed. As the plot shows, the addition of capture to Plant B reduces the net power output by roughly 5% to 40%, depending upon the capture technology chosen, the level of CO_2 emission reduction that is targeted, whether or not some of the flue gas is allowed to bypass the capture system, and if an auxiliary boiler is employed. The use of an auxiliary boiler maintains roughly 80% or more of the plant's power output, with lower levels of capture maintaining the highest electrical output. Figure 8-5 shows the Econamine FG Plus process requires less of the power produced by the plant for capture, whether additional steam is provided by an auxiliary boiler or not. The MEA process is shown to require more steam than the chilled ammonia process. This can be seen by the fact that the MEA process results in a higher power output than the ammonia process when the steam is provided by an auxiliary boiler, yet the fraction of the power output is higher for the chilled ammonia process than for the MEA process when auxiliary steam is not provided.

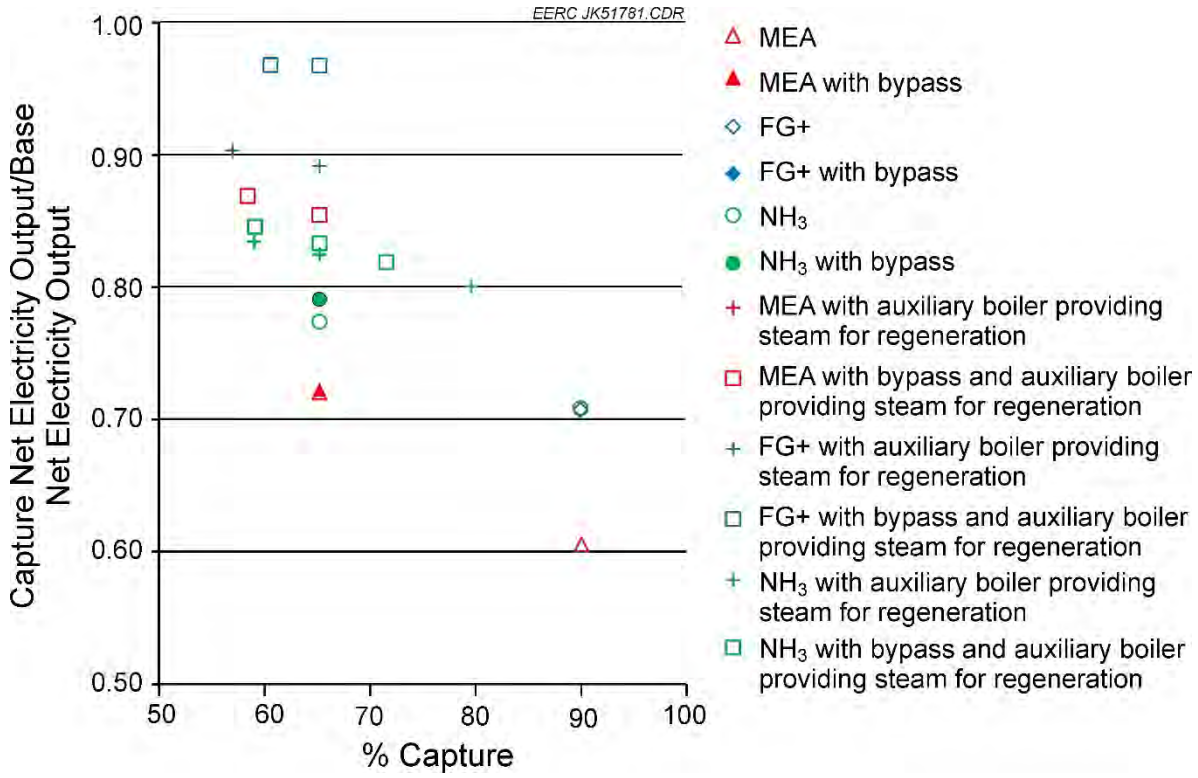

Figure 8-5. Net power output of Plant B, with capture as a fraction of the net power output of the baseline for Plant B.

8.3.2.2 Revenue Required

The revenue required to operate Plant B is the levelized annual cost and includes both the amortized capital costs as well as operating and maintenance costs. For Plant B, the ratio of the revenue required for the plant with capture to the baseline plant indicates that the least expensive approach is to employ the Economine FG Plus process without an auxiliary boiler for steam production. This can be seen in Figure 8-6. The most expensive capture technology to implement is MEA, in cases with or without an auxiliary boiler.

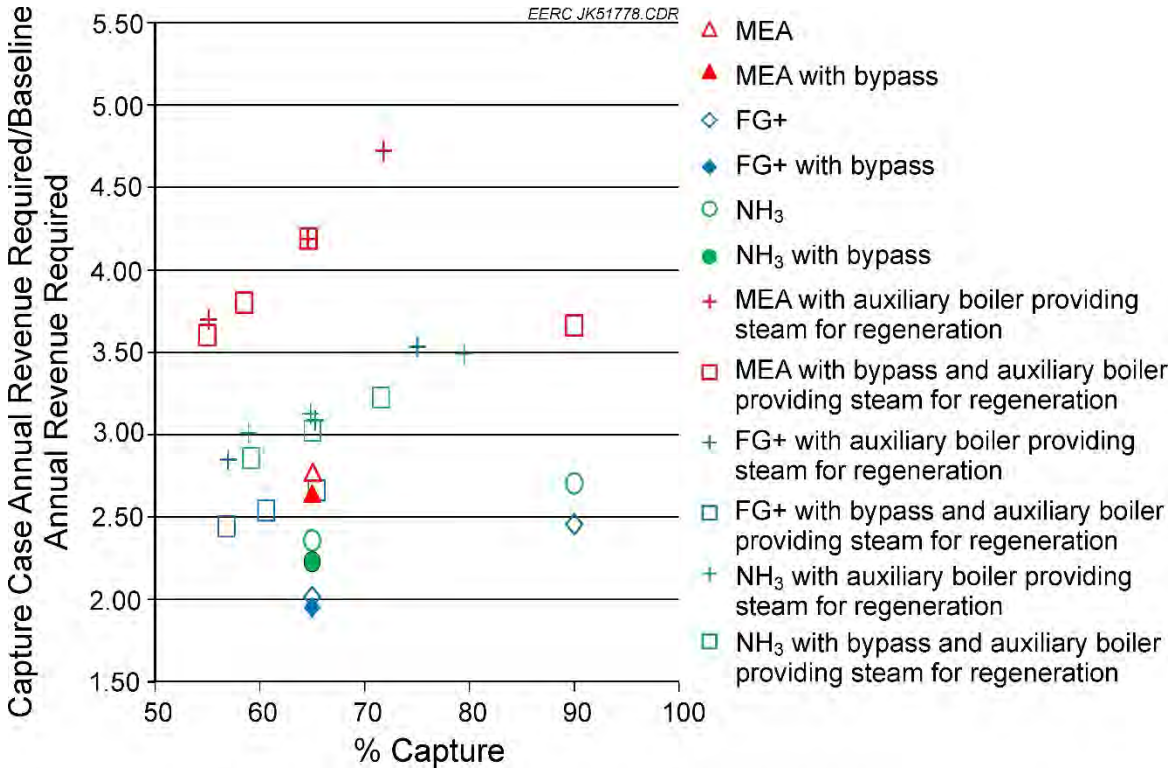

Figure 8-6. Ratio of the annual revenue required to operate Plant B with capture to the baseline revenue required for various capture levels and processes.

Because the use of a capture system reduces the electrical output of the plant, the relationship between annual revenue requirement and electrical output was investigated. This can be seen in Figure 8-7, where the revenue required per MW produced for the various capture cases is shown as a fraction of the equivalent value for the baseline plant. Figure 8-7 shows that the Econamine FG Plus process requires less annual revenue on a per-MW basis than either the MEA process or the chilled ammonia process when applied to Plant B.

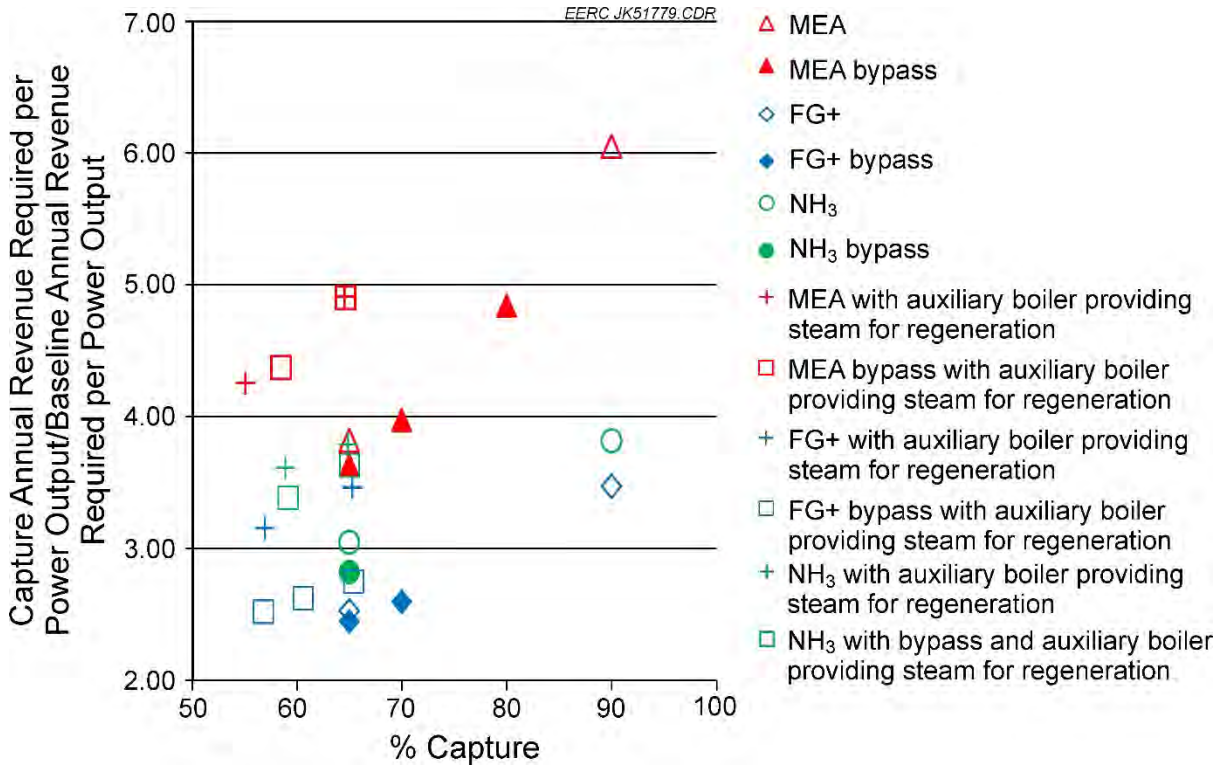

Figure 8-7. The revenue required on a per-MW-produced basis for Plant B as a fraction of the revenue required per MW produced for the baseline plant for various capture levels.

8.3.2.3 Water Use and Waste Production

Total water withdrawal requirement for Plant B is plotted as a fraction of the total water withdrawal requirement of the baseline plant for each of the three capture processes and at various capture levels. This is shown in Figure 8-8. The plot shows that water withdrawl rate is flat across the range of modeled capture levels and that the chilled ammonia process requires considerably less water than either the MEA or Econamine FG Plus process.

During the CO_2 capture process, waste is generated in the reclaimer that typically cannot be treated on-site. Waste generation rates increase as CO_2 capture rates increase. Reclaimer waste must be handled through storage, disposal, or some other means. For Plant B, reclaimer waste is generated at a rate of between 6500 and 9100 lb/hr for MEA and chilled ammonia processes. A much lower waste generation rate of approximately 1000 lb/hr is associated with Econamine FG Plus.

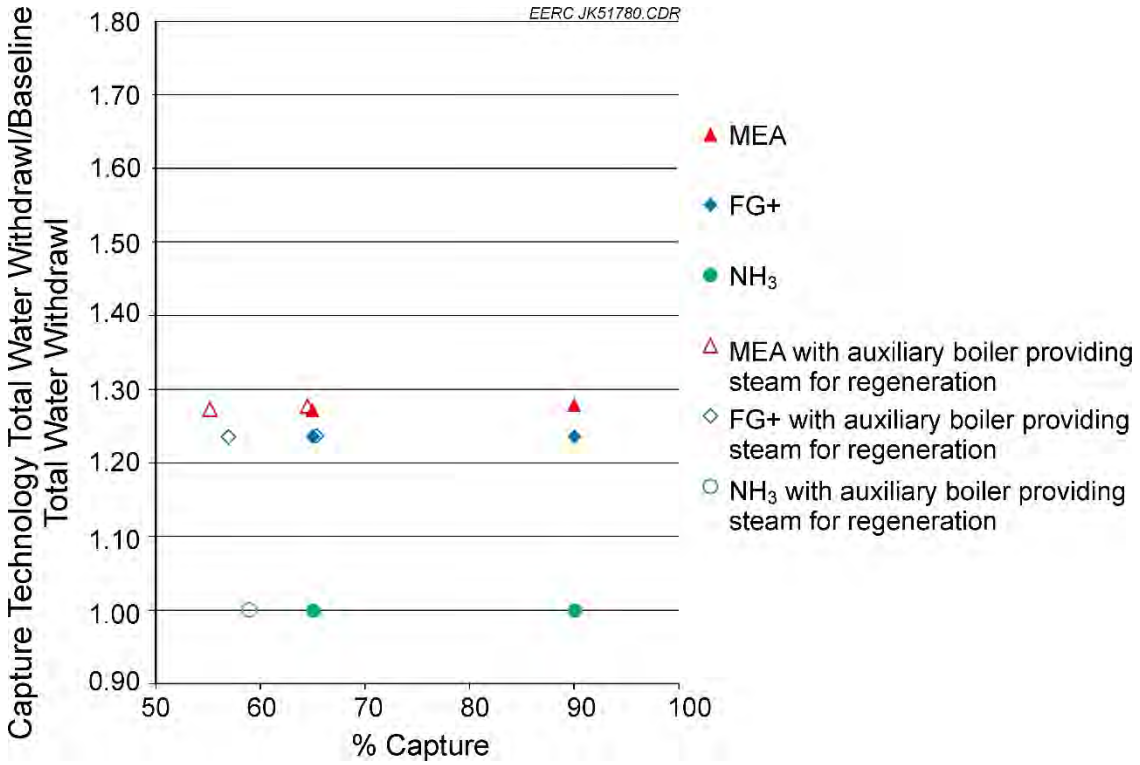

Figure 8-8. Total water withdrawal of various capture processes as a fraction of the total water withdrawal of baseline Plant B for various levels of capture.

8.3.3 Plant C

8.3.3.1 Net Power Output

Figure 8-9 shows the fraction of Plant C's baseline net power output that is achieved when capture is installed. As the plot shows, the addition of capture to Plant C reduces the net power output by about 10% to 45%, depending upon the capture technology chosen, the level of CO_2 emission reduction that is targeted, whether or not some of the flue gas is allowed to bypass the capture system, and if an auxiliary boiler is employed. The use of an auxiliary boiler maintains roughly 80% or more of the plant's power output, with lower levels of capture maintaining the highest power output. It can be seen that, in general, the Econamine FG Plus process requires less of the power produced by the plant for capture, whether additional steam is provided by an auxiliary boiler or not. The MEA process seems to require more steam than the chilled ammonia process, which can be seen by the fact that the MEA process results in a higher power output than the ammonia process when the steam is provided by an auxiliary boiler, yet the fraction of the power output is higher for the chilled ammonia process than for the MEA process when auxiliary steam is not provided.

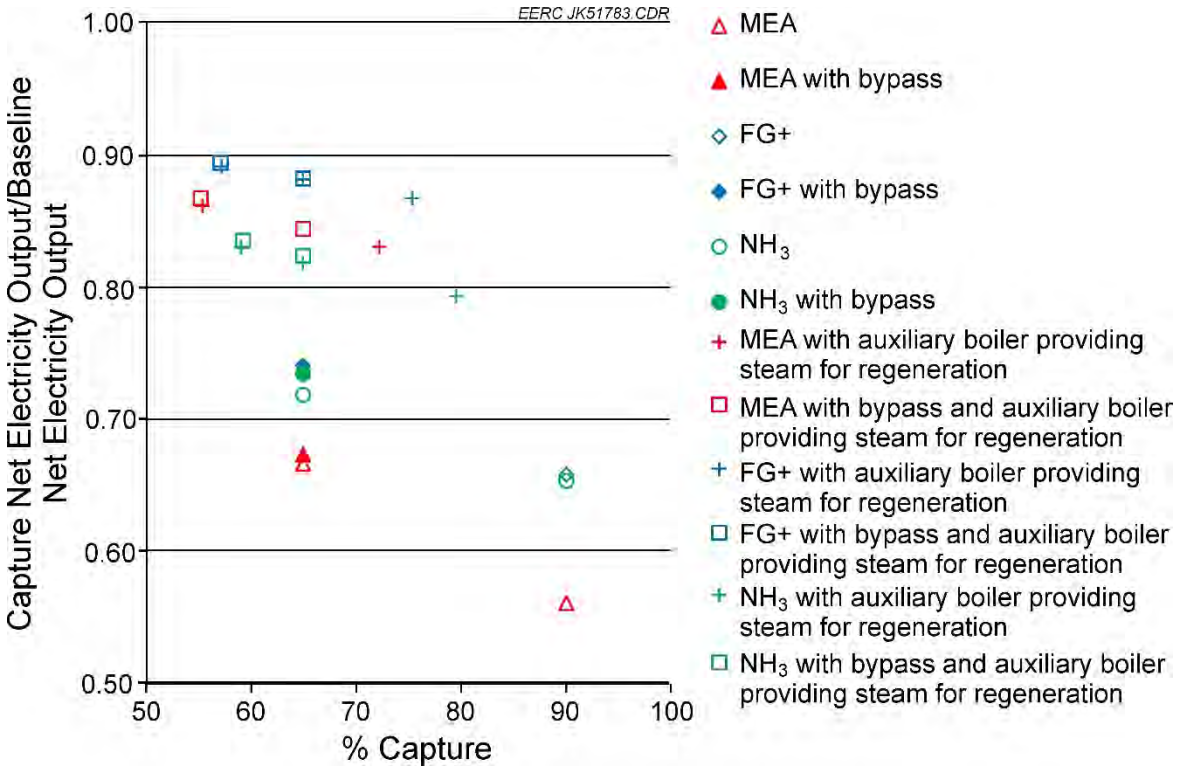

Figure 8-9. Net power output of Plant C with capture as a fraction of the net power output of the baseline for Plant C.

8.3.3.2 Revenue Required

The revenue required to operate Plant C is the levelized annual cost and includes both the amortized capital costs and the O&M costs. For Plant C, the ratio of the revenue required for the plant with capture to the baseline plant indicates that the least expensive approach is to employ the Econamine FG Plus process without an auxiliary boiler for steam production. This can be seen in Figure 8-10.

Because the use of a capture system reduces the amount of power produced by the plant, it was of interest to estimate the annual revenue requirement per MW power produced. This can be seen in Figure 8-11, where the revenue required per MW produced for the various capture cases is shown as a fraction of the equivalent value for the baseline plant. Figure 8-11 clearly shows that the Econamine FG Plus process requires less annual revenue on a per-MW basis than either the MEA process or the chilled ammonia process when applied to Plant C.

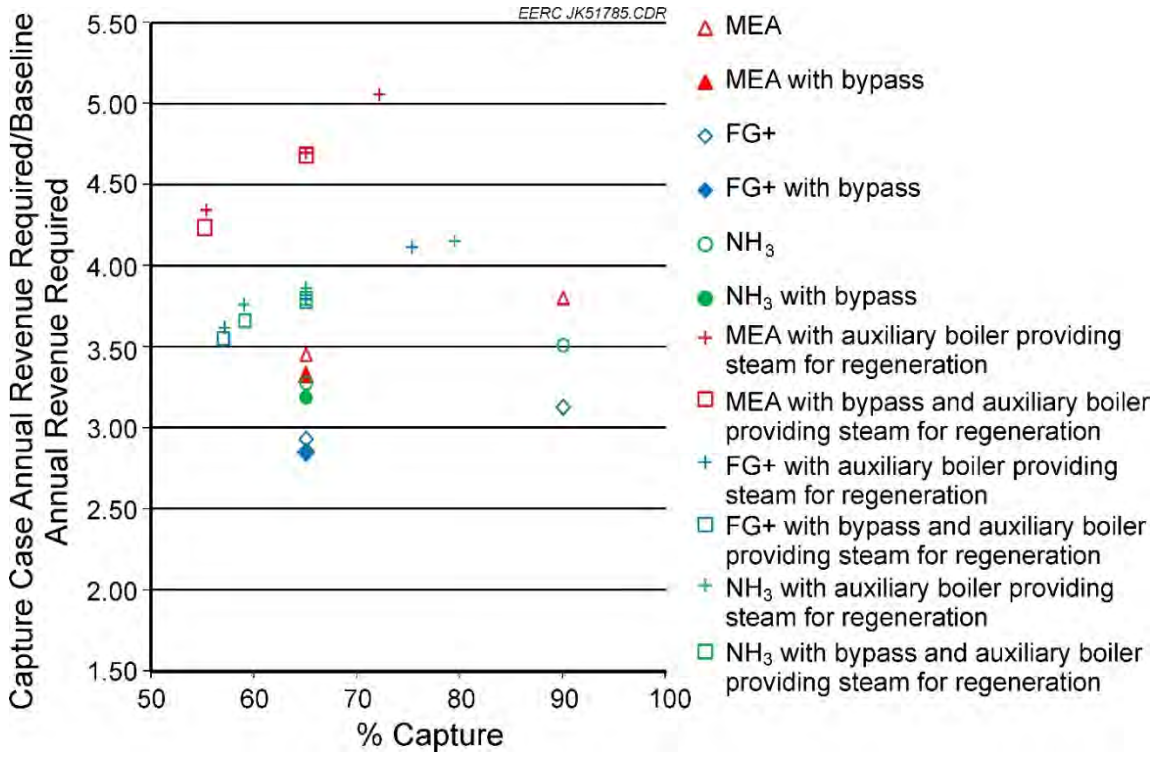

Figure 8-10. Ratio of the annual revenue required to operate Plant C with capture to the baseline revenue required for various capture levels and processes.

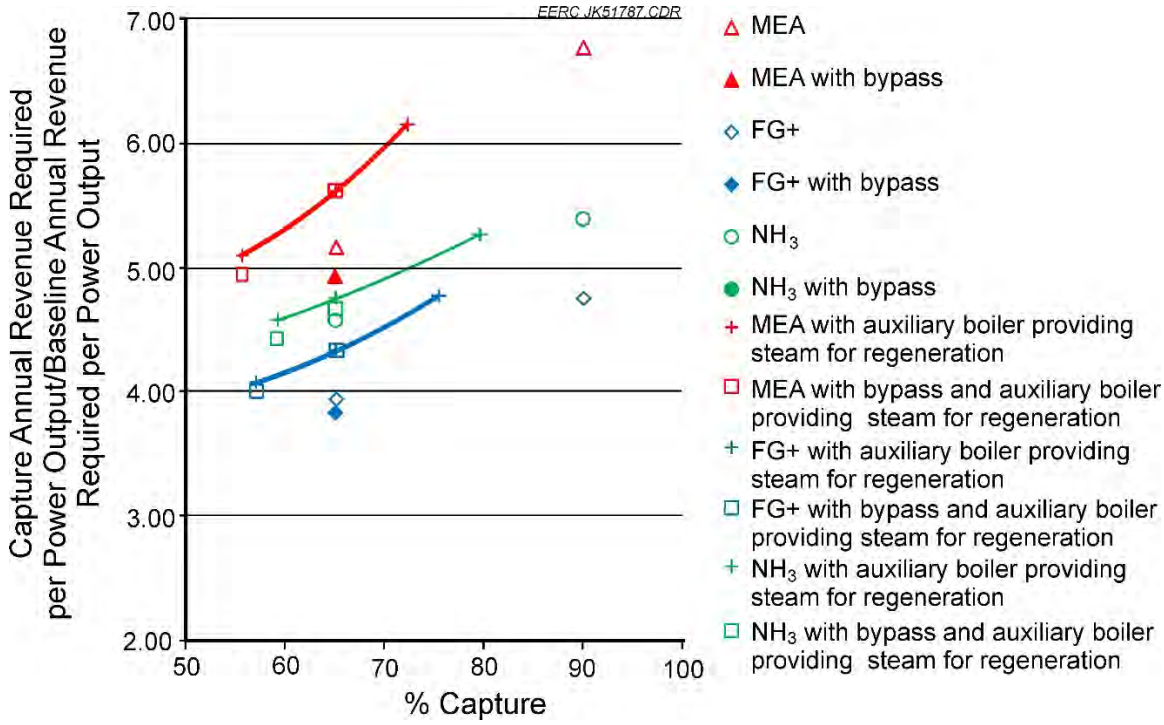

Figure 8-11. The revenue required on a per-MW-produced basis for Plant C as a fraction of the revenue required per MW produced for the baseline plant for various capture levels.

8.3.3.3 Water Use

The total water withdrawal requirement for Plant C was plotted as a fraction of the total water withdrawal requirement of the baseline plant for each of the three capture processes and at various capture levels. This is shown in Figure 8-12. The plot shows that less water is required for lower capture levels and that the chilled ammonia process requires considerably more water than does either the MEA or Econamine FG Plus process. The chilled ammonia process needs less steam to regenerate the solvent than does either the MEA or Econamine FG Plus process. Therefore, when an auxiliary boiler is added to the system, the additional water required is less for the chilled ammonia process than for the MEA or the Econamine FG Plus processes.

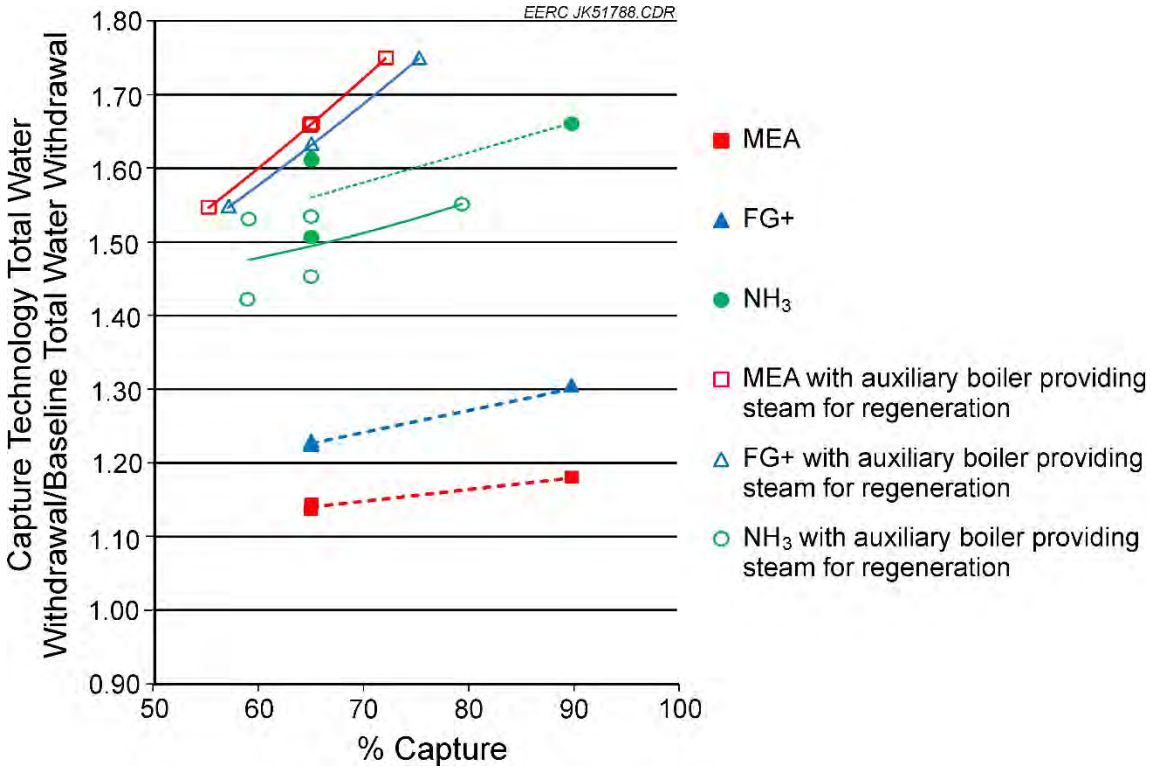

Figure 8-12. Total water withdrawal of various capture processes as a fraction of the total water withdrawal of baseline Plant C for various levels of capture.

8.4 Conclusions and Recommendations

8.4.1 Plant A

The modeling results indicate that the most appropriate capture process of those that were modeled for Plant A is the Fluor Econamine FG Plus. It allows the plant to retain more of its power output and requires less revenue to operate the unit relative to the other capture technologies. Lower levels of capture were more efficient and should be considered if this would allow the unit to meet emission requirements.

8.4.2 Plant B

The modeling results indicate that the most appropriate capture process of those evaluated for Plant B is the Fluor Econamine FG Plus. It allows the plant to retain more of its power output and requires less revenue to operate the unit relative to the other capture technologies modeled. The unit was more efficient at lower capture levels, which should be considered if this would allow the unit to meet emission requirements.

8.4.3 Plant C

The modeling results indicate that the most appropriate capture process of those that were modeled for Plant C is the Fluor Econamine FG Plus. It allows the plant to retain more of its power output and requires less revenue to operate the unit relative to the other capture technologies. Lower levels of capture were more efficient and should be considered if this would allow the unit to meet emission requirements.

8.4.4 Overall Considerations

When determining how to add capture to a power plant, several important points must be considered:

- If a power plant unit does not currently include a sulfur removal device, it will need one to reduce flue gas sulfur levels to less than 20 ppm, the upper boundary of sulfur content that can be tolerated by most capture solvents (amines, ammonia). The installation of a WFGD that removes 98% of the SO_x may eliminate the need for an additional sulfur-scrubbing tower to "polish" the flue gas prior to capture. The cost of a very efficient WFGD may be less than the cost of a less efficient WFGD plus a sulfur-polishing scrubber tower.

- CO_2 capture facilities require a relatively large footprint. Some estimates have placed the amount of space required for a capture plant and attendant unit operations at about 4 acres. (Florin and Fennell, 2010) The amount of space required, and its location relative to ductwork, water lines, etc., may dictate the choice of one capture process over another.

- Space will also be required for on-site storage of solvent and waste from the reclaiming process.

- Capture processes require considerable amounts of water, especially for cooling. Power plants that are in arid areas may find that the addition of a cooling tower would be advantageous in minimizing water usage.

- Use of a bypass to minimize the size of the capture tower(s) results in a slight reduction of revenue required to operate the plant on a per-MW basis when compared to capture of an equivalent amount without a bypass. The inclusion of a bypass should be made on a case-by-case basis, considering the CO_2 emission reduction level that is targeted as well

as the space and location that will be required for the ductwork and blowers needed for the bypass.

9.0 AMINE EMISSION EVALUATION

9.1 Introduction

The use of aqueous amine solvents to capture CO_2 from coal-derived flue gas is widely viewed as a promising technology and has undergone several pilot demonstrations around the world, with varying degrees of success. One common challenge with this technology is the degradation of amine compounds during the capture process and/or during regeneration of the solvent in the stripper unit. As a result, some of the functional amine is lost to degradation, volatilization, or leakage from the handling systems, thus releasing these chemicals into the environment in various forms. This section addresses the emission of amines with the flue gas and evaluates the FT-IR spectroscopy method as a means of amine emission monitoring.

9.1.1 Amine Emission Monitoring

With the lack of full-scale facilities utilizing amine solvents for CO_2 capture, studies on the extent/impact of emissions of amine and its degradation products on the environment are still limited. The Norwegian Technology Centre Mongstad (TCM), which is one of the world's largest CO_2 capture facilities, has conducted some work to evaluate the environmental impact of amine solvents used for CO_2 capture, particularly, amine-derived constituents that enter the environment through stack emissions (Dye and others, 2008). Preliminary results from Phase I Task 3 of that study identified the FT-IR spectroscopy technique as a viable analytical tool for continuous monitoring of stack emissions of some of the amines and/or their degradation products.

In general, the application of FT-IR technology to gas sampling is based on the ability of the instrument to acquire spectra from the gas stream and then compare with previously acquired calibration spectra (reference spectra) under similar conditions using associated software. Thus the FT-IR is amenable to monitoring stack emissions of amines and their degradation products during CO_2 capture from coal-derived flue gas.

9.1.2 Amine Emission Mitigation

Besides monitoring, a potential mitigation approach to amine emissions is believed to involve the use of water wash to scrub the amine and its degradation products from stack gas. However, this method can only remove water-soluble compounds, and a small fraction of insoluble compounds may still be emitted. Previous pilot studies at the EERC have employed the water wash method as way to abate excessive amine volatilization products via the stack. But the viability of a water wash technique in terms of water use, corrosion issues, disposal challenges, etc., for the control of amine emissions has not yet been established, and studies demonstrating this concept are rare. Consequently, this study was conducted as part of PCO_2C Phase III work to review current information about the FT-IR technology for continuous stack monitoring of amine-related emissions and a water wash method for potential abatement of these emissions. Specifically, the

aim is to identify the challenges, advantages and disadvantages, and available potential remedies for any known challenges.

9.1.3 Amine Emission-Monitoring Background

A few studies have been conducted around the world geared toward investigating the impact of amine-related emissions during CO_2 capture from coal- and/or gas-fired utilities. Considering that the need to control such emissions is still growing as the technology matures, the focus has been primarily on finding adequate analytical capabilities and their suitability to detect and quantify amine-related emissions.

One of the pioneer and perhaps largest effort was undertaken by TCM, which is one of the largest CO_2 capture demonstration facilities in the world (Dye and others, 2008; Riley and others, 2010). Although Phase 2 of the project that included most of the demonstration work was cancelled because of political and economic reassessments (Bergman, 2013), a detailed review of analytical techniques performed for TCM by CSIRO (Riley and others, 2010) affirmed FT-IR as one of the leading methods for continuous online monitoring of stack amine-related emissions. The FT-IR technique has also been used to monitor amine emissions at a mobile CO_2 capture facility in Risavika, Norway (Graff, 2010) and the Esbjerg pilot plant in Denmark (Mertens and others, 2012, 2013). A recent review by the Scottish Environment Protection Agency (SEPA) found that the calibration libraries of some FT-IR manufacturers contain amine compounds such MEA, diethanolamine (DEA), and ammonia, with lowest detection limits of about 0.3 ppm for MEA compared to expected emission levels of about 0.5 ppm (Scottish Environment Protection Agency, 2013). Although the FT-IR method can, in theory, be calibrated to analyze nitrosamines, the SEPA study did not find any available reports of nitrosamine detection by FT-IR spectroscopy. Three additional pilot studies have been conducted in Australia, where FT-IR has been used to not only monitor amine emissions but also to measure CO_2 levels in the flue gas (Riley and others, 2010). Mertens and others (2013) have also invested emissions of ammonia and MEA on a long-term basis (~1000 hr) in a pilot facility using FT-IR. The amine-based CO_2 capture unit was run on a continuous basis while monitoring the emissions using FT-IR in an effort to study the effect of process operating conditions of the water wash section on emission control.

In addition to gas sampling, researchers at SINTEF Materials and Chemistry and the Norwegian University of Science and Technology at Trondheim, Norway, have also demonstrated that FT-IR coupled with attenuated total reflectance (ATR), can be used to monitor amine solutions during CO_2 capture (Einbu and others, 2012). A multicomponent calibration was developed from the study, which allowed analysis of both amine concentration and CO_2 loading of the solutions.

9.2 Experimental Methods and Equipment

9.2.1 FT-IR Laboratory Test with MEA Solutions

The EERC operates a pilot-scale facility for testing CO_2 capture from fossil fuel-derived flue gases using alkanolamine solvents. Many proprietary amine solvents have been tested on the EERC postcombustion capture facility over the last 5–10 years for different industry clients, in addition to MEA. Because of the frequency of amine solvent testing at the EERC and in

anticipation of future regulation on amine emissions from pilot- and/or full-scale facilities, this small lab-scale investigation was conducted to identify challenges that may exist in using FT-IR to monitor such emissions. The focus of this lab test was to determine the feasibility of detecting and quantifying any residual amine as well as its degradation products (particularly nitrosamines) that can be potentially emitted to the atmosphere alongside the stack flue gases. The process for conducting this test and the results are described below.

9.2.2 Test Process Description

A flow diagram for the system used to perform this test is shown in Figure 9-1 and the solvent tested was an MEA solution that had been previously exposed to coal-derived flue gases during a PCO_2C test campaign in 2014. The solutions tested included an initial MEA mixture that was not exposed to flue gas (virgin MEA), a rich MEA sample collected from the absorber column, and a lean MEA sample collected from the stripper column. The samples were exposed to flue gas at 100 scfm for about 2 hr in 2014 and were stored in air-tight containers at room temperature until the test. The choice of MEA as the solvent to use in this test was primarily due to the limited number of calibration spectra for relevant amine solvents and their degradation products such as nitrosamines and also because MEA is relatively well-known.

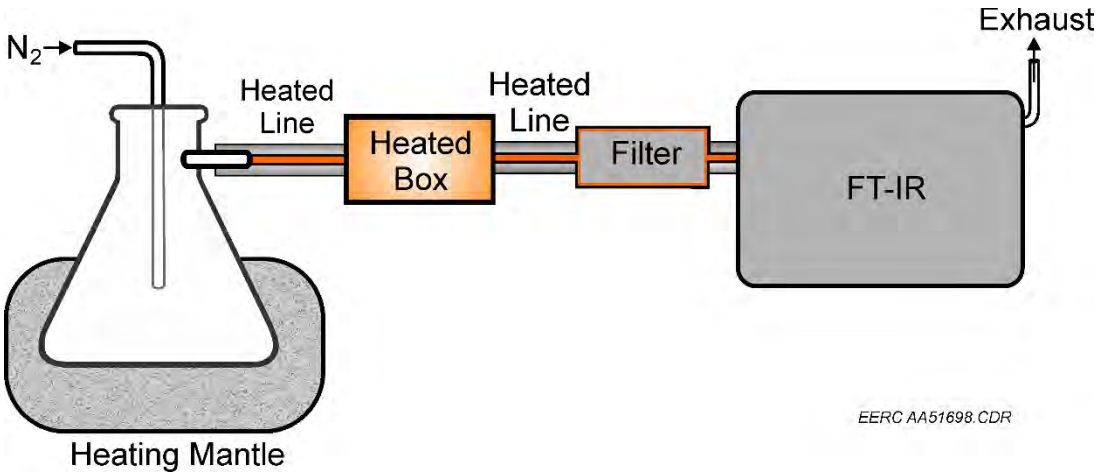

Figure 9-1. Flow diagram of the FT-IR laboratory test with MEA solutions.

The list of nitrosamine compounds with available calibration standards in our current FT-IR calibrations database is shown in Table 9-1 together with the concentration ranges for which they can be quantified at a specific temperature. Calibration standards (reference spectra) for ammonia and other low-molecular-weight organic species such as formaldehyde, acetic acid, and acetone are also available.

Table 9-1. Available Nitrosamine Compounds with Reference Spectra in the Current FT-IR Database

Compound	Concentration Range, ppm	Temperature, °C
Ethanolamine (MEA)	20–1000	150
N-nitrosodibutylamine	93–932	180
N-nitrosodiethylamine	93–932	180
N-nitrosodimethylamine	37–932	180
N-nitrosodipropylamine	93–932	180
N-nitrosomorpholine	70–1827	180
N-nitrosopiperidine	19–932	180
N-nitrosopyrrolidine	93–932	180

9.2.3 Using FT-IR Technique

9.2.3.1 Advantages of FT-IR

There are several advantages to using FT-IR for continuous stack gas sampling (Riley, 2010). FT-IR can determine multiple analytes of interest simultaneously, including conventional flue gas species such as SO_x, NO_x, CO, CO_2, and H_2O. Often, several species can be displayed and tracked simultaneously. FT-IR operators can create a library of reference spectra and calibration curves prior to testing, and raw spectra collected can be saved and processed at a later date if better calibration spectra are developed. This ability makes the FT-IR technique adaptable to a wide range of applications.

9.2.3.2 Disadvantages of FT-IR

There are also disadvantages to FT-IR that have been noted in the literature (Riley and others, 2010). FT-IR has a high sensitivity to the sampling matrix (collisional effects). For amine-related emissions, the FT-IR technique is a novel approach, so there is a general lack of research on the use of FT-IR to measure amine degradation compounds such as nitrosamines. Also, the emission components of interest, including degradation products, are not fully known from specific amines or amine-based technologies. There are some doubts whether currently available commercial systems can meet lowest detection limits of all amine-related emission compounds. Water in the spectra can create water-broadening effects, and interferences can arise in absorption spectra between components of interest and other components or with water.

In addition, for a strong analysis, the operator needs to know the identities of all analytes being tested, and pure forms of these analytes must be available for the development of calibration reference spectra. Good data can only be produced when the instrument is functioning properly and well maintained, and the FT-IR instrument is challenging to maintain. Cleaning instrument components such as mirrors is very delicate, and laser alignment can be very difficult, especially for new users of the instrument.

9.2.4 Amine Emission Mitigation

Amine solvents used to scrub CO_2 from flue gases in coal combustion utilities are soluble in the aqueous phase to form a weakly basic solution. Because of these properties, many aqueous phase approaches are being developed to mitigate amine emissions during postcombustion amine-based CO_2 capture. A recent study by CSIRO (IEA Greenhouse Gas R&D Programme, 2012) outlined several of these techniques, including single- and multiple-stage water wash, combined acid and water wash, and acid wash. These are briefly described below.

9.2.4.1 Single- and Multiple-Stage Water Wash

A single-stage water wash involves installation of a one-stage washing section above the absorber column to scrub any gaseous amine compounds and their soluble degradation products before the lean flue gases exit via the stack. However, the concentration of amine recovered in the washing water can be too high such that the scrubbing process becomes insufficient because of poor partitioning (IEA Greenhouse Gas R&D Programme, 2012). As a result, a large amount of gaseous amine components may remain in the flue gas stream that exits the stack.

In a multiple-stage water wash approach, the absorption column is modified to include multiple water wash sections, with the aim to improve the CO_2-scrubbing performance. According to the CSIRO study, three stages can be added, but the number of stages added depends, in part, on the operating conditions and also on the associated costs. Although installation of multiple stages increases the amine-scrubbing performance, the CSIRO study suggests that the risk of some amine emissions still exists and an optimum number of washing stages would largely depend on acceptable levels of emissions at any given facility (IEA Greenhouse Gas R&D Programme, 2012).

9.2.4.2 Combined Acid and Water Wash

The combined acid and water wash approach utilizes an additional acid wash stage after the water wash stages. The acid pH is maintained in the range 4–6, but the range 3–7 has been found to be effective as well (IEA Greenhouse Gas R&D Programme, 2012). The major role of the acid treatment is to protonate, thus providing stabilization of the amines and other alkaline degradation products in the solution phase for a more efficient removal.

9.2.4.3 Acid Wash

An acid-only wash involves treatment of the gas stream with dilute acid. Bade and colleagues (2010) have found that when sulfuric acid was added to reduce the pH of recycling water to below 6, the MEA concentration in the flue gas dropped below detection limits to about 0.05 ppm. Similar drops in the flue gas levels of ammonia were observed in the study.

9.2.4.4 Economic Impact of a Water Wash Approach

The impact of water wash systems has been rarely studied, but can have significant economic consequences on the overall feasibility of an amine-based CO_2 capture plant. Some of these factors

include amount of water used, corrosion issues, and disposal of wastewater. Brief discussions of these factors are provided below.

9.2.4.5 Water Use and Waste Water Disposal

Currently, there is little or no information in the literature about the economic impacts of water wash processes and/or overall amine-related wastewater effluents. However, a review study conducted by SEPA has suggested that about 2500 tonnes/yr of amine reclaimer wastewater can be expected for a 300-MW_e CO_2 capture power plant (Scottish Environment Protection Agency, 2013). This poses wastewater issues that necessitate treatment prior to disposal, which increases the overall cost to operate a CO_2 capture plant. The use of aqueous amine solvents as a potentially viable CO_2 capture technology is still in active research and development (R&D) and demonstration stages, with no commercial full-scale facilities implemented yet. As a result, many facilities that are involved in demonstration tests are solely engaged in common sense disposal practices. Aqueous amine chemicals and related degradation products are not really novel per se, but their use in the quantities found in CO_2 capture processes is new and poses disposal challenges.

9.2.4.6 Corrosion Issues

At a pilot study in Denmark, a single-stage water wash section was used to control emissions from an MEA CO_2 capture system (Mertens and others, 2013). The results from this study indicate that a single-stage water wash may not be sufficient in removing all amine-related emissions from the flue gas prior to exit to the stack. In addition, levels of ammonia (a key degradation product of MEA) were observed to trend positively with the concentration of iron ions in solution, which was indicative of increased corrosion tendencies for the metal pipes in the CO_2 capture unit. In a recent patent by Bade and colleagues (2010), there is a suggestion to use multiple water wash stages coupled with an acid wash stage for optimal control of the soluble compounds in the gas stream. While this approach may improve the control of emissions of soluble components in the flue gas stream, the presence of acidic conditions can exacerbate corrosion in the system. Thus corrosion is a serious challenge associated with the use of water wash sections to control emissions of amines and the associated degradation products.

9.3 Results and Discussion

9.3.1 FT-IR Lab Test with MEA Solution

The results obtained from the laboratory test are shown in Table 9-2. The rich and lean solutions tested showed the presence of N-nitrosodimethylamine, N-nitrosodiethylamine, N-nitrosopiperidine, and N-nitrosopropylamine in addition to ammonia, water moisture, CO, CO_2, and SO_2. However, the virgin MEA also showed the presence of these components, which suggests an interference issue between the peaks for the nitrosoamines and alkanolamine solvent. The standard deviations obtained were high, and the approximate detection limit estimated by 3σ was even higher, thus suggesting increasing uncertainty related to the quantified results. The spectra from the samples were noisy, and the water reference spectrum used was calibrated for 40% water content, which is not suitable for analyzing a sample with less than 10% water.

Table 9-2. Results Obtained from the Lab Test

Compound	Conc. in Virgin MEA	Conc. in Lean MEA	Conc. in Rich MEA
Ethanolamine (MEA)	>1000 ppm	>1000 ppm	>1000 ppm
N-nitrosodibutylamine	0 ppm	0 ppm	0 ppm
N-nitrosodiethylamine	89.07 ppm	101 ppm	102.20 ppm
N-nitrosodimethylamine	90.72 ppm	100.40 ppm	75.67 ppm
N-nitrosodipropylamine	734 ppm	826.05 ppm	425 ppm
N-nitrosomorpholine	0 ppm	0 ppm	0 ppm
N-nitrosopiperidine	28 ppm	33.13 ppm	23.60 ppm
N-nitrosopyrrolidine	0 ppm	0 ppm	19.80 ppm
NH_3	6.32 ppm	58.40 ppm	11.81 ppm
HCOOH	0 ppm	0 ppm	6.52 ppm
SO_2	13.70 ppm	14.98 ppm	12.24 ppm
CO	0.35 ppm	0.34 ppm	11.94 ppm
CO_2	0.06%	0.07%	0.11%
H_2O	9.77%	4.20%	2.27%

Based on experience from other projects, there is likely water-broadening effects. Consequently, these results only serve to validate the idea that these compounds can be detected and measured by FT-IR, but the accuracy of the quantified data will require further development of suitable reference spectra that remove interferences and proper correction of water-broadening effects and matrix effects.

The upper limit of quantification for a given reference spectrum must be carefully considered prior to setting up recipes for testing. Some reference spectra have nonlinear calibration curves and have more complicated extrapolation profiles. Consequently, if the concentration of an analyte exceeds the upper limit in the reference spectrum, the component is detected but the quantification is wrong.

As shown in the left spectrum in Figure 9-2, the scaled MEA reference spectrum (blue trace), with upper limit of 1000 ppm, does not match the sample spectrum (red trace) completely, and so the quantification of MEA for that sample is inaccurate. The spectrum on the right in Figure 9-2 shows a good fit between the scaled reference spectrum and the sample spectrum because the actual MEA concentration in the sample was 252 ppm, which is within the range of 20–1000 ppm allowed in the reference spectrum. Hence, the quantified MEA concentration is more reliable. In this test, the concentrations of ammonia in the rich and lean solutions were within the limits of the calibration standard, and the match between the scaled reference spectrum and sample spectrum is very good as shown in Figure 9-3.

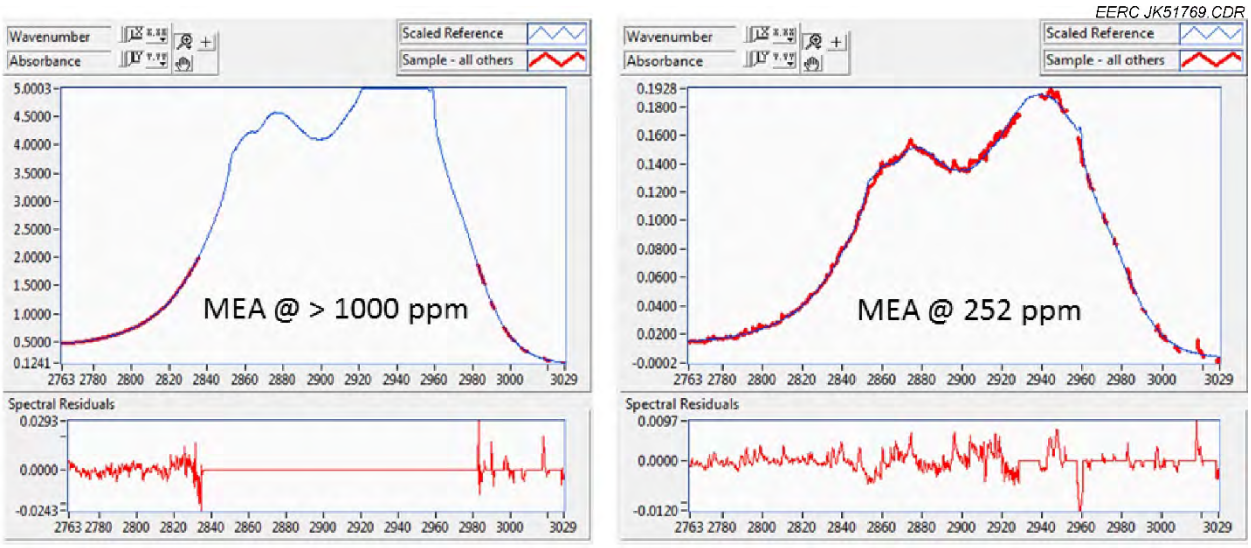

Figure 9-2. Fit between MEA sample spectrum and reference spectrum for (left) above upper limit concentration and (right) below upper limit concentration.

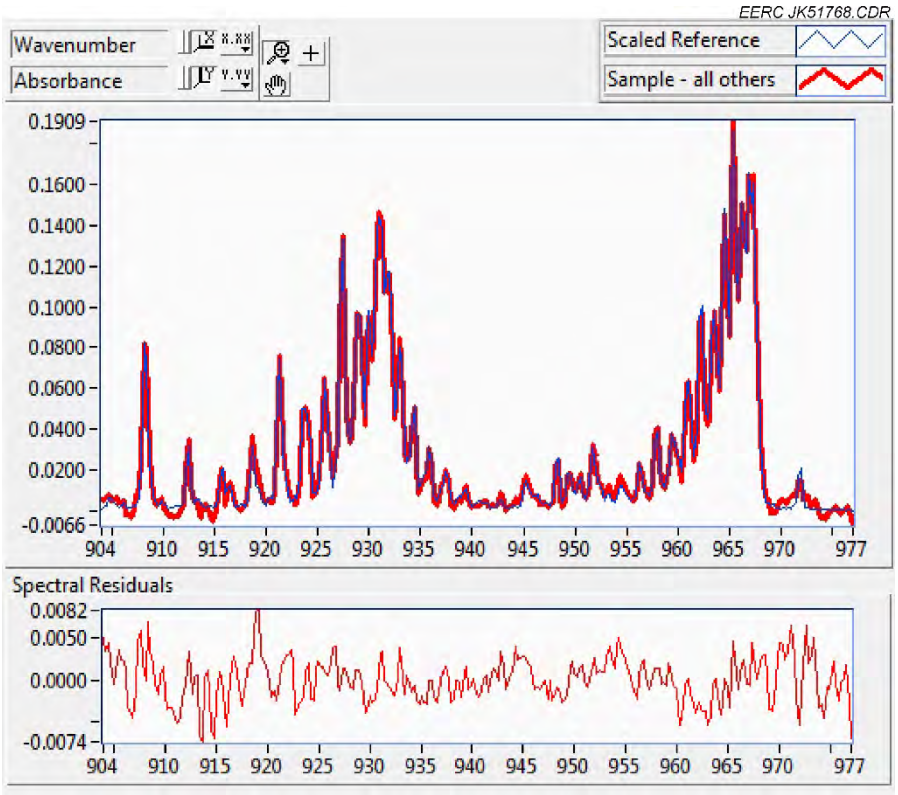

Figure 9-3. Fit between ammonia sample spectrum and the corresponding reference spectrum.

The key finding of this test is that solutions of alkanolamine solvents containing pure solvent components as well as their degradation products and flue gas species can be monitored using the FT-IR technique, as has been established in a few other studies (Riley, 2010; Mertens and others, 2012, 2013; IEA Greenhouse Gas R&D Programme, 2012; Scottish Environment Protection Agency, 2013). However, the reference spectra that are used to perform quantification must be carefully developed to avoid interferences between pure solvent and its degradation products. Also matrix effects including water-broadening and other interferences from flue gas components need to be fully investigated to advance the robustness of the FT-IR technique, especially for advanced proprietary amine solvents. Water sensitivity is crucial, and water calibration must be performed, preferably with the water concentration as close as possible to the expected water level in the flue gas or testing matrix.

9.4 Conclusions

This study suggests that FT-IR is amenable to continuous sampling of stack emissions of aqueous alkanolamines in CO_2 capture utilities. However, very little research has been done on this subject, and many challenges remain to be worked out prior to having the FT-IR technique as a robust method for stack gas-sampling applications. Some of these challenges include:

1. Sensitivity to the sampling matrix.

2. Interferences between desired analytes and other components.

3. Water-broadening effects.

4. Lack of knowledge on the possible degradation products of alkanolamines needed for the development of appropriate reference spectra.

5. Confidentiality barriers involving proprietary solvents hinder or slow the pace of research.

Despite these challenges, the FT-IR technology has strong merits in its ability to detect and quantify many analytes simultaneously where reference spectra are available; raw spectra files can be stored and reprocessed at a later date if improvements are made to the reference spectra files; and the ability to precreate a library of reference spectra and calibration curves that are stored and used as needed.

10.0 SUMMARY OF ACTIVITIES, CONCLUSIONS, AND RECOMMENDATIONS

Studies performed during PCO_2C Phase III focused on the efficient application of capture to electricity-generating facilities and finding ways to decrease the cost of applying capture to such facilities. The activities performed during this phase focused on flue gas pretreatment, pre- and postcombustion capture technologies, capture technology modeling and technoeconomics, power plant modeling, and amine emissions as aerosols in an effort to identify cost-saving approaches to

CO_2 capture. Conclusions and recommendations for each of these activities are included in the summaries that follow.

10.1 Cansolv SO_2 Capture Process

An SO_2 capture solvent developed by Cansolv Technologies Inc. was tested for its ability to remove SO_2 from flue gas. Removal of SO_2 from the flue gas extends the life of a CO_2 capture solvent (thereby decreasing capture cost) by reducing the formation of HSS. The evaluation carried out on the EERC's small pilot-scale combustion and CO_2 capture test system was to determine if Cansolv's new improved formulation exhibited improved operability over the benchmark solvent. Testing was performed with natural gas-fired flue gas that was spiked with various levels of SO_2. Operational challenges were encountered during the testing, primarily related to corrosion of carbon steel components, but these were addressed and solved. The test system operability differences between the solvents were minimal. The improved formulation tended to foam when circulated in the system, but the addition of an antifoaming agent during testing showed that it could be easily remedied. The testing conducted at the EERC indicated that the decision of which solvent to use should be made based on the effectiveness of the SO_2 removal from the flue gas stream as well as the energy input required for solvent regeneration rather than on solvent operability.

10.2 Tri-Mer Flue Gas Filtration Technology

The Tri-Mer flue gas filtration technology combines particulate, NO_x, and SO_2 control. This approach was evaluated using flue gas produced by the EERC's CTF and PTC, with the flows combined to provide the required gas volume for the testing in a device provided by Tri-Mer. Sorbent and ammonia were injected prior to a residence chamber. Two different sorbents, Sorbacal SP and Sorbacal SPS, were evaluated at various residence chamber temperatures. Testing resulted in high levels of capture for particulate, NO_x, and SO_2. As anticipated, NO_x and SO_2 capture were highly dependent on temperature, ammonia injection rate, and amount of sorbent. Differences were also observed between the SP and SPS SO_2 sorbents. SPS sorbent was found to remove more SO_2 than was exhibited by the same quantity of SP sorbent. The Tri-Mer filtration technology was found to be an effective tool for the removal of impurities prior to CO_2 capture, although it may be necessary to further reduce SO_2 levels in some instances.

10.3 KCRC Solvent-B CO_2 Capture Technology

Two new postcombustion capture solvents were tested on the PCO_2C small pilot-scale system. The first solvent tested was Solvent-B from KCRC. This was the first test of the solvent at the pilot scale, and unfamiliarity with the solvent's properties and performance led to some challenges in test operation, including the need for a makeup water stream and reduction of flue gas flow rate in order to achieve the L/G needed for 90% capture. Two test campaigns were run, with capture rates of 70% to 94% observed for Solvent-B. Steady-state data were collected at several different test points. Solvent-B appeared to perform at least as well as 30 wt% MEA. It achieved 90% capture with an estimated 40% lower L/G and 30% lower regeneration energy input than MEA at the same capture level.

10.4 CO_2 Solutions Incorporated Enzyme Solvent

The second postcombustion capture solvent evaluated was developed by CO_2 Solutions Incorporated. CO_2 Solutions' proprietary technology employs the enzyme carbonic anhydrase as a catalyst within a salt solution. The solvent requires that the stripping column be run at a slight vacuum; therefore, the EERC's CO_2 capture test system was modified to include a vacuum pump on the stripping column. Other system modifications included the addition of a hot-water system, auxiliary heat on the solvent heater water inlet, and an inline pH meter. The testing comprised parametric-style and short-term tests in which L/Gs varied and the resulting CO_2 capture rates were measured. Most of the tests were performed with natural gas-derived flue gas, with a few test periods during which solvent performance using coal-derived flue gas was measured. The testing indicated that a plate heat exchanger might have provided better performance than the shell-and-tube reboiler that was used during the testing. Following testing, the south absorber was found to contain a significant buildup of solid residue from the solvent. This was because of column base geometry. Buildup of solids over the course of the test could have reduced the ability of the solvent to capture CO_2. Overall, the CO_2 Solutions test program was successful, meeting objectives including no degradation in performance of the enzyme catalyst and no toxic waste products generated. The most significant result was the demonstrated ability to use low-grade heat for the process for regeneration, significantly reducing the cost to capture CO_2.

10.5 CSIRO Hydrogen Separation Membranes

CSIRO's hydrogen separation membranes for purifying hydrogen from coal-derived syngas were tested on syngas produced in the EERC's FBG. These were the first tests of CSIRO's membranes on actual coal-derived syngas. For the testing, CSIRO provided nine palladium–vanadium metal membranes. During testing, warm-gas cleanup techniques were employed to remove impurities in the syngas stream prior to the CSIRO hydrogen separation membranes.

The membranes' performance increased as the temperature increased and was comparable to the performance of other membranes tested at the EERC. Brittle fractures were observed on two of the separators, indicating that long-term tolerance to syngas impurities should be evaluated. Higher-temperature operation should be the objective of future testing in order to take advantage of the increased performance. The higher temperatures would most likely accelerate membrane material degradation, but this could facilitate materials research that would benefit future membrane development.

10.6 Postcombustion Capture Modeling

A process-modeling effort was undertaken to develop the basis for determining the cost of CO_2 capture using advanced postcombustion capture technologies and techniques, including the KCRC and CO_2 Solutions solvents as well as partial CO_2 capture with MEA. A model was developed using Aspen Plus software that mimics the boiler and steam cycle of Cases 11 and 12 from the DOE report entitled "Cost and Performance Baseline for Fossil Energy Plants, Volume 1: Bituminous Coal and Natural Gas to Electricity" (Black, 2013a). Case 11 represents a 550-MW-net pc-fired power plant with a supercritical steam cycle operating at 39.3% efficiency. Case 12 represents a 550-MW-net pc-fired supercritical power plant with 90% CO_2 capture. The

overall plant size was increased in Case 12 to account for the significant parasitic load of the CO_2 capture process, and the overall efficiency is 28.4%. The models developed in the DOE report served as the basis against which the advanced postcombustion technologies were analyzed.

The results of the Aspen Plus process-modeling effort were used to develop the mass and energy balance for utilization of the KCRC solvent in a 550-MW_e power generation facility. The overall plant performance in the KCRC case is significantly improved over Case 12, primarily because the steam withdrawn from the steam cycle for solvent regeneration is reduced. This results in a much lower coal feed rate and smaller overall plant size. The auxiliary load for CO_2 capture and compression is also lower than that of Case 12. The baseline MEA model uses five CO_2 capture trains, but the reduced L/G for the KCRC solvent enabled the same amount of CO_2 capture in only three trains. This reduces the overall auxiliary load on the plant. The overall efficiency of the plant was improved from 28.4% to 30.8% when compared to Case 12. Overall, the modeling showed that utilization of the KCRC solvent could improve the efficiency of CO_2 capture when compared to MEA.

The modeling effort was also used to develop mass and energy balances for utilization of the CO_2 Solutions solvent at a 550-MW power generation facility. It was assumed that adequate waste heat could be gathered from the power plant to regenerate the solvent and that the solvent will perform in a manner comparable to MEA. The modeling results indicate that if these two assumptions can be met, significant increases in overall plant efficiency and reductions in coal feed rate (compared to Case 12) can be realized. Even if all of the heat required for 90% capture cannot be obtained, the result holds promise for systems that could require partial capture of CO_2. The solvent holds significant potential in this situation to provide low levels of capture with no impact to the overall steam cycle. Additional studies should be performed to verify potential sources of waste heat and heat sources that might impact the overall plant efficiency less, such as hot-water withdrawal. Additional testing is also needed to verify the performance and compare it to that of MEA. Any improvement in performance over MEA will reduce the amount of waste heat needed for regeneration.

Another important factor is the use of vacuum in the stripping column for solvent regeneration. Vacuum is an important component for the performance of CO_2 Solutions solvent but was not included in the modeling analysis. Further investigation of the components necessary and their appropriate sizes is needed to estimate energy demands and costs. The results presented here are a very conservative first step in the economic projection process for this technology.

EPA recently released new rules for each state regarding the emissions of CO_2 from stationary power sources. Emission reduction targets for most states fall within the 25%–45% range. The cost of CO_2 capture is expected to be significantly lower for a capture solvent system that captures only part of the CO_2 than for a system targeting 90% (often called total capture), making partial CO_2 capture a potentially attractive strategy. To estimate this cost, the EERC undertook a detailed techno-economic analysis focused on modeling the mass and energy balance and equipment needs associated with partial capture of CO_2. Several capture targets could be evaluated, but it was decided that 45% capture would be the basis for modeling in this initial study since that represents the potential high end of CO_2 capture requirements for electricity-generating plants. The standard models use five capture trains to achieve 90% CO_2 capture from the base

cases; therefore, several options exist to achieve lower levels of CO_2 separation. These options could include 45% capture from five trains, 75% capture from three trains, or 90% capture from two trains, with a third smaller train still required. As a starting point, it was decided to model 75% capture from three trains using a standard MEA solvent, resulting in 45% overall CO_2 capture.

The total steam turbine power output for the partial capture case was modeled to be 617.4 MW, which represents a reduction of 45.4 MW over Case 12, for the same net power production of 550 MW. Auxiliary power requirements for the CO_2 capture system and the total output of the steam turbines were modeled in detail using Aspen Plus. The power requirements for some of the smaller systems were estimated based on the information provided in the DOE report. Overall, the models showed that a supercritical coal-fired power plant operating with 45% CO_2 capture could achieve net plant efficiencies in excess of 33%.

To estimate the impact that process improvements in CO_2 capture technology can have on the economics of a power plant, the APEA software package was used. APEA is a project-scoping tool that enables engineers to evaluate the economic impact of their process designs. It is most valuable in the early phases of conceptual design to compare competing technologies and evaluate alternative process configurations. Models constructed in Aspen Plus for calculating mass and energy balances were imported into APEA for economic analysis.

KCRC Solvent-B demonstrated improved performance over MEA at the pilot scale. Projecting that performance to full scale indicated that, relative to MEA, the overall efficiency of a plant utilizing the solvent would be increased, the size of the capture system could be reduced because of the reduction in L/G, and that system could be reduced to only three equipment trains. These improvements benefit the overall economic assessment of performance at full scale. Because the solvent is still in the development stage, estimates of solvent cost and usage were kept equivalent to those provided for MEA in the DOE Case 12 evaluation. As more information becomes known about the solvent, the models must be rerun to reflect these changes in values. This first-time economic projection indicates that Solvent-B improves the costs of carbon capture over that of MEA (DOE Case 12) because of the reduced equipment requirements and improved solvent performance. As development continues to larger demonstrations, it is anticipated that the costs will improve even more.

There are components of the carbon capture system that truly do not apply to the CO_2 Solutions capture system. These are components that are not needed for the CO_2 Solutions solvent but are in the Econamine basis for the DOE case studies and include the water wash tower and associated subsystems as well as the solvent reclaimer and its associated subsystems. Exact detail on the precise components cannot be derived as that information is held as proprietary by Fluor and cannot be released by DOE. Nonetheless, an attempt was made to remove those components from the system and the costs estimated by their removal from the case study. The estimated reduction in costs associated with removal of the subsystems not needed to operate with the CO_2 Solutions solvent results in an approximate reduction of the capture cost by 5%, although the associated vacuum costs were not included and need to be explored further. Much of the benefit resides in the low heat requirements for regeneration. If ample low-quality heat sources can be identified at the full scale to provide the regeneration energy required, then the steam cycle can remain unaltered. This concept alone can be the driving factor for a utility to utilize this technology

and results in lower cost as compared to the DOE Case 12 scenario for a plant with carbon capture. Results of this beginning work indicate the strong potential to meet the DOE goal of $40/tonne of CO_2 captured.

10.7 Plant-Specific CO_2 Capture Evaluation

A modeling effort was undertaken at the EERC to provide decision makers with a tool to enable them to assess possible CO_2 emission reduction strategies to meet EPA's CPP. Three power plants from the region were modeled using the Carnegie Mellon IECM to show the effects that the addition of capture would have on their specific net power production, water usage, and revenue requirements for various levels of capture. The work also highlighted potential challenges that may exist for some power plants at which CO_2 capture is being considered. Important findings included that sulfur removal devices must be installed if not already present; space for the capture plant and storage of solvent and reclaimer waste must be available; use of a bypass during partial capture may minimize the size of the capture tower(s), resulting in a reduction of revenue required to operate the capture facility; and power plants in arid areas may find that addition of a cooling tower could minimize water usage. The results reinforced that a one-size-fits-all approach cannot be taken to adding capture to a power plant.

10.8 Amine Emission Evaluation

One common challenge with using amines for CO_2 capture is the degradation of amine compounds during the capture process and/or during regeneration of the solvent in the stripper unit. As a result, some of the functional amine is lost to degradation, volatilization, or leakage from the handling systems, thus releasing these chemicals into the environment in various forms. A small laboratory-scale investigation was performed to identify challenges that may exist in using FT-IR to monitor any residual amines as well as their degradation products (particularly nitrosamines) that can be potentially emitted to the atmosphere with the stack flue gases during CO_2 capture activities. It was found that solutions of alkanolamine solvents containing pure solvent components as well as their degradation products and flue gas species can be monitored using the FT-IR technique. The reference spectra that are used to perform quantification must be carefully developed to avoid interferences between pure solvent and its degradation products. Matrix effects including water broadening and other interferences from flue gas components need to be fully investigated to advance the robustness of the FT-IR technique, especially for advanced proprietary amine solvents. Water sensitivity is crucial, and water calibration must be performed, preferably with the water concentration as close as possible to the expected water level in the flue gas or testing matrix. FT-IR is applicable to continuous sampling of stack emissions at CO_2 capture facilities.

PCO_2C Program Phase III placed a strong emphasis on the integration of technologies into total systems so that substantial economic and environmental benefit could be realized. The type of information gathered during Phase III is important for utility stakeholders as they determine how to cost-effectively reduce their CO_2 emissions in a carbon-constrained world.

11.0 REFERENCES

Adler, J. Supreme Court puts the brakes on the EPA's Clean Power Plan. *The Washington Post,* February 9, 2016. www.washingtonpost.com/news/volokh-conspiracy/wp/2016/02/09/supreme-court-puts-the-brakes-on-the-epas-clean-power-plan/ (accessed March 23, 2016).

Adhikari, S.; Fernando, S. Hydrogen Membrane Separation Techniques. *ACS Publications Industrial & Engineering Chemistry Research* **2006**.

Bade, O.M.; Gorset, O.; Graff, O.F.; Woodhouse, S. *Eliminating/Reducing Emission of Amines and Their Alkaline Degradation Products to Atmosphere from a Plant for Carbon Dioxide Capture from Flue Gas Involves Washing Carbon Dioxide Lean Flue Gas with Acidic Aqueous Solutions*; WO2010102877-A1, WO20102877-A1, BO1D-053/14 201063, Sept 16, 2010.

Bergman, J. Norway Drops "Moon Landing" as Mongstad Carbon Capture Scrapped. www.bloomberg.com/news/articles/2013-09-20/norway-drops-moon-landing-as-mongstad-carbon-capture-scrapped, 2013 (accessed Oct 2, 2015).

Black, J. *Cost and Performance Baseline for Fossil Energy Plants Volume 1: Bituminous Coal and Natural Gas to Electricity*; Revision 2; DOE/NETL-2010/1397; 2010.

Black, J. *Cost and Performance Baseline for Fossil Energy Plants, Volume 1*: *Bituminous Coal and Natural Gas to Electricity*; Revision 2a; DOE/2010/1397; Sept 2013a.

Black, J. *Quality Guidelines for Energy Systems Studies, Capital Cost Scaling Methodology*; DOE/NETL-341/013113; Jan 2013b.

DOW Specialty Amines. www.dow.com/amines/prod/ethano-mea.htm (accessed Jan 2016).

Dye, C.; Schmidbauer, N.; Schlabach, M. Evaluation of Analytical Methods for Amine-Related Emissions and Degradation Products in Emission and Ambient Air – Phase I: CO_2 and Amines Screening Study for Environmental Risks, 2008. http://co2.nilu.no/LinkClick.aspx?fileticket=JDEy5GezzRU%3d&tabid=2549&mid=5547&language=en-US (accessed Oct 12, 2015).

E&E Publishing, LLC. Clean Power Plan—A Summary. EnergyWire, 2015. www.eenews.net/interactive/clean_power_plan/fact_sheets/rule (accessed Feb 1, 2016).

Einbu, A.; Ciftja, A.F.; Grimstvedt, A.; Zakeri, A.; Svendsen, H.F. Online Analysis of Amine Concentration and CO_2 Loading in MEA Solutions by ATR-FTIR Spectroscopy. *Energy Procedia* **2012**, *23*, 55–63.

Ellis, S. Honda Fuel Cell Vehicle Progress. Presented at the Advancing the Hydrogen Economy Action Summit II; Grand Forks, ND; Sept 4, 2008.

Florin, N.; Fennell, P. Assessment of the Validity of "Approximate Minimum Land Footprint for Some Types of CO_2 Capture Plant," 2010. www.gov.uk/government/uploads/system/

uploads/attachment_data/file/43615/CCR_guidance_-_Imperial_College_review.pdf (accessed Jan 2016).

Gabitto, J.; Tsouris, C. Sulfur Poisoning of Metal Membranes for Hydrogen Separation. *International Review of Chemical Engineering* **2009**, *1* (5), 394–411.

Galindo, P.; Schaffer, A.; Brechtel, K.; Unterberger, S.; Scheffknecht, G. Experimental Research on the Performance of CO_2-Loaded Solutions of MEA and DEA at Regeneration Conditions; 8th European Conference on Coal Research and Its Applications. *Fuel* **2012**, *101*, 2–8.

Gerdes, K. *Current and Future Technologies for Gasification Based Power Generation, Volume 2: Carbon Capture, Revision 1*; DOE/NETL-2009/1389; 2010.

Gerdes, K. The Potential of Advanced Gasification Pathways to Reduce CO_2 Capture Costs. Presented at the Gasification Technologies Conference, Colorado Springs, CO, Oct 2009.

Global CCS Institute. Large-Scale CCS Demonstrations and the Kemper Project, 2013. www.globalccsinstitute.com/insights/authors/pamelatomski/2013/10/17/large-scale-ccs-demonstrations-and-kemper-project (accessed Feb 2, 2016).

Graff, O.F. *Emission Measurement and Analysis from Mobile Carbon Capture Test Facility*; IEA Greenhouse Gases R&D Programme Report on meeting at Oslo, Norway, Feb 2010; Report 2010/11; June 2010. Available online at www.ieaghg.org.

Hao, S.; Sholl, D. Comparison of First Principles Calculations and Experiments for Hydrogen Permeation Through Amorphous ZrNi and ZrNiNb Films. *Journal of Membrane Science* **2010**, *350,* 402.

Hao, S.; Sholl, D. Selection of Dopants to Enhance Hydrogen Diffusion Rates in MgH_2 and $NaMgH_3$. *Applied Physics Letters* **2009**, *94,* 171909.

Hao, S.; Sholl, D. The Role of Interstitial H_2 in Hydrogen Diffusion in Light Metal Borohydrides. *Phys. Chem. Chem. Phys*. **2009**, *11*, 11106.

Hoffman, J. Cost and Performance for Low-Rank Coal Power Plants. Presented at the Gasification Technologies Conference, Colorado Springs CO, Oct 2009.

Holmes, M. Coal-to-Hydrogen. Presented at the Advancing the Hydrogen Economy Action Summit II, Grand Forks, ND, Sept 4, 2008.

IEA Greenhouse Gas R&D Programme. *Gaseous Emissions from Amine-Based PCC Processes and Their Deep Removal*; 2012/07; May 2012. Available online at www.ieaghg.org.

Jensen, M.; Schlasner, S.; Sorensen, J.; Hamling, J. *Operational Flexibility of CO_2 Transport and Storage (IEA/CON/13/218)*; Final Report for IEA Greenhouse Gas R&D Programme; Energy & Environmental Research Center: Grand Forks, ND, Dec 2014.

Kamakoti, P.; Sholl, D. Ab Initio Lattice-Gas Modeling of Interstitial Hydrogen Diffusion in CuPd Alloys. *Physical Review B 71*, **2005**, 014301.

Kamakoti, P.; Sholl, D. Towards First Principles-Based Identification of Ternary Alloys for Hydrogen Purification Membranes. *Journal of Membrane Science* **2006**, *279,* 94–99.

Kamakoti, P.; Sholl, D. A Comparison of Hydrogen Diffusivities in Pd and CuPd Alloys Using Density Functional Theory. *Journal of Membrane Science* **2003**, *225*, 145–154.

Kavanagh, D. Paris Climate Agreement—A Three-Point Summary. *Journalytic*, 2015. https://journalytic.wordpress.com/2015/12/15/paris-climate-agreement-a-three-point-summary/ (accessed Feb 1, 2016).

Klara, J.M. IGCC: Coals Pathway to the Future. Presented at the Gasification Technologies Conference, Oct 4, 2006.

Kluiters, S.C.A. *Status Review on Membrane Systems for Hydrogen Separation*; Intermediate Report EU Project MIGREYD NNE5-200-670; Dec 2004.

Kozak, F.; Petig, A.; Rhudy, R.; Thimsen, D.; Morris, E. Chilled Ammonia Field Pilot Program at We Energies. Presented at the 9th Annual Conference on Carbon Capture and Sequestration, Pittsburgh, PA, May 10–13, 2010.

Ma, Y.; Pomerantz, N.; Chen, C. *Sulfur-Tolerant Pd/Cu and Pd/Au Alloy Membranes for Hydrogen Separation with High Pressure CO_2 Sequestration*; Periodic Progress Report; 2007.

Mertens, J.; Lepaumier, H.; Desagher, D.; Thielens, M-L. Understanding Ethanolamine (MEA) and Ammonia Emissions from Amine Based Post Combustion Carbon Capture—Lessons Learned from Field Tests. *International Journal of Greenhouse Gas Control* **2013**, *6*, 72–77.

Mertens, J.; Knudsen, J.; Thielens, M-L; Andersen, J. Online Monitoring and Controlling Emissions in Amine Post-Combustion Carbon Capture—A Field Test. *International Journal of Greenhouse Gas Control* **2012**, *6* (1), 2–11

Nelson, M. CO_2 Capture at the Kemper County IGCC Project. Presented at the 2011 NETL CO_2 Capture Technology Meeting, Pittsburgh, PA, Aug 2011.

NRG Energy. WA Parish CO_2 Capture Project Fact Sheet, 2014. www.nrg.com/documents/business/pla-2014-petranova-waparish-factsheet.pdf (accessed Feb 2, 2016).

O'Brien, C. *Sulfur Poisoning of Pd and PdCu Alloy Hydrogen Separation Membranes*; Doctoral Thesis, Carnegie Mellon University, 2011.

Ockwig, N.; Nenoff, T. Membranes for Hydrogen Separation; *ACS Publications Chemical Review*, 2007.

Plunkett, J. Performance & Cost Comparisons of Alternate IGCC-Based Carbon Capture Technologies. Presented at the Gasification Technologies Conference, Colorado Springs, CO, Oct 2009.

Rao, A.; Rubin, E. A Technical, Economic, and Environmental Assessment of Amine-Based CO_2 Capture Technology for Power Plant Greenhouse Gas Control. *Environ. Sci. Technol.* **2002**, *36* (20), 4467–4475.

Reddy, S.; Johnson, D.; Gilmartin, J. Fluor's Econamine FG Plus^{SM} Technology for CO_2 Capture at Coal-Fired Power Plants. Presented at the Power Plant Air Pollutant Control "Mega" Symposium, Baltimore, MD, Aug 25–28, 2008.

Rhudy, R. *Chilled Ammonia Postcombustion CO_2 Capture System–Laboratory and Economic Evaluation Results*; Electric Power Research Institute Technology Update Report 1012797; Palo Alto, CA, 2006.

Riley, K.W.; Angove, A.; Halliburton, B.; Tibbett, A.; Sharma, S.; Attalla, M.; Azzi, M. CO_2 Capture Mongstad—Project A – Establishing Sampling and Analytical Procedures for Potentially Harmful Components from Post-Combustion Amine-Based CO_2 Capture—Task 3 – Online Sampling and Analysis, Dec 24, 2010, EP105968. www.gassnova.no/no/Documents/Onlinesamplingandanalysis_CSIRO.pdf (accessed Sept 16, 2015).

Rothenberger, K.; Howard, B.; Killmeyer, R.; Ciocco, M.; Morreale, B.; Enick, R. Palladium-Copper Alloy Membrane Performance Under Continuous H_2S Exposure, 2005, pp 11–13. www.netl.doe.gov.

Scottish Environment Protection Agency. Review of Amine Emissions from Carbon Capture Systems Version v1.1, Jan 2013. www.sepa.org.uk/media/155585/review-of-amine-emissions-from-carbon-capture-systems.pdf (accessed Sept 16, 2016)

Sholl, D. Using Density Functional Theory to Study Hydrogen Diffusion in Metals—A Brief Overview. *Journal of Alloys and Compounds* **2007**, *446–447*, 462–468.

Smith, J.; Van Ness, H.; Abbott, M. *Introduction to Chemical Engineering Thermodynamics*, 5th Edition; McGraw Hill: Boston, MA, 1996.

Sondreal, E.A.; Swanson, M.L.; Benson, S.A.; Holmes, M.J.; Jensen, M.D. A Review of Gasification Technology for Coproduction of Power, Synfuels, and Hydrogen from Low-Rank Coals. In *Proceedings of the 20th Symposium on Western Fuels*; Marriott Denver Tech Center, Denver, CO; Oct 24–26, 2006.

Stanislowski, J.; Laumb, J. Gasification of Lignites to Produce Liquid Fuels, Hydrogen, and Power. Presented at the Pittsburgh Coal Conference, Sept 2009.

Stocker, J.; Whysall, M.; Miller, G. *30 years of PSA Technology for Hydrogen Purification*; UOP LLC; 1998.

Subramanian, P.; Laughlin, D. Binary Alloy Phase Diagrams – 2nd Edition; Massalski, T., Ed.; ASM International, 1990; pp 1454–1456.

U.S. Department of Energy. *Effects of a Transition to a Hydrogen Economy on Employment in the United States, Report to Congress,* July 2008a. www.hydrogen.energy.gov/pdfs/epact1820_employment_study.pdf (accessed 2016).

U.S. Department of Energy Hydrogen Program. FY2008 Annual Progress Report, Dec 2008b. www.hydrogen.energy.gov/index.html (accessed 2016).

U.S. Department of Energy National Energy Technology Laboratory Office of Program Planning and Analysis. *Quality Guidelines for Energy System Studies, Cost Estimation Methodology for NETL Assessments of Power Plant Performance*; DOE/NETL-2011/1455; April 2011.

Volkov, A.; Kazantsev, V.; Kourov, N.; Kruglikov, N. Formation of the Structure and Properties of Cu-Pd Alloys During the A1-B2 Phase Transitions. *The Physics of Metals and Metallography* **2008**.

Yang, J.; Nishimura, C.; Komaki, M. Hydrogen Permeation of $Pd_{60}Cu_{40}$ Alloy Covered V-15Ni Composite Membrane in Mixed Gases Containing H_2S. *Journal of Membrane Science* **2008**, *309*, 246–250.

ZeroCO_2.NO. Boundary Dam Integrated CCS Project. www.zeroco2.no/projects/saskpowers-boundary-dam-power-station-pilot-plant (accessed Feb 2, 2016).